Theoretical aspects of relaxation phenomena accompanying core and valence ionization in some organic systems

Cromarty, Benjamin J.

UNIVERSITY OF DURHAM

A thesis entitled

Theoretical Aspects of Relaxation Phenomena Accompanying Core and Valence Ionization in Some Organic Systems

Submitted by

Benjamin J. Cromarty, B.Sc.

A candidate for the degree of Doctor of Philosophy

Grey College

September 1978

To my parents

ACKNOWLEDGEMENTS

The debt to my supervisor, Dr. D.T. Clark, is obvious from the content of this thesis, and I wish to extend my warmest thanks to him for introducing me to the field of theoretical chemistry applied to ESCA, and for the constant enthusiasm, unfailing encouragement and ever-available assistance offered me over the past three years. I should also like to thank my collaborator Professor A. Sgamellotti, whose three brief visits to Durham were thought-provoking and certainly most productive.

Thanks are due to my contemporary and friend, Derek Shuttleworth, and to all those other colleagues whose presence in the laboratories at some time over the past three years have made my stay here such an enjoyable one: Dave Adams, Jim Peeling, Jiri Müller, Ron Thomas, Alan Dilks, Lynne Colling, Herb Beer, and Thomas Fok.

Gratitude is also expressed to the Science Research Council for the provision of a research grant, and computing facilities via the RHEL (Remote 8) Workstation. The patience of the Physics users of the workstation in allowing a mere chemist into their midst is acknowledged, and I am particularly indebted to A.P. Lotts for his kindness and assistance. Thanks are also due to the University of Durham for research and computing facilities; the able assistance of Dr. A.M. Lamont at NUMAC is gratefully acknowledged.

Finally, I would like to thank Mrs. Kay Jones for her considerable skills in assisting with the many diagrams presented in this thesis, and Mrs. Marion Wilson for her great patience and skill in typing this (often illegible) manuscript.

MEMORANDUM

The work described in this thesis was carried out in the University of Durham between September 1975 and September 1978. The work has not been submitted for any other degree, and is the original work of the author except where acknowledged by reference. Parts of this thesis have been the subject of the following publications:

1. D.T. Clark, B.J. Cromarty; "A Theoretical Investigation of Electronic Reorganizations Accompanying Core and Valence Ionization in Simple Hydrogen-Bonded Systems", Theor.Chim.Acta, 44, 181 (1977).
2. D.T. Clark, B.J. Cromarty; "Some Theoretical Aspects of Core-Ionization in Carbocations", in "Progress in Theoretical Organic Chemistry, Volume II", edited I.G. Csizmadia, Elsevier, pp 447 (1977).
3. D.T. Clark, B.J. Cromarty, L. Colling; "On the Relative Energies of the Ground and Core Hole States of the 1-Propyl and 2-Norbornyl Cations", J.C.S. Chem.Comm., 277 (1977).
4. D.T. Clark, B.J. Cromarty, L. Colling; "A Theoretical Investigation of the Core Hole States of the 2-Norbornyl Cation", J.Am.Chem.Soc., 99, 8118 (1977).
5. D.T. Clark, B.J. Cromarty; "A Non-empirical LCAO MO SCF Investigation of Electronic Relaxation Accompanying Core-Ionization in a Series of Saturated Alkanes", Chem.Phys.Lett., 49, 137 (1977).
6. D.T. Clark, B.J. Cromarty, A. Sgamellotti; "Single Orbital Relaxation Accompanying Core-Ionization", Chem.Phys. Lett., 51, 356 (1977).
7. D.T. Clark, B.J. Cromarty, A. Sgamellotti; "A Theoretical Investigation of the Electric Field Dependence of Core-Ionization Phenomena in Carbon Monoxide", Chem.Phys., 26, 179 (1977).

8. D.T. Clark, B.J. Cromarty, A. Sgamellotti; "Orbital Contributions to Relaxation Energies Accompanying Core-Ionizations in the Series CO, COH^+, HCO^+ and H_2CO", J.C.S. Faraday Trans.II, 74, 1046 (1978).

9. D.T. Clark, B.J. Cromarty, A. Sgamellotti; "Single Orbital Relaxations Accompanying Core-Ionization in the Isoelectronic Series CH_4, NH_3, H_2O, HF and Ne", J.Electron Spectros.Rel.Phenom., 13, 85 (1978).

10. D.T. Clark, B.J. Cromarty, A. Sgamellotti; "A Theoretical Investigation of the Ground and Core Hole States of Linear and Bent NiCO: A Prototype for CO Adsorbed on Nickel", Chem.Phys.Lett., 55, 482 (1978).

11. D.T. Clark, B.J. Cromarty, A. Sgamellotti; "A Theoretical Investigation of the Electronic Reorganization Accompanying Core-Ionization in the Isometic Molecules HCN, HNC and HON, HNO", J.Electron Spectros.Rel.Phenom., in press (1978).

12. D.T. Clark, B.J. Cromarty, A. Sgamellotti; "Orbital Relaxation Accompanying Core-Ionization in Carbon Monoxide", Atti Accad.Naz.Lincei,Rend.Classe Sci.Mat.Fis.Nat., in press (presented August 1978).

13. D.T. Clark, B.J. Cromarty, A. Sgamellotti; "A Theoretical Investigation of Single Orbital Relaxation Energy Contributions Accompanying Core-Ionization of N_2", Chem.Phys., in press (1978).

14. D.T. Clark, B.J. Cromarty, A.D. Dilks; "A Theoretical Investigation of Molecular Core Binding and Relaxation Energies in a Series of Oxygen-Containing Organic Molecules, of Interest in the Study of Surface Oxidation of Polymers", J.Polym.Sci., Polym.Chem.Ed., in press (1978).

15. D.T. Clark, B.J. Cromarty, J. Müller, U. Gelius; "Some Theoretical Aspects of Photoionization Phenomena Involving the Valence 2s Levels of a Series of Alkanes", Phys.Scr. (to be submitted).

16. D.T. Clark, B.J. Cromarty, A. Sgamellotti; "Some Theoretical Aspects of Electronic Reorganization Phenomena Accompanying Core-Ionization within the Hartree-Fock Model", Accts.Chem.Res. (to be submitted).

ABSTRACT

Irradiation of molecules by X-rays leads to photo-emission of electons, this forming the basis of XPS or ESCA spectroscopy. The electrons remaining in the molecule experience an effective increase in nuclear charge accompanying photoionization, and undergo a "relaxation" process. The energy associated with this (the relaxation energy) affects not only the intensity and shape of the experimentally measured peak, but also its position (or binding energy) to a significant extent.

By means of well-established quantum mechanical methods, it is possible to calculate theoretically both binding energies and relaxation energies for core-electron photoionization. Specifically, *ab initio* LCAO MO SCF calculations within the Hartree-Fock formalism have been performed on a wide variety of organic systems.

The relaxation energy as a function of increasing chain-length in a series of linear and bent alkanes has been investigated, and found to be responsible for the experimentally observed shifts in core binding energies. The valence (2s) ionized species have also been investigated, with particular emphasis on line-widths. A study of the simple carbocations has been made, a particular point of interest being the classical or non-classical descriptions of the bonding in specific cases.

To investigate the effect of extra-molecular contributions to relaxation energies, a series of hydrogen-bonded dimers has been studied as a simple prototype system. Intermolecular

contributions to relaxation energies are found to be of the same sign, irrespective of the sign for the shift in core binding energy. The core-like, valence (2s) hole-state species are found to have parallel trends in shifts.

A method has been developed for partitioning the total relaxation energy into contributions from each occupied orbital in the molecule of interest. This procedure is shown to be both mathematically rigorous, and in accord with chemical intuition, and is applied to several series of related molecules. From studies of this nature, a clearer understanding of the relationship between chemical bonding, and the reorganization processes accompanying core-ionization is possible.

Finally, as an extension of the investigation into extra-molecular relaxation energies, and a further example of the use of relaxation energy partitioning, some simple prototype systems for the adsorbtion of small molecules onto metal surfaces are considered. In the case of CO on Ni, it is found that a bent conformation is needed to interpret the available XPS data.

CONTENTS

Page No.

Page No.

CHAPTER ONE

MOLECULAR ORBITAL THEORY

1.1 Introduction

The aim of this chapter is to present sufficient background theory to form a basis for discussions presented in subsequent chapters. A concise summary is therefore given of non-empirical molecular orbital theory, with some description of the computational aspects of the theory. A brief discussion of the programs used in this work for the molecular Hartree-Fock calculations is also given. The main emphasis is on computations within the Hartree-Fock formalism, although mention is made of both correlation and relativistic effects. Several excellent texts are available for more detailed discussions of this whole area.[1-8]

1.2 A Brief Summary of Quantum Mechanics

1.2.1 The Schrödinger Equation

Quantum theory ensures that all knowledge of the properties of a system of n electrons is contained in a function ψ, in the sense that $\psi^* \psi$ is a measure of the probability or electron density for a one-electron wavefunction. The function $\psi(r,R)$ for a molecule of N nuclei and n electrons is determined by solving the time-independent Schrödinger Equation:

$$\hat{H} \ \psi(r,R) = E \ \psi(r,R) \qquad (1.1)$$

where

$\hat{H}$ is the Hamiltonian (total energy operator)

E is the total energy of the molecule

and ψ (r,R) is a molecular wavefunction depending upon both the electronic co-ordinates r and the nuclear co-ordinates R.

For such a molecule containing N nuclei, with charges $Z_k e$ and masses M_k (k = 1,2,...N), and n electrons, with charges -e and masses m_e, the Hamiltonian may be written as:

$$\hat{H} = \sum_{k=1}^{N} \frac{-h^2}{8\pi^2 M_k} \nabla^2_k + \sum_{\mu=1}^{n} \frac{-h^2}{8\pi^2 m_e} \nabla^2_\mu \qquad (1.2)$$

$$- \sum_{\mu=1}^{n} \sum_{k=1}^{N} \frac{Z_k e^2}{\kappa_o r_{\mu k}} + \sum_{k<l}^{N} \frac{Z_k Z_l e^2}{\kappa_o r_{kl}} + \sum_{\mu<\nu}^{n} \frac{e^2}{\kappa_o r_{\mu\nu}}$$

where

h is Planck's constant

∇^2 is the Laplacian operator

κ_o is the permittivity of a vacuum

and, for example, $r_{\mu k}$ is the distance between electron μ and nucleus k, where greek subscripts refer to electrons, and roman subscripts to nuclei.

Before going on to discuss the individual terms in this equation, it is convenient to simplify the form of (1.2) by the introduction of atomic units. The definition of atomic units involves setting m_e (the rest mass of the electron), $\hbar(=h/2\pi)$ and e equal to unity. This leads to the definition of the atomic unit of length, the Bohr atomic unit, a_o:

$$a_o = \frac{(h/2\pi)^2}{m_e e^2} = 0.529177 \text{ Å} = 1 \text{ a.u.}$$

The atomic unit of energy, the Hartree atomic unit, E_o, can be derived from Coulomb's Law of electron-electron repulsion:

$$E_o = \frac{e^2}{a_o} = 27.2107\text{eV} = 1 \text{ a.u.}$$

The energy computed in Hartrees is defined for a single particle, in much the same way as for spectroscopic energy units:

1 hartree/particle = 27.2107eV/particle = 219475 cm^{-1}/ particle.

For an Avogadro number of particles, the equivalent amount of energy in CGS or SI units is:

1 hartree/particle ≡ 627.51 kcal/mole = 2625.51 kJ/mole.

Finally, using κ_o as a unit of permittivity further simplifies the equations. The system of atomic units is especially useful since computed results will be independent of the values of the universal constants $\hbar$, e and m_e.

Writing (1.2) in atomic units, then, gives:

$$\hat{H} = \underbrace{-\frac{1}{2}\sum_{k=1}^{N}\frac{1}{M_k}\nabla_k^2}_{(1)} \underbrace{-\frac{1}{2}\sum_{\mu=1}^{n}\nabla_\mu^2}_{(2)} \underbrace{-\sum_{\mu=1}^{n}\sum_{k=1}^{N}\frac{Z_k}{r_{\mu k}}}_{(3)} + \underbrace{\sum_{k<l}^{N}\frac{Z_k Z_l}{r_{kl}}}_{(4)} + \underbrace{\sum_{\mu<\nu}^{n}\frac{1}{r_{\mu\nu}}}_{(5)} \qquad (1.3)$$

The various terms in this equation are:

(1) the kinetic energy of the nuclei;

(2) the kinetic energy of the electrons;

(3) the electron-nucleus attractive potential energy;

(4) the nuclear-nuclear repulsive potential energy;

and

(5) the electron-electron repulsive potential energy.

Certain assumptions and approximations can be made to simplify the solution of (1.1). Of these, the most important is the Born-Oppenheimer Approximation,[9] in which the total wavefunction is separated into two parts:

$$\Psi(r,R) = \psi_R(r)\ \theta(R) \tag{1.4}$$

Here, $\psi_R(r)$ is the electronic wavefunction for fixed nuclear positions, and depends only parametrically upon the nuclear co-ordinates. $\theta(R)$ is the nuclear wavefunction. This assumption is equivalent to the physical idea that the electrons can adjust their motion instantaneously to any nuclear motion, and can be shown to be valid provided that the electronic wavefunction $\psi_R(r)$ is a slowly varying function of the nuclear co-ordinates.[10]

(1.3) can now be rewritten as:

$$\hat{H} = \hat{T}_R + \hat{h} + \hat{V} \tag{1.5}$$

where $\hat{T}_R$ is the kinetic energy operator of the nuclei:

$$\hat{T}_R = -\frac{1}{2} \sum \frac{1}{M_k} \nabla^2_k \tag{1.6}$$

$\hat{h}$ is a sum of monoelectronic operators, each of the form:

$$\hat{h}_\mu = -\frac{1}{2} \nabla^2_\mu - \sum_{k=1}^{N} \frac{Z_k}{r_{\mu k}} \tag{1.7}$$

and $\hat{V}$ is the potential-energy operator for nuclear-nuclear repulsions and electron-electron repulsions:

$$\hat{V} = \sum_{k<l}^{N} \frac{Z_k Z_l}{r_{kl}} + \sum_{\mu<\nu}^{n} \frac{1}{r_{\mu\nu}} \tag{1.8}$$

The operator $(\hat{h} + \hat{V})$ is referred to as the electronic Hamiltonian, and is assumed to satisfy the Schrödinger equation:

$$(\hat{h} + \hat{V})\ \psi_R(r) = E(R)\ \psi_R(r) \qquad (1.9)$$

When the nuclear co-ordinates R are fixed, E(R) is the energy of the n electrons moving in the field of N fixed nuclei PLUS the mutual repulsion energy of the N fixed nuclei.

E(R) is referred to as the molecular energy in the fixed-nuclei approximation. For a diatomic molecule, a plot of E(R) versus the internuclear distance R leads to the well-known potential-energy curve, the existence of which, of course, depends on the validity of the Born-Oppenheimer approximation. More complicated molecules lead to a more complicated functional dependence of the energy on geometry, leading to potential-energy surfaces and hypersurfaces.

The electronic wavefunction is solved for fixed positions of the nuclei by (1.9) to give the electronic energy E(R). The Schrödinger equation describing the nuclei has the form:

$$(\hat{T}_R + E(R))\ \theta(R) = E_N\ \theta(R) \qquad (1.10)$$

The total energy E is the sum of the electronic energy evaluated at the equilibrium configuration, plus the nuclear energy:

$$E = E(R_o) + E_N \qquad (1.11)$$

A second important assumption has been made in writing (1.2), in that there are no terms representing electron spin-orbit interactions, or electron-nuclear spin coupling, for example. The omission of magnetic terms from $\hat{H}$ is deliberate, since magnetic effects are on a very much smaller energy scale than electrostatic effects. It is therefore assumed that the electronic distribution is determined by the non-relativistic,

spin-free, electrostatic Hamiltonian $\hat{H}$, in (1.2). A brief discussion of the magnitudes of the relativistic corrections to this model will be presented in a subsequent section.

Inspection of the form of the molecular electronic Hamiltonian shows that the actual analytical problem presented by the Schrödinger equation (1.9) is a partial differential equation in 3n dimensions: because of the electron-electron repulsion operator ($\sum_{\mu<\nu}^{n} 1/r_{\mu\nu}$), no further reduction into equations of smaller dimension is possible. Thus, it is clear that "exact" solutions of the Schrödinger equation for molecules are not possible. However, if the inter-electronic repulsion term could be neglected, then a simpler equation would result:

$$\hat{H}^{e} \quad \psi' \quad = \quad \hat{h} \quad \psi' \quad = \quad E \ \psi' \qquad (1.12)$$

where the prime shows this is a simplification. This equation can now be broken down into n separate equations:

$$\hat{h}(i) \quad \phi_j(i) \quad = \quad \varepsilon_j \ \phi_j(i) \qquad (1.13)$$

where $\phi_j(i)$ and ε_j are the eigenfunctions and eigenvalues of $\hat{h}(i)$, respectively. Then:

$$\psi' \quad = \quad \phi_1(1) \quad \phi_2(2) \ \ldots\ldots \phi_k \ (n) \qquad (1.14)$$

and:

$$E \quad = \quad \varepsilon_{j1} \quad + \quad \varepsilon_{j2} \quad + \quad \ldots\ldots \quad \varepsilon_{jn} \qquad (1.15)$$

In these expressions, the functions ϕ are orbitals, in the sense of the definition that "an orbital is a solution of any real or model single-electron Schrödinger equation."

Clearly, the fact that the true molecular Hamiltonian

does contain electron repulsion terms means that Ψ' is not the true molecular wavefunction. However, the idea of a one-electron function (the orbital approximation) is conceptually simple, and it is therefore very useful to consider products of one-electron functions, and to determine how close it is possible to approach the exact functions. Within the orbital approximation it is possible to describe adequately the average repulsion experienced by an electron due to the other electrons in the system; it is not possible, however, to incorporate the instantaneous correlations of electron motions.

Associated with each electron is a spin ($M_s = \pm \frac{1}{2}$). The two possible spin functions for an electon i are written as $\alpha(i)$, where $M_s = \frac{1}{2}$, and $\beta(i)$, where $M_s = -\frac{1}{2}$. The product of a spatial orbital, as is defined above, and a spin function, is known as a spin orbital:

$$\psi_1(i) = \begin{cases} \phi_1(i) \quad \alpha(i) \\ \phi_1(i) \quad \beta(i) \end{cases} \tag{1.16}$$

The spin functions α and β are orthonormal, i.e.:

$$\begin{aligned} \int \alpha(i)^* \, \alpha(i) \, dM_s &= 1 \\ \int \alpha(i)^* \, \beta(i) \, dM_s &= 0 \end{aligned} \tag{1.17}$$

It should be noted that the separation of spin orbitals into spatial and spin functions is only possible because the non-relativistic, spin-free Hamiltonian was used.

It is convenient at this point to recapitulate the orbital model: if it is possible to partition, in some approximate way, the n-electron Hamiltonian into n separate one-electron Hamiltonians, then an approximate solution of the full Schrödinger

equation is given by a linear combination of products of the orbitals defined by the one-electron Schrödinger equation. Thus, many-electron wavefunctions may be constructed as products of one-electron spin-orbitals (where the prime from (1.14) has now been dropped):

$$\Psi(1,2,\ldots,N) = \psi_1(1)\ \psi_2(2)\ldots\psi_N(N) \qquad (1.18)$$

This total wavefunction must be in accord with the Pauli antisymmetry principle, which allows for the fact that electrons are indistinguishable from each-other. Thus, any permutation of the labels of (1.18) should also be a satisfactory wavefunction, yielding therefore N! terms:

$$\Psi(1,2,\ldots,N) = \hat{A}\{\psi_1(1)\ \psi_2(2)\ \ldots\ \psi_N(N)\} \qquad (1.19)$$

where $\hat{A}$ is the antisymmetrizing operator. The right-hand-side of (1.19) is in fact the formula for a determinant:

$$\Psi(1,2,\ldots,N) = \frac{1}{\sqrt{N!}} \begin{vmatrix} \psi_1(1) & \ldots & \psi_N(1) \\ \vdots & & \vdots \\ \psi_1(N) & \ldots & \psi_N(N) \end{vmatrix} \qquad (1.20)$$

where $1/\sqrt{N!}$ is a normalizing constant (for an orthonormal set of orbitals). The spin-orbitals may be replaced by the product of a space and spin function:

$$\Psi(1,2,\ldots 2M) = \frac{1}{\sqrt{(2M)!}} \begin{vmatrix} \phi_1(1)\alpha(1) & \phi_1(1)\beta(1) & \ldots & \phi_M(1)\alpha(1) & \phi_M(1)\beta(1) \\ \phi_1(2)\alpha(2) & \phi_1(2)\beta(2) & \ldots & \phi_M(2)\alpha(2) & \phi_M(2)\beta(2) \\ \vdots & \vdots & & \vdots & \vdots \\ \phi_1(2M)\alpha(2M) & \phi_1(2M)\beta(2M) & \ldots & \phi_M(2M)\alpha(2M) & \phi_M(2M)\beta(2M) \end{vmatrix} \qquad (1.21)$$

Clearly, exchange of any two electrons interchanges two rows of the determinant, thereby reversing the sign of the wavefunction and ensuring the required antisymmetry. Furthermore, if two electrons are placed in the same spin-orbital, the value of the determinant is zero, since two rows would be identical; this accounts for the Pauli exclusion principle. This form of a wavefunction is referred to as a Slater determinant, and is customarily abbreviated by writing only the diagonal elements, the normalization factor being understood:

$$\Psi(1,2,\ldots,2M) =$$

$$\left| \phi_1(1)\alpha(1) \quad \phi_1(2)\beta(2) \ldots\ldots \phi_M(2M-1)\alpha(2M-1) \quad \phi_M(2M)\beta(2M) \right| \qquad (1.22)$$

$$= \left| \phi_1 \quad \bar{\phi}_1 \quad \phi_2 \cdots\cdots \phi_M \quad \bar{\phi}_M \right| \qquad (1.23)$$

where α-spin is understood, and β-spin denoted by the bar, $\bar{\ }$.

1.2.2 The Variation Theorem

Almost all calculations of molecular energy within the orbital approximation have been variational in nature. The variation theorem[11] states that any approximate wavefunction $\tilde{\Psi}$ will produce an energy $\tilde{E}$ which is higher than the exact energy E given by the exact wavefunction Ψ . As the approximate wavefunction approaches the exact ($\tilde{\Psi} \rightarrow \Psi$), then the approximate energy will also approach the exact ($\tilde{E} \rightarrow E$). Before considering the use of the variational method in the solution of the Schrödinger equation, it should be recalled that the wavefunction Ψ must be continuous, single-valued, and have an integrable square (thereby allowing normalization):

$$\int \Psi_i^* \Psi_i \, d\tau = 1 \qquad (1.24)$$

Furthermore, due to the Hermitian symmetry of the operator $\hat{H}$,

it can be shown that different eigenfunctions of the same Hamiltonian corresponding to different eigenvalues are mutually orthogonal. Thus:

$$\int \psi_i^* \psi_j \, d\tau = \delta_{ij} \quad \text{where } \delta = 1 \text{ for } i=j, \; \delta = 0 \text{ for } i \neq j \qquad (1.25)$$

where δ_{ij} is known as the Kronecker delta.

Considering now the solution of the Schrödinger equation:

$$\hat{H} \psi = E \psi$$

premultiplying by ψ^* and integrating gives:

$$\int \psi^* \hat{H} \psi \, d\tau = E \int \psi^* \psi \, d\tau$$

or:

$$E = \frac{\int \psi^* \hat{H} \psi \, d\tau}{\int \psi^* \psi \, d\tau} \qquad (1.26)$$

From the variation theorem, if ψ is replaced by some approximate function $\tilde{\psi}$ in (1.26), then the value of the computed approximate energy expression $\tilde{E}$ is always higher than the lowest true solution of the Schrödinger equation:

$$\tilde{E} = \frac{\int \tilde{\psi}^* \hat{H} \tilde{\psi} \, d\tau}{\int \tilde{\psi}^* \tilde{\psi} \, d\tau} > E \qquad (1.27)$$

In transforming the Schrödinger equation from the differential equation form to the apparently equivalent variational form (1.27), some finer points of the solution have been lost. A variational solution of (1.27) is obtained by minimizing the value of an *integrated* expression; the solution is the best possible solution of the model type *in the mean*. The differential Schrödinger equation has *point by point* solutions; it is therefore not surprising that any variationally-determined

approximate solution of the Schrödinger equation will not, in principle, give a good description of molecular properties which depend on the value of $\tilde{\Psi}$ at *particular points* in space. Molecular properties depending on various integrations of $\tilde{\Psi}$ should, however, be well reproduced. The most important "point properties" are spin hyperfine coupling constants.

This gives a technique for the computation of the approximate, orbital model, wavefunction:

$$\Psi = \sum_k D_k \Phi_k \qquad (1.28)$$

where

$$\Phi_k = |\psi_1(1) \quad \psi_2(2).....\psi_N(N)|$$

and

$$\psi_1(1) = \phi_1(1)\,\alpha(1) \quad \text{or} \quad \phi_1(1)\,\beta(1)$$

Since we shall be concerned only with approximate wavefunctions from now on, the tilde above Ψ has been dropped. (1.28) is substituted into the variational expression (1.27), which is then minimized with respect to the coefficients D_k, and any parameters contained in the definition of the spatial orbitals ϕ. In practice, this "full" optimization (called the Multi-Configuration Self-Consistent Field method) is too complex and time-consuming for many-electron systems of chemical interest, and is only rarely carried out. The most widely used approach (the Molecular Orbital model) is to retain only a single term in (1.28), viz.,

$$D_1 = 1 \qquad D_i = 0, \; i > 1$$

and devote all the computational effort into choosing the best

possible orbitals in this single configuration. The other method, which uses fixed orbitals ϕ and optimizes the coefficients D_i of an essentially multi-configuration wavefunction is the Valence-Bond method, which is widely used qualitatively, but has found little quantitative application.

The computation of optimum linear expansion coefficients, D_i of (1.28), when the functions Φ are not optimized, is particularly easy to formulate in general. Thus, if:

$$\Psi = \sum_k D_k \Phi_k$$

then substitution into (1.27) gives:

$$\tilde{E} = \frac{\sum_{i,j} D_i D_j H_{ij}}{\sum_{i,j} D_i D_j S_{ij}} \qquad (1.29)$$

where

$$H_{ij} = \int \Phi_i \hat{H} \Phi_j \, d\tau \qquad (1.30)$$

and

$$S_{ij} = \int \Phi_i \Phi_j \, d\tau \qquad (1.31)$$

Rearranging (1.29) gives:

$$\sum_i S_{ij} \tilde{E} = \sum_i D_i D_j H_{ij} \quad (j=1,2,\ldots.)$$

Forming $\partial E / \partial D_j$ for each value of j, and equating each partial derivative to zero, ensures a minimum in (1.29).

The resulting equations are best collected in matrix form:

$$(\mathbf{H} - \tilde{E}\mathbf{S})\mathbf{D} = \mathbf{0} \qquad (1.32)$$

or

$$\mathbf{H}\,\mathbf{D} = \tilde{E}\,\mathbf{S}\,\mathbf{D}$$

where $\mathbf{H}$ and $\mathbf{S}$ are matrices whose elements are defined by (1.30) and (1.31) respectively, and $\mathbf{D}$ is a column matrix of the coefficients D_i. In particular, if a set of orthogonal Φ functions is chosen, then $\mathbf{S} = \mathbf{I}$, and

$$\mathbf{H}\,\mathbf{D} = \tilde{E}\,\mathbf{D} \qquad (1.33)$$

an obvious matrix analogue of the Schrödinger equation.

1.3 The Self-Consistent Field Method for Closed Shell Systems

1.3.1 The Hartree-Fock Equations

The basis of the self-consistent field (SCF) treatment of molecules lies in the extension of the treatment of atomic systems by Hartree,[12] which was modified by Fock[13] and Slater[14] to include the anti-symmetry of the wavefunctions. The method consists of minimizing the energy resulting from a single-determinantal wavefunction of the type (1.21), to derive a set of integrodifferential equations known as the Hartree-Fock equations. The Hartree-Fock (HF) wavefunction is the best (in the variational sense) wavefunction which can be constructed by assigning each electron to a separate orbital, or function, depending only on the co-ordinates of that electron. The Hartree-Fock equations can only be solved in closed form for one-electron systems such as the hydrogen atom; however, for atoms, the equations may be solved to a high degree of accuracy by numerical integration.[15] For molecules, the orbitals are

expanded in terms of a set of analytical basis functions. Since it is never possible to use a mathematically complete set of functions in molecular calculations of a practical nature, only approximate solutions of the Hartree-Fock equations are obtained. The best (lowest energy) single determinantal wavefunction constructed within a finite basis set is the SCF wavefunction.

The aim, then, of the molecular orbital (MO) method is to find the best possible one-configuration (single determinantal) approximate solution of:

$$\hat{H}\,\psi = E\,\psi$$

where $\hat{H}$ is the full, non-relativistic molecular Hamiltonian, and Ψ is a determinant of spin-orbitals, whose spatial components are the molecular orbitals ϕ_i. The simplest and most commonly occurring case is the closed-shell, ground state function:

$$\Psi_o \equiv \Psi_o\,(1,2,\ldots,2M) = |\phi_1\,\phi_1\,\phi_2\cdots\phi_M| \qquad (1.34)$$

The computational method is to assume a physically plausible form for the functions ϕ_i, which contains adjustable parameters which may be optimized within the variational principle. A convenient form for the approximate molecular orbitals ϕ_i is a linear combination of atomic orbitals, η_i.

The electronic Hamiltonian for a 2M electron system may be written as:

$$\hat{H} \equiv \hat{H}\,(1,2,\ldots,2M) = \sum_{\mu=1}^{2M} \hat{h}_\mu + \sum_{\mu>\nu}^{M(2M-1)} \hat{g}_{\mu\nu} \qquad (1.35)$$

where $\hat{h}_\mu$ is often referred to as the one-electron, or core

Hamiltonian, consisting of the kinetic-energy operator and electron-nuclear attraction terms for electron μ:

$$\hat{h}_\mu = -\tfrac{1}{2}\nabla^2_\mu - \sum_k \frac{Z_k}{r_{\mu k}} \tag{1.36}$$

The second term in (1.35), $\hat{g}_{\mu\nu}$ is the electron-electron interaction:

$$\hat{g}_{\mu\nu} = \frac{1}{r_{\mu\nu}} \tag{1.37}$$

The energy value after substitution of Ψ_o and $\hat{H}$ into the expectation value equation is:

$$E = \int \Psi_o^* \hat{H} \Psi_o \, d\tau \equiv \langle \Psi_o | \hat{H} | \Psi_o \rangle \tag{1.38}$$

where we have introduced the bra-ket notation of Dirac.

Substituting (1.34) and (1.35) into (1.38), and integrating out the spin-variables, gives:

$$E = 2 \sum_p^M \langle \phi_p(1) | \hat{h}_1 | \phi_p(1) \rangle + \tag{1.39}$$

$$\sum_p^M \sum_q^M \left[2 \langle \phi_p(1) \phi_q(2) | \hat{g}_{12} | \phi_p(1) \phi_q(2) \rangle - \langle \phi_p(1) \phi_p(2) | \hat{g}_{12} | \phi_q(1) \phi_q(2) \rangle \right]$$

The two-electron integrals in the double-summation of (1.39) are the Coulomb and Exchange integrals, respectively. Note that in the Coulomb integrals, electron (1) is associated with orbital ϕ_p only, whereas in the Exchange integrals, electron (1) is associated with both orbital ϕ_p and ϕ_q. This distinction between Coulomb and Exchange terms becomes clearer in the "charge cloud" or electron density formalism, where orbitals associated with electron (1) are collected in front of the operator. Thus:

$$E = 2 \sum_{p}^{M} I(\phi_p|\phi_p) + \sum_{p}^{M}\sum_{q}^{M}\left[2(\phi_p \phi_p|\phi_q \phi_q) - (\phi_p \phi_q|\phi_p \phi_q)\right] \tag{1.40}$$

is exactly equivalent to (1.39). This expression may be further abbreviated to:

$$E = 2 \sum_{p}^{M} h^{\phi}_{pp} + \sum_{p}^{M}\sum_{q}^{M} (2J^{\phi}_{pq} - K^{\phi}_{pq}) \tag{1.41}$$

where J_{pq} and K_{pq} symbolize the Coulomb and Exchange integrals, and h_{pp} is the one-electron term, or core potential. The superscript ϕ indicates that these matrix representatives are over the MO basis. Note that $J_{pp} = K_{pp}$. The relative magnitudes of these quantities are:

$$0 \leq K_{pq} \leq J_{pq} \leq \tfrac{1}{2}(J_{pp} + J_{qq}) \tag{1.42}$$

The J and K integrals may conveniently be expressed as pseudo one-electron integrals, by defining pseudo one-electron operators $\hat{J}_p$ and $\hat{K}_p$ as:

$$\hat{J}_p \ \phi_p = \langle \phi_q | \hat{g}_{12} | \phi_q \rangle \ \phi_p$$

and $$\hat{K}_q \ \phi_p = \langle \phi_q | \hat{g}_{12} | \phi_p \rangle \ \phi_q$$

such that
$$\begin{aligned} J^{\phi}_{pq} &= \langle \phi_p(1) \ \phi_q(2) | \hat{g}_{12} | \phi_q(2) \phi_p(1) \rangle \\ &= \langle \phi_p \ | \ \hat{J}_q \ | \ \phi_p \rangle \\ &= \langle \phi_q \ | \ \hat{J}_p \ | \ \phi_q \rangle \end{aligned} \tag{1.43}$$

and

$$K_{pq}^{\phi} = \langle\phi_p(1)\phi_p(2)|\hat{g}_{12}|\phi_q(1)\phi_q(2)\rangle$$
$$= \langle\phi_p(1)\phi_q(1)|\hat{g}_{12}|\phi_q(2)\phi_p(2)\rangle$$
$$= \langle\phi_p \mid \hat{K}_q \mid \phi_p\rangle$$
$$= \langle\phi_q \mid \hat{K}_p \mid \phi_q\rangle \qquad (1.44)$$

The energy expression may then be written as:

$$E = 2\sum_{p}^{M}\langle\phi_p|\hat{h} + \sum_{q}^{M}{}'(2\hat{J}_q - \hat{K}_q)|\phi_p\rangle$$
$$\equiv 2\sum_{p}^{M}\int\phi_p^*\{\hat{h} + \sum_{q}^{M}{}'(2\hat{J}_q - \hat{K}_q)\}\phi_p\, d\tau \qquad (1.45)$$

where the prime ' indicates summation for p>q only.

According to the Variation Theorem, the energy may be optimized by variation of ϕ. Thus, to minimize E with respect to ϕ_p requires that:

$$\delta E = 0$$

subject to the constraint that the orbitals ϕ_p remain orthonormal:

$$S_{pq} \equiv \langle\phi_p|\phi_q\rangle \equiv \int\phi_p^*\,\phi_q\, d\tau = \delta_{pq} \qquad (1.46)$$

This leads to a restriction in the variation of ϕ_p, viz:

$$\delta S_{pq} = \int(\delta\phi_p^*)\phi_q d\tau + \int(\delta\phi_q)\phi_p^*\, d\tau = 0 \qquad (1.47)$$

Consideration of an arbitrary variation in E caused by an infinitesimal variation in the MO, $\delta\phi_p$, gives:

$$\delta E = 2\sum_{p}^{M}\int(\delta\phi_p^*)\left\{\hat{h} + \sum_{q}^{M}{}'(2\hat{J}_q - \hat{K}_q)\right\}\phi_p d\tau$$
$$+ 2\sum_{p}^{M}\int(\delta\phi_p)\left\{\hat{h}^* + \sum_{q}^{M}{}'(2\hat{J}_q^* - \hat{K}_q^*)\right\}\phi_p^*\, d\tau = 0 \qquad (1.48)$$

Defining the Fock operator, $\hat{F}$, as:

$$\hat{F} = \left\{ \hat{h} + \sum_{q}^{M} {}' (2\hat{J}_q - \hat{K}_q) \right\} \qquad (1.49)$$

gives:

$$\delta E = 2 \sum_{p}^{M} \int \delta \phi_p^* \hat{F} \phi_p d\tau + 2 \sum_{p}^{M} \int \delta \phi_p \hat{F}^* \phi_p^* d\tau = 0 \qquad (1.50)$$

Introduction of undetermined Lagrangian multipliers, and the appropriate combination of (1.47) and (1.50) leads to the Hartree-Fock expression originally formulated by Roothaan:[16]

$$\hat{F} \phi_p = \phi_p \varepsilon_p \qquad (1.51)$$

where the ε_p were originally introduced as a specific case of undetermined Lagrangian multipliers, which may be interpreted as "orbital energies".

1.3.2 Matrix Formulation of MO Theory

We require now to replace the MO ϕ_p by a linear combination of atomic orbitals, η_i; it is convenient at this stage to introduce a brief discussion of the use of matrix algebra in MO theory. An orbital ϕ may be represented as a linear combination of basis functions:

$$\phi = C_1\eta_1 + C_2\eta_2 + \ldots . C_n\eta_n = \sum_{1}^{n} C_i\eta_i \qquad (1.52)$$

This may be written in vector form:

$$\phi = (C_1 C_2 \ldots . C_n) \begin{pmatrix} \eta_1 \\ \eta_2 \\ \vdots \\ \eta_n \end{pmatrix} = (\eta_1 \eta_2 \ldots . \eta_n) \begin{pmatrix} C_1 \\ C_2 \\ \vdots \\ C_n \end{pmatrix} \qquad (1.53)$$

or $\underline{\phi} = \underline{C}\underline{\eta} = \underline{\eta}\underline{C}$

where the single-bar subscript refers to a row or column vector. Now, in quantum chemistry, the molecular orbitals ϕ are obtained by a transformation from some set of basis functions such as a linear combination of atomic orbitals, η. The transforming matrix $\mathbf{C}$ is then referred to as the coefficient matrix. The number of occupied MO must be less than or equal to the number of basis functions:

$$\underline{\phi} = \underline{\eta}\,\mathbf{C}$$

or in detail:

$$\underbrace{(\phi_1 \phi_2 \cdots \phi_m}_{m \text{ occupied MO}} \underbrace{\cdots \phi_n)}_{(n-m) \text{ virtual MO}} = \underbrace{(\eta_1 \eta_2 \cdots \eta_n)}_{n \text{ AO}} \begin{pmatrix} C_{11} & C_{12} \cdots C_{1m} \cdots C_{1n} \\ C_{21} & C_{22} \cdots C_{2m} \cdots C_{2n} \\ \vdots & \vdots \quad \vdots \quad \vdots \\ \vdots & \vdots \quad \vdots \quad \vdots \\ \vdots & \vdots \quad \vdots \quad \vdots \\ \vdots & \vdots \quad \vdots \quad \vdots \\ C_{n1} & C_{n2} \cdots C_{nm} \cdots C_{nn} \end{pmatrix} \quad (1.54)$$

To introduce in more detail the meaning of the expression "matrix representative", consider $\Psi = \hat{A}\phi$, where both Ψ and ϕ belong to the orthonormal vector space η_i. The inner product between Ψ and ϕ, in terms of $\{\eta\}$, may be generated by expressing ϕ as a linear combination of the set $\{\eta\}$:

$$\phi = \sum_{i}^{n} \eta_i C_i = \underline{\eta}\,\underline{C}$$

Now the inner product, or overlap integral, is given as:

$$S_{ij} = \langle \eta_i | \eta_j \rangle$$

Thus.

$$\langle \phi \mid \psi \rangle = \langle \phi | \hat{A} \phi \rangle \equiv \langle \phi | \hat{A} | \phi \rangle$$

$$= \langle \sum_i^n C_i \eta_i \mid \hat{A} \mid \sum_j^n \eta_j C_n \rangle$$

$$= \sum_i^n \sum_j^n C_i^* \langle \eta_i \mid \hat{A} \mid \eta_j \rangle C_j$$

$$= \sum_i^n \sum_j^n C_i^* \quad a_{ij} \quad C_j \qquad (1.55)$$

$\langle \phi | \hat{A} | \phi \rangle$ is frequently called the expectation value of the operator $\hat{A}$. Writing (1.55) in matrix form:

$$\langle \phi | \psi \rangle = (C_1^* C_2^* \ldots C_n^*) \begin{pmatrix} a_{11} & a_{12} \ldots a_{1n} \\ a_{21} & a_{22} \ldots a_{2n} \\ \vdots & \vdots \quad \vdots \\ a_{n1} & a_{n2} \ldots a_{nn} \end{pmatrix} \begin{pmatrix} C_1 \\ C_2 \\ \vdots \\ C_n \end{pmatrix} \qquad (1.56)$$

$$\langle \phi \mid \psi \rangle = \underline{C}^{\dagger} \mathbf{A} \underline{C} \qquad (1.57)$$

Here, matrix $\mathbf{A}$ is the matrix representative of the operator $\hat{A}$ in the basis $\{\eta_i\}$, best written with a superscript showing the basis: $\mathbf{A}^{\eta}$, with matrix elements $\langle \eta_i | \hat{A} | \eta_j \rangle$.

Having a matrix representative of an operator over the AO basis, say, it is often necessary to obtain a similar matrix representative of another basis, such as the MO basis. Let

$$\underline{\psi} = \underline{\phi}\, \mathbf{U} \qquad (1.58)$$

where both $\{\phi_i\}$ and $\{\psi_i\}$ are the basis vectors of two n-dimensional orthonormal vector spaces. Thus, (1.58) written

in full is:

$$(\psi_1\psi_2\ldots\psi_n) = (\phi_1\phi_2\ldots\phi_n)\begin{pmatrix} U_{11} & U_{12} & \ldots & U_{1n} \\ U_{21} & U_{22} & \ldots & U_{2n} \\ \vdots & \vdots & & \vdots \\ U_{n1} & U_{n2} & \ldots & U_{nn} \end{pmatrix}$$

Correspondingly,

$$\underline{\psi}^\dagger = \mathbf{U}^\dagger \underline{\phi}^\dagger \tag{1.59}$$

We wish to express $\mathbf{A}^\psi$ in terms of $\mathbf{A}^\phi$, because $\mathbf{A}^\phi$ is given, and the unitary matrix $\mathbf{U}$ connecting $\underline{\psi}$ and $\underline{\phi}$ is available. Now:

$$\mathbf{A}^\psi = \begin{pmatrix} \langle\psi_1|\hat{A}|\psi_1\rangle & \langle\psi_1|\hat{A}|\psi_2\rangle & \ldots & \langle\psi_1|\hat{A}|\psi_n\rangle \\ \langle\psi_2|\hat{A}|\psi_1\rangle & \langle\psi_2|\hat{A}|\psi_2\rangle & \ldots & \langle\psi_2|\hat{A}|\psi_n\rangle \\ \vdots & \vdots & & \vdots \\ \langle\psi_n|\hat{A}|\psi_1\rangle & \langle\psi_n|\hat{A}|\psi_2\rangle & \ldots & \langle\psi_n|\hat{A}|\psi_n\rangle \end{pmatrix} \tag{1.60}$$

From (1.55), a given matrix element may be expressed as:

$$\langle\psi_k|\hat{A}|\psi_l\rangle = \sum_i^n \sum_j^n U_{ki}^* \; a_{ij} \; U_{jl} \tag{1.61}$$

$$= (U_{k1}^* \; U_{k2}^* \ldots U_{kn}^*) \begin{pmatrix} a_{11} & a_{21}\ldots a_{1n} \\ a_{21} & a_{22}\ldots a_{2n} \\ \vdots & \vdots \\ a_{n1} & a_{n2}\ldots a_{nn} \end{pmatrix} \begin{pmatrix} U_{11} \\ U_{21} \\ \vdots \\ U_{n1} \end{pmatrix}$$

or

$$a^{\psi}_{kl} = \underline{U}_k^{\dagger} \mathbf{A}^{\phi} \underline{U}_l \tag{1.62}$$

Thus, the whole matrix may be written as:

$$\begin{pmatrix} a_{11}^{\psi} & a_{12}^{\psi} \cdots a_{1n}^{\psi} \\ a_{21}^{\psi} & a_{22}^{\psi} \cdots a_{2n}^{\psi} \\ \vdots & \vdots \quad \vdots \\ a_{n1}^{\psi} & a_{n2}^{\psi} \cdots a_{nn}^{\psi} \end{pmatrix} = \begin{pmatrix} U_{11}^{*} & U_{21}^{*} \cdots U_{n1}^{*} \\ U_{12}^{*} & U_{22}^{*} \quad U_{n2}^{*} \\ \vdots & \vdots \quad \vdots \\ U_{1n}^{*} & U_{2n}^{*} \cdots U_{nn}^{*} \end{pmatrix} \begin{pmatrix} a_{11}^{\phi} & a_{12}^{\phi} \cdots a_{1n}^{\phi} \\ a_{21}^{\phi} & a_{22}^{\phi} \cdots a_{2n}^{\phi} \\ \vdots & \vdots \quad \vdots \\ a_{n1}^{\phi} & a_{n2}^{\phi} \cdots a_{nn}^{\phi} \end{pmatrix} \begin{pmatrix} U_{11} & U_{12} \cdots U_{1n} \\ U_{21} & U_{22} \cdots U_{2n} \\ \vdots & \vdots \quad \vdots \\ U_{n1} & U_{n2} \cdots U_{nn} \end{pmatrix}$$

or:

$$\mathbf{A}^{\psi} = \mathbf{U}^{\dagger} \mathbf{A}^{\phi} \mathbf{U} \tag{1.63}$$

This equivalence is usually referred to as a similarity transformation.

The eigen-problem equation for an n-dimensional space may be written as:

$$\hat{Q} \phi_i = \varepsilon_i \phi_i$$

or

$$\hat{Q} \underline{\phi} = \underline{\phi} \boldsymbol{\epsilon} \tag{1.64}$$

where $\boldsymbol{\epsilon}$ is a diagonal matrix. Taking the inner product with ϕ_i gives:

$$\langle \phi_i | \hat{Q} | \phi_i \rangle = \langle \phi_i | \phi_i \rangle \varepsilon_i$$

or

$$\mathbf{Q}^{\phi} = \mathbf{S}^{\phi} \boldsymbol{\epsilon}$$

Thus, iff:

$$\mathbf{S}^{\phi} = \mathbf{I}$$

then:

$$\mathbf{Q}^{\phi} = \boldsymbol{\epsilon} \tag{1.65}$$

This implies that the matrix representative of an operator over the eigenvector space is a diagonal matrix.

If $\{\phi_i\}$ represents the MO, which are unknown, then $\mathbf{Q}^{\phi}$ must be obtained by means of a similarity transformation from the known $\mathbf{Q}^{\eta}$, where $\{\eta_i\}$ is the chosen set of AO:

$$\underline{\phi} = \underline{\eta}\,\mathbf{C}$$

Substituting into the eigenproblem equation (1.64) gives:

$$\mathbf{Q}^{\phi} = \mathbf{C}^{\dagger}\,\mathbf{Q}^{\eta}\,\mathbf{C} = \mathbf{C}^{\dagger}\,\mathbf{S}^{\eta}\,\mathbf{C}\,\boldsymbol{\epsilon} \qquad (1.66)$$

Expanding $\underline{\phi}$ in terms of an orthonormal AO basis set $\{\chi\}$, noting that:

$$\underline{\phi} = \underline{\chi}\,\mathbf{U} \text{ and } \underline{\phi}^{\dagger} = \mathbf{U}^{\dagger}\,\underline{\chi}^{\dagger} \qquad (1.67)$$

then:

$$\begin{aligned}\mathbf{Q}^{\phi} &= \mathbf{U}^{\dagger}\,\mathbf{Q}^{\chi}\,\mathbf{U} = \mathbf{U}^{\dagger}\,\mathbf{S}^{\chi}\,\mathbf{U}\,\boldsymbol{\epsilon} && \{\chi\} \text{ is orthonormal, therefore } \mathbf{S}^{\chi} = \mathbf{I}\\ &= \mathbf{U}^{\dagger}\,\mathbf{U}\,\boldsymbol{\epsilon} && \mathbf{U} \text{ is unitary, thus } \mathbf{U}^{\dagger} = \mathbf{U}^{-1}\\ &= \boldsymbol{\epsilon} && (1.68)\end{aligned}$$

In practice, one works with real orbitals, and thus $\mathbf{U}$ is orthogonal, whilst $\mathbf{Q}^{\chi}$ is real, symmetric. Consequently, diagonalization of a real symmetric matrix is of utmost importance, since the matrix ($\mathbf{U}$) that diagonalizes $\mathbf{Q}^{\chi}$ via a similarity transformation is the matrix that transforms the orthogonal AO basis set $\{\chi\}$ to the MO basis set $\{\phi\}$.

A widely used method for the diagonalization of a real, symmetric matrix is that of Jacobi, based on successive plane rotations. If the original real, symmetric matrix is $\mathbf{Q}_o$, the

matrix obtained after rotation in the first plane $\mathbf{U}_1$, etc., and the final diagonal matrix $\boldsymbol{\epsilon}$, then the method may be represented as:

$$\mathbf{Q}_o \rightarrow \mathbf{Q}_1 \rightarrow \cdots \mathbf{Q}_{k-1} \rightarrow \mathbf{Q}_k \rightarrow \cdots \rightarrow \boldsymbol{\epsilon}$$

The matrix in the k^{th} step is related to the previous matrix by:

$$\mathbf{Q}_k = \mathbf{U}_k^{\dagger} \mathbf{Q}_{k-1} \mathbf{U}_k$$

where $\mathbf{U}_k$ is an orthogonal matrix associated with the rotation in the k^{th} plane - in general, the elements of the matrix involving rotation in the r,s plane are:

$$\left.\begin{array}{l} U_{rr} = U_{ss} = \cos\alpha \\ U_{rs} = -U_{sr} = -\sin\alpha \end{array}\right| \left.\begin{array}{l} U_{ii} = U_{jj} = 1 \\ U_{ij} = U_{ji} = 0 \end{array}\right\} \; i,j \neq r,s$$

Here, α is the angle of rotation. Values of $\mathbf{U}_k$ and $\mathbf{U}_k^{\dagger}$ are substituted into the above equation, and off-diagonal elements associated with the r,s plane eliminated. This is done successively, and the final orthogonal matrix $\mathbf{U}$ incorporating all of the rotational matrices $\mathbf{U}_k$ is in fact the product matrix of all $\mathbf{U}_k$. In practice, each $\mathbf{U}_k$ matrix is multiplied by the previous products of $\mathbf{U}_k$, so that one obtains successively $\mathbf{U}_1$, $(\mathbf{U}_1\ \mathbf{U}_2)$ and so on.

Returning to the discussion of the Fock eigenvalue equation (1.51), it should now be apparent that the elements of the Fock matrix over the MO basis, $\mathbf{F}^{\phi}$, may be written as:

$$F^{\phi}_{st} \equiv \langle \phi_s | \hat{F} | \phi_t \rangle \qquad (1.69)$$

Converting the Hartree-Fock operator equation (1.51) to matrix form gives:

$$\mathbf{F}^{\phi} = \boldsymbol{\epsilon} \qquad (1.70)$$

since:

$$\mathbf{S}^{\phi} = \mathbf{I} \quad \text{or} \quad S^{\phi}_{st} = \langle \phi_s | \phi_t \rangle = \delta_{st} \tag{1.71}$$

thanks to the orthonormality of the MO basis (1.46). Because ϕ is unknown, substitution of:

$$\underline{\phi} = \underline{\eta}\,\mathbf{C} \quad \text{and} \quad \underline{\phi}^{\dagger} = \mathbf{C}^{\dagger}\,\underline{\eta} \tag{1.72}$$

gives the Hartree-Fock matrix equation over the AO basis:

$$\mathbf{C}^{\dagger}\,\mathbf{F}^{\eta}\,\mathbf{C} = \mathbf{C}^{\dagger}\,\mathbf{S}^{\eta}\,\mathbf{C}\,\boldsymbol{\epsilon} \tag{1.73}$$

where

$$\mathbf{F}^{\eta} = \mathbf{H}^{\eta} + 2\,\mathbf{J}^{\eta} - \mathbf{K}^{\eta} \tag{1.74}$$

and

$$S^{\eta}_{ij} = \langle \eta_i | \eta_j \rangle \tag{1.75}$$

These molecular integrals (in pseudo one-electron form) are:

$$h^{\eta}_{ij}(1) = \langle \eta_i(1) | \hat{h} | \eta_j(1) \rangle \tag{1.76}$$

$$J^{\eta}_{ij}(1) = \sum_{k}^{N} \sum_{l}^{N} (\eta_i \eta_j | \eta_k \eta_l) \rho_{kl} \tag{1.77}$$

$$K^{\eta}_{ij}(1) = \sum_{k}^{N} \sum_{l}^{N} (\eta_i \eta_k | \eta_j \eta_l)\, \rho_{kl} \tag{1.78}$$

where ρ_{kl} is the kl^{th} element of the density matrix.

$$\boldsymbol{\rho} = \mathbf{C}_M\,\mathbf{C}_M^{\dagger} \tag{1.79}$$

Thus:

$$F^{\eta}_{ij} = h^{\eta}_{ij} + \sum_{k}^{N} \sum_{l}^{N} \left[2(\eta_i \eta_j | \eta_k \eta_l) - (\eta_i \eta_k | \eta_j \eta_l) \right] \rho_{kl}$$

or

$$F^{\eta}_{ij} = h^{\eta}_{ij} + 2J^{\eta}_{ij} - K^{\eta}_{ij} \tag{1.80}$$

Writing E in terms of the AO integrals from (1.41) gives:

$$E = 2 \sum_{i}^{N} \sum_{j}^{N} \rho_{ij} h^{\eta}{}_{ji} + 2 \sum_{i}^{N} \sum_{j}^{N} \rho_{ij} J^{\eta}{}_{ji} - \sum_{i}^{N} \sum_{j}^{N} \rho_{ij} K^{\eta}{}_{ji} \tag{1.81}$$

Rearranging this to include the Fock matrix explicitly:

$$\begin{aligned} E &= \sum_{i}^{N} \sum_{j}^{N} \rho_{ij} h^{\eta}{}_{ji} + \sum_{i}^{N} \sum_{j}^{N} \rho_{ij} (h^{\eta}{}_{ji} + 2J^{\eta}{}_{ji} - K^{\eta}{}_{ji}) \\ &= \sum_{i}^{N} \sum_{j}^{N} \rho_{ij} h^{\eta}{}_{ji} + \sum_{i}^{N} \sum_{j}^{N} \rho_{ij} F^{\eta}{}_{ji} \\ &= \sum_{i}^{N} \sum_{j}^{N} \rho_{ij} (h^{\eta}{}_{ji} + F^{\eta}{}_{ji}) \end{aligned} \tag{1.82}$$

The innermost summation over j will eliminate the running index j, leaving only ii elements. Thus, the outermost summation over i is simply a summation of the diagonal elements of a diagonal matrix - the trace of the matrix:

$$E = \mathrm{tr} \left\{ \boldsymbol{\rho} (\mathbf{H}^{\eta} + \mathbf{F}^{\eta}) \right\} \tag{1.83}$$

It is also of interest to relate the orbital energies to the total energy. (1.70) shows that the matrix representative of the Fock operator over the MO basis is simply the MO energy matrix. When matrix elements $F^{\phi}{}_{pp}$ are transformed to the AO basis, the following equivalence holds:

$$\varepsilon_p \equiv F^{\phi}{}_{pp} \equiv \langle \phi_p | \hat{F} | \phi_p \rangle = \sum_{i}^{N} \sum_{j}^{N} C_{ip} \langle \eta_i | \hat{F} | \eta_j \rangle C_{jp} \tag{1.84}$$

Summing all occupied MO energies results in:

$$\sum_{p}^{M} \varepsilon_p = \sum_{i}^{N} \sum_{j}^{N} \rho_{ij} \langle \eta_j | \hat{F} | \eta_i \rangle = \sum_{i}^{N} \sum_{j}^{N} \rho_{ij} F^{\eta}{}_{ji} \tag{1.85}$$

Recalling from (1.80) that:

$$h^{\eta}_{ji} = F^{\eta}_{ji} - (2J^{\eta}_{ji} - K^{\eta}_{ji})$$

and substituting into (1.82) gives:

$$E = \sum_{i}^{N} \sum_{j}^{N} \rho_{ij} \left\{ 2F^{\eta}_{ji} - (2J^{\eta}_{ji} - K^{\eta}_{ji}) \right\}$$

$$= 2 \sum_{i}^{N} \sum_{j}^{N} \rho_{ij} F^{\eta}_{ji} - \sum_{i}^{N} \sum_{j}^{N} \rho_{ij} (2J^{\eta}_{ji} - K^{\eta}_{ji}) \qquad (1.86)$$

From (1.85) then gives:

$$E = 2 \sum_{i}^{M} \epsilon_i - \sum_{i}^{N} \sum_{j}^{N} \rho_{ij} (2J^{\eta}_{ji} - K^{\eta}_{ji}) \qquad (1.87)$$

The total electronic energy E is thus seen to be twice the sum of the doubly occupied MO minus the electron-electron repulsion.

1.3.3 The SCF Procedure

Developing the discussion of (1.80) and (1.81), the basic problem is that even when all the integrals are known, $\mathbf{F}^{\eta}$ (required for the Hartree-Fock equation (1.73)) and E cannot be calculated, since both depend on $\boldsymbol{\rho}$, which depends on $\mathbf{C}$, which is what we want to obtain from the Hartree-Fock equations. This requires that the eigen-problem equation be solved in an iterative manner by the process referred to as the Self-Consistent Field (SCF) method.

Consideration of the orthogonality problem is required. The basis set $\{\eta\}$ is not orthogonal, so that the coefficient matrix $\mathbf{C}$ which diagonalizes $\mathbf{F}$ cannot be found by an orthogonal transformation. Consequently, it is necessary to

transform the non-orthogonal set $\{\eta\}$ into an orthogonal set $\{\chi\}$, and correspondingly, $\mathbf{F}^{\eta}$ into $\mathbf{F}^{\chi}$. $\mathbf{F}^{\chi}$ may then be diagonalized by an orthogonal transformation (such as Jacobi's diagonalization), permitting the calculation of the coefficient matrix. Since orthogonalization may be regarded as a special type of transformation, the $\mathbf{C}$ matrix is separated into two matrices $\mathbf{V}$ and $\mathbf{U}$:

$$\underline{\phi} = \underline{\eta}\,\mathbf{C} = \underline{\eta}\,\mathbf{V}\,\mathbf{U} = \underline{\chi}\,\mathbf{U} \qquad (1.88)$$

This process is schematically illustrated in Figure 1.1.

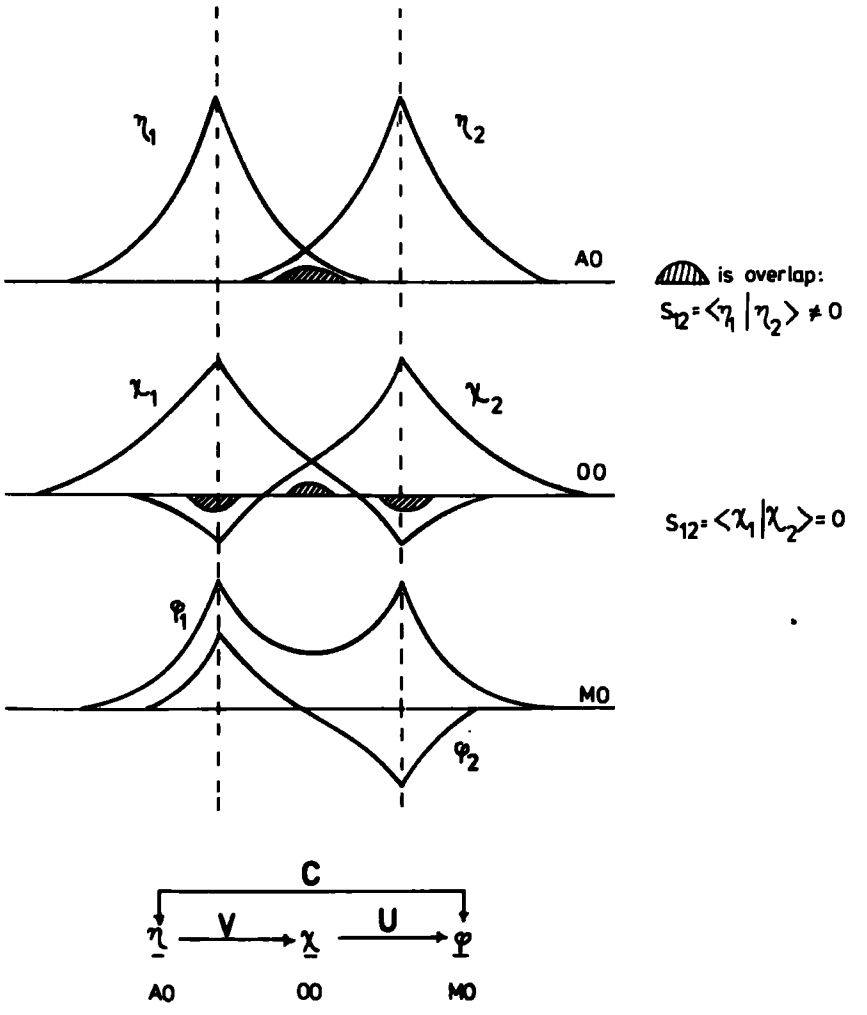

Fig.(1.1) Schematic illustration for the transformation of AO to MO.

(1.88) gives:

$$\underline{\phi}^{\dagger} = \mathbf{U}^{\dagger}\,\mathbf{V}^{\dagger}\,\underline{\eta}^{\dagger} = \mathbf{U}^{\dagger}\,\underline{\chi}^{\dagger} \qquad (1.89)$$

Substituting into the Hartree-Fock equation (1.73), since

$\mathbf{C} = \mathbf{V}\mathbf{U}$, gives:

$$\begin{aligned} \mathbf{U}^{\dagger}\;\underbrace{\mathbf{V}^{\dagger}\;\mathbf{F}^{\eta}\;\mathbf{V}}\;\mathbf{U} &= \mathbf{U}^{\dagger}\;\underbrace{\mathbf{V}^{\dagger}\;\mathbf{S}^{\eta}\;\mathbf{V}}\;\mathbf{U}\;\boldsymbol{\epsilon} \\ \mathbf{U}^{\dagger}\qquad\mathbf{F}^{\chi}\qquad\mathbf{U} &= \mathbf{U}^{\dagger}\qquad\mathbf{I}\qquad\mathbf{U}\;\boldsymbol{\epsilon} \end{aligned} \qquad (1.90)$$

since $\mathbf{S}^{\eta} = \mathbf{I}$ for orthonormality. Then:

$$\mathbf{U}^{\dagger}\;\mathbf{F}^{\chi}\;\mathbf{U} = \boldsymbol{\epsilon} \qquad (1.91)$$

$\boldsymbol{\epsilon}$ is a diagonal matrix, so that $\mathbf{F}^{\chi}$ may be diagonalized by $\mathbf{U}$. Löwdin[17] showed that the orthogonalizing matrix $\mathbf{V}$ may be chosen to be $\mathbf{S}^{-\frac{1}{2}}$. This is known as the symmetric, or Löwdin, orthogonalization. Thus:

$$\mathbf{F}^{\chi} = \mathbf{S}^{-\frac{1}{2}}\;\mathbf{F}^{\eta}\;\mathbf{S}^{-\frac{1}{2}} \qquad (1.92)$$

The iterative SCF procedure may conveniently be presented in the form of a flow-chart, shown in Figure (1.2).

In the course of a well-behaved SCF procedure, the total energy E is lowered in each iteration cycle (i.e., E_n becomes more negative as n increases). Convergence may be measured by the difference between the energy-values associated with two successive iterations, as in Figure (1.2). Alternatively, it is possible to judge convergence in terms of the density matrix:

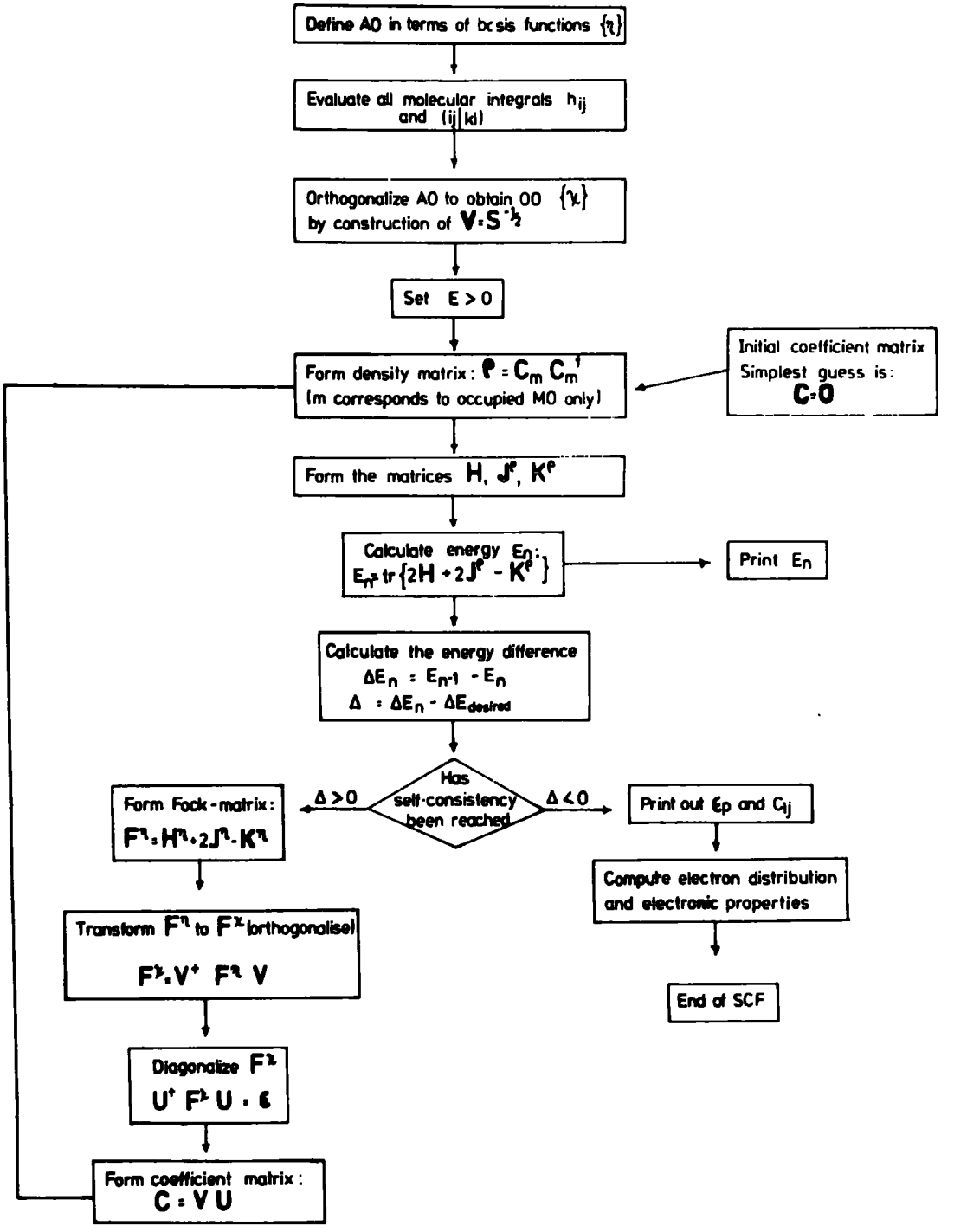

Fig. (1.2) Flow-chart for the iterative SCF method.

$$\Delta \rho_n = \rho_{n-1} - \rho_n \qquad (1.93)$$

Convergence is illustrated schematically in Figure (1.3).

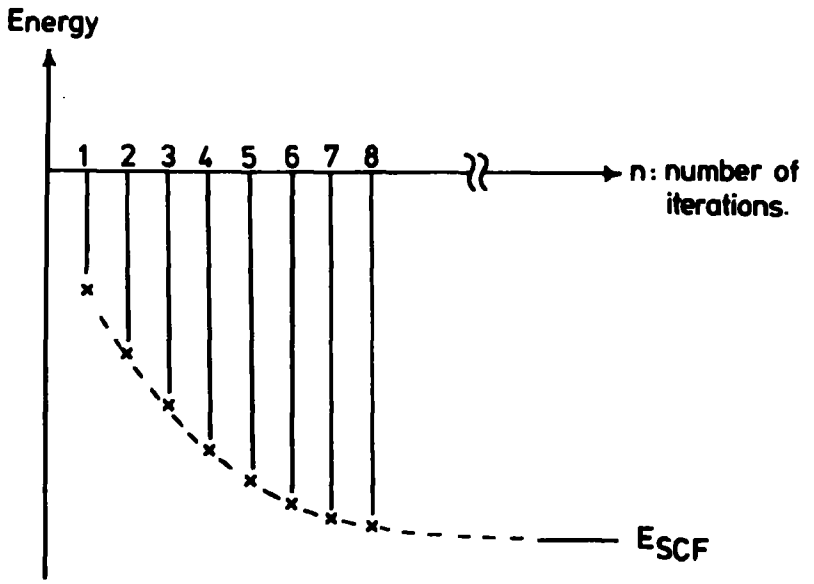

Fig. (1.3) Schematic illustration for the convergence of an SCF calculation.

Another point of interest is the consequence of choosing $\mathbf{C} = \mathbf{0}$. In this event, $\boldsymbol{\rho} = \mathbf{0}$, and terms that incorporate the density matrix (e.g. $\mathbf{J}^{(\rho)}$ and $\mathbf{K}^{(\rho)}$) will vanish. However, the Fock-matrix will not, and the approximation $\mathbf{F}^{n} = \mathbf{H}^{n}$ will be operative.

1.4 Open-Shell SCF Theory

1.4.1 Unpaired Electrons

The methods discussed in Section 1.3 are limited to "closed shell" systems: the electronic structure is

described by a single determinant of doubly occupied spatial orbitals. However, transition metal compounds, many cationic and free-radical species, and transient species such as core-ionized systems have unpaired electrons, or "open-shell" electronic structures. A brief discussion of the LCAO MO open-shell theory is therefore given.

The spin multiplicity of a system is essential to the classification of open-shell systems:

$$\text{spin multiplicity} = 2|s_Z| + 1 \qquad (1.94)$$

where s_Z is the expectation value of the total spin angular momentum with respect to one arbitrary axis (Z), computed by summing the spin eigenvalues ($\pm\frac{1}{2}$) of the individual electrons of the system, as given by:

$$S_Z = \sum_{i}^{\text{all electrons}} s_Z(i) \qquad (1.95)$$

In constructing a proper determinantal wavefunction for an open-shell system, it is generally required that the wavefunction be a simultaneous eigenfunction of the $\hat{S}_Z$ and $\hat{S}_Z^2$ spin angular momentum operators. Now, a commonly-occurring open-shell electronic configuration is one in which there is only one electron outside closed shells. In such a situation, two equivalent wavefunctions may be constructed for the doublet state, as illustrated for a three-electron system:

$$\Phi_\alpha = |\phi_1(1)\,\alpha(1)\phi_1(2)\beta(2)\phi_2(3)\alpha(3)| \qquad \Phi_\beta = |\phi_1(1)\alpha(1)\phi_1(2)\beta(2)\phi_2(3)\beta(3)|$$

$$\hat{S}_z\,\Phi_\alpha = \tfrac{1}{2}\,\Phi_\alpha \qquad \hat{S}_z\,\Phi_\beta = -\tfrac{1}{2}\,\Phi_\beta$$

These two spin states are equivalent in the absence of a magnetic field, and it is therefore sufficient to treat only one of them. By convention, the one yielding the largest spin eigenvalue is chosen, which in this example is ϕ_α.

As far as the $\hat{S}^2$ operator is concerned, the situation for a doublet and triplet state may be exemplified as follows:

$$\hat{S}^2 \ \phi_\alpha = \tfrac{1}{2}(\tfrac{1}{2} + 1) \ \phi_\alpha = 0.75 \ \phi_\alpha$$

$$\hat{S}^2 \ \phi_{\alpha\alpha} = 1(1 + 1) \ \phi_{\alpha\alpha} = 2.00 \ \phi_{\alpha\alpha}$$

The 0.75000... and 2.00000... are measures of the spin purity of the state for doublet and triplet multiplicities respectively. This purity is guaranteed in the Restricted Hartree-Fock (RHF) method. However, if it is required only that the wavefunction be a variational solution of the Schrödinger equation satisfying the Pauli principle, then the spin Unrestricted Hartree-Fock (UHF) method is obtained, in which spin purity is no longer guaranteed. This latter method is also known as the "Different Orbitals for Different Spins" (DODS) method, and the distinction between the two formalisms, RHF and UHF, is illustrated schematically in Figure (1.4).

Each of these methods is outlined below.

1.4.2 Restricted Hartree-Fock Formalism

Roothaan's open-shell RHF approach[18] reduces the open-shell equations for a large number of cases to pseudo-eigenvalue form by absorbing off-diagonal multipliers (which cannot in general be eliminated simply by a unitary transformation, due to the coupling of the closed and open shell) into the effective Hamiltonian; i.e., by redefining the Fock operator.

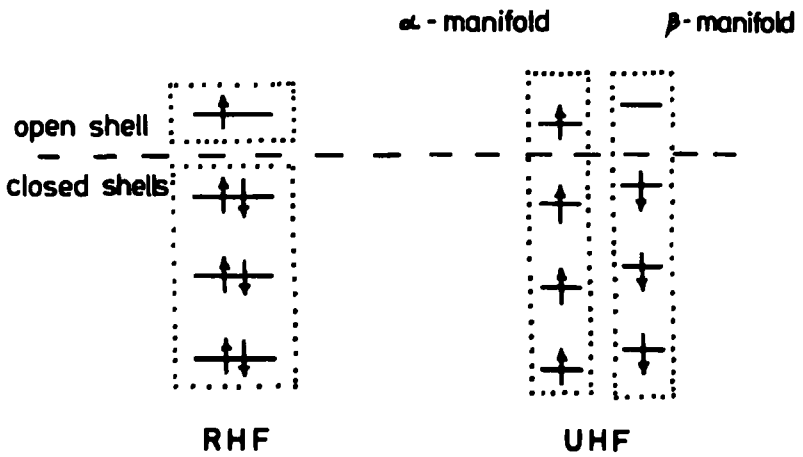

Fig. (1.4) Schematic illustration of the difference between the RHF and UHF formalisms.

Consider the MO, ϕ , of a system divided into closed-shell MO ϕ_c, and open-shell MO ϕ_o, which are restricted to be orthonormal:

$$\phi = (\phi_c, \phi_o) \tag{1.96}$$

If the wavefunction is constructed from these MO as a single Slater determinant, then the molecular electronic energy for an arbitrary open shell may be written as:

$$E = \underbrace{2\sum_{k}^{n_c} H_k + \sum_{k}^{n_c}\sum_{l}^{n_c} (2J_{kl} - K_{kl})}_{\text{closed shell}}$$

$$+ \; 2 \sum_{m=n_c+1}^{n_o} H_m + \sum_{m=n_c+1}^{n_o} \sum_{m=n_c+1}^{n_o} (2J_{mn} - K_{mn})$$

open shell

$$+ \sum_{k}^{n_c} \sum_{m=n_c+1}^{n_o} (2J_{km} - K_{km}) \qquad (1.97)$$

closed-shell - open-shell interaction

where

k,l are the running indices for closed-shell orbitals

m,n are the running indices for open-shell orbitals

n_c is the number of MO in the closed shell

n_o is the number of MO in both the closed and open shell

(i.e. n_o-n_c is the number of MO in the open shell only)

For a relatively large class of systems, the energy may be written more generally as:

$$E = 2 \sum_{k}^{n_c} H_k + \sum_{k}^{n_c} \sum_{l}^{n_c} (2J_{kl} - K_{kl})$$

$$+ f \left[2 \sum_{m}^{n_s} H_m + \sum_{m}^{n_s} \sum_{n}^{n_s} (2a\, J_{mn} - b\, K_{mn}) \right]$$

$$+ 2f \sum_{k}^{n_c} \sum_{m}^{n_s} (2J_{km} - K_{km}) \qquad (1.98)$$

Here, a and b depend on the specific spin state of a given configuration. The fractional occupancy, f, varies between zero and unity ($0 \leq f \leq 1$), where zero is the value for an

unoccupied shell, and unity is the value of f for a closed shell. Note that n_s is the number of degenerate spatial orbitals within the open shells:

for triple degeneracy, t_{2g} $\quad n_s = 3$

for double degeneracy, e_g $\quad n_s = 2$

for no degeneracy, $\quad n_s = 1$

A number of important cases fall within the range of this method, including the half-closed shell, and partially occupied degenerate sets of orbitals. A slightly more general expression for the energy allows for the case of two open shells of different symmetry to be handled.[19]

The two sets of orbitals, ϕ_c and ϕ_o, are eigenfunctions of two molecular Fock operators:

$$\begin{aligned} \hat{F}_c \phi_c &= \phi_c \varepsilon_c \quad \text{(for closed shells)} \\ \hat{F}_o \phi_o &= \phi_o \varepsilon_o \quad \text{(for open shells)} \end{aligned} \tag{1.99}$$

Where the corresponding Fock matrices are:

$$\mathbf{F}_c = \mathbf{H} + 2\mathbf{J}_c - \mathbf{K}_c + 2\mathbf{J}_o - \mathbf{K}_o + 2\alpha\mathbf{L}_o - \beta\mathbf{M}_o \tag{1.100}$$

$$\mathbf{F}_o = \mathbf{H} + 2\mathbf{J}_c - \mathbf{K}_c + 2a\mathbf{J}_o - b\mathbf{K}_o + 2\alpha\mathbf{L}_c - \beta\mathbf{M}_c$$

The L and M operators are defined as follows:

$$\hat{L}_c = \sum_k^{n_c} |\phi_k\rangle\langle\phi_k| \hat{J}_o \qquad \hat{M}_c = \sum_k^{n_c} |\phi_k\rangle\langle\phi_k| \hat{K}_o$$

$$\hat{L}_o = f \sum_m^{n_s} |\phi_m\rangle\langle\phi_m| \hat{J}_o \qquad \hat{M}_o = f \sum_m^{n_s} |\phi_m\rangle\langle\phi_m| \hat{K}_o \tag{1.101}$$

where

$$\alpha = \frac{1 - a}{1 - f} \quad \text{and} \quad \beta = \frac{1 - b}{1 - f} \tag{1.102}$$

1.4.3 Unrestricted Hartree-Fock Theory

In the UHF method, the equivalence restriction by which the spatial parts of each closed-shell pair of spin-orbitals are identical is removed.[20] Thus, the wavefunction is now written as a single determinant of α orbitals, ϕ^{α}, which are occupied by electrons of α spin, and β orbitals, ϕ^{β}, which are occupied by electrons of β spin, where $\alpha \neq \beta$. Again, two Hartree-Fock problems are considered, one for the α-spin manifold, and one for the β-spin manifold:

$$\hat{F}^{\alpha} \phi^{\alpha} = \phi^{\alpha} \varepsilon^{\alpha} \tag{1.103}$$

$$\hat{F}^{\beta} \phi^{\beta} = \phi^{\beta} \varepsilon^{\beta}$$

where

$$\underline{\phi}^{\alpha} = \underline{\eta}\, \mathbf{C}_{\alpha} \tag{1.104}$$

$$\underline{\phi}^{\beta} = \underline{\eta}\, \mathbf{C}_{\beta}$$

The two Fock matrices may be written as:

$$\mathbf{F}^{\alpha} = \mathbf{H} + \mathbf{J} - \mathbf{K}^{\alpha} \tag{1.105}$$

$$\mathbf{F}^{\beta} = \mathbf{H} + \mathbf{J} - \mathbf{K}^{\beta}$$

where $\mathbf{K}^{\alpha}$ and $\mathbf{K}^{\beta}$ depend on $\boldsymbol{\rho}^{\alpha}$ and $\boldsymbol{\rho}^{\beta}$, the respective density matrices:

$$\boldsymbol{\rho}^{\alpha} = \mathbf{C}_{\alpha}\, \mathbf{C}_{\alpha}^{\dagger} \qquad \boldsymbol{\rho}^{\beta} = \mathbf{C}_{\beta}\, \mathbf{C}_{\beta}^{\dagger} \tag{1.106}$$

Elements of the $\mathbf{J}$, $\mathbf{K}^{\alpha}$ and $\mathbf{K}^{\beta}$ matrices are defined as:

$$J_{rs} = \sum_t \sum_n (\rho^{\alpha}_{tu} + \rho^{\beta}_{tu}) \langle \eta_r(1)\eta_r(2) | g_{12} | \eta_s(1)\eta_r(2) \rangle$$

$$K^{\alpha}_{rs} = \sum_t \sum_n \rho^{\alpha}_{tu} \langle \eta_r(1)\eta_t(2) | g_{12} | \eta_u(1)\eta_s(2) \rangle \qquad (1.107)$$

$$K^{\beta}_{rs} = \sum_t \sum_n \rho^{\beta}_{tu} \langle \eta_r(1)\eta_t(2) | g_{12} | \eta_u(1)\eta_s(2) \rangle$$

The total electronic energy of the system may be written as:

$$E = \sum_i^{\alpha+\beta} H_i + \tfrac{1}{2} \sum_i^{\alpha+\beta} \sum_j^{\alpha+\beta} J_{ij} - \tfrac{1}{2} \left(\sum_i^{\alpha} \sum_j^{\alpha} K^{\alpha}_{ij} + \sum_i^{\beta} \sum_j^{\beta} K^{\beta}_{ij} \right) \qquad (1.108)$$

The wavefunction obtained by the UHF method is not a pure spin state, and this is, in a sense, unrealistic, since it is a wavefunction "contaminated" by spin states of higher multiplicity. An important consequence of this contamination is that the energy computed is not a quantum mechanically rigorous upper bound for the energy of a molecule. In other words, the energy already incorporates a small (and undesired) fraction of the correlation energy, leading to an energy-lowering over the RHF method of the order of 1/10 eV.[21] The most straightforward way of making the UHF wavefunction an exact eigenfunction of $\hat{S}^2$ is to apply a spin projection operator;[22] however, the projected wavefunction is not strictly variational.

1.5 Molecular Properties

1.5.1 Mulliken's Population Analysis

Although the electron density distribution within a molecule is continuous, it is a useful concept to assign a charge to each atom in the molecule. Such populations are

given by a Mulliken population analysis.[23]

In general, the MO are expressed as a linear combination of AO:

$$\phi_i = \sum_j \eta_j C_{ji} \tag{1.109}$$

Thus

$$\phi_i^2 = \left(\sum_j \eta_j C_{ji} \right)^2 = \left(\sum_j \eta_j C_{ji} \right) \left(\sum_k \eta_k C_{ki} \right)$$

$$= \sum_j \sum_k \eta_j \eta_k C_{ji} C_{ki} \tag{1.110}$$

Integrating over all space, the orbital population N_i is:

$$N_i = N_i \int \phi_i^2 \, d\tau = N_i \sum_j \sum_k C_{ji} C_{ki} \int \eta_j \eta_k d\tau$$

$$= N_i \sum_j \sum_k C_{ji} C_{ki} S_{jk} \tag{1.111}$$

where S_{jk} is the overlap integral $\int \eta_j \eta_k d\tau \equiv \langle \eta_j | \eta_k \rangle$.

Summing over all occupied MO gives:

$$N = \sum_i N_i = \sum_i N_i \sum_j \sum_k C_{ji} C_{ki} S_{jk}$$

$$= \sum_j \sum_k S_{jk} \left(\sum_i C_{ji} C_{ki} \right) \tag{1.112}$$

where N is the total number of electrons. In the general case, the orbital occupancy N_i would be incorporated into the density matrix (i.e., (1.79) would be modified). In a closed-shell system, $N_i = 2$ for all the occupied MO, so a factor 2 may be brought outside the summation. Thus, from (1.79):

$$\rho_{jk} = \sum_{i}^{\text{occupied MO}} C_{ji}\, C_{ik}^{\dagger} = \sum_{i}^{\text{occ.MO}} C_{ji} C_{ki}^{*} = \sum_{i} C_{ji} C_{ki} \qquad (1.113)$$

since the MO are real. Thus (1.112) becomes:

$$N = 2 \sum_{j} \sum_{k} \rho_{jk}\, S_{jk} \qquad (1.114)$$

A population matrix $\mathbf{P}$ may be defined by

$$P_{ij} = 2\rho_{ij}\, S_{ij} \qquad (1.115)$$

The diagonal elements P_{ii}, equal to $2\rho_{ii}$ (since $S_{ii} = 1$), represent the electronic populations, or the "atomic charge" in units of number of electrons, whilst the off-diagonal elements P_{ij} are overlap populations, related to the simple idea of "bond order". Note that $P_{ij} = P_{ji}$, since both $\boldsymbol{\rho}$ and $\mathbf{S}$ are symmetric. Further, from (1.114),

$$\sum_{i} \sum_{j} P_{ij} = N \qquad (1.116)$$

The final result of the Mulliken Population Analysis is given in (1.115). The P-matrix provides an orbital population analysis. Summation of all P_{ij} elements associated with atomic orbital i gives the gross orbital charge of AO_i, GOC_i:

$$GOC_i = P_{ii} + (\tfrac{1}{2}) \sum_{j \neq i} P_{ij} + (\tfrac{1}{2}) \sum_{j \neq i} P_{ji}$$

$$= P_{ii} + (\tfrac{1}{2}) \sum_{j \neq i} (P_{ij} + P_{ji})$$

$$= P_{ii} + \sum_{j \neq i} P_{ij}$$

$$= \sum_{j} P_{ij} \qquad (1.117)$$

since $P_{ij} = P_{ji}$. It should be noted that the distribution of the overlap density P_{ij} equally between orbitals i and j is somewhat arbitrary.

The summation of all the P_{ij} elements associated with a given pair of atoms A and B reduces the "orbital by orbital" population matrix $\mathbf{P}$ to an "atom by atom" matrix $\mathbf{R}$:

$$R_{AB} = \sum_{i}^{\text{AO on A}} \sum_{j}^{\text{AO on B}} P_{ij} \qquad (1.118)$$

The total number of electrons associated with atom A, N_A, is given by:

$$N_A = R_{AA} + (\tfrac{1}{2}) \sum_{B \neq A}^{\text{atoms}} R_{AB} + (\tfrac{1}{2}) \sum_{B \neq A}^{\text{atoms}} R_{BA}$$

$$= R_{AA} + \sum_{B \neq A}^{\text{atoms}} R_{AB}$$

$$= \sum_{B}^{\text{all atoms}} R_{AB} \qquad (1.119)$$

Once again, the electrons are partitioned equally between A and B. The net charge Q_A associated with A is given by

$$Q_A = Z_A - N_A \qquad (1.120)$$

where Z_A is the nuclear charge of atom A. This definition of the populations P_{ij}, R_{AB} and R_A has the property:

$$N = \sum_{i,j} P_{ij} = \sum_{A,B} R_{AB} = \sum_{A} R_A \qquad (1.121)$$

1.5.2 Orbital Density Contours

Demand for a visual representation of the shapes

and sizes of molecular orbitals is evidenced by several recent reviews of just this area,[24-27] and extensive use of contour plots has been made in this thesis.

The electron density D_p associated with the p^{th} MO is defined as $|\phi|^2$; or more precisely, as $\phi\phi^\dagger$:

$$D_p(x,y,z) = \phi_p(x,y,z)\,\phi_p^{\dagger}(x,y,x) \qquad (1.122)$$

The density may be calculated at any point (x,y,z) of the 3-D physical space in terms of the AO basis $\{\eta\}$ and the MO coefficient matrix, $\mathbf{C}$:

$$D_p \equiv \phi_p\phi_p^{\dagger} = f_p(\eta_1\eta_2\cdots\eta_N)\begin{pmatrix} C_{1p} \\ C_{2p} \\ \vdots \\ C_{Np} \end{pmatrix}(C_{1p}C_{2p}\cdots C_{Np})\begin{pmatrix} \eta_1 \\ \eta_2 \\ \vdots \\ \eta_n \end{pmatrix}$$

$$= f_p(\eta_1\eta_2\cdots\eta_N)\begin{pmatrix} \rho_{11}^p & \rho_{12}^p & \cdots & \rho_{1N}^p \\ \rho_{21}^p & \rho_{22}^p & \cdots & \rho_{2N}^p \\ \vdots & \vdots & & \vdots \\ \rho_{N1}^p & \rho_{N2}^p & \cdots & \rho_{NN}^p \end{pmatrix}\begin{pmatrix} \eta_1 \\ \eta_2 \\ \vdots \\ \eta_N \end{pmatrix}$$

where $\boldsymbol{\rho}^p$ is the density matrix of the p^{th} MO. When summed over all the occupied MO, it yields the total density matrix $\boldsymbol{\rho}$, with elements defined as:

$$\rho_{ij} = \sum_p^M \rho_{ij}^p \qquad (1.124)$$

Thus D_p may be written as:

$$D_p(x,y,z) = f_p\underline{\eta}(x,y,z)\;\boldsymbol{\rho}^p\,\underline{\eta}(x,y,z)$$

$$= f_p\sum_i^N\sum_j^N \eta_i(x,y,z)\,\rho_{ij}^p\,\eta_j(x,y,z) \qquad (1.125)$$

The factor f_p is the integrated spin part of the orbital, which is 2 if the orbital is doubly occupied, 1 if it is singly occupied, and 0 if it is empty. The sum of the M doubly occupied MO densities is then:

$$D(x,y,z) = \sum_{p}^{M} D_p(x,y,z) = 2 \sum_{i}^{N} \sum_{j}^{N} \eta_i(x,y,z)\, \rho_{ij} \eta_j(x,y,z) \qquad (1.126)$$

The problem is simply to calculate the individual orbital electron density values D_p at every intersection of a given mesh around the molecule. Typically, 9409 points (i.e., a 97 x 97 mesh) provides a fine enough grid for a 10 x 10 $bohr^2$ area. Electron densities are interpolated between points so that density contours may be recorded by a 2-D (x,y) plotter.

Density difference functions, of the general form:

$$\Delta D(x,y,z) = \sum_{p}^{M} D_p(x,y,z) - \sum_{q}^{M} D_q(x,y,z) \qquad (1.127)$$

are particularly revealing. Two examples of the value of such molecular density difference functions are:

(a) in illustrating the effect on molecular charge distribution resulting from an extension of the basis set:

$$\Delta D(x,y,z) = D^{\text{extended}}_{\text{mol}}(x,y,z) - D^{\text{minimal}}_{\text{mol}}(x,y,z) \qquad (1.128)$$

(b) in illustrating the reorganization of charge density on core-ionization:

$$\Delta D(x,y,z) = D^{\text{ground}}_{\text{mol}}(x,y,z) - D^{\text{core-hole}}_{\text{mol}}(x,y,z) \qquad (1.129)$$

1.5.3 Computation of Molecular Properties

A full treatment of the computation of observable molecular properties (other than orbital energies) demands the use of perturbation theory.[28] The method of detection of dipole moments, polarisabilities, nmr chemical shifts, etc., corresponds to adding (ideally) small terms to the molecular Hamiltonian and computing the way in which the molecular electron density responds to such perturbations. However, it is possible (both computationally and conceptually) to regard the so-called first-order properties of the molecule as existing in their own right, independent of the measuring process.

In Quantum mechanics, the observable (Ω) is written as the expectation value of the appropriate operator ($\hat{\Omega}$) that describes the physical quantity in question over the many-electron wavefunction Φ_ν for a given state :

$$\Omega_\nu \equiv \langle \Phi_\nu (1,2,3,\ldots) | \hat{\Omega}_{1,2,3,\ldots} | \Phi_\nu (1,2,3,\ldots) \rangle \qquad (1.130)$$

where 1,2,3,... symbolise the co-ordinates of electrons 1,2,3,... . For all our purposes, the wavefunction is an antisymmetrized orbital product (a single Slater determinant for closed-shell species).

The operator $\hat{\Omega}_{1,2,3,\ldots}$ may be written as a sum of operators:

$$\hat{\Omega} = \hat{\Omega}_o + \hat{\Omega}_i + \hat{\Omega}_{ij} \qquad (1.131)$$

Here, $\hat{\Omega}_o$ is a no-electron operator, operating on the nuclear wavefunction. The electronic operators may be classified as

one-electron operators $\hat{\Omega}_i$ dependent on the co-ordinates of a single electron, and two-electron operators $\hat{\Omega}_{ij}$, dependent on the co-ordinates of two electrons simultaneously.

Quantities involving the two-electron operators are not trivial to compute, since they include calculation of a great many two-electron integrals of the type:

$$< \phi_p(1)\, \phi_q(2) |\, \hat{\Omega}_{1,2} \,| \phi_r(1)\, \phi_s(2) > \qquad (1.132)$$

where the $\{\phi_\eta\}$ are the individual MO. However, these operators are very important, describing a number of physical properties. Most important is the Hamiltonian operator (including a two-electron operator $\hat{g}_{ij} = {}^1/r_{ij}$) responsible for the computation of molecular energies.

The second class of quantum chemical operators include only the first two terms in (1.131); the properties (P) that may be computed with the aid of such operators are referred to as one-electron properties:

$$\begin{aligned} P &= \langle\Phi|\hat{P}_o + \sum_i \hat{P}_i|\Phi\rangle \\ &= \langle \Phi|\, \hat{P}_o|\Phi\rangle + \sum_i \langle\Phi|\, \hat{P}_i|\Phi\rangle \\ &= P_o + \sum_i P_i \end{aligned} \qquad (1.133)$$

where individual P_i have the general form:

$$P_i = < \phi_q(1)|\, \hat{P}_1 \,|\phi_r(1) > \qquad (1.134)$$

Many properties fall into this category, but amongst the most noteworthy is the dipole moment, μ. The accuracy of the computed μ is very sensitive to the quality

of the wavefunction. The computation of the dipole moment value μ^{oo} for the electronic ground state Φ_o may be written as:

$$\mu^{oo} = \langle \Phi_o(1,2,3,\ldots)|\hat{\mu}_o + \sum_i \hat{\mu}_i|\Phi_o(1,2,3,\ldots)\rangle$$

$$= \langle \Phi_o(1,2,3,\ldots)|\hat{\mu}_o|\Phi_o(1,2,3,\ldots)\rangle$$

$$+ \sum_i \langle \Phi_o(1,2,3,\ldots)|\hat{\mu}_i|\Phi_o(1,2,3,\ldots)\rangle$$

$$= \mu_o^{oo} + \sum_i \mu_i^{oo} \qquad (1.135)$$

The dipole moment for the ν^{th} excited state, $\mu^{\nu\nu}$, may be similarly defined. The transition dipole moment, $\mu^{o\nu}$, of the molecule between the ground and excited states requires the computation of the following integral:

$$\mu^{o\nu} = \langle \Phi_o(1,2,3,\ldots)|\hat{\mu}_o + \sum_i \hat{\mu}_i|\Phi_\nu(1,2,3,\ldots)\rangle$$

$$= \mu_o^{o\nu} + \sum_i \mu_i^{o\nu} \qquad (1.136)$$

1.6 Basis Functions and Basis Sets

1.6.1 Molecular Integral Considerations

The use of a basis set of analytical functions in which to expand the unknown MO has been discussed previously at several points. Historically, basis functions were chosen on the basis of their relationship to AO - hence the term LCAO MO. The initial choice of a basis set is of prime importance: it will fix forever the reliability of the results of a calculation. The determination of carefully optimized and balanced basis sets is an extremely time-consuming process, but a

necessary one.

Historically, the basis functions were chosen by physical analogy to orbitals. At present, the emphasis is on the computability of the three- and four-centre two-electron integrals. The necessity of the rapid computation of integrals becomes clear when it is noted that the number of computationally difficult two-electron integrals increases with the number of basis function as N^4. Thus, the more "physically" realistic Slater type orbitals (STO) have been replaced by the more mathematically and computationally convenient Gaussian type functions (GTF), for many purposes. The basic advantage of GTF is due to the fact that the product of any two gaussians is also a gaussian, with its centre on a line between the centres of the two original gaussian functions, as illustrated in Figure (1.5).

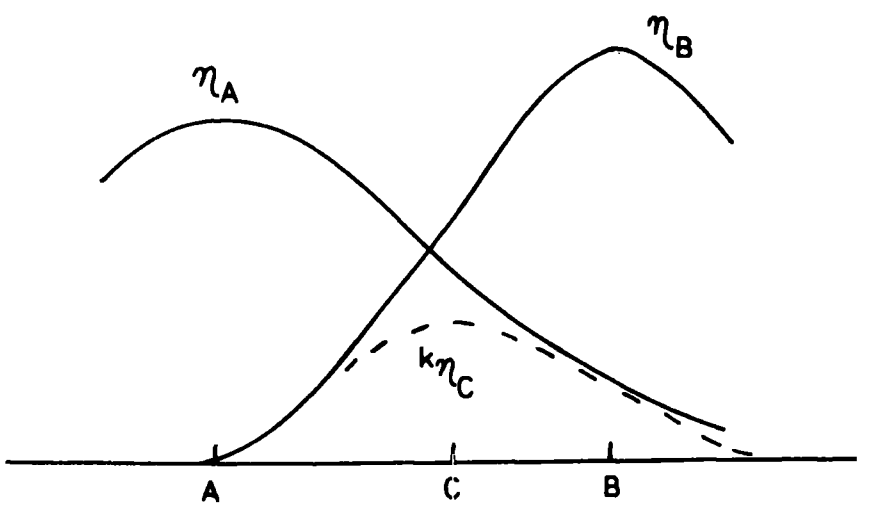

Fig.(1.5) An illustration of the theorem that the product of two gaussians is also a gaussian.

Consequently, all integrals have explicit analytical expressions, and may be evaluated rapidly. A similar theorem does not exist for STO. The principal disadvantages of GTF are their smooth behaviour (lack of a cusp) at the nucleus, and their too rapid (e^{-r^2} rather than e^{-r}) decrease at large distances, as illustrated in Figure (1.6).

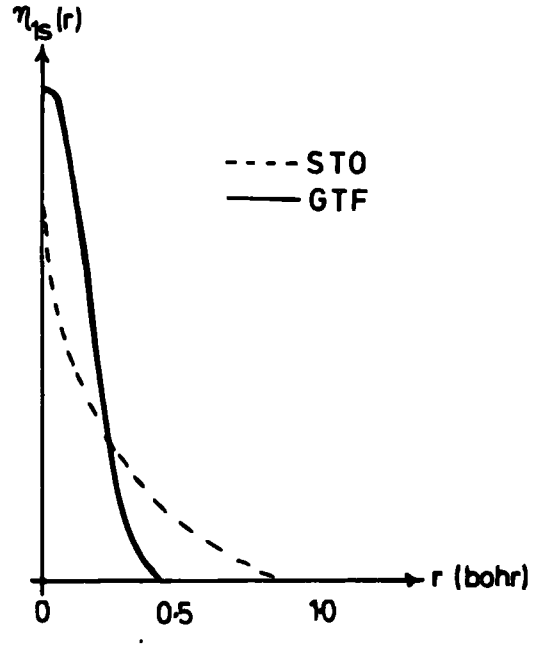

Fig.(1.6) A schematic comparison of a 1s-STO and 1s-GTF as a function of r.

This improper asymptotic behaviour requires the use of a larger number of GTF than STO for equivalent accuracy. However, the much greater speed per integral with GTF as opposed to STO allows for this greater total number of integrals.

1.6.2 Slater Type Functions

Prior to the early 1960's, almost all MO calculations were performed with STO. The functions are analogous to the actual solutions of the Schrödinger equation for the

hydrogen atom, but possess different nodal properties. The functions are given by:[29]

$$\eta_{nlm}(r,\theta,\phi) = A_n\, r^{n-1}\, e^{-\zeta r}\, Y_{lm}(\theta,\phi) \qquad (1.137)$$

where

n,l,m are principal, azimuthal and magnetic quantum numbers respectively;

r, θ, ϕ are spherical polar co-ordinates;

A_n is a normalizing factor;

and $Y_{lm}(\theta, \phi)$ are the spherical harmonics introducing the required angular dependence.

A minimal basis set of STO includes one such function for every AO occupied in the separated atoms (e.g. for carbon: 1s, 2s, $2p_x$, $2p_y$). The choice of the orbital exponents ζ must be made. These were originally chosen on the basis of a set of empirical rules (Slater's Rules[29]), where:

$$\zeta = \frac{(Z - S)}{n^*} \qquad (1.138)$$

Here,

Z is the actual charge on the nucleus;

S is a screening constant;

and n^* is an effective quantum number.

More recently, Clementi et al[30,31] have variationally optimized ζ values for the ground electronic states of the free atoms. In principle, the exponents should be re-optimized for the molecule; in practice, the optimization of ζ values in the molecular environment is prohibitively expensive, and the atom-optimized orbital exponents are used directly in

Hartree-Fock LCAO MO SCF calculations.

Minimal basis sets occupy a unique position in the history of quantum mechanics. Virtually all the current semi-empirical SCF methods are in principal based on a minimum set of STO, and many of the concepts in organic chemistry (e.g. hybridisation, resonance structures) can only be discussed in terms of a minimum basis set.

A considerable improvement in energy is obtained by using the double zeta basis set,[32,33] in which free atom occupied AO are represented by two STO with orbital exponents ζ and ζ', optimized variationally; the larger ζ value corresponds to a "tight" orbital, the smaller to a "loose" orbital. Any basis set beyond the double zeta level may be considered an extended basis set. Of particular importance is the addition of functions with higher l values,[34] i.e., d,f,... on first row atoms, and p,d,... on hydrogen. These are termed polarization functions. The exponents of the polarization functions should in principle be optimized for the molecule in question, but this is not usually done, for economic reasons. It appears that the calculated total energies are not too sensitive to small variations in the exponents of the polarization function, and thus a reasonable choice might be based on small molecule calculations,[35-38] e.g., for STO, a ζ (2p) of 2.0 for H, and ζ (3d) = 2.0 for C are not unreasonable.

1.6.3 Gaussian Type Functions

In recent years, most large-scale MO calculations have used GTF[39,40]. The radial dependence of a gaussian function may be written:

$$\eta = r^n e^{-\alpha r^2} \qquad (1.139)$$

A normalizing factor and angular dependence may be introduced as was done for STO. For gaussians, the latter is frequently introduced not by a spherical harmonic factor $Y_{lm}(\theta,\phi)$, but by:

$$Cx^p\ y^q\ z^s\ e^{-\alpha r^2} \qquad (1.140)$$

where p,q and s are integers, thus yielding cartesian gaussians. In addition to cartesian gaussians, the gaussian lobe method[41,42] uses only s-type gaussians, but floats the centres of these functions away from the atomic centres to simulate s,p,d..... orbitals, as illustrated in Figure (1.7).

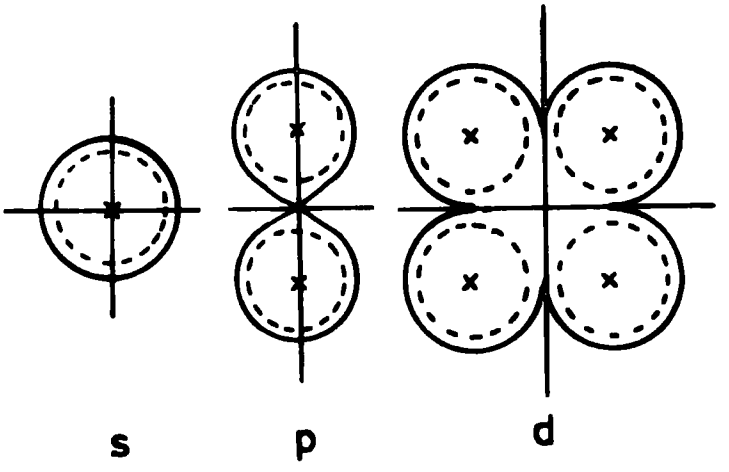

Fig.(1.7) The floating of gaussian lobe functions (broken lines) to simulate s,p,d,... orbitals (solid lines).

A minimal basis set which retains the concept of an STO, but replaces the actual STO by a linear combination of n GTF is termed an STO-nG basis set;[43-45] despite its name, this is fundamentally a gaussian basis set. The convergence to the correct STO results as the number of gaussians n used in the least-square fit to the STO is increased has been investi-

gated. Even when n=6, the total molecular SCF energies are ~1 eV above the exact STO energies. However, energy differences are more important than absolute energies in chemistry, and for most chemical purposes, four gaussian expansions are suitable replacements for STO. STO-3G is also widely used for large molecules.[44,45] It is worth mentioning that GTF exponents are usually listed for an STO exponent of unity, and must be multiplied by the square of the actual STO exponent to obtain the best fit for that particular orbital.

A significant improvement on STO-nG basis sets may be obtained by splitting the valence-shell of each heavy atom into two parts, giving a more flexible description of the valence orbitals to allow for their distortion on bond-formation. As a commonly-used example, in the split-valence-shell STO-4.31G basis set,[46] the inner (1s) shell of the first-row atoms is represented by a fixed sum of 4 GTF, whilst the valence (2s, 2p) shells are divided into "inner" and "outer" components represented by 3 and 1 GTF respectively. Hydrogens are represented by a split 1s shell, again comprising of an "inner" (3 GTF) and an "outer" (1 GTF) part. A further improvement is obtained by addition of a single set of gaussian d functions to the description of each heavy atom, a commonly-used basis set being STO-6.31G*;[47] addition of a single gaussian p-type function to the representation for each hydrogen atom gives a basis set denoted by STO-6.31G**.[47] As with STO, calculated total energies are not too sensitive to small variations in polarization function exponents, and reasonable values would be $\alpha(1s)=1.0$ for hydrogen, and $\alpha(3d)=0.8$ for first-row atoms. The general trend is for the optimum 3d exponents

of both STO and GTF to increase in going from Be to Ne.

Although integral evaluation is considerably speeded-up by the use of GTF as opposed to STO, the number of integrals to be computed can become very large if a GTF basis set of STO quality is used, requiring considerable storage-space. Furthermore, the SCF step can become prohibitively time-consuming due to the larger size of the various matrices to be manipulated, and the use of large basis sets may also necessitate more iterations in order to attain convergence. For these reasons, calculations carried out directly in terms of primitive gaussians may become uneconomical, and the use of *contracted* GTF was introduced. These are linear combinations of primitive GTF with fixed coefficients;[42,48] only the coefficients in each SCF orbital of the contracted functions are variationally determined in the SCF procedure. This approach allows one to exploit the analytic properties of the GTF in integral evaluation, yet keep the time required for the SCF iterations at a reasonable level.

The contraction of gaussian basis sets requires considerable care.[49] Perhaps the most obvious type of contraction would be a complete contraction to atomic SCF orbitals. Thus, for a gaussian (11s 7p) basis set, such a contraction would be designated (11s 7p / 2s 1p). The molecular calculation would then be carried out in terms of a minimum basis set (1s, 2s, 2p) for first row atoms. However, such a basis set leads to erroneous descriptions of molecular properties (e.g. unrealistically large bond-distances and small dissociation energies) because the basis does not have sufficient flexibility to describe the rearrangement in the electron

distribution accompanying molecule formation. Indeed, a minimum STO basis set is preferable to such an energetically superior overcontracted gaussian basis set. Perhaps the greatest amount of effort as regards the contraction of functions has gone towards the goal of obtaining contracted gaussian basis sets comparable to the double zeta STO basis sets. Perhaps the most effective double zeta gaussian basis set (in which two contracted GTF contribute to each AO) is Dunning's contraction[49] of Huzinaga's basis set[50] for boron to fluorine, designated (9s 5p/4s 2p).

1.6.4 Basis Set Optimization and Quality

The term "basis set optimization" almost always refers to the variational determination (with respect to energy) of a set of function exponents for a free atom. Even for the atom, there is no guarantee that the exponents so obtained will also yield the best values for other properties (such as the moments of charge distribution). Moreover, optimum *atomic* exponents are not necessarily optimum *molecular* exponents, although in general, carefully optimized atomic exponents are used in molecular calculations.

The term "quality" used with respect to a basis set is a relative one; however, certain general conclusions are in order. Clearly, a minimal basis set (even if carefully optimized) is *not* capable of yielding reliable values for sensitive one-electron properties such as the dipole moment; however, at least the gross features of molecular geometry, and trends in bond-lengths and angles should be reasonably accurately predicted. At the double-zeta or split-valence basis set level, such features should be given more accurately;

however, most one-electron properties require the use of polarization functions for accurate description. Finally, in addition to the size and type of basis set, it is necessary to consider the *balance* of the basis set: all constituent parts of the molecule must be described equally well. Unfortunately, it is difficult to define precisely the "degree of optimization".

1.7 The Hartree-Fock Limit and Beyond

1.7.1 The Concept of the Hartree-Fock Limit

It is useful at this stage to recall the various approximations that have been made in developing a computationally feasible theory of molecular electronic structure, as shown in Figure (1.8).

Thus, calculation of the "true" total energy of a molecule is not possible using a non-relativistic Hamiltonian; a total energy higher than the experimental energy is obtained. The limiting energy value that can be computed with the non-relativistic Hamiltonian is referred to as the non-relativistic limit (NRL); the difference between the experimental energy and that associated with the NRL is the relativistic energy (E_R).

When the total single-determinantal wavefunction is constructed from the most accurate set of MO, a limiting total energy value higher than the NRL value is reached. This is referred to as the Hartree-Fock limit (HFL), the energy difference between the two limits (NRL, HFL) being called the correlation energy (E_{cor}). The SCF energy (E_{SCF}) that is computed by non-empirical MO theory constitutes an upper bound

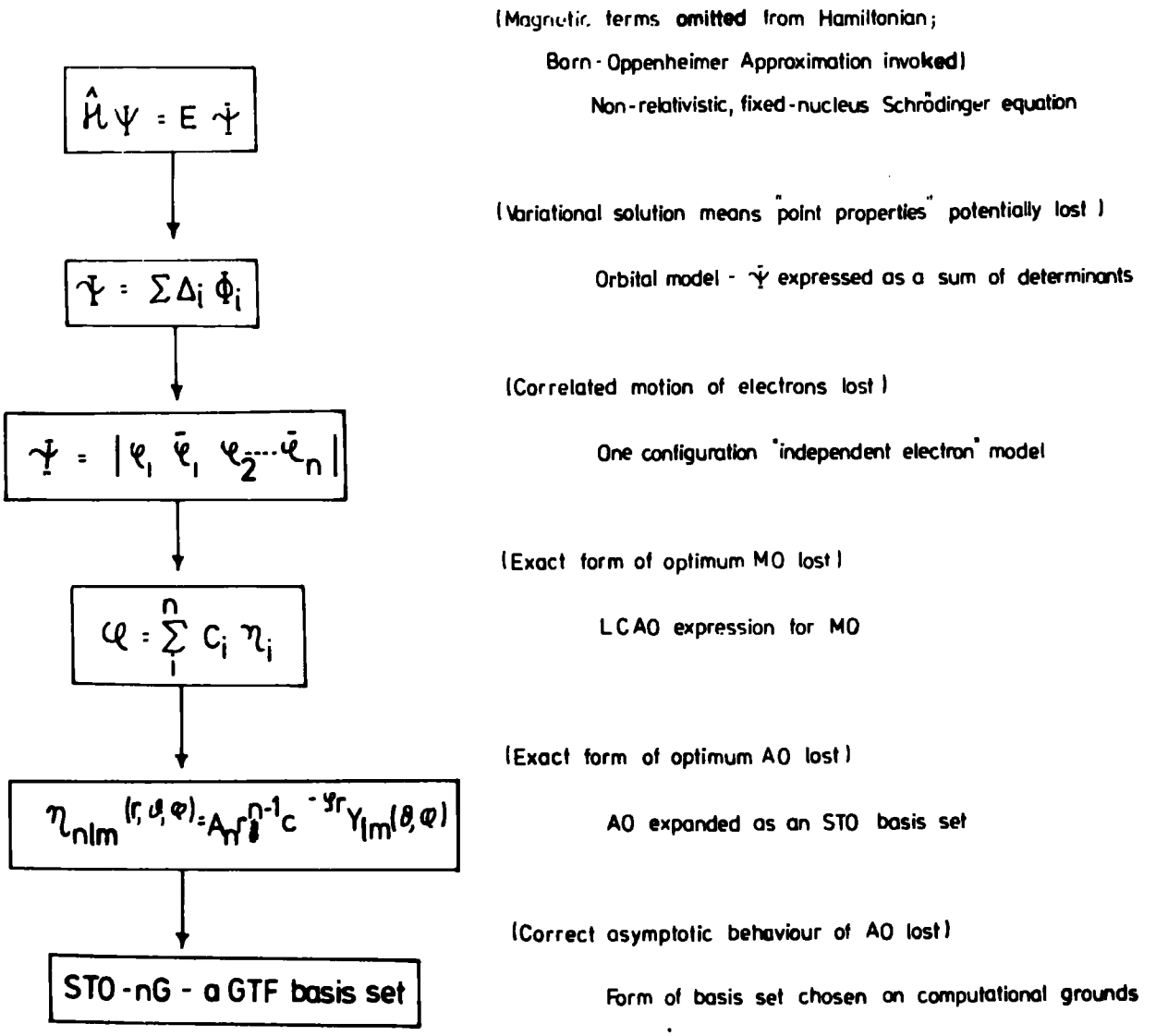

Fig. (1.8) Hierarchy of approximations involved in the MO model.

on the Hartree-Fock energy (E_{HF}); only at the HFL will E_{SCF} equal E_{HF}. However, to achieve this result requires a complete basis set of infinite dimension, which is not possible for large molecules. The inter-relationship between these quantities is illustrated in Figure (1.9) for CO.

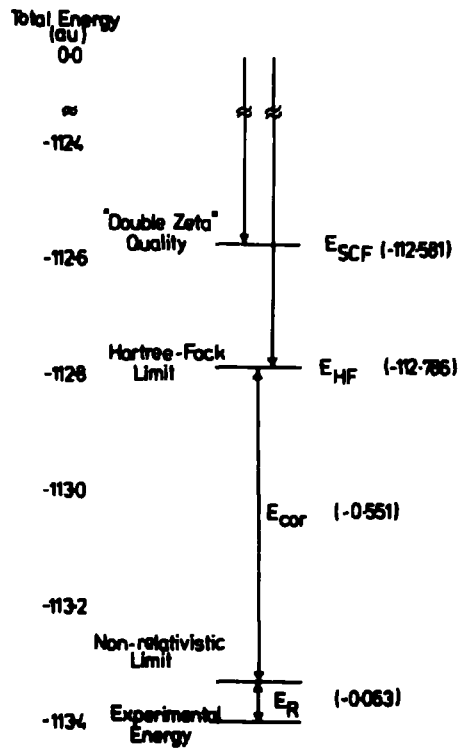

Fig. (1.9) Breakdown of total energy for CO.

1.7.2 The Relativistic Correction

The relativistic correction is the energetic consequence of the relativistic effects suffered by the electrons as they pass the nucleus, since from the Virial Theorem ($V = -2T$, where V is the potential energy and T the kinetic energy) it is apparent that an electron in a region of high potential will have a correspondingly high kinetic energy. The correction is a function of atomic number, being comparatively small for the light atoms up to Ne, but appreciable for heavier elements. Furthermore, for core electrons, relativistic effects may become important in heavier elements, this having potential significance with regard to calculations on photoionization. Fortunately, relativistic corrections to

shifts in core-electron binding energies are small. Customarily, it is assumed that the relativistic correction of atoms is unchanged on formation of molecules, so that:

$$E_R^{\ mol} = \sum_{i}^{\text{all atoms}} (E_R^{\ atom})_i \qquad (1.141)$$

Extensive tabulations of relativistic expectation values for atoms have been made,[51] allowing detailed comparisons with non-relativistic results. In addition, neutral atom ΔSCF binding energies from relativistic HF calculations ($2<Z<106$) have been published,[52] allowing a comparison between the Koopmans' and ΔSCF relativistic binding energies to be made.

1.7.3 Correlation Energy

In the Hartree-Fock approximation, the motion of each electron is solved for in the presence of the average potential created by the remaining electrons. As such, this neglects the instantaneous (rather than averaged) repulsions between pairs of electrons. The contribution to the total energy due to instantaneous repulsions is called the correlation energy,[53] E_{cor} (see Figure (1.9)). E_{cor} is usually a relatively small percentage of the total energy of an atom or molecule; however, this amount is larger than or comparable to the energy associated with physical or chemical phenomena. Nevertheless, there are many problems in chemistry where Hartree-Fock theory is perfectly adequate: for example, molecular geometries, and some one-electron properties predicted from Hartree-Fock theory are frequently in good agreement with experiment. Furthermore, since energy differences are of prime importance to chemists, if E_{cor} were constant as a function of

molecular geometry, it would be hoped that accurate dissociation energies and potential energy surfaces could be obtained from HF wavefunctions. Generally, changes in E_{cor} are small for barriers to rotation,[54] and heats of isodesmic reactions.[55] Also, as illustrated in Figure (1.10) for a diatomic molecule, some important aspects of potential energy surfaces are well-reproduced within the Hartree-Fock formalism.

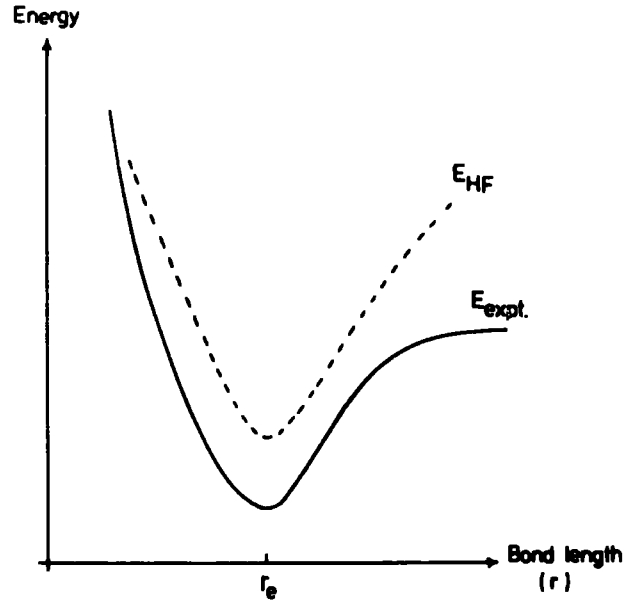

Fig. (1.10) Diagrammatic comparison of computed (HF) and experimental potential energy surfaces for a typical diatomic molecule.

Thus, although the HF curve lies above the experimental curve, it virtually parallels it at the minimum. As a result, computed equilibrium bond-lengths, r_e, are very close to the observed values, with the vibrational frequencies (and thus force constants) generally being slightly overestimated.[56] A similar situation holds for polyatomic molecules.

However, Figure (1.10) also illustrates the main

drawback of the HF method: its incorrect behaviour at large internuclear separations, leading to an inability to correctly describe molecule formation and dissociation.[57] Thus, in many circumstances, the theoretician must go beyond the HFL to make a contribution to the solution of problems of chemical interest. The most frequently used method for approaching the electron correlation problem is configuration interaction (CI).[58]

1.7.4 Configuration Interaction

For any atom or molecule, there are an infinite number of orbitals in addition to the HF orbitals, which can be used to construct other configurations. A CI wavefunction is just a linear combination of such configurations, with coefficients variationally determined. More precisely, the CI wavefunction is of the form:

$$\Psi_e = \sum_i c_i \Phi_i \qquad (1.142)$$

The coefficients c_i are determined to minimize the energy $\int \Psi_e^* \hat{H}_e \Psi_e d\tau$. Application of the Variation Theorem leads to the eigenvalue problem, discussed previously (1.32):

$$(\mathbf{H} - E\mathbf{I}) \mathbf{C} = 0 \qquad (1.143)$$

$\mathbf{H}$ is composed of matrix elements between configurations:

$$H_{ij} = \int \Phi_i^* \hat{H}_e \Phi_j d\tau \qquad (1.144)$$

Hamiltonian matrix elements H_{ij} between configurations i and j of different symmetries are zero, greatly simplifying the secular equation. Sophisticated and efficient algorithms for the determination of the lowest eigenvalue and corres-

eigenvector of large, real symmetric matrices have been developed,[59,60] of particular value in large CI calculations.

It is necessary here to introduce the terminology to be used in the discussion of CI. An *orbital occupancy* (or *electron configuration*) is a collection of orbitals written without regard to those quantum numbers which do not affect the orbital energy. For example,

Ne (ground state) is $1s^2\ 2s^2\ 2p^6$

O_2 is $1\sigma_g^2\ 1\sigma_u^2\ 2\sigma_g^2\ 2\sigma_u^2\ 3\sigma_g^2\ 1\pi_u^4\ 1\pi_g^2$

A *configuration* is defined as a symmetry-adapted linear combination of Slater determinants, *symmetry-adapted* implying that the chosen linear combination of determinants possesses all the symmetry of the molecular state being described by the approximate wavefunction. The configuration Φ is written:

$$\Phi = \sum c_i D_i \qquad (1.145)$$

where D_i is the Slater determinant (1.20). It is often found that a single orbital occupancy gives rise to several different configurations; to determine what they are it is only necessary to consider the electrons outside the closed shell. Having determined the manifold (Σ, Π or Δ type) for a given orbital occupancy,[61] it is then necessary to find which combinations of all possible determinants of that manifold give rise to the desired spin multiplicity. A less tedious approach to the problem than the direct application of angular momentum operators is the use of projected wavefunctions.[62] In particular, Nesbet's method[22] is simple to apply, and time-saving in CI studies in that it reduces the number of terms involved in matrix elements.

It is often found that a CI wavefunction is dominated by a single configuration, the HF wavefunction. In such cases it is found that 95% or more of the correlation energy can be accounted for by configurations which differ by one or two orbitals from the HF or reference configuration. A singly excited configuration (*single excitation*) is obtained by promoting one electron from the $k^{\underline{th}}$ to $\mu^{\underline{th}}$ spin orbital. Similarly, a *double excitation* is a configuration generated by the promotion of two electrons out of spin-orbitals contained in the reference configuration. These classes of determinantal functions are thus defined as:

Reference (or HF) configuration $D_o = |\phi_a \phi_b \cdots \phi_k \cdots \phi_l \cdots \phi_n|$

Single excitation $D_k^{\mu} = |\phi_a \phi_b \cdots \phi_{\mu} \cdots \phi_l \cdots \phi_n|$

Double excitation $D_{kl}^{\mu\nu} = |\phi_a \phi_b \cdots \phi_{\mu} \cdots \phi_{\nu} \cdots \phi_n|$

Evaluation of the matrix elements H_{ij} in terms of determinantal functions D_i is facilitated by the use of Slater's Rules for the Calculation of Matrix Elements,[63] summarized in Table One.

The electronic wavefunction may now be written as:

$$\Psi_{el} = C_o D_o + \sum_{k,\mu} C_k^{\mu} D_k^{\mu} + \sum_{k,l,\mu,\nu} C_{kl}^{\mu\nu} D_{kl}^{\mu\nu} + \ldots \quad (1.146)$$

This is known as the CI expansion. In HF Theory, the expansion is limited to the first determinant with a coefficient of unity. The best way to proceed is the Multiconfigurational SCF method (MC SCF) in which both the orbitals ϕ and the CI coefficients c are simultaneously varied to give the lowest energy multiconfiguration HF wavefunction. However, solution of the MC SCF equations is computationally difficult, and very time-consuming.

TABLE ONE - A Collection of Pertinent Slater Rules

1. Overlap Integral

$$\langle D_o | D_o \rangle = 1 \qquad \langle D_o | D_k^{\mu} \rangle = \langle D_o | D_{kl}^{\mu\nu} \rangle = 0$$

2. One-electron Operators

$$\langle D_o | \sum_i \hat{\Omega}(i) | D_o \rangle = \sum_k^{\text{occupied orbitals}} \langle \phi_k(1) | \hat{\Omega}(1) | \phi_k(1) \rangle$$

$$\langle D_o | \sum_i \hat{\Omega}(i) | D_k^{\mu} \rangle = \langle \phi_k(1) | \hat{\Omega}(1) | \phi_{\mu}(1) \rangle$$

$$\langle D_o | \sum_i \hat{\Omega}(i) | D_{kl}^{\mu\nu} \rangle = 0$$

3. Two-electron Operators

$$\langle D_o | \sum_{i<j} \hat{\Omega}(i,j) | D_o \rangle = \sum_{k<l}^{\text{occupied orbitals}} \left\{ \langle \phi_k(1)\phi_l(2) | \hat{\Omega}(1,2) | \phi_k(1)\phi_l(2) \rangle - \langle \phi_k(1)\phi_l(2) | \hat{\Omega}(1,2) | \phi_k(2)\phi_l(1) \rangle \right\}$$

$$\langle D_o | \sum_{i<j} \hat{\Omega}(i,j) | D_k^{\mu} \rangle = \sum_k^{\text{occupied orbitals}} \left\{ \langle \phi_k(1)\phi_l(2) | \hat{\Omega}(1,2) | \phi_k(1)\phi_{\mu}(2) \rangle - \langle \phi_k(1)\phi_l(2) | \hat{\Omega}(1,2) | \phi_k(2)\phi_{\mu}(1) \rangle \right\}$$

$$\langle D_o | \sum_{i<j} \hat{\Omega}(i,j) | D_{kl}^{\mu\nu} \rangle = \langle \phi_k(1)\phi_l(2) | \hat{\Omega}(1,2) | \phi_{\mu}(1)\phi_{\nu}(2) \rangle - \langle \phi_k(1)\phi_l(2) | \hat{\Omega}(1,2) | \phi_{\mu}(2)\phi_{\nu}(1) \rangle$$

$$\langle D_o | \sum_{i<j} \hat{\Omega}(i,j) | D_{klm}^{\mu\nu\rho} \rangle = 0$$

where

$\sum_i \hat{\Omega}(i)$ is a general one-electron operator

$\sum_{i<j} \hat{\Omega}(i,j)$ is a general two-electron operator

Since calculations in this thesis have not made use of any CI, no further discussion of the various methods currently in use will be given here. A brief introduction to the topic is given in Schaefer;[2] more detailed coverage is given in several recent texts.[64,65]

1.8 Computational Aspects

1.8.1 Introduction

Although MO theory was largely elaborated during the 1920's and 1930's, it has only been the advent of modern electronic computers in the 1960's, together with accurate, well-tested, well-documented computer programs that has led to the rapid growth of the *ab initio* technique as a well-established tool in modern chemistry. The writing and development of these programs has required man-years of effort, usually from teams of people, and they are readily available through the Quantum Chemistry Program Exchange (QCPE).[66] Some commonly-used programs are IBMOL V,[67] POLYATOM(2),[68] MOLECULE,[69] ALCHEMY[70] and GAUSSIAN 70.[71] Calculations in this thesis have been performed using the ATMOL 2[72] and ATMOL 3[73] sets of programs, and this section will be limited to a brief discussion of some particular points of interest in these programs. Further description of the programs is available in the appropriate ATMOL documentation.[72,73] In common with most *ab initio* programs, ATMOL has the following essential stages:

(i) The computation of molecular integrals over basis functions, together with the transformation of integrals (if required) over contracted functions.

(ii) Assembly and diagonalization of the Fock matrix until the required self-consistency is reached.

(iii) Analysis of the molecular wavefunction in the form of (for example) Mulliken population analysis, electron density contour plots, and expectation values of some 1-electron properties.

1.8.2 Integral Evaluation

The computation, storage and retrieval of AO integrals is generally the most time-consuming part of any orbital basis valence calculation. The two main areas of continuing research in this field are the rapid and accurate computation of the integrals, and the design of an efficient file structure for storing the computed integrals for subsequent use. The electron repulsion (or two-electron) integrals present the most difficulties from both points of view; however, ATMOL has extensive integral file handling facilities provided by a SERVICE program, useful for copying, editing, and merging integral files. In addition, the program has a restart facility, and a library file containing standard contractions is available for use, thus reducing the amount of input required.

The general problems involved in molecular integral evaluation are touched upon in Cook.[4] Details of the numerical procedures used for the evaluation of molecular integrals over GTF, together with a discussion of the general strategy employed, are given by Saunders.[74] For STO, one-centre two-electron integrals are computed analytically; all other two-electron integrals are computed by the alternate Gaussian transform technique of Shavitt and Karplus.[75] In addition, it is worth pointing out that the symmetry properties of the molecule may be used to improve the efficiency of the two-electron integrals calculation. Centres of symmetry are declared in the input,

which may include local symmetry as well as symmetry centres for the molecule as a whole.

The one-electron integrals may be conveniently stored, space being saved by keeping only the $\frac{1}{2}N(N+1)$ distinct elements of the N by N matrix, where N is the number of basis functions. For example, for the overlap integral, S_{ij}, symmetry considerations give:

$$S_{ij} = \langle x_i | x_j \rangle = S_{ji}$$

The value of the integral S_{ij} is then stored at position SM(I+J*(J-1)/2) of the one-dimensional vector SM.

Treatment of the four-index two-electron integrals is quite different. A four-dimensional array is out of the question for two reasons:

(i) such an array would have N^4 elements, permitting only the treatment of very small systems;

(ii) equalities among the integrals (ij|kl) permit considerable space saving; $1/8(N^4+2N^3+3N^2+2N)$ locations being used instead of N^4.

The equality of the integrals:

$$(ij|kl) = (ji|kl) = (ij|lk) = (ji|lk)$$
$$= (kl|ij) = (lk|ij) = (kl|ji) = (lk|ji) \qquad (1.147)$$

is independent of molecular symmetry; thus only *one* of the above need be computed and stored. The ordering convention used by ATMOL is:

$$i \geq j \; ; \; k \geq l \; ; \; [ij] \geq [kl] \qquad (1.148)$$

where $[ij] = \frac{1}{2}i(i-1) + j$. This converts the 4-dimensional matrix (ij|kl) to a pseudo-2-dimensional matrix.

The integrals are stored in blocks, the steps in the process being:

(i) assign a block of storage in fast store (a "buffer") for the temporary storage of the integrals;

(ii) set up loops ranging over i, j, k and l satisfying the ordering convention;

(iii) using the current labels i, j, k, l, and the input (i.e., molecular geometry, orbital specifications, etc.), compute the current integral $(ij|kl)$;

(iv) store the computed integral in the buffer; if it fills the buffer, go to (v); if not, go to (vi);

(v) write contents of buffer to disk (or tape) file;

(vi) increment i,j,k,l consistent with the ordering convention;

(vii) if the loops on i,j,k and l are exhausted, go to (viii); if not, go to (iii);

(viii) close the integral storage file and finish.

The values of the labels i,j,k and l are stored in the file together with the value of the integral $(ij|kl)$; this allows zero integrals to be omitted from the file.

1.8.3 The SCF Procedure for the Closed-Shell Case

The SCF calculation proceeds in an iterative way, each iteration including essentially three steps:

(i) building the Fock matrix (1.74);

(ii) solving the pseudoeigenvalue equation (1.73);

(iii) recognising whether or not self-consistency has been reached; if not, a new set of trial vectors ($\mathbf{C}$ in (1.73)) must be defined as input for the next cycle in the iteration.

Each of these steps requires some auxiliary calculations such as the formation of the density matrix ρ (1.79) from a given set of vectors C_m; the calculation of the total energy E (1.83) at each iteration; and an orthonormalization process to ensure that the set of trial vectors is orthonormalized. In this section, some of the general computational aspects of these points will be discussed, with explicit reference to the ATMOL programs where relevant.

Building of the Fock matrix requires the density matrix, ρ (1.79), and a list of two-electron integrals, $(ij|kl)$, calculated making use of the integral equalities of (1.147) and ordered using (1.148). The general term of the Fock matrix from (1.81) may be written as:

$$F_{ij} = h_{ij} + G_{ij} = h_{ij} + \sum_{kl} \rho_{kl} \left[2(ij|kl) - (ik|jl) \right] \quad (1.149)$$

Since the reading of an external file is a slow process, it is necessary to list all the contributions of a given integral $(ij|kl)$ to the G matrix; since this is symmetric, only the lower half ($j \leq i$) need be considered. It is then possible to write a simple algorithm for the formation of the G matrix.[76]

Two techniques are currently used for the solution of the Roothaan equation. The first, probably easier, way for closed-shell systems, transforms the problem into a standard eigenvalue problem by subjecting the basis set to a Löwdin orthogonalization;[17] the eigenvalues and eigenvectors of the real, symmetric matrix are then obtained by one of the many available techniques, such as Jacobi diagonalization. Both these topics have been outlined in previous sections, and will

not be further discussed here. The second technique in use, the Single Vector Diagonalization (SVD);[77] is an iterative method by which a more accurate eigenvector of the Roothaan equation is calculated from some trial eigenvector. This technique is of interest when only a few eigenvectors are wanted (as in atomic calculations), or when one has to be sure to pick the right eigenvector out of many possible solutions. In this case, starting with some trial vector which is known to represent a good approximation to the solution ensures the right choice amongst many solutions. This has been found useful for the open-shell problem, and the multi-configuration problem.

In the SCF procedure, one starts with a set of trial vectors which are input to the calculation, calculates the density matrix ρ from these eigenvectors, and then the Hamiltonian, to obtain new eigenvectors. The process is repeated until the input and output vectors agree within a certain threshold. This procedure raises three different points of interest which will be commented on in turn:

(i) what choice of trial vectors can be made?

(ii) can the convergence be guaranteed, and speeded up?

(iii) how is SCF convergence recognized?

The choice of good initial vectors is the most obvious way to reduce the number of iterations, and reduces the possibility of trapping the solution in a local minimum. One trial choice is a set of zero vectors: although this may lead to convergence, it is nevertheless a very poor choice. Trial vectors do not need to be accurate, but must have some

qualitative relationship with the final vectors. It is relatively easy to have fairly accurate trial vectors for molecular inner-shells from atomic calculations. In some cases, trial vectors may be obtained from the results of previous calculations either for molecular fragments, or a related molecule. For example, trial vectors for borazane (BH_3NH_3) could start with the SCF vectors of borane (BH_3) and ammonia (NH_3). ATMOL has flexible file-handling capabilities to facilitate such choices of starting vectors. In addition, ATMOL trial vectors may be formed by diagonalization of the one-electron Hamiltonian operator matrix. The vectors are ordered according to increasing eigenvalue. A better possibility in ATMOL is the generation of a set of trial vectors from the negatives of the expected values of the diagonal elements of the Fock matrix (in the basis set representation) at self-consistency. These values, termed ALPHAS, remain approximately invariant under change in molecular environment for a given basis set, and so a "library" of appropriate ALPHAS can be built up. For example, a study of methane will yield ALPHAS appropriate for carbon and hydrogen in other molecular environments for that particular basis set.

Extrapolation is an attempt to compute a better approximation to the SCF solution from the results of a few successive iterations. Thus:

Iteration number	Trial vector	Final vector	Energy
i	C_i	C_{i+1}	E_i
$i+1$	C_{i+1}	C_{i+2}	E_{i+1}

(1.150)

Let the complete set of vectors representing all the occupied orbitals be collected into one vector, C. Then C_i represents the approximate vectors where i denotes the iteration. The

difference of these vectors from the actual solution is $\Delta C_i = C_i - C$. One commonly used extrapolation procedure called the Aitken method is based on the assumption that each element of C approaches its limit with a geometric decrease of error. It is found that each component of the extrapolated SCF solution is obtained from the corresponding components of three sets of vectors, connected by two successive SCF iterations. Although useful, experience has shown that the scheme may fail in some cases, usually when the vectors are too far away from the exact solution. A general procedure called damping has been found useful,[78] and is used in ATMOL. It consists of scaling down the changes in the vectors produced by one iteration: thus, the input to the iteration i+2 will be taken as:

$$\begin{aligned} C &= \alpha C_i + (1 - \alpha)\, C_{i+1} \quad \text{if } E_i < E_{i+1} \\ \text{or} \quad C &= (1 - \alpha)\, C_i + \alpha C_{i+1} \quad \text{if } E_{i+1} < E_i \end{aligned} \tag{1.151}$$

where α, the damping factor, is a positive number whose value is less than unity (typically 0.7).

An unconditional guarantee of convergence may be obtained according to a procedure proposed by Saunders and Hillier,[79] in ATMOL. For a 2n electron system with a basis set of m basis functions, a set of m - n virtual orbitals can be constructed such that all MO form an orthonormal set. Denoting the set of doubly-occupied MO (DOMO) as ϕ_1, and the set of virtual MO (VMO) as ϕ_2, then:

$$(\phi_1 \vdots \phi_2) = (\eta) \qquad (C_1 \vdots C_2) = \underline{\eta}\,\mathbf{C} \tag{1.152}$$

ROW VECTOR — COLUMN VECTOR — M X M MATRIX

It is perfectly possible to consider the basis set at any

iteration as being the set of trial MO at that iteration. In this new basis, (1.152) becomes:

$$(\phi_1 \vdots \phi_2) = (\phi_1 \vdots \phi_2) \begin{pmatrix} I & \vdots & 0 \\ \cdots & \vdots & \cdots \\ 0 & \vdots & I \end{pmatrix} \qquad (1.153)$$

where I is a unit matrix. Arbitrary but small variations in the DOMO may be written as:

$$\phi_1' = (\phi_1 \vdots \phi_2) \begin{pmatrix} I \\ \cdots \\ \Delta \end{pmatrix} \qquad (1.154)$$

where ϕ_1' denotes the row vector of perturbed DOMO, I is the identity matrix of order n, and Δ is the (m-n) x n mixing matrix, whose elements are arbitrary but presumed "small". This equation (1.154) clearly does not consider mixing amongst the trial DOMO, since the total wavefunction and energy are invariant to such mixing. With these variations, the DOMO remain orthonormal to first order, since their overlap matrix is given by:

$$\mathbf{S} = \underline{\phi}_1'^{\dagger}\,\underline{\phi}_1' = (I \vdots \Delta^{\dagger}) \begin{pmatrix} \phi_1 \\ \cdots \\ \phi_2 \end{pmatrix} (\phi_1 \vdots \phi_2) \begin{pmatrix} I \\ \cdots \\ \Delta \end{pmatrix}$$

$$= (I \vdots \Delta^{\dagger}) \begin{pmatrix} I \\ \cdots \\ \Delta \end{pmatrix}$$

$$= I + \Delta^{\dagger}\Delta \qquad (1.155)$$

From perturbation theory, the electronic energy change accompanying the variation in the DOMO may be written as:[80]

$$E' \rightarrow E_o + 4 \sum_{i}^{\text{occupied}} \sum_{k}^{\text{virtual}} \Delta_{ki} F^{\phi}_{ki} + \text{higher terms} \qquad (1.156)$$

where F^{ϕ}_{ki} stands for the matrix elements of the Fock operator in the basis set of the trial MO. Clearly, if values of Δ_{ki}

are chosen of opposite sign to corresponding F_{ki}^{ϕ} (making the first-order energy contribution negative), and sufficiently small so that the higher terms in (1.156) are smaller than the first-order term, the energy of the perturbed wavefunction will not be higher than that of the unperturbed function. This would give a method of guaranteeing convergence to a stationary point on the energy surface, though not necessarily the ground state.

Performing an iteration using the basis set of the trial MO is easily achieved by construction of the Fock matrix $\mathbf{F}^{\eta}$ and transforming it to the MO basis by a similarity transformation:

$$\mathbf{F}^{\phi} = (C_1 \vdots C_2)\ \mathbf{F}^{\eta}\ (C_1 \vdots C_2)$$

$$= \begin{pmatrix} C_1^{\dagger}F^{\eta}C_1 & \vdots & C_1^{\dagger}F^{\eta}C_2 \\ \cdots\cdots & \vdots & \cdots\cdots \\ C_2^{\dagger}F^{\eta}C_1 & \vdots & C_2^{\dagger}F^{\eta}C_2 \end{pmatrix} \qquad (1.157)$$

For the purpose of this analysis, the diagonal blocks of $\mathbf{F}^{\phi}$ are assumed to be diagonal. Consider now the diagonalization of a matrix identical to $\mathbf{F}^{\phi}$, save that the elements of the off-diagonal blocks $C_1^{\dagger}F^{\eta}C_2$ and $C_2^{\dagger}F^{\eta}C_1$ have been multiplied by a small positive factor, λ, corresponding to a damping factor of the type in (1.151). If λ is sufficiently small to allow first-order perturbation theory to be used, the result of the diagonalization may be written in the form of (1.154), where:

$$\Delta_{ki} = \frac{\lambda F_{ki}^{\phi}}{F_{ii}^{\phi} - F_{kk}^{\phi}} \qquad (1.158)$$

It has been assumed that the "aufbau" principle ($F_{kk}^{\phi} > F_{ii}^{\phi}$) has been obeyed. In this situation, then, the Δ_{ki} *will* be of opposite sign to the corresponding F_{ki} in (1.156); however, it is not possible to guarantee that the magnitudes of Δ_{ki} be sufficiently small to assure convergence. Furthermore, if the trial wavefunction is far from convergence, then the analysis is less clear, since the application of first-order perturbation theory may be invalid. However, convergence may be ensured by adding a positive constant b to the diagonal elements of the block $C_2^{\dagger}\ F^{n} C_2$ in $\mathbf{F}^{\phi}$, to give a modified or "level-shifted" Hamiltonian:

$$\mathbf{F}^{\text{mod.}} = \begin{pmatrix} C_1^{\dagger}F^{n}\ C_1 & \vdots & \lambda C_1^{\dagger}F^{n}\ C_2 \\ \cdots\cdots & \vdots & \cdots\cdots\cdots \\ \lambda C_2^{\dagger}F^{n} C_1 & \vdots & C_2^{\dagger}F^{n}\ C_2 + bI_2 \end{pmatrix} \qquad (1.159)$$

where I_2 is the unit matrix of order m-n.

This modified matrix is now diagonalized, and the resulting eigenvectors ordered according to the "aufbau" principle on the resulting eigenvalues. First-order perturbation theory now yields:

$$\Delta_{ki} = \frac{\lambda F_{ki}^{\phi}}{F_{ii}^{\phi} - F_{kk}^{\phi} - b} \qquad (1.160)$$

The damp factor λ is normally chosen to be unity. If b is chosen positive and sufficiently large:

(i) the first-order perturbation theory used will be valid;

(ii) no swapping of MO can occur from one iteration to the next;

(iii) all Δ_{ki} have the opposite sign to the corresponding F_{ki};

(iv) all Δ_{ki} will be sufficiently small to ignore higher order terms in (1.156).

Thus, for a sufficiently large level-shifter b, the output wavefunction energy will be lower than or equal to the input wavefunction energy, providing an unconditional guarantee of convergence to some stationary point on the energy surface.

To prevent any build-up of round-off errors, a Schmidt orthonormalization of the trial vectors is performed after each iteration. Note that trial vectors are needed for the whole set of MO (both occupied and virtual) in the level-shifting procedure. Also, orbital energies of the VMO will be displaced upward by an amount equal to the level-shifter: this is taken into account by the ATMOL routines. This level-shifting procedure has been found efficient for a large number of systems. Relatively large values of the level-shifter ($\sim$4 to 5 a.u.) are used in the first few iterations when the trial vectors are rather inaccurate. After a few cycles, however, the use of large values slows down the convergence unnecessarily and smaller values ($\sim$0.3 to 1.0 a.u.) are typically used.

If, for each component of all the vectors corresponding to the occupied orbitals, the computed value at a given iteration differs from the value used in building the Fock matrix by less than an appropriate threshold, the calculation is said to have converged. However, this method has some drawbacks: if the threshold is set too stiffly, an otherwise perfect calculation may be rejected because it "diverges"; if set too loosely, the results will be unnecessarily inaccurate. Generally, programs will look for vector convergence only after

some convergence for the energy value has been achieved, since this converges much more rapidly than the vectors. The relationship between the total energy and orbital energies (1.87) may also provide a test for the achievement of self-consistency. The magnitude of the off-diagonal elements between occupied and virtual orbitals of the Fock matrix in the MO basis may also be considered, since they are zero at convergence.

1.8.4 The SCF Procedure for the Open-shell Case

With respect to many points, the SCF calculation will proceed for the open-shell case in the same way as for the closed-shell case. However, since there are now two sets of equations (see sections 1.4.2 and 1.4.3), the program will deal with the closed- and open-shell equations, either simultaneously or successively, at each iteration. In this respect, the computational burden is potentially twice that of the closed-shell case. Furthermore, an optimal use of fast store is now needed to handle the many matrices which appear in the construction of the Fock matrices.

The open-shell calculations reported in this thesis were carried out using the ATMOL RHF SCF program. This minimizes the energy of a single-determinantal wavefunction constructed from doubly- and singly-occupied MO. The aims of this program[73] and those of Roothaan[18] are identical in all cases where the state studied is not orbitally degenerate. In the case where states are orbitally (spatially) degenerate, the ATMOL program yields MO which optimally describe only one component of the degenerate manifold, whilst Roothaan's procedures yield MO which are used to construct the set of degenerate wavefunctions. Thus, the ATMOL programs always minimize

a one-component energy expression of the form:

$$\langle \Psi | \hat{H} | \Psi \rangle \Big/ \langle \Psi | \Psi \rangle \tag{1.161}$$

whereas Roothaan's procedures minimize

$$\left(\sum_{i=1}^{g} \langle \Psi_i | \hat{H} | \Psi_i \rangle \Big/ \langle \Psi_i | \Psi_i \rangle \right) \Big/ g \tag{1.162}$$

where each wavefunction Ψ_i is constructed from a common set of MO, and g denotes the state degeneracy. In general, the energy of a degenerate state produced by ATMOL will be lower than that given by Roothaan's procedure. Furthermore, the discontinuities in the energy surface with Roothaan's "symmetry equivalenced" procedures when Jahn-Teller distortions of the molecular geometry are studied, do not occur using the sptaially unrestricted methods of ATMOL. However, the total wavefunction produced by ATMOL may not be an eigenfunction of all the symmetry operators which commute with the total Hamiltonian, whilst that produced by the methods of Roothaan will.

A "level-shifting" technique to permit guaranteed convergence for the open-shell case has been developed[81] as a logical extension of the closed-shell case discussed in the previous section. The single Hamiltonian procedure of Roothaan is included as a special case of the energy-minimization scheme. The general strategy adopted is similar to the closed-shell case; the situation is more complicated, however, due to the presence of singly-occupied MO (SOMO) as well as DOMO and VMO. This means that the single Hamiltonian

matrix defined in the MO basis (analogous to (1.159) for the closed-shell case) now has three distinct damp factors λ, and two level shifters b. This is a consequence of the fact that mixing is now possible between VMO and DOMO; VMO and SOMO; and DOMO and SOMO. The appropriate Hamiltonian matrix is diagonalized, and after suitable ordering, the resulting eigenvectors are used to define iterated MO as linear combinations of the trial MO. Ordering may be according to the "aufbau" principle, or by the use of a LOCK directive, which causes iterated MO to be selected on the principle of maximum overlap with the trial MO. This directive is particularly useful in the study of excited states, such as the core hole state species encountered in the calculation of core binding energies, as outlined in the following chapter.

CHAPTER TWO

X-RAY PHOTOELECTRON SPECTROSCOPY

2.1 Introduction

In this chapter a brief description of the basic processes and theory of X-ray Photoelectron Spectroscopy (XPS) will be presented. Although of considerable interest and importance, photoelectron spectroscopy of valence electrons using relatively low-energy photons (say, less than 100 eV) - commonly referred to as Ultraviolet Photoelectron Spectroscopy (UPS) - will not be treated *per se* here: it has been extensively reviewed elsewhere.[82,83] After introducing the fundamental processes involved in XPS, mention will be made of the instrumentation involved, and of the main features of the spectra obtained. There are presently several excellent texts available giving full coverage of the technique,[84-89] in addition to the key works of Siegbahn et al.[90,91] The remainder of the chapter will concentrate on the various methods for the calculation of electron binding energies (BE) and relaxation energies (RE). The emphasis will be on *ab initio* quantum mechanical methods, although brief mention will be made of many-body perturbation theory approaches. Several detailed review articles are available on the theoretical aspects of XPS.[92-96]

2.2 Processes involved in XPS

The technique of XPS, as used today, was developed and named ESCA (Electron Spectroscopy for Chemical Applications) by Siegbahn and coworkers in Uppsala in the 1950's, although some earlier investigations (notably by Robinson[97] and de Broglie[98]) into the energies of photoelectrons emitted from

samples irradiated by X-rays had previously been carried out. A recent review[99] describes the development of XPS from 1900 to 1960, whilst much of the early work of the Uppsala group is well-documented in the two ESCA books of Siegbahn.[90,91]

2.2.1 Photoionization

In XPS, the sample being studied is irradiated with a monoenergetic beam of soft X-rays, typically $Mg_{K\alpha_{1,2}}$ or $Al_{K\alpha_{1,2}}$ with energies of 1253.7 and 1486.6 eV, respectively. Electrons which have a binding energy less than the energy of the exciting radiation may be photoemitted, allowing the study of both core and valence electron-levels. The total kinetic energy of the emitted photoelectron, KE (which may include contributions from the vibrational, rotational and translational motions), is given by:

$$KE = h\nu - BE - E_r \qquad (2.1)$$

where $h\nu$ is the energy of the incident photon,

h is Planck's constant,

ν is the frequency of the X-ray radiation,

BE is the binding energy of the photoemitted electron, defined as the positive energy required to remove an electron to infinity with zero kinetic energy,

and E_r is the recoil energy of the sample.

The recoil energy is usually negligible, except where high-energy X-rays are used with light atoms (e.g., for Li using $Al_{K\alpha}$ (1486.6 eV) and $Ag_{K\alpha}$ (22,000 eV), the recoil energies are 0.1 and 2 eV, respectively).[90] The effect has been studied in some detail by Cederbaum and Domcke,[100] who have

recently shown that the vibrational band envelopes in the XPS spectra of molecules differ from those predicted by the Franck-Condon principle; energy shifts in the $Al_{K\alpha}$ excited electron bands of up to several tenths of an eV due to recoil-induced vibrational and rotational excitation, in addition to the translational recoil energy of the molecule, have been predicted. However, in this work, since comparison is generally made with experimental data using low-energy X-rays ($Al_{K\alpha}$ or $Mg_{K\alpha}$) pertaining to molecules containing atoms higher in the Periodic Table than lithium, the recoil energy is neglected, and the equation for the BE of an electron in a gaseous sample (2.1) reduces to:

$$KE = h\nu - BE \qquad (2.2)$$

The complementary technique of UPS is based on the same principles, and normally employs He I radiation (21.22 eV), although other radiation (mainly He II (40.8 eV))[101] has been used. Typically, only the outer valence-electrons can be studied; however, since the total line-widths in UPS ($\sim$0.015 eV) are much less than those in XPS ($\sim$1 eV), vibrational fine-structure may be resolved. This is both the principle advantage of UPS over XPS, since it allows considerable information to be derived concerning the nature of the valence orbitals, which determine the chemical and physical properties of the molecules, but also a drawback, since the assignment of each band in the UPS spectrum of a molecule may be a very difficult task.

2.2.2 Relaxation, Shake-up and Shake-off

Figure 2.1 shows schematically the relationship between direct photoionization, relaxation and shake-up in XPS.

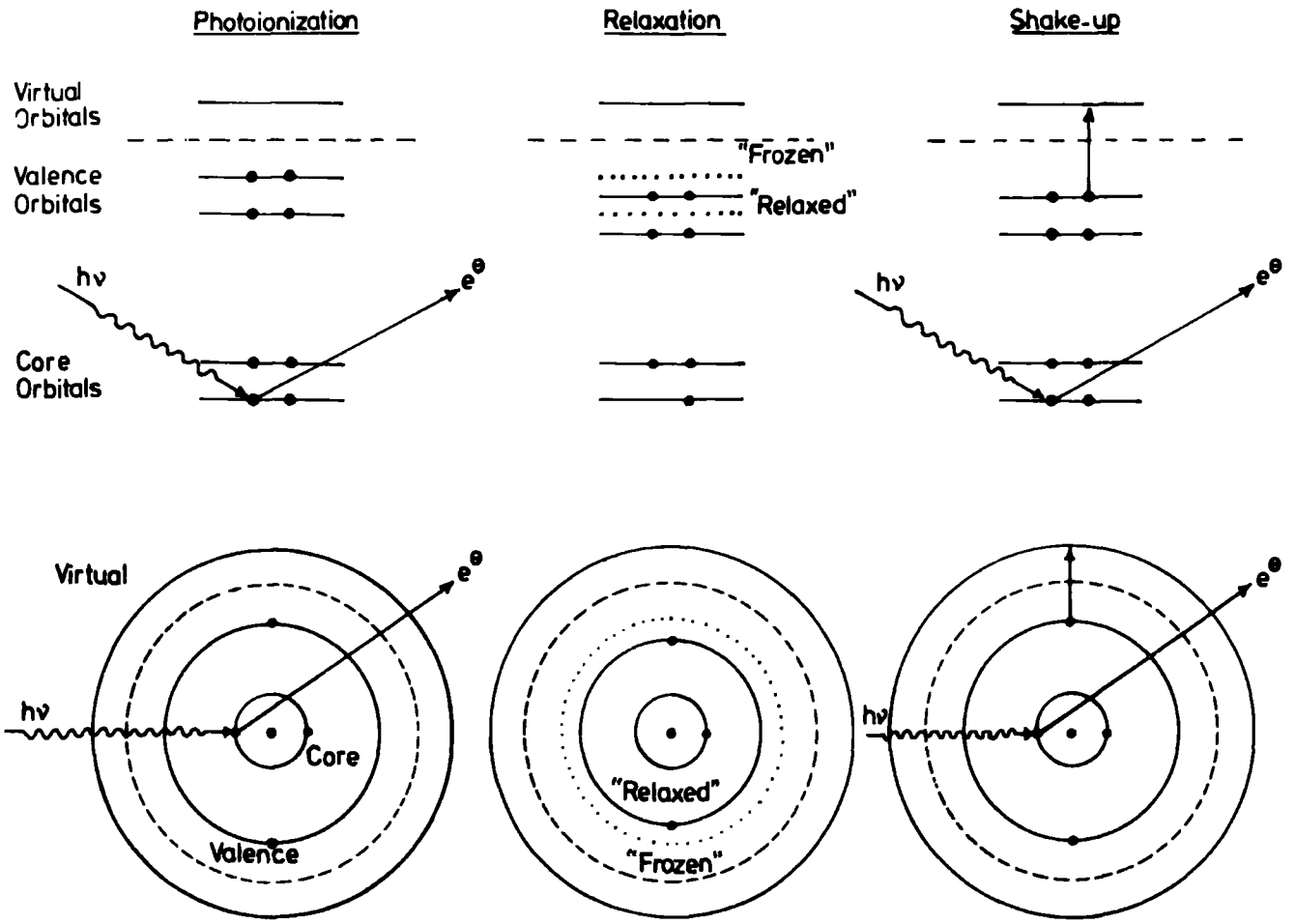

Fig.(2.1) A schematic representation of the basic processes in XPS.

Although core-electrons are sufficiently localized in space in the proximity of the nucleus not to take any part in bonding, the major contribution to the total energy of an atom or molecule arises from its core-electrons, which closely monitor valence-electron distributions. The removal of such a tightly-bound core-electron, which is almost completely screening as far as the valence-electrons are concerned, leads to substantial electronic reorganization or "relaxation" accompanying core-ionization, predominantly associated with the valence-electrons; although it is convenient to conceptually separate

the processes of photoionization and relaxation, they should strictly be regarded as occurring concurrently. This relaxation process is a sensitive function of the electronic structure of the molecule, and is of considerable importance in determining not only the absolute BE of a core-electron, but also in determining the lineshapes of observed peaks by means of vibrational fine-structure. These and other aspects of the relaxation process will be considered in some detail in subsequent chapters of this thesis.

The sudden perturbation of the valence-electron cloud accompanying core-ionization gives rise to a finite probability for photoionization to be accompanied by simultaneous excitation of a valence-electron from an occupied orbital to a virtual orbital (shake-up), as illustrated in Figure (2.1), or even simultaneous emission of a valence-electron (shake-off). This gives rise to satellite peaks on the low kinetic-energy side of the direct photoionization peak, which may be thought of as arising from excited states of the core-hole state species. Thus, a revision of (2.2) is needed to account for these multi-electron processes:

$$KE = h\nu - BE - \bar{E} \qquad (2.3)$$

where $\bar{E}$ is the energy of the multi-electron process. In the sudden approximation, transition intensities are directly related to the sums of one centre overlap terms involving the occupied orbitals of the initial system and virtual orbitals of the hole-state species. Thus, the probability of exciting an electron from the orbital denoted by nlj of the neutral atom, to the orbital n'lj of the ion, is given by:[102]

$$P_{n'lj \leftarrow nlj} = N \left| \int \psi^{*}_{nlj} \, \psi'_{n'lj} \, d\tau \right|^2 \qquad (2.4)$$

where N is the number of electrons in orbital nlj

and ψ_{nlj}, $\psi'_{n'lj}$ are the wavefunctions of orbitals nlj, n'lj in the atom and ion respectively.

It follows that excitations to these states follow monopole selection rules:

$$\Delta J = \Delta L = \Delta S = \Delta M_J = \Delta M_L = \Delta M_S = 0 \qquad (2.5)$$

Considering excitations involving a core hole state in the doublet manifold, as depicted in Figure 2.2, it is clear that within a simple orbital model, there are two

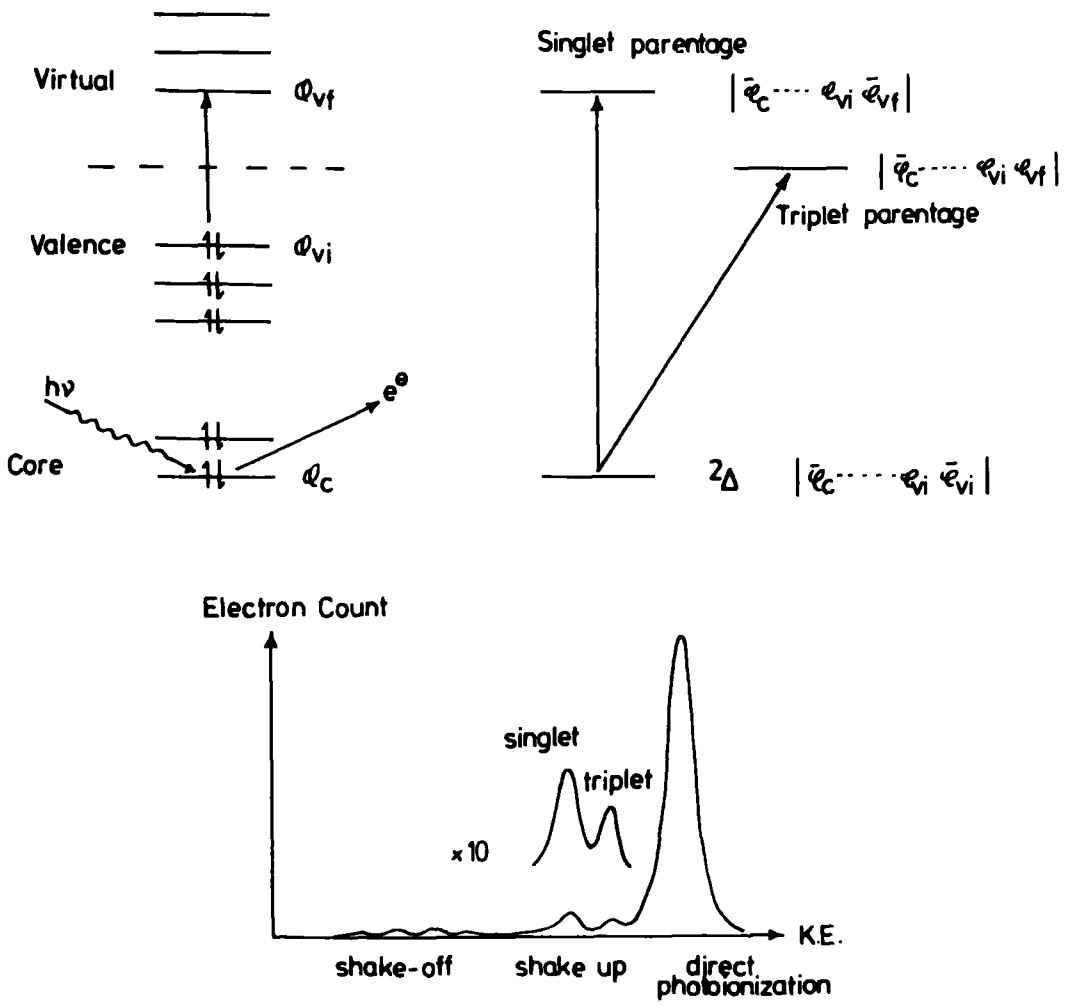

Fig.(2.2) Schematic illustration of single-triplet shake-up

possibilities. Either the unpaired electron in the valence-level and that excited to the virtual orbital will have opposite spins ("singlet origin"), or they both have the same spin, whilst the remaining core-electron has the opposite spin ("triplet origin"). This "triplet" state is lower in energy than that of singlet origin; however, since both represent doublet states, transitions from the groundstate of the core hole state may be viewed as both being allowed. In principle, therefore, it should be possible to experimentally observe the energy-separations and intensities for the components of the shake-up states of a given excitation configuration, the singlet state naively being expected to be the more intense. Of course, the detailed theoretical interpretation of shake-up states[103] is by no means as simple as has been portrayed here, but this simplistic model provides an adequate starting-point for discussions in subsequent chapters.

The relationship between relaxation and shake-up and shake-off has been clearly elaborated by Manne and Åberg.[104] Shake-up and shake-off transitions obey monopole selection rules; if there were no relaxation accompanying core-ionization, clearly such transitions would have zero intensity, since eigen-functions of the same Hamiltonian corresponding to different eigenvalues are orthogonal. Manne and Åberg showed that the weighted average over the direct photoionization and shake-up and shake-off peaks corresponds to the BE appropriate to the unrelaxed system (given by Koopmans' theorem), illustrated schematically in Figure 2.3. Since RE fall within a narrow range for a given core-level (e.g., for C_{1s}, a typical BE for a neutral system is $\sim$290 eV, whilst RE might typically fall in the range 12 ± 2 eV), it is clear that shake-up and shake-

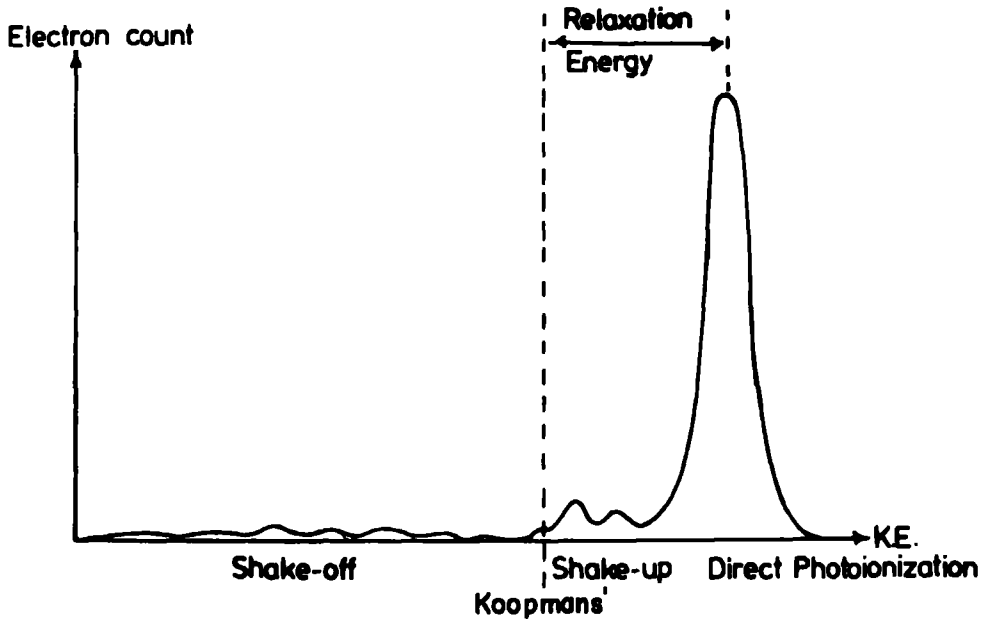

Fig.(2.3) The relationship between RE, Koopmans' theorem and the direct photoionization and multi-electron satellite peaks.

off are perfectly general phenomena present in every system; only the weighting coefficients (probabilities) for each transition vary from system to system. Transition probabilities for high-energy shake-off processes should be relatively small, and thus transitions of highest probability will fall reasonably close to the weighted mean. In principle, the RE should be available from experiment, provided all of the relevant shake-up and shake-off processes can be estimated in terms of energies and intensities. In practice, this is not feasible, since the overall situation is considerably complicated by the presence of the general inelastic tail, arising from photoemission from a given core-level, followed by energy loss by a variety of scattering processes. This gives rise to a broad energy distribution, usually peaking (for organic systems) $\sim$20 eV below the direct photoionization peak, generally obscuring any underlying high-energy shake-off processes, at least in the solid state.

2.2.3 Auger Emission and X-ray Fluorescence

Core-ionization leaves an atom or molecule in a highly excited state: de-excitation of the hole-state may occur by both fluorescence and Auger processes, as illustrated schematically in Figure 2.4. Auger emission may be viewed

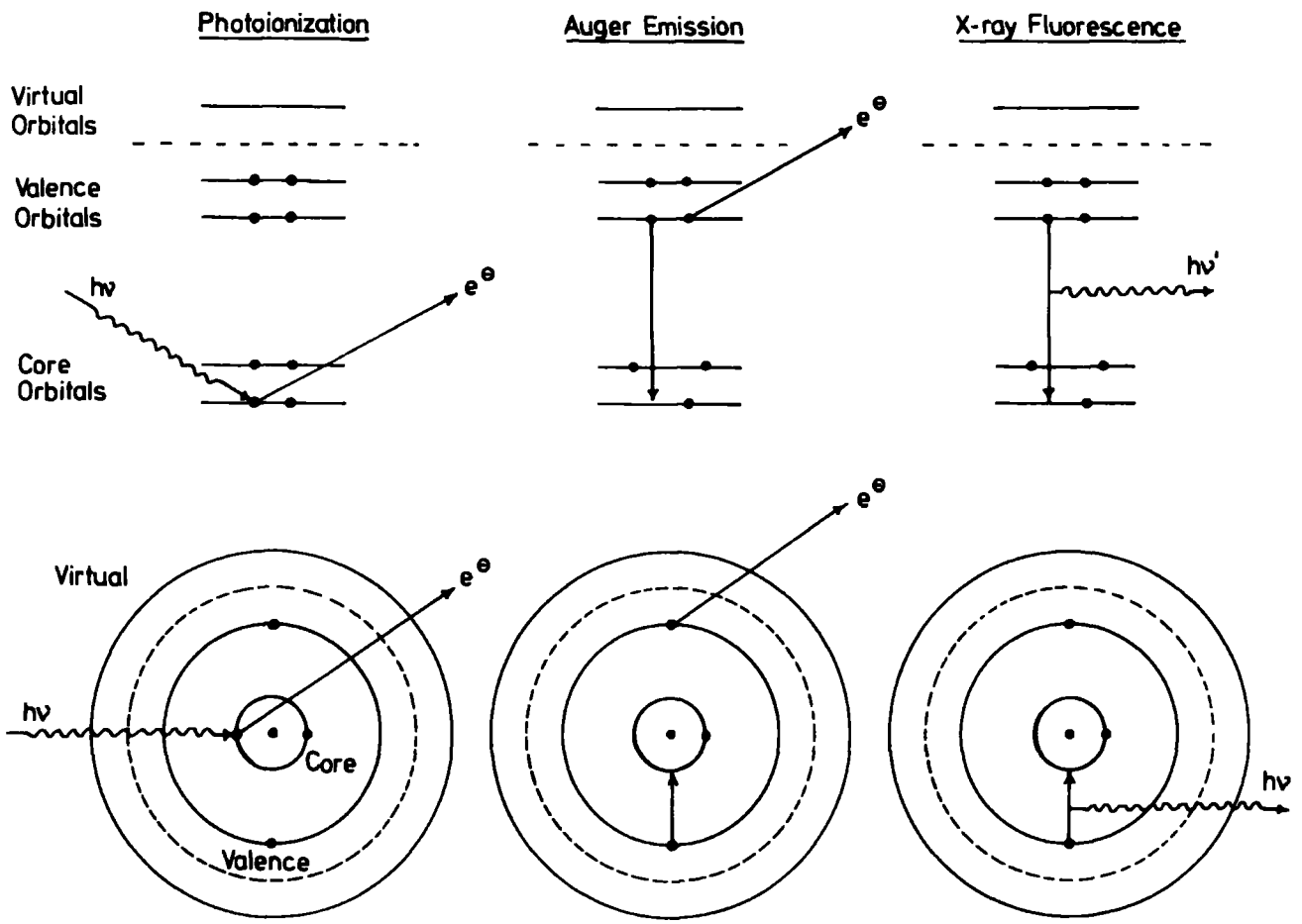

Fig.(2.4) De-excitation of a core hole state by Auger and X-ray Fluorescence.

as a two-step process, in which the ejection of a core-electron by a photon is followed by an electron dropping down from a higher (valence) level to fill the inner-shell vacancy, with the simultaneous emission of a second electron from some valence-shell.[105-110] Unlike shake-up or shake-off, which may be termed two-electron processes, Auger emission is a

three-electron process, involving a set of levels KLM. If one of the final vacancies is in the same shell as the primary vacancy, the process is known as a Coster-Kronig transition. This process is very efficient, leading to short life-times of the primary hole-state, with a concomitant broadening in the XPS spectrum.[109,110] The wavefunction overlap is such that the probability for Coster-Kronig processes is more than an order of magnitude greater than for Auger processes involving valence-electrons. For a Coster-Kronig process, the difference in the BE of the two inner shells must be sufficiently large to eject an electron from an orbital in a higher shell. This situation generally only arises in elements of atomic number greater than 40.

Auger electrons are also recorded in the XPS spectrum; however, since their energies are independent of the exciting radiation (provided it is sufficiently great to create the primary vacancy), they may readily be distinguished from photoelectrons by changing the energy of the exciting radiation. Chemical shifts have been observed in Auger spectra;[90] interpretation of Auger spectra may not be straightforward, however, since *differences* in energy-levels are involved. Auger Electron Spectroscopy (AES) as conventionally applied is based on the analysis of the energy of electrons that are ejected from a sample as a consequence of excitation by primary electron beams (typically $\sim$2 kV), rather than X-ray photons. This technique is truly a surface analysis technique in that the penetration depth for the exciting electrons is typically around 5 atomic layers. Under ideal conditions, atoms have been detected down to 10^6 atoms cm^{-3} at the surface.

The emission of X-rays instead of electrons leads to X-ray fluorescence (XRF), an excellent means of qualitative analysis for constituents of atomic number greater than eight. Concentrations of 0.1% for most elements, and 0.01% for elements around Fe, Co and Ni have been detected.[111] X-ray emission is very inefficient for the lighter elements, and negligible for energies less than 500 eV, with Auger emission being more probable, as illustrated in Figure 2.5. Auger efficiency is approximately comparable to X-ray emission at about 2000 eV.

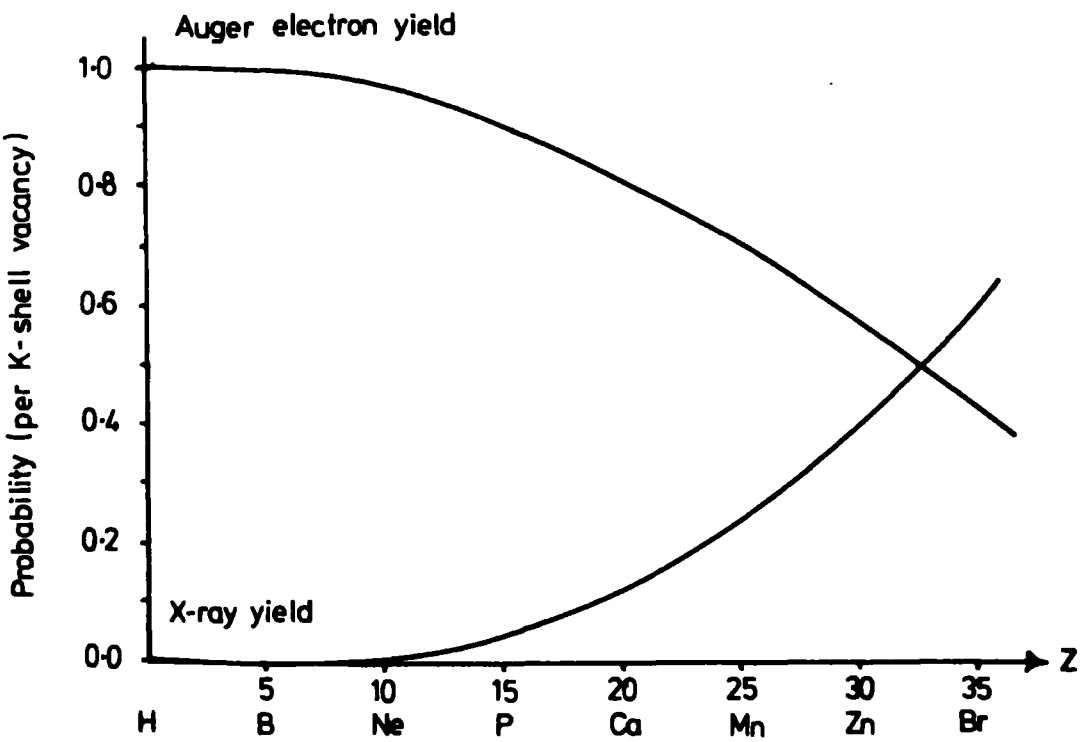

Fig. (2.5) Probability of Auger Electron Emission and X-ray Fluorescence as a function of Atomic Number.

2.3 Instrumentation

The first commercial XPS instrument appeared in 1969; since that time, several designs have been placed on the market. A schematic of the essential components of a typical XPS spectrometer (an A.E.I. ES200 AA/B) is given in Figure 2.6.

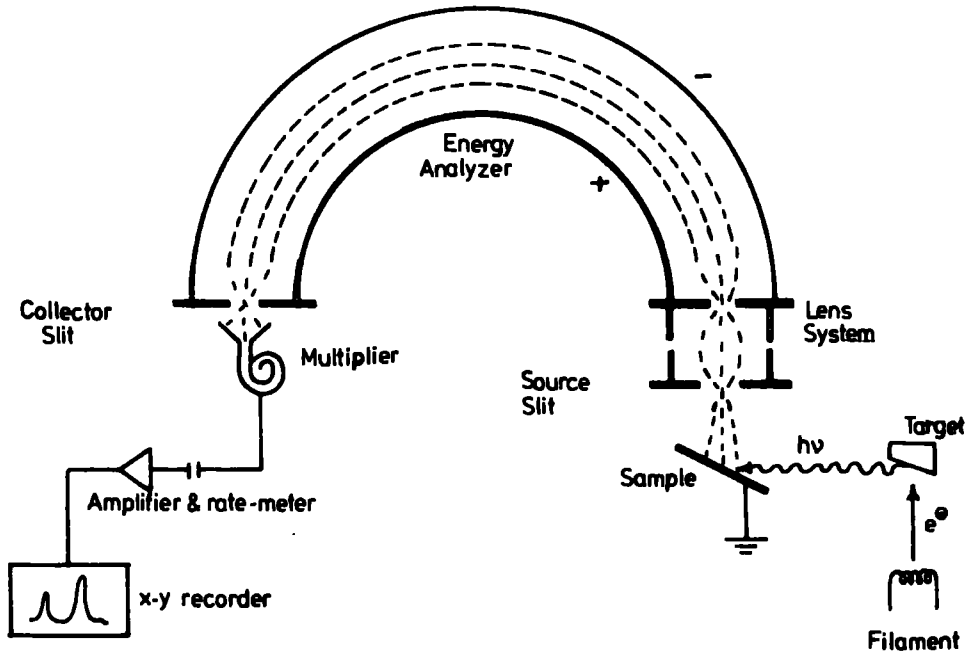

Fig.(2.6) A schematic of XPS instrumentation

2.3.1 X-ray Generator

The most commonly-used X-ray sources are non-monochromatized $Mg_{K\alpha_{1,2}}$ (typical operating conditions: $<10^{-5}$ torr; 12 kV, 15 mA) and monochromatized $Al_{K\alpha_{1,2}}$ ($<10^{-6}$; 15 kV, 35 mA). The X-ray flux is of the order of 0.1 rad/sec.,[112] which for the majority of samples causes little or no radiation damage. The component linewidths for non-chromotized X-ray sources in the case of Mg and Al targets are ∿0.7 eV and 0.9 eV, respectively.[90] In the case of the Al source, the linewidth may be reduced by monochromatization,[91] thereby improving resolution, and eliminating unwanted background and X-ray satellites. The wavelength λ of $Al_{K\alpha}$ radiation is 8.34 Å, and by diffraction from the $(10\bar{1}0)$ plane of quartz at an incident angle θ of 78.5°, the required conditions for the Bragg equation:

$$n\lambda = 2d \sin\theta \quad \text{where} \quad \begin{array}{l} n \text{ is an integer} \\ d \text{ is the interatomic spacing} \end{array} \qquad (2.6)$$

are satisfied.[91] After separating the $Al_{K\alpha}$ radiation from the background, the linewidth may be reduced by one of three techniques:

(a) 'slit-filtering' (passing through a slit);

(b) 'dispersion compensation' (passing through a lens system to allow for the peak-shape of the Kα radiation);

(c) 'fine-focussing' (using an electron-gun and a rotating anode).

In principle, an ultimate linewidth of 0.2 eV can be attained by these techniques.

2.3.2 Sample Region

The sample region of the spectrometer is separated from the X-ray generator by a thin (∿0.003") Al window, which ensures that electrons scattered from the target or filament in the X-ray gun do not enter the sample region. Samples may be studied on the tip of a probe, which may be inserted into the sample region via a system of insertion locks without letting the sample region up to atmosphere; however, this limits the base-pressure of the system to $\sim 10^{-8}$ torr. The probe-tip may be heated to over 250°C, or cooled by using liquid nitrogen, and can be oriented in the X-ray beam to obtain maximum signal intensity, or to perform angular dependent studies. Solid samples are mounted on the probe-tip usually by means of double-sided 'Scotch' insulating tape. The facility for cooling the sample probe-tip allows liquid or volatile solid samples to be studied in the condensed phase, whilst gases may be analyzed directly, using a leak value.

2.3.3 Analyzer

The electron energy analyzer on the A.E.I. ES 200 AA/B is a hemispherical double-focussing electrostatic analyzer,[113] enclosed within two mu-metal cans for magnetic shielding. The resolution of the analyzer is given by:

$$\frac{\Delta E}{E} = \frac{R}{W} \qquad (2.7)$$

where E is the energy of the electrons;

R is the mean radius of the hemisphere;

and W is the combined widths of entrance and exit slits.

Resolution can thus be improved by reducing the slit widths (which also reduces the signal intensity); increasing the radius of the hemispheres (increases engineering difficulties and creates pumping difficulties); or by retarding the electrons before they enter the analyzer.

The overall resolution, $\Delta E_m/E$, also depends on contributions from sources other than the analyzer:

$$(\Delta E_m)^2 = (\Delta E_x)^2 + (\Delta E_{el})^2 + (\Delta E_s)^2 \qquad (2.8)$$

where ΔE_x is the width of the X-ray line inducing the emission;

ΔE_{el} is the natural width of the electron energy distribution in the level being studied;

and ΔE_s is the line-broadening due to spectrometer irregularities.

2.3.4 The Detector and Data Acquisition

The electrons passing through the collector slit are detected by an electron multiplier, and the pulses obtained are amplified and fed into the counting electronics. Spectra may be generated by one of two methods:

(a) the continuous scan, in which the electrostatic field is increased from the starting kinetic energy continuously, while the signals from the multiplier are monitored by a rate-meter. If the signal is sufficiently strong, and the signal to background ratio sufficiently high, then the spectrum (a graph of counts per second vs. electron kinetic energy) is plotted out directly on an x-y recorder.

(b) the step scan, in which the field is increased by pre-set increments (typically 0.1 eV): at each setting, either a fixed number of counts may be timed, or the counts may be measured for a fixed length of time. The data so obtained is stored in a multi-channel analyzer (MCA), so that many scans can be accumulated to average random fluctuations in the background.

2.4 Reference Levels

It is important to understand the relationship that exists between BE observed experimentally by XPS for solids, as opposed to free molecules, and values calculated theoretically by *ab initio* LCAO MO SCF treatments. The most convenient reference level for a conducting sample is the Fermi level,[90] defined in a metal as the highest occupied level. The work-function for a solid, ϕ_s, is defined as the energy gap between the free electron (or vacuum) level and the Fermi level in the solid. Since the sample and spectrometer are in electrical contact, their Fermi levels are the same; however, the vacuum levels for the solid and the spectrometer may be different, and then the electron will experience either an accelerating or retarding potential equal to $\phi_s - \phi_{spec}$, where ϕ_{spec} is the work-function of the spectrometer.[114,115] In XPS, it is the kinetic energy KE of the electron when it enters the analyzer that is

measured; this will in general be different from the kinetic energy KE' which it had on emerging from the sample. Taking zero BE to be at the Fermi level of the sample gives (from (2.2)):

$$BE = h\nu - KE - \phi_{spec} \qquad (2.9)$$

This is illustrated in Figure 2.7.

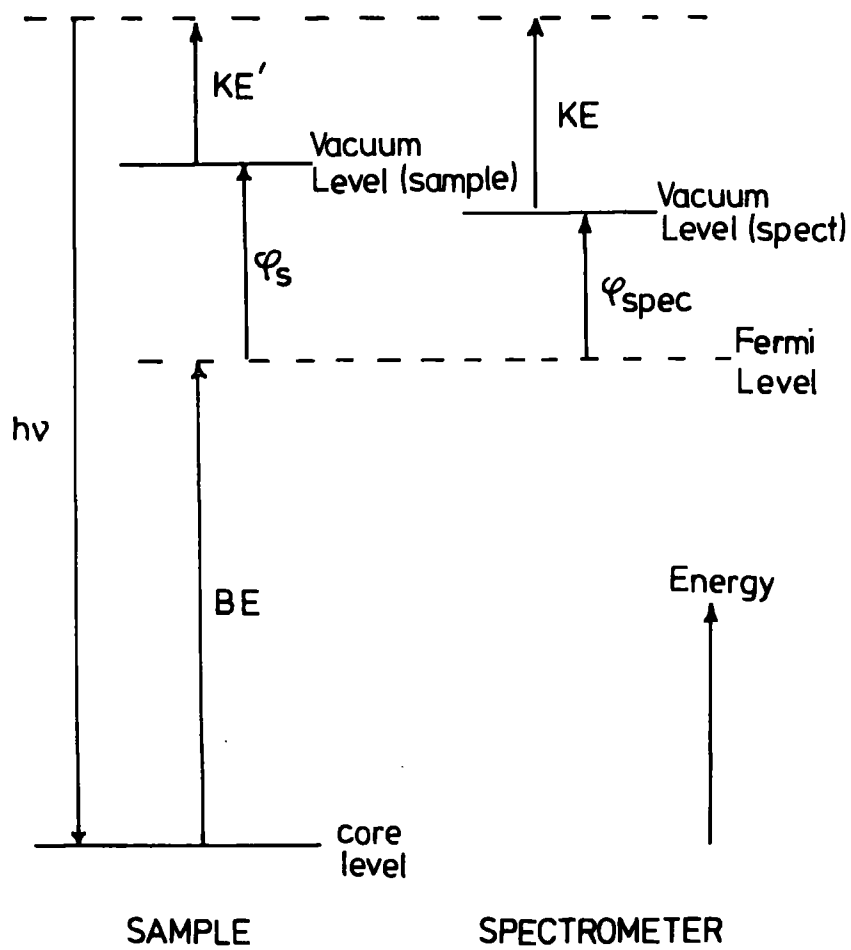

Fig. (2.7) BE reference level in solids.

The BE referred to the Fermi level does not depend on the work-function of the sample, but only on that of the spectrometer, ϕ_{spec}; this represents a constant correction to all BE. In practice, the problem of extracting absolute BE is circumvented by the use of reference standards for calibration of the BE scale.[116]

2.5 Important Features of XPS Spectra

2.5.1 Binding Energies and Chemical Shifts

The BE of core-electrons, which are essentially localized, are characteristic of a particular element. Typical examples of approximate core-electron BE for some elements are shown in Table 2.1.

Table 2.1 Experimental core-level electron BE of the light elements (eV)[a]

	Li	Be	B	C	N	O	F	Ne
1s	57.2	115.6	191	289.3	409.9	543.1	696.7	870.4[b]
2s[b]	5.4	9.3	14.1	19.4	25.4	32.3	40.3	48.5
ϕ[c]	2.4	3.9		4.6				

	Na	Mg	Al	Si	P	S	Cl	Ar
1s	1074.0	1306.7	1562.4	1843	2153	2476	2827	3205.9[b]
2s	65.7	92.3	112.2	153	193	233	274	326.3[b]
$2p_{\frac{1}{2}}$	32.9	53.2	77.3	104	140	169	206	250.6[b]
$2p_{3/2}$	32.6	52.9	76.9	103	139	168	204	248.6[b]
ϕ[c]	2.3	3.7	4.2					

(a) All values are quoted from Ref. 117.

(b) These values are free-atom; all others are standard-state.

(c) The BE are quoted as referenced to the vacuum level: to obtain BE referenced to the Fermi level, the work-function ϕ must be subtracted. Where blank, the work-function is either not applicable, or negligible.

Knowledge of BE thus allows the ready detection or identification of elements in a sample.[90] Although some core-levels are too tightly bound to be studied with Mg or Al x-rays, there are generally less tightly bound core-levels which can be studied.

Variations of BE within a given core-level are a sensitive function of the electronic environment of an atom,[90,91,118] and thus differences in the electronic environment of a given atom in a molecule give rise to a small range of BE, or *chemical shifts*, often representative of a particular structural feature. The classic illustration of chemical shifts is the C_{1s} spectrum of ethyl trifluoroacetate,[91] Figure 2.8. Shifts in BE of over 10 eV have been observed for a given level. Models for the interpretation of chemical shifts will be discussed in more detail later. For a given core-level (with due allowance for any shake-up or shake-off processes), the peak intensities are proportional to the number of atoms in a particular environment.

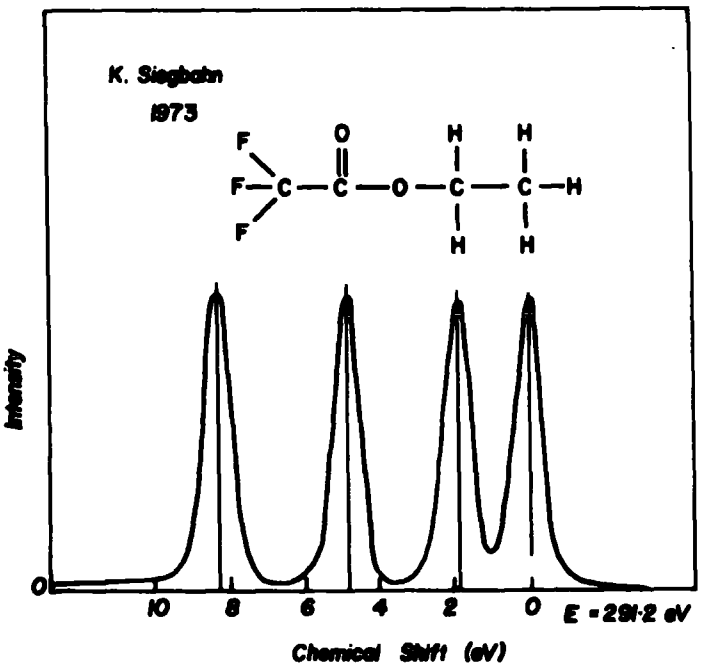

Fig.(2.8) C_{1s} spectrum of ethyl trifluoroacetate.

2.5.2 Multiplet Splitting

Multiplet splittings in XPS occur if the system being studied contains unpaired electrons, since exchange interaction affects core-electrons with differing spins in a different way.[119] The interpretation is relatively straightforward

only for s hole states.[120] If S is the total spin of the 1^n configuration in the ground-state, then the two possible final states have a total spin of $S \pm \frac{1}{2}$. The energy difference between the $S + \frac{1}{2}$ and $S - \frac{1}{2}$ states, ΔE, is proportional to the multiplicity of the ground state:

$$\Delta E = (2S + 1)\, K \qquad (2.10)$$

where K is the exchange integral between the core (c) and valence (v) electrons under consideration, defined by

$$K = \langle \phi_v(1)\, \phi_c(2) \mid 1/r_{12} \mid \phi_v(2)\, \phi_c(1) \rangle$$

The intensities of the peaks are proportional to the degeneracies of the final spin states, viz:

$$\begin{aligned} (2(S + \tfrac{1}{2}) + 1) : (2(S - \tfrac{1}{2}) + 1) &= 2S + 2 : 2S \\ &= S + 1 : S \end{aligned} \qquad (2.11)$$

Multiplet splittings in XPS have been discussed in detail by Fadley.[121] The magnitude of the splitting for a given ion can give valuable information concerning the localization or delocalization of the unpaired valence-electrons in compounds:[90,122,123] the greater the spin-density on an atom, the greater the splitting.

A simple example of multiplet splitting is provided by Siegbahn et al.[91] In a gas-phase study of N_2, NO and O_2, they found that whilst the N_2 molecule did not possess core-level splitting, the NO and O_2 molecules did, as shown in Figure 2.9. Thus, on photoemission from an O_{1s} or N_{1s} core-level in NO, the molecular NO^+ ion is left in either a triplet or singlet state. The splitting observed in the 1s spectra can be attributed to the exchange interaction between the core and unpaired 2π electrons, giving rise to different energies

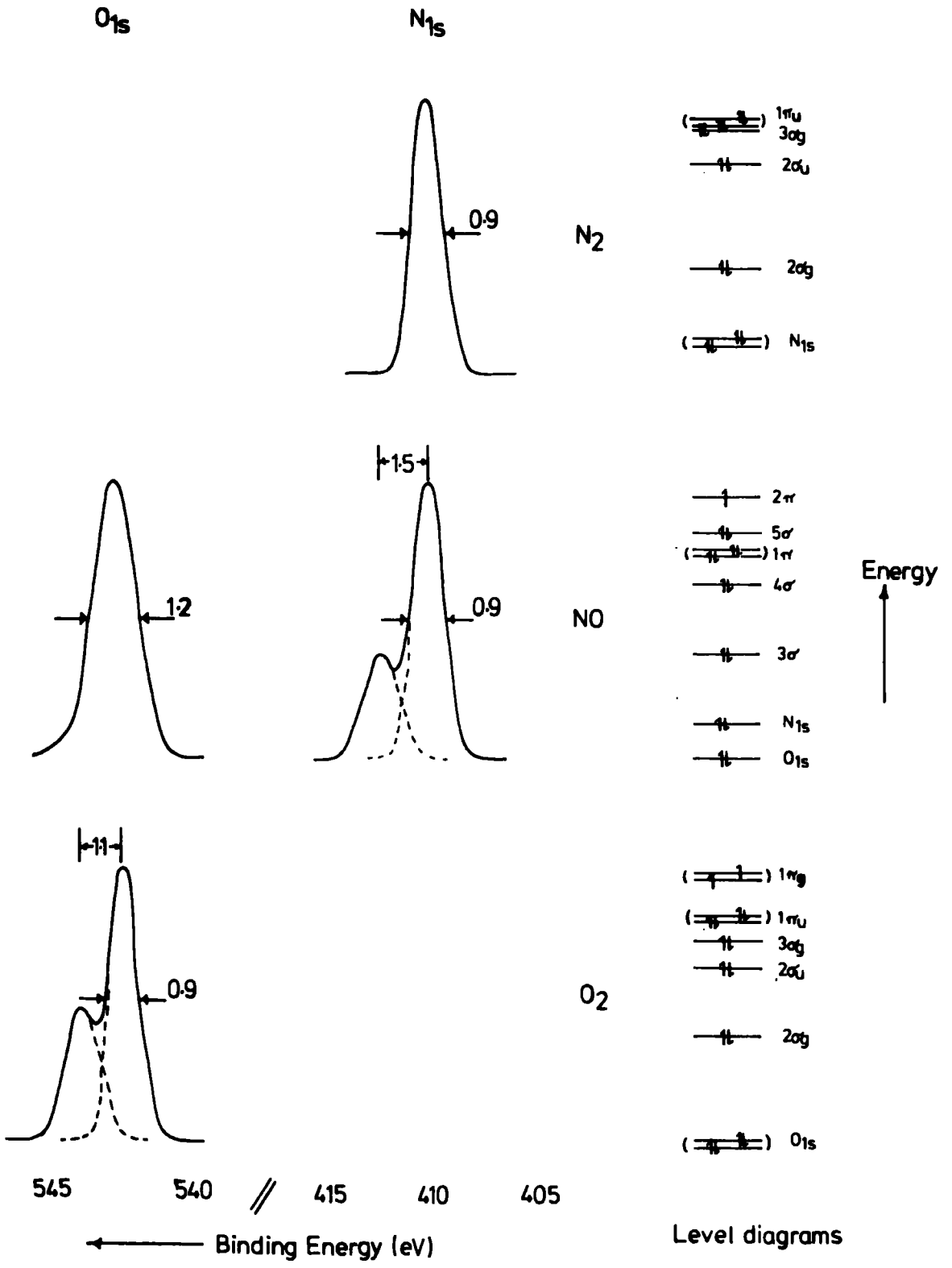

Fig. (2.9) O_{1s} and N_{1s} core-level spectra of N_2, NO and O_2

for those states. For the N_{1s} level, there is an energy separation of 1.5 eV; in the case of the O_{1s} level, the separation of 0.7 eV leads to line-broadening of 0.3 eV. A similar situation arises for the O_2 molecule.

2.5.3 Spin-Orbit Splitting

If photoionization occurs from an orbital with an orbital quantum number l greater than 1, then a doublet structure will be observed in the XPS spectrum.[90] This arises from coupling between the spin and angular moments, S and L respectively, giving rise to two possible values of the total momentum J for the hole-state formed. The intensities of the peaks in the doublet are proportional to the ratios of the degeneracies of the states (2J + 1). The relevant intensity ratios are shown in Table 2.2.

TABLE 2.2 Intensity Ratios for Different Levels

	Orbital quantum number	Total quantum number		Intensity ratio
	l	$J = (l \pm s)$		(2J+1) : (2J+1)
s	0	$\frac{1}{2}$		No splitting
p	1	$\frac{1}{2}$	$3/2$	1:2
d	2	$3/2$	$5/2$	2:3
f	3	$5/2$	$7/2$	3:4

2.5.4 Electrostatic Splitting

Splittings in the $5p_{3/2}$ levels of uranium and thorium metals and their compounds, and in some compounds of gold,[124,125] have been observed, and interpreted as arising from the differential interaction of the internal electrostatic field with the $M = \pm\frac{1}{2}$ and $M = \pm 3/2$ spin states of the $5p_{3/2}$

electrons. A definite correlation between this type of splitting, and the quadrupole splittings obtained in Mössbauer spectroscopy (arising from the interaction of the nuclear quadrupole moment with an inhomogeneous electric field),[126] has been found. Bancroft et al. have recently observed such splittings in the spectra of some tin compounds.[127]

2.5.5 Satellite Peaks

Satellite peaks arising from shake-up (and shake-off) processes occur on the low kinetic energy side of the direct photoionization peak. This has been discussed in section 2.2.2, and a detailed theoretical framework for calculating such satellite peaks has been given by Shirley.[128] Other satellite peaks may be observed:

(1) "Configuration Interaction" peaks arise whenever there are final states with the same symmetry and with energies close to, but greater than, the single hole-state energy.[129] They may be considered as arising from *doubly* excited states of the hole-state, as opposed to shake-up and shake-off, which are *singly* excited states. Such peaks have been observed in some alkali metal halides.[129,130]

(2) In solids, discrete peaks can arise from surface and bulk loss, and interband transitions.[90]

(3) In gases, satellite peaks may be caused by energy loss of the photoelectron after emission, if it undergoes a secondary collision with an atom or molecule, leading to excitation of that atom or molecule.[91]

(4) The X-ray source itself may be a cause of satellite peaks with a higher kinetic energy than the direct photoionization peak. These peaks are formed by the small percentage of $K_{\alpha_{3,4}}$ and $K_{\alpha_{5,6}}$ radiation,[91] but may be eliminated by monochromatization of the X-ray source.

2.5.6 Linewidths

The effects contributing to the total line-width ΔE_m have been discussed in (2.8). The natural full-width at half-maximum (FWHM) of the core-level under investigation, ΔE_{cl} and that of the incident radiation, ΔE_x, (unless monochromatization is used) depend on the Uncertainty Principle:[130]

$$\Delta E \cdot \Delta t \simeq h/2\pi \qquad (2.12)$$

where Δt is the lifetime of the state.

Some natural linewidths of core-levels derived from X-ray spectroscopic studies are given in Table 2.3. A linewidth of $\sim$1 eV corresponds to a life-time of approximately 6.6×10^{-16} s, from (2.12).[130] Table 2.3 emphasizes the fact that there is no particular virtue in studying the innermost core-level: for Au, for example, the halfwidth of $\sim$54 eV for the 1s level would swamp any chemical shifts.

TABLE 2.3 Approximate natural linewidths, ΔE_{cl}, for some core levels (eV).

Level	S	Ar	Ti	Mn	Cu	Mo	Ag	Au
1s	0.35	0.5	0.8	1.05	1.5	5.0	7.5	54
$2p_{3/2}$	0.10	-	0.25	0.35	0.5	1.7	2.2	4.4

2.6 Methods for the Calculation of Binding Energies and Relaxation Energies

2.6.1 Koopmans' Theorem

In the derivation of the Hartree-Fock equations (Section 1.3.1), Lagrangian multipliers ε_{pq} are introduced to guarantee that all pairs of Hartree-Fock orbitals ϕ_p and ϕ_q will be orthogonal.[131] Upon solution of the HF equations, only the diagonal elements ε_{pp} have non-zero values. These diagonal elements are generally designated ε_p and called *orbital energies*; Koopmans' Theorem[132] states that these orbital energies for a closed-shell system may be associated with the BE (or ionization potentials) of the atom or molecule for which the SCF wavefunction has been obtained:

$$BE = -\varepsilon_p \tag{2.13}$$

More precisely, the orbital energy may be written as:

$$\begin{aligned} \varepsilon_p &= I(\phi_p|\phi_p) + \sum_q^M \left[2(\phi_p\phi_p|\phi_q\phi_q) - (\phi_p\phi_q|\phi_p\phi_q)\right] \\ &= h_{pp}^{\phi} + \sum_q^M (2J_{pq}^{\phi} - K_{pq}^{\phi}) \end{aligned} \tag{2.14}$$

Consider now a two-step process:

(1) Calculate an SCF wavefunction for a neutral molecule, and evaluate its total energy using (1.41):

$$E = 2\sum_p^M h_{pp}^{\phi} + \sum_p^M \sum_q^M (2J_{pq}^{\phi} - K_{pq}^{\phi})$$

(2) Using the SCF orbitals from the above neutral molecule calculation, remove one spin-orbital and evaluate the single determinantal energy of the resulting

positive ion.

Koopmans showed that the energy difference (or ionization potential) calculated in this way is just the orbital energy ε_p given by (2.14).

The defects of using Koopmans' Theorem as a quantative model for BE are well known:[133] it does not allow for the reorganization or "relaxation" of the remaining electronic structure upon ionization; nor does it include any accounting for defects inherent in the MO model itself, viz., correlation and relativistic corrections. Nevertheless, this simple model has many useful qualitative and semi-quantative applications. In particular, although core-orbital energies will not represent quantatively the *absolute* values of core BE, provided a physically balanced basis set of double zeta quality or better is used,[134] and provided the relaxation, correlation and relativistic corrections are constant or vary in a regular manner, a reasonable quantative description of *shifts* in BE within a series of molecules can be obtained. This is illustrated in Table 2.4, from which it is clear that there is considerable

TABLE 2.4 C_{1s} BE shifts for fluoromethanes from Koopmans' Theorem (in eV)[a]

Molecule	STO-3G	STO-4.31G	"Double Zeta"[b]	Experimental
CH_4	0(305.43)[c]	0(304.35)[c]	0 (304.95)[c]	0 (290.7)[c]
CH_3F	4.21	3.08	2.80	2.8
CH_2F_2	8.47	6.47	5.86	5.6
CHF_3	12.81	10.05	9.13	8.3
CF_4	17.26	13.61	12.43	11.0

(a) Values taken from ref. 135.

(b) A (9s 5p/5s 3p) basis set, contracted according to the principles outlined by Dunning,[49] of approximately Double Zeta quality.

(c) Absolute binding energy.

basis set dependence in the BE shifts. Even for the "double zeta" basis set, however, the shift between CH_4 and CF_4 is overestimated by some 20%, and absolute values of the BE are considerably overestimated.

2.6.2 The ΔSCF Method and Relaxation Energy

The major drawback of Koopmans' Theorem, as far as calculations of core BE are concerned, is that it relies solely on the *ground-state* properties of the wave-function; however, the BE also depends on the properties of the final (ionized) state. In the ΔSCF method, the BE of an electron is calculated as the difference between the energies of the ground-state and ionized state of an atom or molecule:

$$BE = E^{*}_{HF} - E_{HF} \qquad (2.15)$$

where the asterisk indicates a vacancy in a core-level. However, for the hole-state calculations, there is no absolute guarantee that variational upper bounds to the true total energies for the ionized species are obtained, since the computed hole-states are not necessarily orthogonal to all lower energy states of the same symmetry.[136] They are, therefore, strictly speaking not protected from variational collapse. The ATMOL suite of programs discussed previously (Section 1.8) allows one to force a core-orbital to be singly occupied; the core-hole configuration can then be "locked" to that of the ground-state, with initial trial MO for the hole-state being taken as the ground-state eigenvectors. The core hole states are found to be so far away from other bound states of the ionized system that there is no attempted "mixing", and are thus not subject to variational collapse.[134,135]

Bagus[136] first performed ΔSCF calculations for various ions of Ne and Ar; Schwartz[137] carried out the first calculations of this type on molecules (the first-row hydrides). As shown from the examples given in Table 2.5, the hole-state results are in good overall agreement with the experimental values, and appear to confirm Bagus' contention that single-configuration SCF wavefunctions can provide practical, but not rigorous upper bounds to the energies of inner-shell hole-states.[136]

TABLE 2.5 Δ SCF BE for 1s ionization in first-row hydrides (in eV)

Molecule	GTO basis[a]	"Double Zeta"[b]	Hartree-Fock[c]	Experimental[d]
CH_4	292.8	291.0	290.8	290.7
NH_3	407.6	405.7	-	405.6
H_2O	541.6	539.4	539.1	539.7
HF	-	693.3	-	694.2[e]
Ne	872.2	868.8	868.6	870.2

(a) Ref. 138

(b) (10s 5p / 6s 3p) for central atom; (5s / 2s) for hydrogen atoms: ref. 137

(c) CH_4, ref. 139; H_2O, ref. 140; Ne, ref. 136

(d) Ref. 91

(e) Ref. 141

In molecules containing no equivalent centres, there is no doubt of the localized nature of the core-hole. However, many molecules of interest have several equivalent sites for the core-hole, e.g., N_2, C_2H_2, C_2H_4, F_2. The problem therefore arises of whether the core-hole is localized, or delocalized over the equivalent sites. With this in mind, Bagus and Schaefer[142] performed calculations on the localized

and delocalized 1s hole-states of O_2. They found that the hole-state calculations with gerade or ungerade symmetry imposed on the 1s hole-state gave a BE of 554.4 eV, whereas relaxing the symmetry restriction (equivalent to a localized 1s hole on an oxygen atom) gave a BE of 542.0 eV, in reasonable agreement with the experimental value of 543.1 eV. There is now a large body of evidence in the literature in favour of a localized description of core hole-states.[142-146] It should be noted, however (as pointed out by H. Siegbahn),[146] that the difference in the energies of localized and delocalized hole-state species for a given system disappears when a CI procedure (which takes correlation into account) starting from either localized or delocalized Hartree-Fock wavefunctions, is adopted.

The largest defect in Koopmans' Theorem for core-orbitals is the neglect of electronic relaxation. The relaxation (or reorganization) energy, RE, may be defined as the difference between the BE of an electron described by Koopmans' Theorem, and the ΔSCF method:

$$RE = (-\varepsilon) - \Delta SCF\ BE \qquad (2.16)$$

The physical interpretation of the relaxation process is clear: following photoionization from a core-level, the remaining valence-electrons in the atom or molecule will experience an increased nuclear potential. This will cause the electrons to "relax" or reorganize, to minimize the energy of the system. Since Koopmans' Theorem uses the ground-state wavefunction only, no account is taken of the change in spatial distribution of the electrons caused by photoionization; for the ΔSCF calculations, however, this effect is explicitly considered. The relationship between Koopmans' Theorem, ΔSCF BE and experimental BE is shown in Figure 2.10.

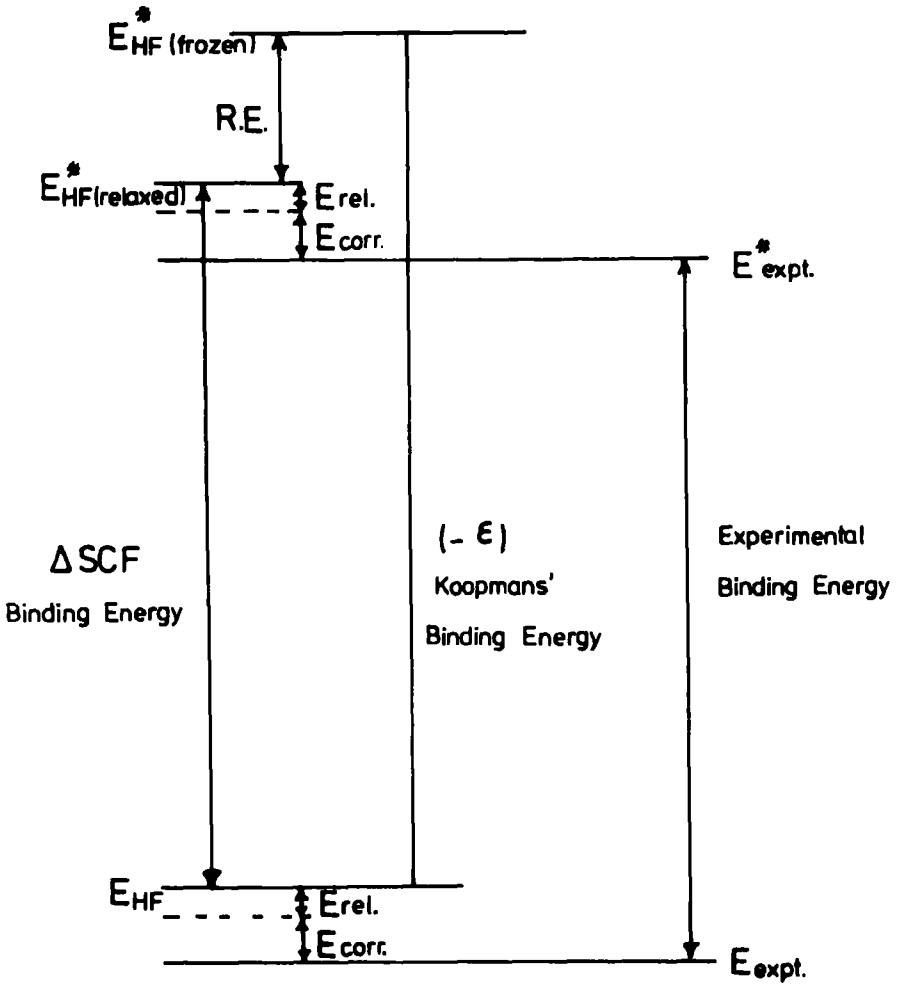

Fig. (2.10) The relationship between Koopmans' Theorem, Δ SCF and experimental BE.

Relaxation energies are by no means negligible for core-ionization, as illustrated for both atoms and molecules in Table 2.6. The change of nuclear potential caused by valence-electron ionization will be much smaller than for core-electron ionization, since valence-electrons have much smaller screening coefficients. This is reflected in the RE values, which are smaller by a factor of ten for valence-electron ionization. For example, the RE for O_{1s} and O_{2s} holes in water are calculated to be 15.3 eV and 2.2 eV, respectively, using a Slater double-zeta basis set.

TABLE 2.6 ΔSCF Relaxation Energies for some atoms and Molecules (in eV)

Atom	RE[a]	Molecule	RE[b]
B	10.6		
C	13.7	CH_4	13.9
N	16.6	NH_3	17.1
O	19.3	H_2O	20.0
F	22.0	HF	21.9
Ne	23.2		

(a) Ref. 147

(b) Ref. 137

Most of the electronic relaxation which occurs on core-ionization is associated with the valence-electrons. This point will be discussed in much more detail in subsequent chapters, but may be illustrated by considering the radial expectation values of various electrons, obtained from Hartree-Fock calculations on neon and its hole-states,[136] Table 2.7.

TABLE 2.7 Radial expectation values for electrons in Ne and its hole-states (in au)[a]

	Ground-state	1s hole	2s hole
$\langle r \rangle_{1s}$	0.1576	0.1545	0.1578
$\langle r \rangle_{2s}$	0.8921	0.8171	0.8536
$\langle r \rangle_{2p}$	0.9652	0.7993	0.8841

(a) Values taken from ref. 136

Removal of a 1s electron has little effect on the radius of the remaining 1s electron, but the outer electrons contract markedly. Since relaxation is associated largely with the valence-electrons, the RE would be expected to vary somewhat

with electronic environment. Indeed, a trend between shifts in BE and RE has been established for several series of molecules,[148,149] and this point will also be elaborated in subsequent chapters where it will become clear that in some series of molecules, it is the variation in RE that leads to changes in BE.

So far, it has been assumed that both the molecule and its core hole state are in their vibrational ground-states, and zero point energies have not been considered. Although vibrational fine-structure accompanying valence-ionization in UPS is well-documented and comparatively well-understood,[82,83] it is only with the advent of high-resolution XPS instrumentation, incorporating fine-focus X-ray monochromatization,[150,151] that the presence of vibrational fine-structure accompanying core-ionization, manifest as a broadening and asymmetry of the observed photoionization peak, has been observed. When a core-electron leaves a molecule, there will be a change (generally a decrease) in the bond-lengths; a new equilibrium bond-distance, with a different force constant, in the core-ionized species will replace the previous ground-state values. Two types of ionization potential may now be calculated:

(1) a vertical transition, which is a transition involving the most likely vertical change from a vibrational level $\nu'' = 0$ in the ground state. This implies that no changes in nuclear geometry occur during photoemission. This assumption is substantiated by consideration of the time-scale of photoemission ($\sim 10^{-17}$ s)[152] as compared with a typical vibrational frequency ($\sim 10^{-13}$ s)[153];

(2) an adiabatic transition, representing a change from a vibrational level $\nu'' = 0$ in the ground-state to a vibrational level $\nu' = 0$ in the core-ionized species.

The new, core-ionized potential contains various vibrational states which will be populated by Franck-Condon transitions. The Franck-Condon principle[154-156] gives the transition probability between vibrational states $\psi_{\nu''}$ and $\psi_{\nu'}$ as:

$$P_{\nu'',\nu'} \propto \left| \int \psi_{\nu''} \psi_{\nu'} d\tau \right|^2 \qquad (2.17)$$

These quantities are commonly referred to as Franck-Condon factors.

In the harmonic approximation, the Franck-Condon factors depend on the three parameters $\alpha_{\nu''}$, $\alpha_{\nu'}$ and $\Delta r = r_{\nu''} - r_{\nu'}$, where Δr is the difference in equilibrium bond-length, $\alpha_{\nu i} = (\mu k_{\nu i})^{\frac{1}{2}}/\hbar$, μ is the reduced mass for the system, and $k_{\nu i}$ is the molecular force constant for the state i. Thus, from knowledge of the potential surfaces (equilibrium bond-lengths, force-constants) for the ground and core hole states, and from the recurrence relationships defined by Ansbacher,[157] it is possible to compute the Franck-Condon factors. These may be used to quantatively explain line-structure in XPS peaks, as illustrated in Figure 2.11 for methane, using the CI calculations of Meyer,[139] and the experimental data of Siegbahn[158] et al. Further examples of such vibrational excitation will be discussed in subsequent chapters.

Since this thesis will largely be concerned with detailed studies of electronic relaxation phenomena, it is worthwhile emphasizing the importance of the relaxation process. Thus, relaxation is of considerable importance not only in determining the absolute BE of a molecule, but also in determining the overall lineshape of the observed peak by means of vibrational fine-structure. Furthermore, the relaxation process provides the perturbation which leads to the shake-up and

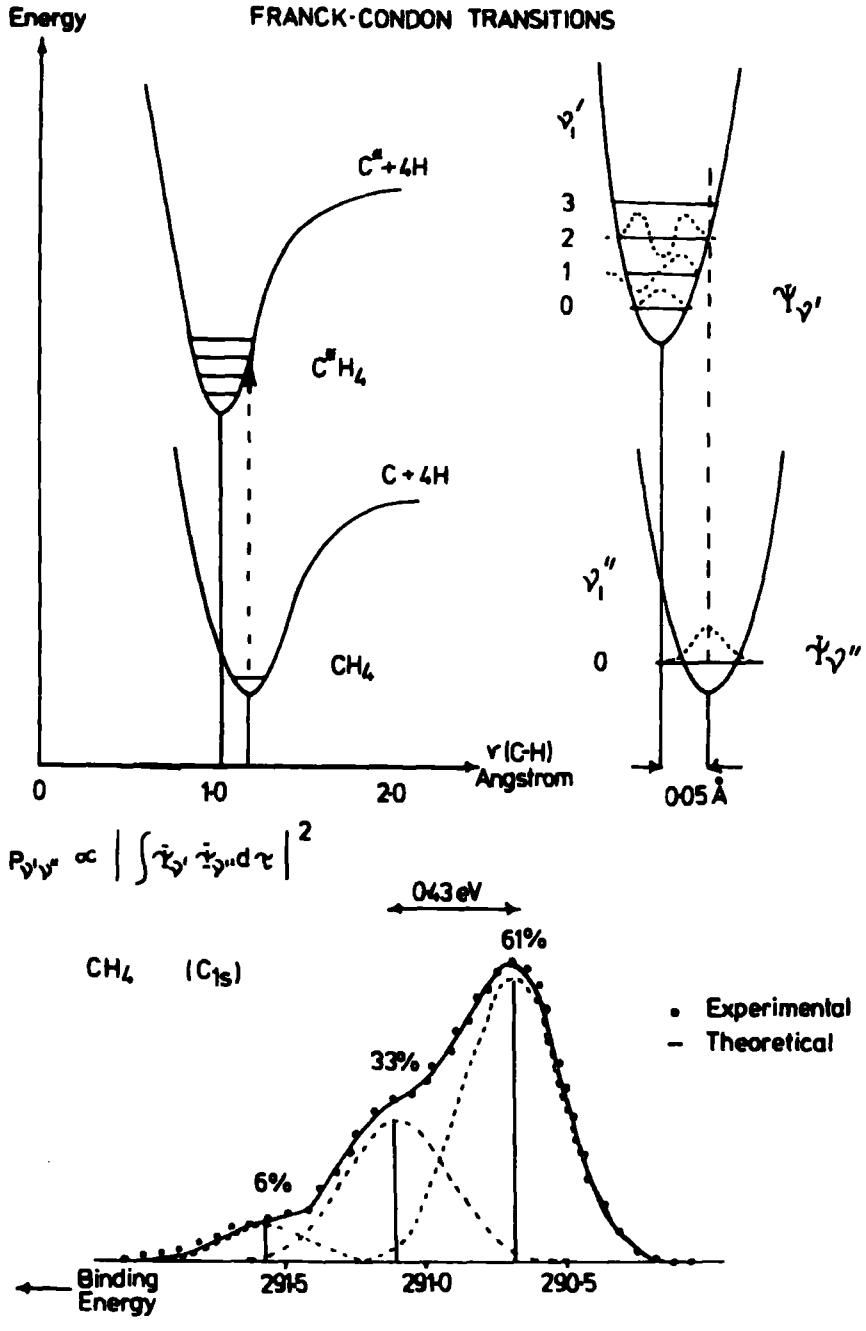

Fig.(2.11) A schematic representation of the vibrational excitation in methane, with the C_{1s} peak in methane

shake-off satellite peaks. A final feature of core-ionization of some interest is in the enhancement of weak interactions between or within molecules.

The failure of Koopmans' Theorem to agree with experimental BE need not solely be due to relaxation effects.

The BE may more precisely be defined as:

$$BE = \Delta E_{HF} + \Delta E_{cor} + \Delta E_{R} \qquad (2.18)$$

where ΔE_{HF} is the difference in the Hartree-Fock energies between the ground and core hole states, previously defined as the ΔSCF BE (2.15);

ΔE_{cor} is the difference in correlation energies;

and ΔE_{R} is the difference in relativistic energies.

Strictly, a term $\Delta E_{vib.}$, the difference between the vertical and adiabatic ionization potential, should also be included in (2.18); however, in the few cases where this has been investigated, $\Delta E_{vib.}$ is small enough to be ignored.[159]

In Section 1.7.2, it was pointed out that relativistic energies for light atoms are reasonably small. Shirley[93] has made rough estimates of the magnitude of the relativistic energies in atoms; he obtained, for example, estimates of ∿0.01 au and ∿1.2 au for C and Ar, which compare well with the accurate values of 0.01381 au and 1.76094 au obtained by Veillard and Clementi.[160] For reference, the relativistic energies (in eV) for the ground-states of first-row atoms are given here.[161]

Li	Be	B	C	N	O	F	Ne
-0.015	-0.060	-0.164	-0.376	-0.755	-1.344	-2.255	-3.570

It has generally been assumed that the relativistic contribution of any subshell is independent of the number of electrons in the outer shells, and simple $1s^2$ relativistic corrections are applied.[162] Generally, for core-ionization of first-row atoms, ΔE_{R} can be neglected,[163] although for heavier atoms, it may be of importance.

There have been few accurate correlated wave-function calculations for core-electron ionization. Some of these are summarized in Table 2.8.

TABLE 2.8 Correlation energy corrections to ΔSCF BE for 1s ionization (in eV)

System	Configuration	E_{cor}	Reference
C^{4+}	$1s^2$	1.24	164
C	$1s^2\ 2s^2\ 2p^2$	-0.21	165
CH_4	$1s^2\ 2a_1^2\ 1t_2^6$	-0.08	139
CO (C_{1s})	$1\sigma^2\ 2\sigma^2\ 3\sigma^2\ 4\sigma^2\ 1\pi^4\ 5\sigma^2$	0.41	159
O^{6+}	$1s^2$	1.24	164
O	$1s^2\ 2s^2\ 2p^4$	-0.24	165
H_2O	$1s^2\ 2a_1^2\ 1b_2^2\ 3a_1^2\ 1b_1^2$	0.50	140
CO (O_{1s})	$1\sigma^2\ 2\sigma^2\ 3\sigma^2\ 4\sigma^2\ 1\pi^4\ 5\sigma^2$	0.54	159
Ne^{8+}	$1s^2$	1.24	164
Ne	$1s^2\ 2s^2\ 2p^6$	0.60	166

It had been naively assumed that the nearly constant correction of 1.2 eV for the $1s^2$ He-like ions could be used to correct the ΔSCF BE (ΔE_{HF}) for correlation in all systems involving 1s ionization.[93,95] This is clearly not the case; the value of ΔE_{cor} is smaller for the molecules due to the contraction of the outer orbitals in these systems, resulting in an increase in the correlation energy of the core-hole species (compared to the He-like systems). Although ΔE_{cor} is relatively small, and may be ignored in many cases (particularly where BE shifts rather than absolute BE are being considered), the need for a careful, systematic correlation energy study for core-ionization in molecules is apparent.

2.6.3 The Equivalent Cores Approximation

It is generally recognized that core-electrons are closely bound to the nucleus, and that they are relatively inert and inaccessible compared to the valence-electrons. It is therefore reasonable to assume that the valence-electrons will be affected by the ionization of a core-electron in essentially the same way as they would by the addition of a proton to the nucleus. This approximation, in which an atomic core which lacks one electron is considered chemically equivalent to the complete core of the next element in the periodic table, is called the *equivalent cores* approximation. Use of this approximation in the prediction of chemical *shifts* in core BE was first reported in 1970 by Jolly and Hendrickson.[167] When the experimental thermodynamic data required to calculate BE shift are not available, SCF calculations on the molecules and ions in their ground-states may be used to obtain the required heats of reaction, and for the isodesmic reactions involved in the equivalent cores method, it has been found that even minimal (e.g. STO-3G) basis set calculations can reliably reproduce heats of reaction.[135,168]

As an example of the use of this approach, Table 2.9 shows the equivalent cores BE shifts in the CH_4 to CF_4 series. There is an improvement in accuracy as the basis set flexibility increases; the basis set dependence is much smaller than is the case for either Koopmans' Theorem (Table 2.4) or Δ SCF calculations. Furthermore, BE shifts are reasonably well-predicted even at the computationally modest STO-3G level, though they tend to be overestimated.

TABLE 2.9 Equivalent cores BE shifts for fluoromethanes (in eV)[a]

Molecule	STO-3G	STO-4.31G	"Double Zeta"	Experimental
CH_4	0	0	0	0
CH_3F	2.95	3.05	2.82	2.8
CH_2F_2	6.34	6.31	5.99	5.6
$CH F_3$	10.16	9.66	9.31	8.3
CF_4	14.37	12.92	12.64	11.0

(a) Values taken from ref. 135

An interesting development of this approach, first suggested by McWeeny and Velenik,[169] is the use of modest basis sets such as STO-3G or STO-4.31G using the ΔSCF method, but employing valence exponents of the equivalent core species for the core hole state wavefunction. This is an intuitively reasonable suggestion, since the valence-electrons of the core hole state and the equivalent cores species both experience a similar potential due to nucleus and core-electrons which will be different from that experienced in the neutral molecule. Indeed, a detailed investigation of basis set optimization for CO by Clark and Müller[130] led to the conclusion that for small basis sets (such as STO-4.31G), the calculated absolute BE with the optimum best-atom valence exponents on the core-hole atom is in close agreement with that calculated using valence exponents appropriate to the equivalent cores species. Basis sets using the valence exponents of the equivalent species for the core-hole atom are somewhat loosely referred to as "optimized" basis sets, and as illustrated in Table 2.10 for an STO-4.31G basis set, are found to give excellent values of the *absolute* BE. Differences in BE, however, are adequately described with "ordinary" ΔSCF calculations at the 4.31G level, certainly for molecules composed of first-row elements.

TABLE 2.10 The effect of using "optimized" valence exponents.[a]

Molecule	Unoptimized	"Optimized"	Experimental
CH_4	294.18	290.71	290.8
H_2O	545.49	539.12	539.4
CO (C_{1s})	300.78	296.71	296.2
CO (O_{1s})	548.47	541.89	542.3

(a) Values taken from ref. 149

2.6.4 Perturbation Theory Methods

The ΔSCF method, as an improvement on Koopmans' Theorem, is very successful for core-ionizations, where the dominant effect is the electronic relaxation. This is not the case for valence ionizations, however; here, although the ΔSCF method does represent the best one-configurational MO model, it does present some problems. Firstly, when there are many ionic states of the same symmetry in the same energy region, a single configuration is a poor quantative description of such near degeneracy, and there may be a tendency toward variational collapse to a lower-energy configuration of the same symmetry.[137,171] A second problem arises even when several ionic states are the lowest of their symmetries, but the SCF MO model contains different correlation defects for the different states. Here, the ΔSCF method may not even give the correct ordering of valence-electron BE. The next step in improving the calculations must take into account the electron correlation energy explicitly by some type of CI procedure, and several studies have now appeared, using for example the PNO-CI and CEPA methods of Meyer.[172]

Since the BE is a total energy difference between

two states, it has been of interest to calculate the difference *directly* by a perturbation-type calculation on a reference state, rather than by taking a relatively small difference between two separate calculations which are each subject to different kinds and magnitudes of errors. The study of valence-ionization by UPS has inspired several perturbation approaches. These include the Transition Operator Method of Gosinski and Pickup,[173] the Equations-of-Motion method developed by Rowe[174] and extended by Simons et al.[175] to describe ionization; Rayleigh-Schrödinger Perturbation Theory developed by Chong et al;[176] and Time-Independent Perturbation Theory developed and applied by Hubač and Kvasnička.[177] Several authors have used Green's function techniques to calculate corrections to Koopmans' Theorem. In particular, a general survey of the Green's function has been given by Csanak et al.,[178] and more specific aspects have been discussed by Linderberg and Öhrn.[179] Cederbaum et al.[180] at Munich have developed an approach based on the second-quantization formulation of many-body perturbation theory, in which the BE are found from the negative real parts of the poles of the one-particle Green's function. With a Hartree-Fock reference state for the perturbation scheme, the zero-order poles correspond to BE = $-\varepsilon_p$ for the occupied MO, which is just Koopmans' Theorem. First-order terms vanish in this formulation, and higher-order terms are analyzed by diagram techniques. The second-order expansion of the self-energy operator contains sums over three orbital indices, and it becomes increasingly difficult to consider higher-order expansions, though methods have been developed to do this.

From the calculations published,[180] this approach seems to be an attractive one. As an illustrative example,

the valence-level BE for N_2 calculated by various methods are shown in Table 2.11.

TABLE 2.11 Valence electron BE for N_2 (in eV)

Orbital	Koopmans' Theorem[a]	ΔSCF[a]	MBPT[b]	Experimental[c]
$3\sigma_g$	17.28	15.85	15.50	15.60
$1\pi_u$	16.75	15.50	16.83	16.98
$2\sigma_u$	21.17	19.80	18.59	18.78

(a) Ref. 181

(b) Ref. 182

(c) Ref. 82

This "direct" approach, rather than dealing with initial and final-state wavefunctions, is of use not only in the accurate calculation of BE, but also in the calculation of vibrational fine-structure, in both UPS and XPS, where the "traditional" calculation of separate accurate potential-energy surfaces for initial- and final-states would seem to be applicable only to the smallest polyatomic molecules. Finally, a "direct" approach would seem to have considerable promise for calculations of many-electron processes such as shake-up accompanying core-ionization, and the Auger process.[183]

CHAPTER THREE

SOME THEORETICAL ASPECTS OF PHOTOIONIZATION PHENOMENA INVOLVING THE CORE (1s) AND VALENCE (2s) LEVELS OF A SERIES OF ALKANES

Ab initio LCAO MO ΔSCF C_{1s} binding energies and relaxation energies have been computed at the STO-4.31G level for linear and branched alkanes (up to C_6) and are compared with experimental data. The structural dependence of binding energies and relaxation energies is discussed, and it is concluded that binding energy shifts in these alkanes (compared with methane) arise mainly from relaxation energy changes.

A similar study for the valence 2s binding energies and relaxation energies has been carried out. These orbitals are found to be sufficiently core-like in character to allow a reasonably good description of the binding energy shifts to be obtained at the ΔSCF level, even with a modest basis set.

Changes in equilibrium geometries and force constants consequent upon both core- and valence (2s)- ionization have been investigated for methane and ethane. Some comment on the relative line-broadenings found in the XPS spectra of these molecules is made, and some general comments for the higher members of the alkanes series are made based on Mulliken population analyses.

3.1 Electronic Relaxation Accompanying Core-Ionization

3.1.1 Introduction

For a given structural class of materials, it has been recognized for some time that absolute and relative

binding energies of core-electrons are subtly dependent on substitution patterns and that a significant proportion of differences in relative binding energies for a given core-level can arise from differences in relaxation energies accompanying core-ionization.[134,149] The factors which determine both absolute and relative binding energies for saturated hydrocarbons are sufficiently short-range in nature that the similarity in valence electronic environment about any given carbon atom compresses the total shift range into a narrow region of the binding energy scale, which for gas-phase samples extends over ∿0.6 eV (methane to tridecane).[184] Indeed, for a given hydrocarbon system with inequivalent carbons the shift is often so small that there are even ambiguities in assignments derived from line-shape analysis. Thus in the particular case of neopentane, correlation of binding energies with model systems led Thomas and co-workers[185,186] to assign the higher binding energy component to the carbons of the methyl groups; however the only detailed attempt at interpreting the data theoretically indicated that the overall line-shape could be equally well-fitted with the alternative assignment of the methyl carbons at lower binding energy.[187] To resolve such ambiguities, and to shed new light on changes in relaxation energy as a function of branching and chain-length in saturated hydrocarbons, the results of non-empirical LCAO MO SCF computations on the ground and localized core hole states of the series methane, ethane, propane, n-butane, n-pentane and n-hexane, and iso-butane and neopentane, are reported here.

The theoretical work described here complements the definitive experimental study of the absolute core binding

energies of a series of linear alkanes recently discussed by Siegbahn and co-workers.[184] By comparing the experimental shifts in core binding energies with those calculated from Koopmans' Theorem employing either STO-4.31G or STO-3G basis sets, it was inferred that the shift in binding energy in going from methane to hexane ($\sim$-0.5 eV) arises from the much larger relaxation energy associated with photoionization of core-electrons in the extended-chain molecule; this was qualitatively confirmed by direct estimates of relaxation energies using the transition potential model[173] within the CNDO/2 formalism. In this section, relaxation energies as a function of electronic environment are analyzed; it is shown that the conclusion previously drawn on the basis of the experimental studies is substantially correct.[184]

3.1.2 Computational Details

Previous investigations have shown that shifts in core binding energies, and differences in relaxation energies, are well-described at the STO-4.31G level, within the ΔSCF formalism.[135,149,170,188] Calculations have therefore been carried out on the ground- and localized core-hole states, using Clementi and Raimondi's best-atom exponents.[30] Where available, optimized geometries were taken from the literature;[189] however, for n-butane, isobutane, n-pentane and n-hexane, standard geometries were employed along the lines suggested by Pople and Gordon.[190] Calculations were carried out with the ATMOL[72,73] suite of programs, implemented on an IBM 370/195.

3.1.3 Results and Discussion

The calculated core binding energies and relaxation

energies are displayed in Table 3.1. Using the ΔSCF method with an STO-4.31G basis set, it is well-known that the absolute magnitudes of the relaxation energies tend to be slightly underestimated; as a result, the calculated absolute binding energies are somewhat larger than those determined experimentally. It is clear from the data displayed in Table 3.1 that the shifts in binding energy, both within a given molecule with inequivalent core-holes and between sites in different molecules, are small. Since the experimental data largely pertain to the peak maxima (centroids), which obviates any necessity of line-shape analysis, it is convenient to discuss the theoretical results on the same basis. Accordingly, Figure 3.1 shows a plot of the centroids of the calculated ΔSCF core binding energies and relaxation energies as a function of chain-length. The decrease in binding energy as

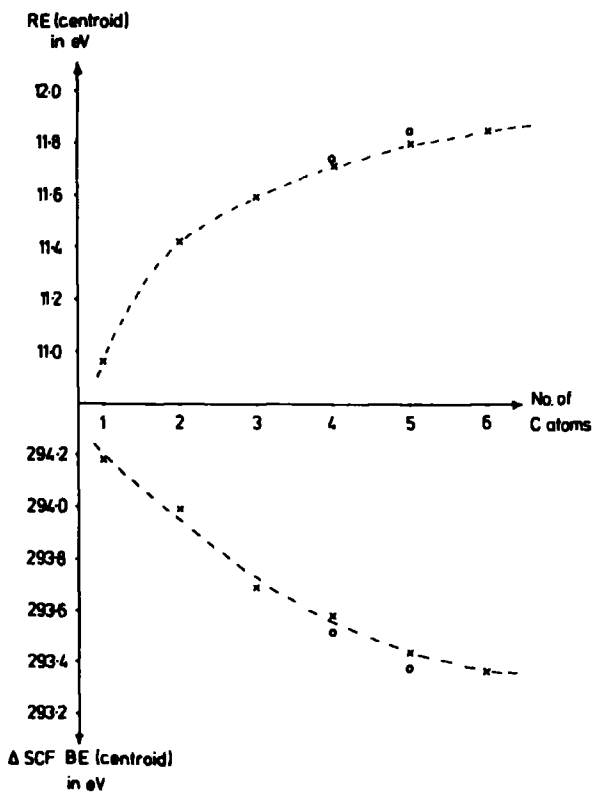

Fig.(3.1) ΔSCF C_{1s} BE (centroid) and RE (centroid) for linear (x) and branched-chain (o) alkanes as a function of chain-length.

TABLE 3.1 ΔSCF Binding Energy, Koopmans' Binding Energies, Relaxation Energies and Experimental Values of Core Binding Energy Centroids

Molecule		ΔSCF B.E.	ΔSCF B.E.	ΔSCF (centroid) B.E.	ΔSCF (centroid) ΔB.E.	Koopmans' B.E.	Koopmans' ΔB.E.	R.E.	ΔR.E.	Experimental (centroid)[a] B.E.	Experimental (centroid)[a] ΔB.E.
Methane		294.18	(0)	294.18	(0)	305.14	(0)	10.96	(0)	290.83	(0)
Ethane	C_1, C_2	293.95	-0.23	293.95	-0.23	305.36	+0.22	11.42	+0.46	290.71	-0.12
Propane	C_1, C_3	293.70	-0.48	293.69	-0.49	305.20	+0.06	11.50	+0.54	290.57	-0.26
	C_2	293.66	-0.52			305.42	+0.28	11.76	+0.80		
n-Butane	C_1, C_4	293.66	-0.52	293.58	-0.60	305.23	+0.09	11.57	+0.61	290.48	-0.35
	C_2, C_3	293.49	-0.69			305.34	+0.20	11.85	+0.89		
n-Pentane	C_1, C_5	293.58	-0.60	293.44	-0.74	305.18	+0.04	11.60	+0.64	290.42	-0.41
	C_2, C_4	293.39	-0.79			305.31	+0.17	11.91	+0.95		
	C_3	293.27	-0.91			305.23	+0.09	11.96	+1.00		
n-Hexane	C_1, C_6	293.56	-0.62	293.37	-0.81	305.17	+0.03	11.61	+0.65	290.36	-0.47
	C_2, C_5	293.32	-0.86			305.29	+0.15	11.93	+0.97		
	C_3, C_4	293.20	-0.98			305.20	+0.06	12.01	+1.05		
Isobutane											
central C		293.47	-0.71	293.52	-0.66	305.56	+0.42	12.08	+1.12	-	-
others		293.53	-0.65			305.16	+0.02	11.62	+0.66		
Neopentane											
central C		293.29	-0.89	293.38	-0.80	305.66	+0.52	12.37	+1.41	290.40[b]	-0.43
others		293.40	-0.78			305.11	-0.03	11.72	+0.76		

a) Experimental values from reference 184.
b) References 185, 186.

a function of increase in chain-length is well-reproduced by the ΔSCF calculations and the absolute magnitude of the change as a function of the incremental change in chain-length shows good agreement with experiment. By contrast, shifts calculated from Koopmans' Theorem have the incorrect sign; thus the shift between methane and n-hexane of +0.1 eV compares with the experimentally determined shift of -0.5 eV and that appropriate to the ΔSCF computation of -0.8 eV. Figure 3.1 clearly shows that increasing chain-length is associated with increasing relaxation energy and that this determines the overall shift as a function of chain-length. The data for the branched-chain systems (isobutane and neopentane) accord with that for their straight-chain counterparts. An analysis of the shifts in core binding energy within a given molecule in the series n-propane, n-butane, n-pentane and n-hexane indicates that the terminal-CH_3 groups are the highest binding energy components, since the relaxation energy is lowest for these structural features. On this basis, therefore, it might be anticipated that in the branched-chain systems of isobutane and neopentane, the methyl groups should in each case form the higher binding energy component. That this is the case is readily confirmed by the direct hole state calculations; however, the shifts are small (~0.1 eV in both cases). The results would therefore support the original assignment for neopentane[185,186]; however, the difficulties of analyzing line-shapes for systems in which the shift range is small can lead to considerable ambiguity.

The available data from these computations allows a relatively complete investigation of the structural dependence of relaxation energy. Figure 3.2 shows the calculated

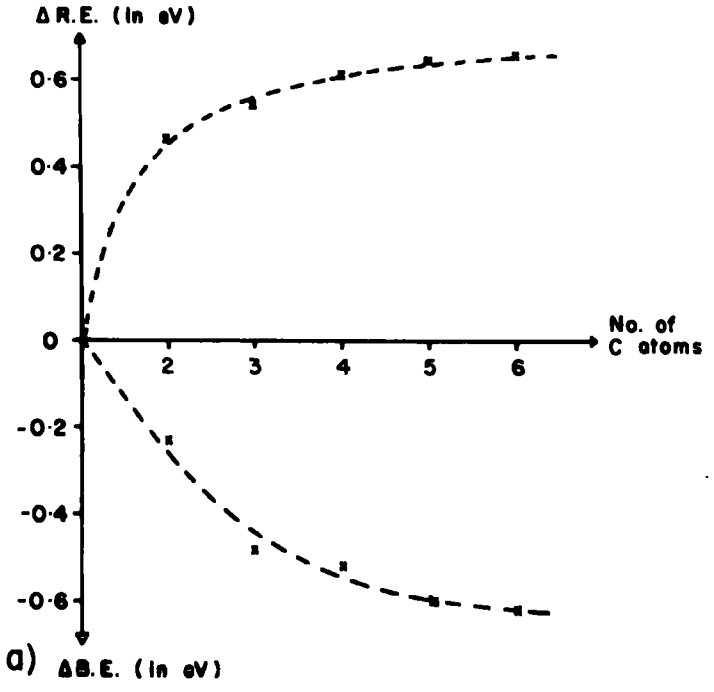

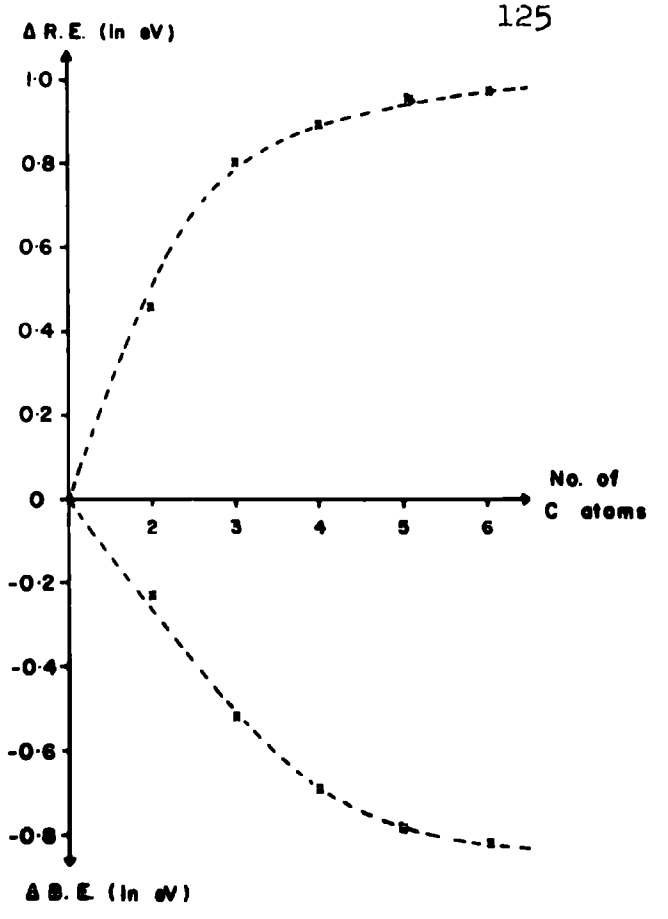

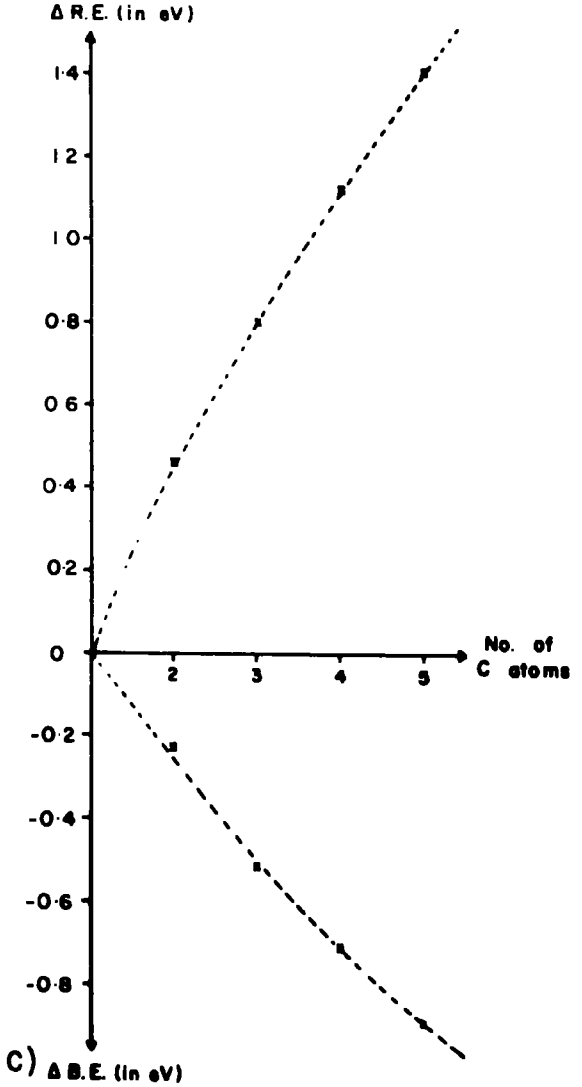

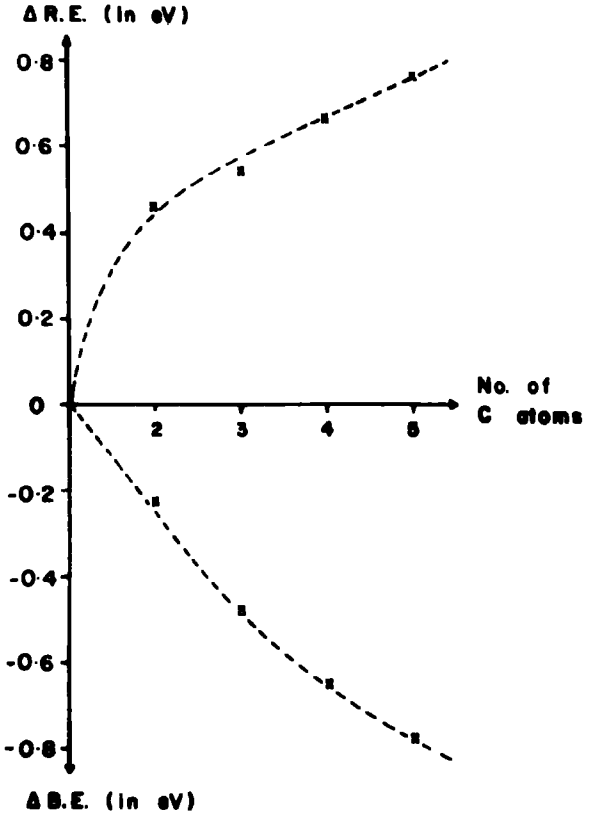

Fig.(3.2) Shifts in core BE and RE, relative to methane (in ev)

C_{1s} shifts in binding energy and relaxation energy for:

(a) the terminal $-CH_3$ carbon atom in the linear alkanes;

(b) the "adjacent" (first methylene, $-\underline{C}H_2-CH_3$) carbon atom in the linear alkanes;

(c) the central carbon atom in the branched-chain alkanes; and

(d) the "terminal" carbon atom in the branched-chain alkanes.

Considering the terminal methyl carbon binding energy and relaxation energy changes as a function of increasing chain-length in the linear alkanes, (a), it is found that the regular decrease in binding energy closely approaches an asymptotic value of $\sim$0.65 eV at n-hexane, this being paralled by an increase in relaxation energy. If the first methylene group is now considered, (b), a steeper initial decrease in binding energy to an asymptotic value of $\sim$0.9 eV at n-hexane is again mirrored by increasing relaxation energy to a near asymptotic value of $\sim$1.0 eV.

In going from methane to neopentane, the calculated shift in binding energy for the central carbon, (c), of -0.9 eV is largely attributable to the increase in relaxation energy of 1.4 eV concomitant with replacing hydrogen by the more polarizable methyl groups. Indeed, the almost linear decrease in ΔSCF binding energy for the central carbon atom in the branched-chain alkane series is almost exactly mirrored by the increase in relaxation energy. Finally, the decrease in binding energy for the "terminal" carbon in the branched-chain alkanes, (d), is much steeper than in the equivalent case for linear alkanes, although not as dramatic as for the central carbon atom in the branched-chain series.

By performing Mulliken population analyses on the

ground- and core-hole states of the alkanes, it is possible to obtain the charge flow accompanying core-ionization. This should only be used as a qualitative guide to the electronic reorganizations accompanying ionization, however; for more detailed consideration, the appropriate density difference should be consulted. Figure 3.3 shows the Mulliken charge flow accompanying core-ionization in the linear alkanes. A negative value indicates an *increase* in electron-density, consequent

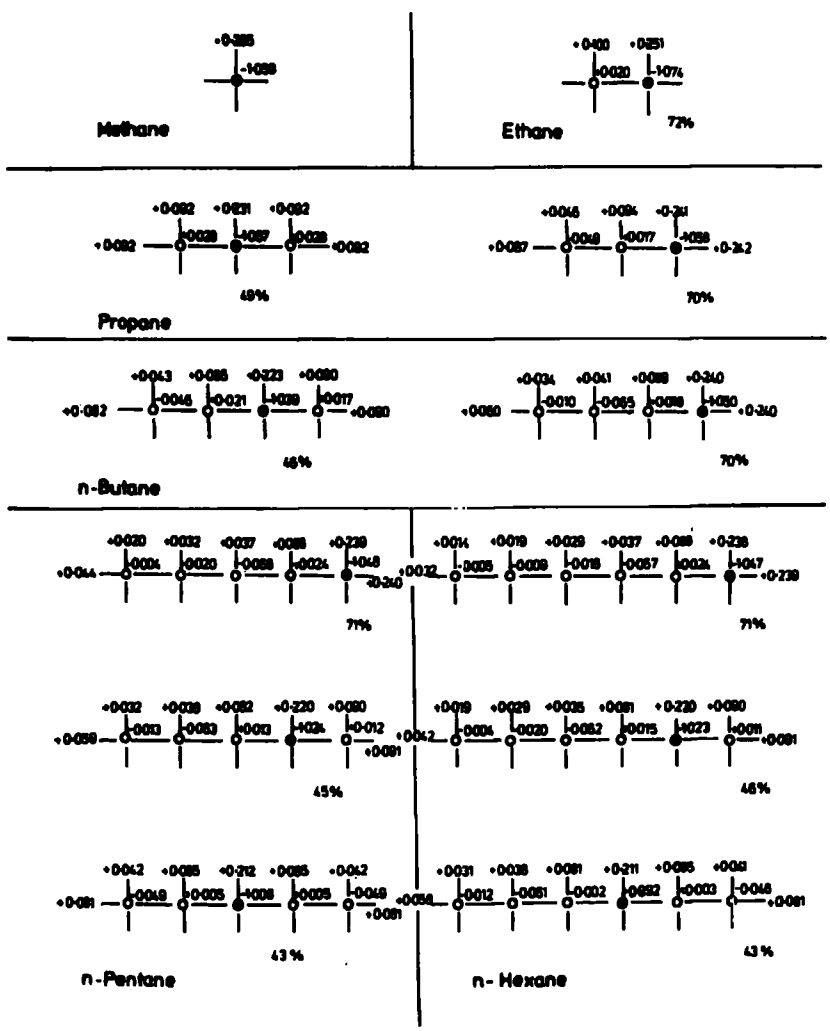

Fig. (3.3) Mulliken charge flow accompanying core-ionization

on core-ionization; thus for methane, there is a net flow of over one electron to the core-ionized carbon atom, corresponding to 0.265 electrons from each hydrogen. The percentage values given in Figure 3.3 show the amount of charge flow (relative to the total charge flow to the core-ionized atom) from the four nearest neighbours. For core-ionization on the terminal (methyl) carbon the percentage of charge flow is fairly constant at around 70%, this coming mainly from the neighbouring hydrogen atoms. This being the case, there is a dramatic decrease in this percentage value (to around 45%) when methylene carbon atoms are core-ionized. The pattern of charge flow for the carbon atoms in the chain is also of interest. In nearly all cases, the immediate neighbours to the core-hole carbon atom show a loss of charge; after that, however, there is a build-up of charge on the carbons in the chain, decreasing along the chain until it is virtually zero (as in the terminal methyl group in n-pentane and n-hexane, with core-ionization on the opposite methyl group).

Figure 3.4 shows the charge flow accompanying core-ionization for the branched-chain alkanes. As in the linear

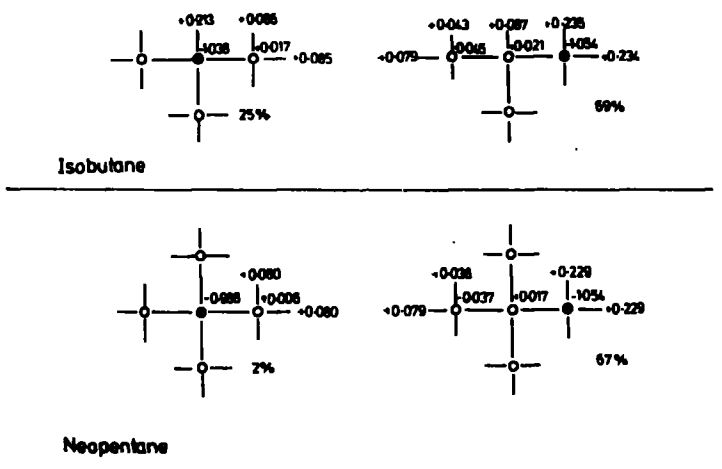

Fig. (3.4) Mulliken charge flow accompanying core-ionization

alkanes, the percentage of charge flow from the immediate neighbouring atoms to the core-ionized atom is relatively constant for the "terminal" methyl atom (69% and 67%). For the central carbon atoms, the percentage flow decreases regularly as the number of nearest-neighbour carbon atoms increases, the appropriate values being 100% for methane with no nearest-neighbour carbon atoms, 72%, 49%, 25% and 2% for neopentane with all nearest-neighbour carbon atoms, showing clearly that the charge-flow arises mainly from the hydrogen atoms attached to the core-ionized carbon.

It has previously been noted that in the particular case of the C_{1s} levels, there is a direct relationship between core binding energy and relaxation energy,[149] which can be understood intuitively in terms of a charge potential type model for both.[191] This contrasts strongly with the more complex behaviour found for N_{1s}, O_{1s} and F_{1s} levels;[149] it should be noted, however, that the range of electronic environments and structural types for O_{1s} levels previously studied[149,192] was somewhat limited, and a recent, more extensive study[193] has shown that clear trends are exhibited if attention is focussed on a given structural type. Over the restricted range of binding and relaxation energies encompassed by the alkanes, the trend for higher binding energy to be associated with lower relaxation energy, previously found for the C_{1s} levels,[149] is also evident here, and this is shown in Figure 3.5. The numerals by the points in the plot indicate the number of carbon atoms in the alkane: o represents the central carbon atom in the branched-chain alkanes; x represents the terminal carbon atoms, and + indicates the methylene carbon atoms. The plot of ΔSCF binding energy against

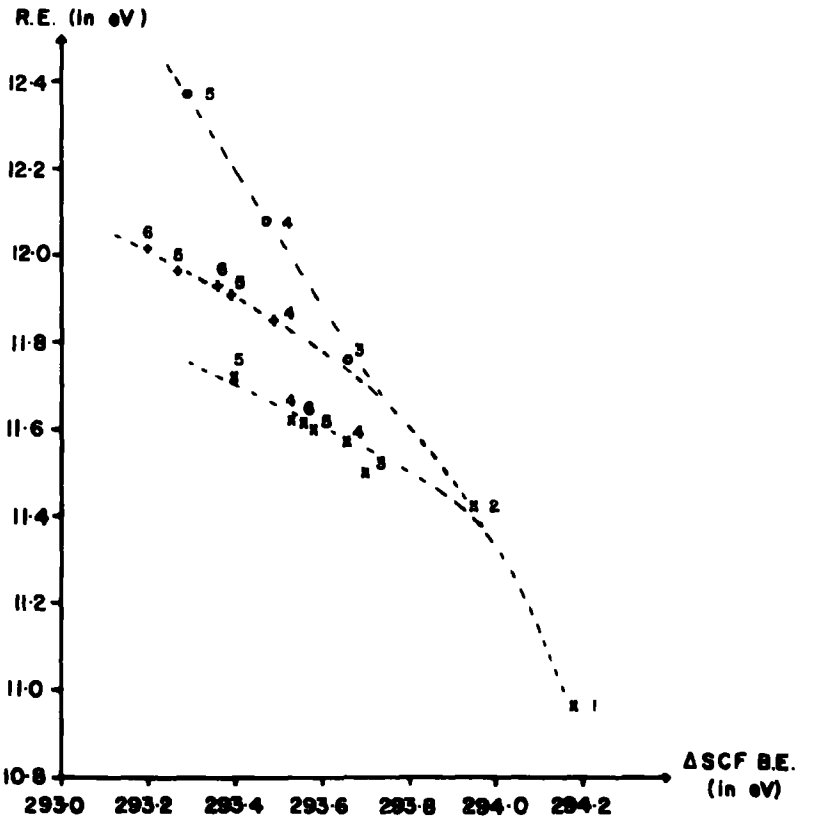

Fig. (3.5) Δ SCF BE versus RE

relaxation energy is interesting in that, despite the small shift range available, the component parts fall into these three clearly-defined groups: the central carbon atoms in branched-chain series; methylene groups in linear alkanes; and terminal methyl groups for both linear and branched-chain alkanes.

3.2 Electronic Relaxation Accompanying Valence (2s) Ionization

3.2.1 Introduction

Whilst the main efforts in high resolution X-ray photoelectron spectroscopy (XPS) and in ultraviolet photoelectron spectroscopy (UPS) have been directed towards the investigation of core-levels and higher-lying valence-levels

respectively, rather less emphasis has hitherto been placed on the investigation of deeper-lying valence-levels, such as those predominantly of 2s character for molecules involving first-row atoms.[194] The advent of high intensity fine-focus X-ray monochromators, coupled with the design of efficient discharge lamps for the production of He(II) radiation, and the increasing interest in the applications of synchrotron radiation,[195] has led to an upsurge of interest in this portion of the photoelectron spectrum of simple molecules. The motivation for this is not difficult to understand, since the ability to study the *complete* valence bands of molecules as opposed to just the highest few levels with ionization energies <21.21 eV generates data of considerable interest to theoreticians concerned with the dependence of differential changes in photoionization cross-sections on photon energies,and in the investigation of asymmetry parameters.[196] Whilst the advent of high resolution, high sensitivity XPS spectrometers has led to an increasing interest in vibrational fine-structure accompanying core-ionizations,[158,120,197-200] and in the investigation of shake-up and shake-off satellites,[201-205] there has been much less emphasis to date in studies of the corresponding phenomena for the deeper-lying valence-levels of simple molecules.[206] This also contrasts with the situation in UPS, where the study of vibrational fine-structure and configuration interaction bands for levels with ionization energies attainable with a high intensity He(I) source is well-developed.

Some attempts at rectifying this situation have appeared recently. Thus in a pioneering series of studies, Price and co-workers[207,208] have investigated at comparatively

low resolution the deeper-lying 2s-like valence-levels of a number of simple molecules and this has been developed into a systematic approach by Heilbronner and co-workers.[194] With a He(II) source, however, despite the small inherent width of the photon source, the cross sections for photoionization are quite small and the typical signal to noise ratios achieved in such studies are relatively poor compared with those normally achieved by He(I) studies of the higher-lying valence-levels. The most comprehensive and systematic study reported to date pertains to a detailed investigation of the deeper-lying valence-levels of the alkanes employing a fine-focus X-ray monochromator, with advantage being taken of the relatively high cross section for photoionization compared with the higher-lying valence-levels.[184]

In this section, therefore, the results of *ab initio* LCAO MO SCF calculations on the ground and valence (2s) hole-states of the series methane, ethane, propane, n-butane and n-hexane, and also isobutane and neopentane are reported.

3.2.2 Computational Details

The valence (2s) hole-state calculations were performed for the above molecules using the geometries and exponents previously discussed (section 3.1.2).

3.2.3 Results and Discussion

The computed ΔSCF valence (2s) binding energies and relaxation energies for the complete series of alkanes studied in this investigation are displayed in Figure 3.6, in which it has been convenient to separate the data into the series of linear and branched-chain alkanes. Least-squares plots of calculated versus experimentally determined 2s binding

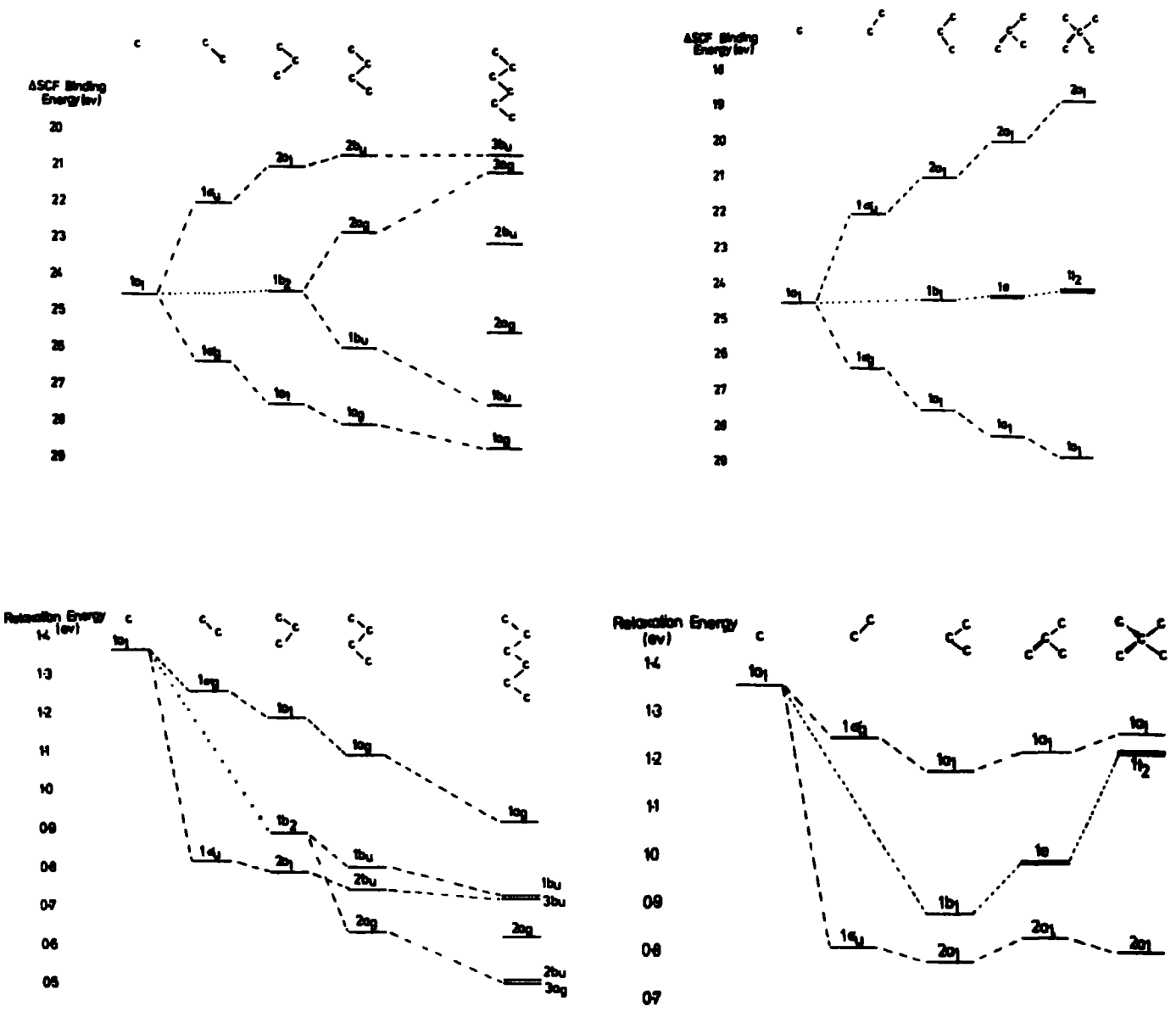

Fig. (3.6) ΔSCF valence (2s) BE and RE

energies have been performed, to give an indication of the adequacy of the theoretical treatment (Figure 3.7).

Considering firstly the linear alkanes, the development of the energy level pattern as a function of chain-length is readily understandable in terms of a simple Hückel model, as has previously been pointed out by Heilbronner.[194] Using the commonly-accepted designation of labelling orbitals with respect to the valence-levels, the ionization potential

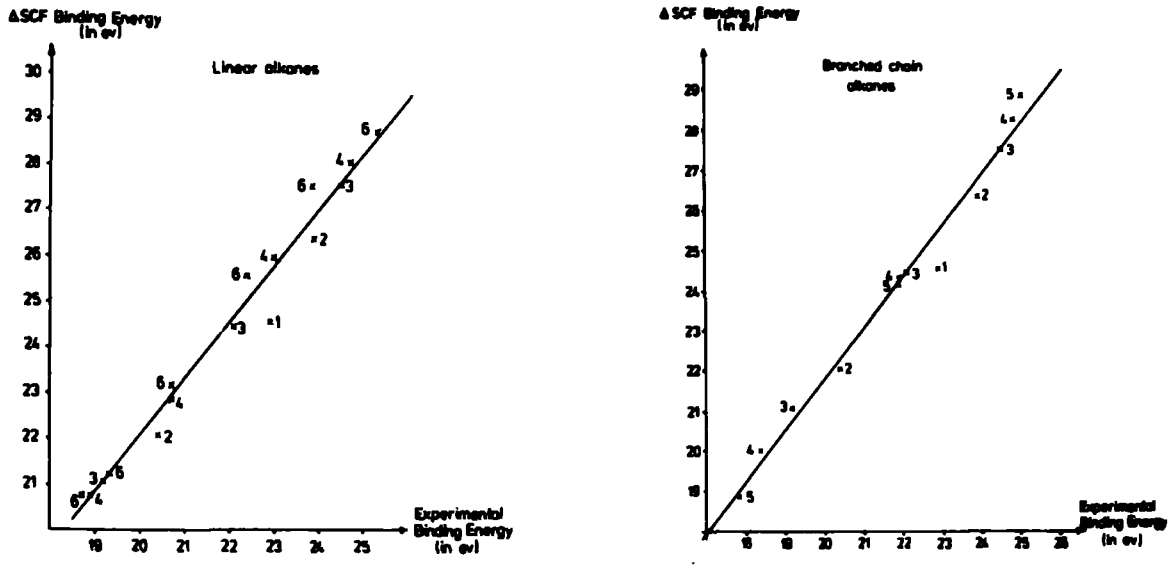

Fig. (3.7) A comparison of theoretical versus experimental C_{2s} BE.

of the $1b_2$ "non-bonding" level of propane is calculated to be closely similar to that for methane (24.4 eV vs. 24.6 eV), and this reproduces quite closely the experimental data (22.1 eV vs. 22.9 eV). For n-hexane, the most tightly bound 2s level has not as yet been experimentally determined; however it would appear from the calculations that the energy gap for the $1a_g$ and $1b_u$ levels is likely to be quite small ($\lesssim$1 eV) and thus may not be resolved. The relaxation energies follow a rather interesting sequence, which contrasts strongly with the situation for the core hole states. Thus for the localized C_{1s} hole-states as discussed in section 3.1.3,[210] the relaxation energy increases with the size of the molecule, as might have been anticipated on polarizability arguments. Extensive delocalization of the valence 2s levels however, leads to a decrease in relaxation energy as a function of the increase in size of the molecule. A least-squares plot of the calculated versus experimentally determined 2s binding energies

provides a slope of 1.2 and an intercept of -2.7 eV, the correlation coefficient r^2 being 0.97. It is interesting to note that the computations indicate quite large differences in relaxation energies for the 2s levels. For example, the computed relaxation energy for the σ_g orbital is $\sim$50% larger than for the σ_u orbital in ethane.

Turning to the corresponding data for the branched-chain alkanes, a plot of the experimental versus the ΔSCF computed binding energies yields a least-squares fit with a slope of 1.28 and intercept -3.7 eV, the correlation coefficient r^2 being 0.98. The computed relaxation energies again span a significant range. Thus for the $1a_1$ orbital of neopentane, which is predominantly the C_{2s} orbital of the central carbon, the relaxation energy is some 50% higher than for the $2a_1$ orbital which corresponds to the symmetric 2s combination of the methyl carbons.

For the 2s levels, correlation energy changes are important. For example the 2s binding energy of methane is overestimated by $\sim$1.6 eV, which is in the opposite sense to that typically found for the outermost (p type) valence-levels, where the correlation energy for the ion is typically smaller than for the neutral molecule.[140] This has been well-documented in the literature for a number of small molecules. The correlation energy changes within this closely related series of molecules are nevertheless very similar, so that shifts in binding energies and changes in relaxation energies are described to a good degree of accuracy within the Hartree-Fock ΔSCF formalism, as demonstrated above.

3.3 A Theoretical Investigation of Vibrational Fine-Structure Accompanying Core-Ionization

3.3.1 Introduction

Vibrational excitation as a manifestation of the changes in potential energy surfaces consequent upon core-ionization represents a topic of considerable current interest, both from an experimental and theoretical stand-point. The published experimental data to date has been limited to CH_4, CO and N_2;[158] this was interpreted initially in terms of Franck-Condon factors derived from calculations on equivalent cores species.[158] Recent theoretical work, however, indicated a significant difference in bond-length and force constant between the equivalent cores and core hole state species,[149] which led Clark and Müller to a further theoretical study of CO and N_2.[170] It was found that the experimental C_{1s}, O_{1s} and N_{1s} spectra were well-reproduced using Franck-Condon factors derived from hole-state calculations at the "triple zeta" level. An alternative approach has been developed by Cederbaum and Domcke, using Many Body Perturbation Theory employing Green's functions[180] to generate one-particle coupling constants, and hence vibrational envelopes.[211] This method also leads to excellent agreement with experiment.[197]

It has been shown that optimization of exponents within the spirit of the equivalent cores concept[169] provides a means of accurately describing both absolute and relative binding energies,[212] and geometry and force constant changes accompanying core-ionization,[149,170] with basis sets at the STO-4.31G level. Accordingly, the analysis of vibrational fine-structure accompanying core-ionization has been extended at this level to a series of somewhat more complicated systems.[199,200]

To provide a suitable background for the discussion in the next section on vibrational fine-structure accompanying valence (2s) ionization in alkanes, and to allow comparison to be made with core-ionization, the results of such calculations on methane and ethane are presented here.

3.3.2 Computational Details

Non-empirical ΔSCF LCAO MO SCF calculations have been carried out within the Hartree-Fock formalism for the ground- and core-hole state species. This approach is known to provide an essentially quantitative description of core binding energies, at least for first row atoms, due to the essentially atomic nature of relativistic and correlation effects.[213] The basis set used was STO-4.31G, with best-atom exponents[30] for the ground-state, while for core hole states, the valence exponents used were those appropriate to the equivalent cores species (a so-called "optimized" STO-4.31G). The vibrational analysis presented here is within the harmonic approximation; to generate the potential energy surfaces, the experimental geometry was taken as a starting point and a parabola computed corresponding to extensions or compressions in bond-length of 0.1 au. A process of successive refinement was then carried out until the intervals were decreased to final values of 0.01 au. Having computed energy minima, it is important to establish that the shape of the potential energy curve in the vicinity of the minimum is also adequately described; accordingly, extensions or compressions of ∿0.15 au were examined and fitted to a parabola, to give the force constants. Having established the equilibrium bond-lengths and force constants for the ground- and core-hole state species, the Franck-Condon factors were computed using the recurrence

relationships derived by Ansbacher.[157] The changes in vibrational separation due to anharmonicity have been shown to be negligible.[170]

Of the 3N-6 vibrational modes for a non-linear N-atomic molecule, only the stretching modes in which local symmetry was not destroyed were considered, since only even quanta (viz., $\nu''=0$ to $\nu'=0,2,4....$) may be excited.[82] Such modes are perhaps more properly denoted as internal displacement coordinates. Bending modes were not explicitly considered since:

(a) the vibrational quanta are small leading to an asymmetry in the spectra which would be largely undetectable with present instrumentation;

and (b) vibrational fine-structure is infrequently observed even in the field of valence-level photoelectron spectroscopy (UPS).[82]

For these reasons, coupled with the considerable computational expense which an investigation of bending vibrations would incur, this work was restricted to a study of selected stretching modes only.

For ethane, the modes discussed are the symmetric C-H stretch (ν_{C-H}^{sym}), the antisymmetric stretch (ν_{C-H}^{anti}) and the C-C stretch (ν_1, ν_5 and ν_3 respectively, using the notation of Herzberg).[61] ν_{C-H}^{sym} was studied in CH_4.

3.3.3 Results and Discussion

The binding energies and relaxation energies are shown in Table 3.2. Clearly, use of the "optimized" STO-4.31G basis provides a computationally inexpensive means for the accurate description of absolute as well as relative binding

TABLE 3.2 C_{1s} BE and RE (in eV) for methane and ethane

	Methane	Ethane
Binding Energy		
Vertical, STO-4.31G	294.2	293.9
Vertical, "optimized" STO-4.31G	290.8	290.5
Experimental[a]	290.8	290.7
Adiabatic, "optimized" STO-4.31G	290.6	290.5
Relaxation Energy		
STO-4.31G	11.0	11.4
"optimized" STO-4.31G	14.4	14.4

(a) References 91 and 185.

energies. The relaxation energies illustrate the expected increase in absolute value for the "optimized" relative to the basic STO-4.31G basis set.

The equilibrium bond-lengths and force constants for the neutral molecules and core-ionized species, together with the calculated Franck-Condon factors, are shown in Table 3.3.

Considering firstly methane, the equilibrium neutral molecule CH bond-length and force constants are in good agreement with those determined from experimental data, and compare very favourably with those reported by Blom and coworkers[215] using a comparable 4.31G basis. Blom et al. also investigated the harmonic force constants for the CC and symmetric CH stretch in ethane and the results reported here are in good agreement. Although the computed bond-lengths are in good agreement with the experimental data, there is a tendency for the 4.31G basis set computations to slightly underestimate and the STO-4.31G to overestimate the bond-lengths.

TABLE 3.3 (i) Theoretical Bond-Lengths (R_e, atomic units) and Some Stretching Force Constants (k, millidynes/Å) for Methane and Ethane, and their Respective Changes on Core-Ionization

Molecule		Neutral Molecule				C_{1s} hole-state		
		R_e	expt.(c)	k	expt.(d)	R_e	(Δ)	k
CH_4	ν^{sym}_{C-H}	2.076	2.066	5.76	5.92	1.958	(0.119)	7.59
CH_3CH_3	ν_{c-c}	2.950	2.899	4.98	4.50	2.902	(0.048)	4.67
	ν^{sym}_{C-H}	2.079	2.066	5.68	4.79	2.007	(0.07)	6.67
	ν^{anti}_{C-H}	2.079		5.66		2.0131(a) 2.1449(b)	(0.07)	5.53

(a) C^*-H (b) C-H (where * indicates the core-hole)

(ii) Franck-Condon factors

Transition	Methane: ν^{sym}_{C-H}	Ethane: ν_{c-c}	ν^{sym}_{c-H}	ν^{anti}_{C-H}
00	62.52	93.29	87.15	89.23
01	28.06	6.51	11.18	10.18
02	7.66	0.20	0.98	0.56
03	1.50	-	0.69	0.03
04	0.26	-	-	-
Separation (eV)	0.45	0.12	0.39	0.36

For comparison purposes, the theoretical data of Blom et al[215] are as follows

	R_e C-C	k C-C	R_e C-H	k C-H
methane			2.044	5.84
ethane	2.889	4.57	2.047	5.31

(c) Ref. 214 (d) Ref. 61

For methane, previous theoretical studies have established that for the core-ionized species the equilibrium bond-length is shorter and force constant for the symmetric CH stretch larger than for the neutral molecule. This is in fact found to be a general feature.[200] Thus, for the localized core-hole state of ethane, the equilibrium CH bond-length is considerably smaller than for the neutral molecule, the reduction in bond-length being somewhat similar to the comparable situation for methane. In the case of the antisymmetric CH_3 stretching mode, the equilibrium bond-length corresponds to a reduction in CH bond-length for the hydrogens attached to the carbon bearing the core-hole and a concomitant increase for the other methyl group. In consequence, whilst the force constant for the symmetric CH_3 stretch increases on core-ionization, that for the antisymmetric mode remains essentially the same as for the neutral molecule.

Turning now to the C-C bond, core-ionization of the C_{1s} level in ethane leads to a decrease in equilibrium bond-length, the absolute magnitude of the change being somewhat smaller than for the CH bonds. The force constant also changes by a relatively small amount, actually decreasing slightly. As an ancillary point, the barrier to rotation in ethane for both the neutral and core-ionized species has been computed. This would indicate a small decrease in going to the ionized species (calculated 3.2 kcal mol^{-1} and 2.5 kcal mol^{-1} respectively).

From the data presented in Table 3.3 it is possible to make a few broad generalizations concerning the likely vibrational profiles accompanying core-ionization. Rather

complete discussions have previously been presented for methane,[139,197] and the calculated band-profile has been shown in Figure 2.11. It is clear that in going from methane to ethane there should be a substantial reduction in the composite line-width for the C_{1s} levels, since the changes in both equilibrium geometry and force constants are substantially smaller. Computations of Franck-Condon factors taking only the three stretching modes discussed previously into account suggests >90% of the signal intensity in the 00 transition, compared with ∿62% in the case of methane. Although high-resolution spectra for the C_{1s} levels of ethane are not currently available, the spectra recorded at medium resolution indicate that the FWHM for the C_{1s} levels of methane are significantly broader than for ethane.

3.4 A Theoretical Investigation of Vibrational Fine-Structure Accompanying Valence (2s) Ionization

3.4.1 Introduction

One of the most significant and interesting features to emerge from the detailed studies of Siegbahn et al. on the deeper-lying valence-levels of the alkanes[184] was the fact that individual components in the predominantly C_{2s} manifold had significantly different composite linewidths. Thus in ethane, the full width at half maximum (FWHM) for the in-phase (gerade), essentially C_{2s} levels is some 12% larger than for the out-of-phase (ungerade) component. Moreover, under the same instrumental conditions, whilst the FWHM for the C_{1s} level of methane is ∿0.8 eV, that for the C_{2s} level is ∿1.27 eV. Even allowing for the small difference in analyzer contributions to the linewidth originating in the differences in kinetic energy for the photoemitted electrons (∿1196 eV and ∿1464 eV for the C_{1s} and C_{2s} levels respectively), there is

still a substantial difference in linewidth for the two levels. Although there will be a significant contribution to the composite observed FWHM originating from the inherent width of the irradiating soft X-ray beam, this is not expected to change from level to level. *A priori*, the difference in linewidth might arise from differences in lifetimes for the hole-states (uncertainty broadening), or from differences in vibrational fine-structure, or indeed from contributions from both sources. Since the inherent width for the C_{1s} level is known to be ~0.1 eV and since it would seem unlikely that the lifetime for the 2s hole-state would be very significantly shorter (i.e. differing by greater than an order of magnitude) than for the 1s level, the most likely explanation for differences in linewidths and asymmetries of peaks would seem to be differences in vibrational fine-structure. (Although of course differences in lifetimes could give rise to broadening, this should be symmetrical; the asymmetry of overall line-profiles in the absence of low energy shake-up satellites or of discrete energy-loss peaks can only in principle be attributed to unresolved vibrational fine-structure). This would not be unreasonable, since vibrational excitation accompanying the removal of a non-bonding core-electron originates in the substantial reorganization of the valence-electrons in response to the electron demand which is created.[158,130,199,200] By contrast, relaxation or reorganization phenomena involving photoionization of the valence-levels themselves are quite small; however, since electrons are being removed from orbitals with certain bonding and antibonding characteristics, we might anticipate substantial vibrational fine-structure which would only fortuitously correspond to that for the core-levels.

In this section, therefore, some aspects of the vibrational fine-structure accompanying photoionization of the C_{2s} levels of methane and ethane have been investigated in detail.

3.4.2 Computational Details

Calculations were performed for the C_{2s} hole-states of methane and ethane in a similar manner to that described in section 3.3.2, using an "optimized" STO-4.31G basis set. The vibrational modes investigated were those previously detailed for the C_{1s} levels.

Using the STO-4.31G basis set described in sections 3.1.2 and 3.2.2, Mulliken population analyses were performed on the neutral molecules and corresponding ionized states for the series methane, ethane, propane and n-butane to provide bond overlap populations. In the particular case of ethane, density difference contours for the core and valence 2s ionized states were computed with respect to the neutral molecule. A mesh of 97 x 97 points was used, with the same geometry for both ground and ionized states; the planes studied were the "molecular" plane containing the C-C bond (11 x 11 au), and a plane bisecting the C-C bond (8 x 8 au). Since the difference contours are ground state minus hole state , the negative contours (dashed lines) represent an increase in electron density on ionization. Contour lines are drawn from 0.004 au, successively doubling in value to a maximum of 0.8 au.

3.4.3 Results and Discussion

(a) Methane

The available experimental data[184,216] suggest that there is considerable asymmetry in the high resolution

spectrum of the 2s level of methane, and this in itself would mitigate against any explanation of the larger composite FWHM for this level compared with that for the 1s level based on differences in lifetimes for the relevant hole-states. As has been noted, the differences in composite linewidths are of the order of 50%, a small proportion of which may be attributed to the slightly larger contribution originating from the electron optics. The available high resolution C_{1s} spectra for methane have previously been quantitatively described[139,197] in terms of vibrational excitation of the symmetric CH stretching mode consequent upon the large difference in potential energy surface for ground and core hole state species. The equilibrium CH bond-length and force constant for the hole-state are computed to be shorter and larger respectively than for the neutral molecule. By comparison, the asymmetric nature of the overall line-profile for the 2s level of methane might also, therefore, be expected to arise from vibrational excitations. The larger inherent FWHM could then arise merely from a more extended vibrational envelope, implyinga much greater change in potential energy surface on valence- as opposed to core-ionization; superimposed on this, however, could be differences in lifetimes for the 2s compared with the 1s level.

The equilibrium bond-length and force constant for the 2s hole-state of methanehave been computed. The relevant data are displayed in Table 3.4. Whilst for the core-ionized species (Table 3.3), the equilibrium bond-length is computed to be considerably shorter with respect to the neutral molecule, the change in bond-length and force constants are larger in absolute magnitude, and in the opposite sense for

TABLE 3.4 Theoretical Bond-Lengths and Force Constants for Methane and Ethane, and their Respective Changes on Valence (2s) Ionization.

	Equilibrium Bond-Length (au)	Force Constant (millidyne/Å)	Koopmans' Equilibrium Bond-Length	Koopmans' Force Constants	ΔSCF Binding Energies (eV)	Relaxation Energies (eV)
Methane						
C-H stretch (symmetric), ν^{sym}_{C-H}						
Ground State	2.0761	5.760				
C_{2s} hole state	2.2442	4.126	2.232	4.865	24.56	1.36
Ethane						
C-C stretch, ν_{C-C}						
Ground State	2.9503	4.982				
C_{2s} gerade	3.2848	3.269			26.38	1.25
C_{2s} ungerade	2.7998	7.006			22.05	0.81
C-H stretch (symmetric), ν^{sym}_{C-H}						
Ground State	2.0790	5.683				
C_{2s} gerade	2.1470	5.008				
C_{2s} ungerade	2.1868	4.515				
C-H stretch (antisymmetric), ν^{anti}_{C-H}						
Ground State	2.0790	5.657				
C_{2s} gerade	2.1470	5.864				
C_{2s} ungerade	2.1868	3.425				

Franck-Condon Factors

	Methane	Ethane					
	ν^{sym}_{C-H}	ν_{C-C}		ν^{sym}_{C-H}		ν^{anti}_{C-H}	
Transition	C_{2s}	C_{2s} (g)[a]	C_{2s} (u)	C_{2s} (g)	C_{2s} (u)	C_{2s} (g)	C_{2s} (u)
00	43.19	5.35	49.14	88.26	74.40	99.23	97.39
01	38.60	17.52	32.65	10.73	22.63	-	-
02	14.34	25.45	13.24	0.54	2.76	0.07	2.61
03	3.27	23.40	3.86	0.02	0.21	-	-
04	0.60	15.50	0.90	-	-	-	-
05	-	7.93	0.21	-	-	-	-
Separation (eV)	0.33	0.10	0.15	0.34	0.32	0.37	0.28

Not all of the Franck-Condon factors are shown here.

the 2s valence-ionized state. Meyer has presented a large scale CI computation of aspects of the potential energy surfaces for the ground, core and valence (2s) ionized states of methane,[139] and it is gratifying to note that the limited basis set computations reported here exactly reproduce the predicted changes in equilibrium geometry on ionization. The computed Franck-Condon factors (also shown in Tables 3.3 and 3.4) reveal more extended vibrational fine-structure accompanying the valence (as opposed to core) photoionization, with up to 5 vibrational quanta excited. This is also apparent from Meyer's work;[139] however, he only considered the first three vibrational quanta there, and it is therefore difficult to compare directly with the work reported here. To partially offset the larger FWHM which might be inferred from this more extended vibrational series compared with the 1s levels, it should be noted that the vibrational frequency for the 2s hole-state is considderably lower than for the 1s hole-state, since the changes in bond-length are opposite in sign. If as a starting point it is assumed that the instrumental and other factors contributing to the overall linewidth are the same for both the 1s and 2s levels, then with the computed Franck-Condon factors it may be shown that the FWHM for the overall band-profiles is a few per cent larger for the C_{2s} levels. Although this is in the correct sense, the experimental data indicate that the FWHM for the latter are $\sim$100% larger than for the 1s levels. Since the kinetic energies of the photoemitted electrons are not greatly different ($\sim$1197 eV and 1464 eV for the 1s and 2s levels respectively), it would seem unlikely that the contribution arising from the electron optics would be drastically different for the two levels; the only reasonable conclusion

would seem to be that the inherent width (lifetime) for the 2s hole-state is somewhat greater (shorter) than for the 1s hole-state. The difference in lifetimes could be well within an order of magnitude to explain the results, and this would not be unreasonable on the basis of efficient de-excitation of the 2s hole involving electrons from orbitals dominantly of 2p character, since no change in principal quantum number is involved.

Inspection of the available data for the 2s levels of the higher alkanes shows in particular cases rather narrow linewidths for individual components, and the interpretation of such data will be presented in a subsequent section. However, the narrowest component, for which the theoretical calculations would suggest a rather small probability of vibrational excitation, has a linewidth of $\sim$1.1 eV. With a component linewidth of this magnitude, the overall computed band-profile for the C_{2s} level of methane is in good overall agreement with the experimental data, as is clear from the data presented in Figure 3.8. Although the possibility of so-called configuration interaction resonances contributing to the overall band-profiles cannot be discounted, the clear-cut nature of the spectra for the 2s levels of methane and the higher alkanes (with little evidence of extensive satellite structure to higher kinetic energy, at least in the regions within a few eV of the direct photoionization peaks), would make it seem unlikely that such interactions, if present, contribute to the overall profiles. The consistent nature of the interpretation of variations in linewidths and asymmetries of the 2s levels which is presented subsequently lends strong support to an analysis based on underlying vibrational

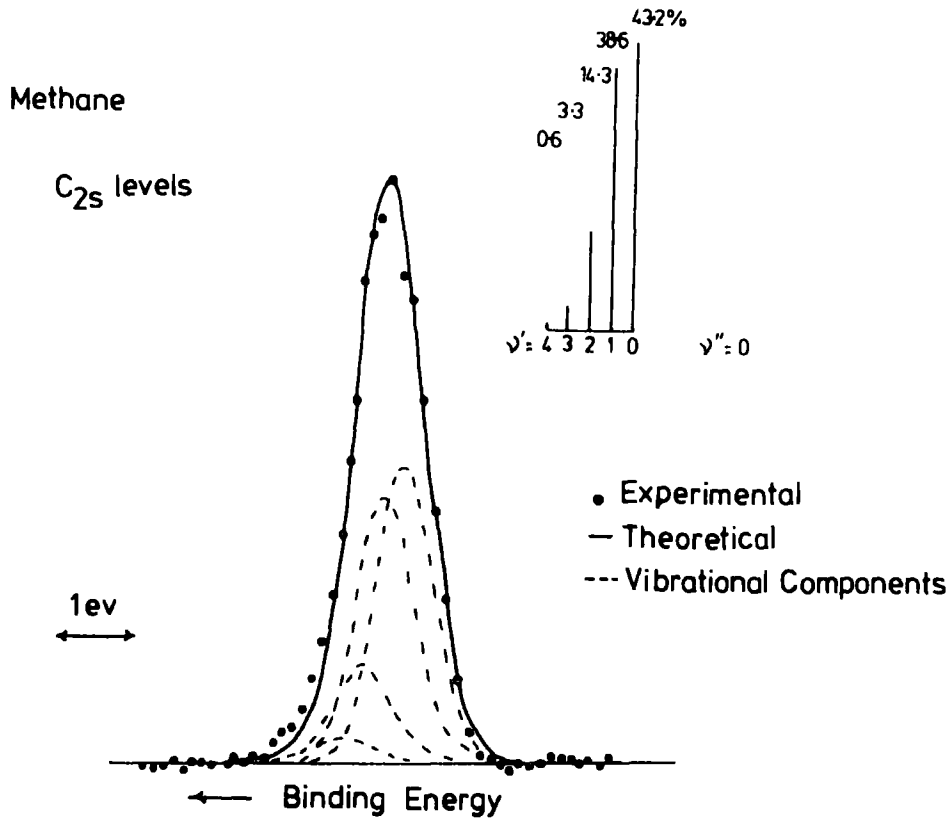

Fig. (3.8) The C_{2s} spectrum of methane. Vibrational components have a FWHM of 1.1 eV, separated by 0.33 eV.

fine-structures.

It is of interest to compare the directly computed changes in equilibrium bond-lengths and force constants with those derived from Koopmans' Theorem. It is clear from this that without due consideration for relaxation accompanying ionization, although the predicted bond-length changes are quite close to those calculated directly, the changes in shape of the potential energy surfaces are poorly described. The manifestations of electronic relaxations are apparent in

the potential energy surfaces which in the case of the 1s level is calculated to be narrow and steep, with a significantly increased force constant, which contrasts with the situation for the 2s levels, where the surface is relatively broad and flat with a substantially reduced force constant.

(b) Ethane

The C_{1s} hole-states of ethane have previously been discussed (section 3.3.3); it is clearly of interest to investigate the corresponding situation for the C_{2s} hole-states, more particularly since the experimental data show two clearly resolved components which differ significantly in their FWHM.

The relevant theoretical data are presented in Table 3.4. Considering firstly the ν_{CC} stretching mode, there is a striking contrast in behaviour for the core as opposed to valence 2s ionizations. Whilst for the core-levels (Table 3.3) removal of an electron results in a relatively small decrease in equilibrium bond-length and concomitant change in force constant, for the symmetric combination of the 2s orbitals there is a large increase and for the antisymmetric combination a large decrease in equilibrium CC bond-length. This is readily understood in terms of the bonding and anti-bonding characteristics of these orbitals respectively, as far as the carbon-carbon bond is concerned. For the σ_g orbital, removal of an electron to produce the 2s valence-ionized species results in a substantial change in potential energy surface with the force constant for the ν_{CC} mode being significantly less than for the neutral molecule. The manifestation of this is that the ν_{CC} mode is computed to be

strongly excited on photoionization. The corresponding data for the σ_u level are also shown in Table 3.4, and it is clear that the computed profile shows considerably less extended vibrational excitation than for the σ_g level. Turning now to the symmetric C-H stretching modes, ionization is computed to lead to a lengthening of the CH bonds and concomitant decrease in force constants for both the σ_g and σ_u levels. The computed Franck-Condon factors indicate a somewhat more extended series for the σ_u as compared to the σ_g orbital. For the antisymmetric stretch, only even vibrational quanta may be excited and whereas the force constant for the σ_g ionized state is computed to be somewhat larger than for the neutral molecule, for the σ_u state the force constant is substantially smaller. Clearly, there should be substantial broadening for both the σ_g and σ_u 2s levels of ethane. The computed Franck-Condon factors, taken with a component linewidth of 1.1 eV, do indeed reveal a slightly larger linewidth for the σ_g component as compared with the σ_u; however, the composite linewidths are smaller than those observed experimentally (1.64 eV and 1.46 eV respectively). It is a straightforward matter to show on energetic grounds that predissociation is likely to be of considerable importance in ethane for the valence 2s levels, and since there is strong coupling to the CC stretching mode there is a direct channel to methyl cation plus methyl radical. Such a predissociative pathway is likely to be less important for methane since the valence 2s ionized state only couples to the symmetric CH stretching mode and the corresponding channel to methyl cation and hydrogen atom is therefore less accessible. The net effect would be an increased broadening of the 2s levels for ethane, that for the σ_g level being the larger since the

electron being removed provides substantial C-C bonding.

The calculated absolute and relative binding and relaxation energies for the 2s levels in methane and ethane are also displayed in Table 3.4. Since there is an increase in correlation energy in going from the neutral to the valence 2s ionized species, the ΔSCF computations actually overestimate the ionization potentials; however, it has been seen in section 3.2.3 that the correlation energy contribution changes in a consistent manner across the series, and the relative binding energies and shifts for the 2s levels are well-reproduced by the computations at the STO-4.31G level. In summary, therefore, the difference in linewidth for the 2s levels of ethane may be qualitatively understood in terms of the differences in potential energy surfaces for the ground and ionized species. The C_{2s} relaxation energy of methane computed in this work is in excellent agreement with the more extended basis set computations of Meyer.[139]

(c) Higher Alkanes

One of the most interesting aspects of the investigations which have been reported to date[184] is the considerable variation in linewidth for the components of the 2s levels of the alkanes. Although the localization characteristics of the individual molecular orbitals which are dominantly of 2s character differ significantly across the series of alkanes of interest to this work, the variations in correlation energy corrections will not be sufficient to cause any reordering of states with respect to that produced from the ΔSCF calculations. For propane, the order of increasing ionization potentials is $2a_1 < 1b_2 < 1a_1$ (Figure 3.6). The experimentally determined

FWHM fall in the order $1a_1 > 1b_2 > 2a_1$. As a starting point in the discussion of this data, it might be anticipated that by analogy with the data previously presented for ethane, removal of an electron which contributes a bonding interaction between a pair of atoms will result in an increase in that equilibrium bond-length for the ionized species. Correspondingly, for an antibonding interaction the bond-length would be expected to decrease. In a simplistic model, since it might be anticipated that bond extension would be energetically less expensive than bond compression, the absolute magnitude of the change in bond-length should be larger for removal of a bonding interaction compared with that appropriate to removal of an antibonding interaction. On this basis, it is clear that the removal of an electron from the most strongly bonding of the valence 2s levels in propane, namely the $1a_1$ orbital, should lead to substantial excitation of both C-C and CH stretching modes. The Mulliken population analysis shown in Figure 3.9 reveals a substantial decrease in the C2-C1(C3) bond overlap populations and smaller changes in the C2-H populations. Although in a relative sense the Mulliken population analysis may be used as a qualitative guide to the electronic reorganizations accompanying ionizations, the subtle details of changes in electron distributions in the inter-bonding regions may only be inferred from detailed consideration of appropriate density difference contours.

Before considering the alkanes in greater detail, it is worthwhile illustrating this point by reference to ethane. Whilst core and valence ionization of the σ_u orbitals leads to a decrease in equilibrium C-C bond-length, for the σ_g orbital there is a substantial increase in computed

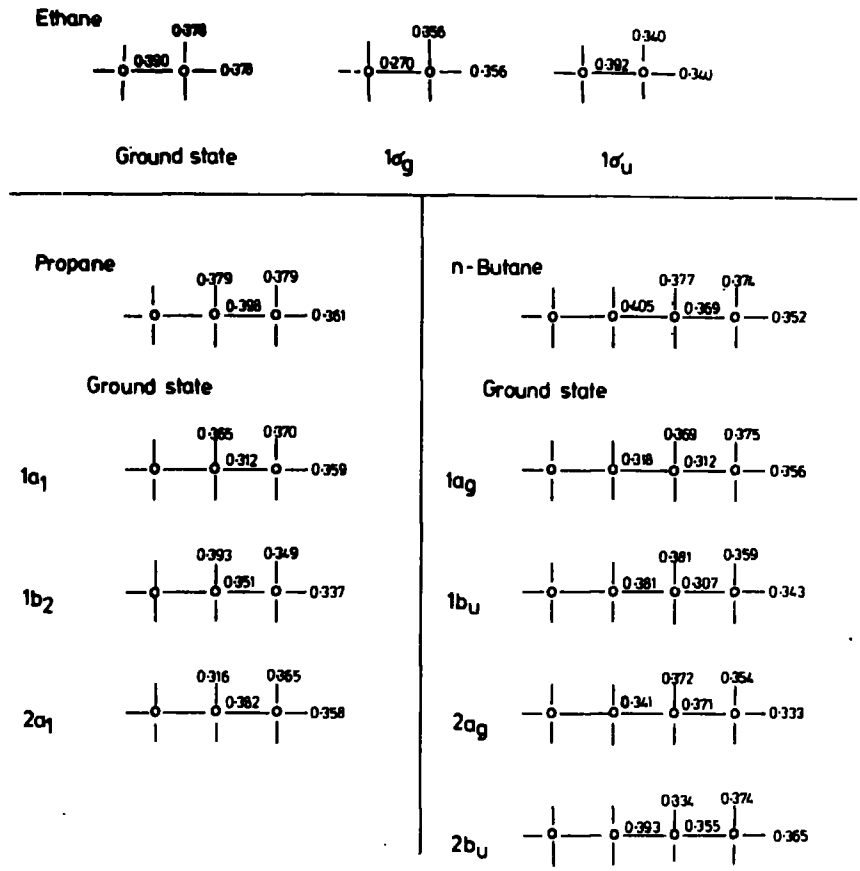

Fig. (3.9) Mulliken bond overlap populations

equilibrium bond-length. The corresponding CC bond overlap populations (evaluated at the equilibrium bond-length for the neutral molecule) qualitatively reflect these changes in geometry, being 0.28, 0.39 and 0.27 for the ls, σ_u and σ_g ionized species respectively. Comparison with the bond overlap computed for the neutral molecule (0.39) illustrates the limitations of the Mulliken population analysis in rationalizing the data, since although the bond overlap population for the ls ionized state is substantially less than for the

neutral molecule, the computed equilibrium bond-length is shorter than for the neutral molecule.

The reason for this is readily apparent on considering density difference contours computed for a plane bisecting the molecular axis (Figure 3.10). Although the total bond overlap populations for the 1s core and σ_g valence ionized states are both smaller than for the neutral molecule,

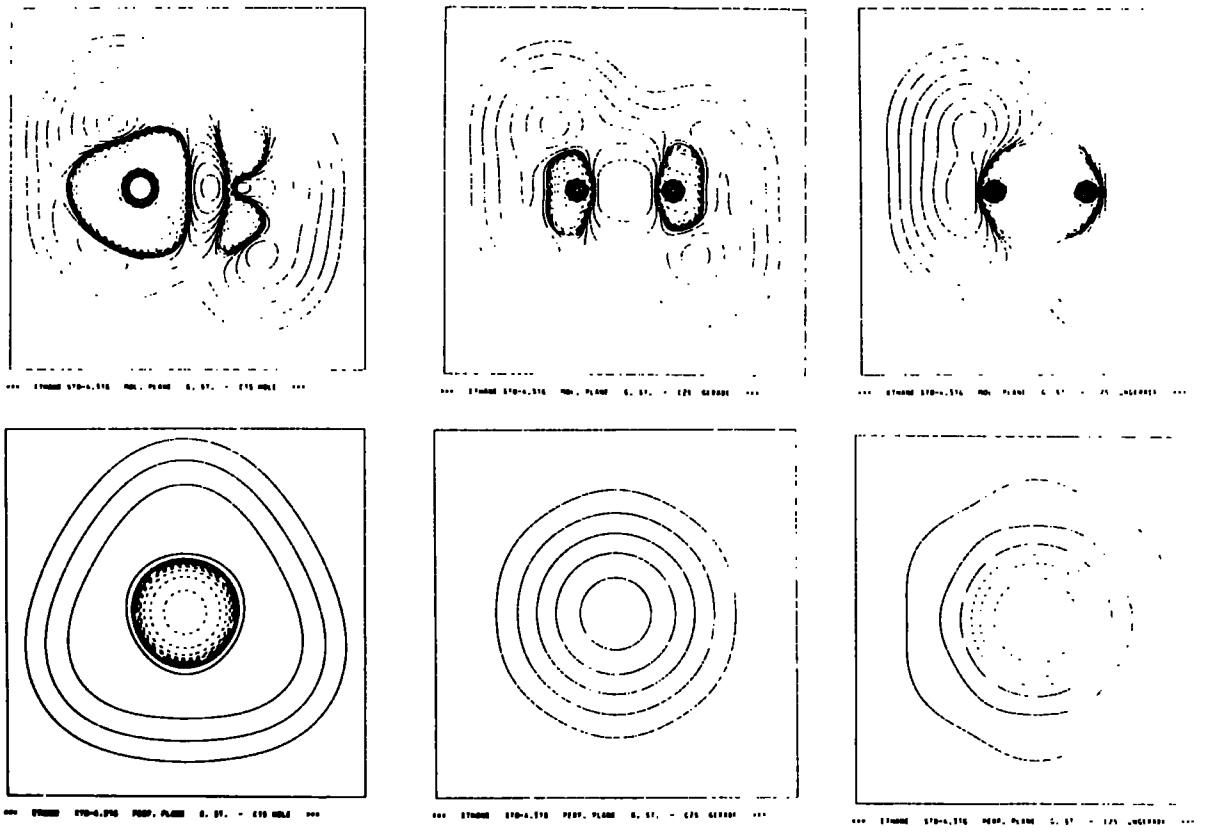

Fig. (3.10) Density difference contours for C_{1s}, C_{2s} gerade and C_{2s} ungerade ionization of ethane.

the contours reveal that for the former there is actually a build up of electron density in the bonding region close to the internuclear axis at the expense of the regions remote from the axis. On this basis the shorter equilibrium bond-length for the core-ionized species is readily understandable.

Ionization from the σ_u orbital leads to a significant increase in valence population in the bonding region, and it is thus possible to understand why the equilibrium bond-length is decreased, despite the fact that the total bond overlap population is almost the same as for the neutral molecule. By contrast, the substantial decrease in bond overlap population for the σ_g orbital is accompanied by a uniform decrease in population in the CC bonding regions, and the equilibrium bond-length is therefore computed to be substantially larger than for the neutral molecule.

Returning now to the results of the population analysis for the valence 2s ionized states of propane, the change in CC bond overlap populations in going from the neutral molecule to valence-ionized species falls in the order $1a_1 > 1b_2 > 2a_1$. Comparison with the population analysis for ethane suggests that the $1a_1$ and $1b_2$ valence-ionized states should have significantly longer C-C bond-lengths, the changes, however, being somewhat smaller than for ethane. For the $2a_1$ orbital, there is a small percentage decrease ($\sim 5\%$) in CC bond overlap population and again by comparison with ethane this would suggest a small change in equilibrium bond-length on ionization.

As far as the CH bond overlaps are concerned, whilst the methylene CH bond overlap populations for the $2a_1$ ionized species are much smaller than for the neutral molecule, those for the $1b_2$ ionized state are somewhat larger and for the $1a_1$ ionized state somewhat smaller than for the neutral molecule. For the methyl CH bonds, the bond overlap populations for the $1a_1$ and $2a_1$ valence-ionized states are not too

different than for the neutral molecule; however, for the $1b_2$ ionized state there is a significant decrease in population. On the basis of the foregoing discussion, it is not unreasonable that the overall FWHM for the individual valence 2s levels should occur in the order $1a_1 > 1b_2 > 2a_1$ based on the expected contributions from the likely vibrational modes which would be excited.

Although linewidth variations are clearly apparent for the higher alkanes, the experimental data has only been subjected to a detailed analysis for the series up to and including n-butane.[216] The linewidth variation for the individual components is substantial, ranging from $\sim$2.2 eV for the most tightly-bound $1a_g$ to 1.1 eV for the $2b_u$ ionized states. Analysis of the CC and CH bond overlap populations provides a qualitative rationale for these observations. Thus for the $1a_g$ ionized species, the CC and methylene CH bond overlap populations decrease significantly compared with the ground-state molecule, suggesting that the symmetric CC and CH stretching modes would contribute significantly to the overall band-profiles. By contrast, for the $2b_u$ ionized state the major difference in bond overlap populations is in respect of the methylene CH groups. An interesting situation is apparent for the $1b_u$ and $2a_g$ ionized states, since the linewidth for the latter is significantly larger than for the former. Whereas for the $1b_u$ ionized state the major changes in bond overlap population with respect to the ground state are for the C1(C3)-C2(C4) bonds, for the $2a_g$ ionized state there are substantial changes for the C2-C3 bond overlap and for the methyl CH bond overlap populations. It would not seem unreasonable therefore that the linewidth should be somewhat

smaller for the $1b_u$ compared with the $2a_g$ ionized state.

A detailed analysis of the asymmetric band-shape associated with ionization of the predominantly 2s orbital of methane in terms of vibrational fine-structure would seem to indicate that the lifetime for the hole is significantly smaller than for the core-ionized species. An elementary analysis of the lineshape associated with ionization from the corresponding σ_g and σ_u orbitals of ethane in terms of changes in potential energy surfaces accompanying ionization provides a qualitative basis for rationalizing the experimental data. In the particular cases of propane and n-butane, a qualitative discussion of the substantial differences in overall band-profiles may be presented in terms of vibrational excitations as evidenced by changes in bond overlap populations. It would appear therefore that a consistent picture may be presented of the differences in linewidth for individual components of the valence 2s regions of the alkanes in terms of differences in vibrational excitations accompanying ionization.

CHAPTER FOUR

SOME THEORETICAL CONSIDERATIONS OF CORE-IONIZATION IN CARBOCATIONS

Δ SCF calculations on simple carbocations at the STO-4.31G level are reported. Readily understood trends in binding energy shifts and differences in relaxation energy are found. The potential of XPS as a tool for investigating such systems is pointed out. For the particular cases of t-butyl cation, and 2-norbornyl cation, comparison is made with the available XPS experimental data. Excellent agreement with experiment is found in both cases only if the non-classical form of the 2-norbornyl system is considered. Finally, for the classical and non-classical forms of ethyl, 1-propyl and 2-norbornyl cation, it is found that the energetic preferences of the core-ionized species magnify the small energy-differences of the ground-state systems.

4.1 Electronic Relaxation Accompanying Core-Ionization in Some Simple Carbocation Systems

4.1.1 Introduction

Ab initio MO theory has played an impressive role in the discussion of the structure and stability of reactive chemical intermediates.[217-220] Such species are generally too short-lived to be amenable to direct spectroscopic observation and characterization, with the result that theoretical rather than experimental probes have been used extensively to gain insight into the properties of these species. It should however be stressed at the outset that theoretical calculations refer to the isolated ion in the gas phase. The calculations,

therefore, reflect the fundamental electronic properties of the isolated ion, and caution must be exercised in making comparisons with experimental data in solution, where the results may depend strongly on interactions with solvent molecules. The problem of differential solvent effects is only now beginning to be studied from a quantum mechanical viewpoint.[237-240]

Carbonium ions occupy a special place in the realm of reactive chemical intermediates, as evidenced by the comprehensive volumes edited by Olah and Schleyer[221] on the subject. In order to account properly for their properties, Olah[222] proposed two classes of carbocation (the most general name for all cationic carbon compounds, cf. carbanions for the negative ions):

(i) carbenium ions, which are trivalent ("classical") ions with an electron-deficient central carbon atom;

(ii) carbonium ions, which are penta- (or tetra-) coordinated ("non-classical") ions.

The topic of non-classical carbocations has aroused much controversy; recent reviews by Kramer,[223] Brown[224] and Olah[225] give good accounts of the differing viewpoints, and a recent book[226] attempts to provide a critical examination of the whole field.

It was recognized at an early stage[227,228] that the core binding energy shifts would make XPS a particularly suitable technique for the study of carbocations. In view of the XPS data already published,[227,229-232] and as a logical extension of the previous chapter on alkanes, a study of the core binding energies, and of the electronic relaxation

accompanying core-ionization in some simple model-system linear and branched carbocations is presented in this section. This represents the first detailed systematic study of carbocation systems at the ΔSCF level; previous studies of individual carbocations relied on Koopmans' Theorem. Since differential relaxation effects might be anticipated to be important in such charged species, it might be expected that Koopmans' Theorem provides only a poor estimate of the binding energy in such systems.

4.1.2 Computational Details

ΔSCF calculations at the STO-4.31G[46] level employing best-atom exponents[30] were performed on the following series of simple carbocations: methyl, ethyl, bridged ethyl, n-propyl (methyl-staggered 1-propyl), "bent" propyl (methyl-eclipsed 1-propyl), corner-protonated cyclopropane, isopropyl (2-propyl), n-butyl, and tertiary-butyl cation. Where available, the STO-4.31G (or STO-3G) optimized geometries[218,219] were used; for t-butyl cation, the partially-optimized geometry quoted by Hehre[220] was used, whilst for n-butyl cation, a model geometry along the lines suggested by Pople et al.[190,234] was employed.

4.1.3 Results and Discussion

The calculated binding energies and relaxation energies are shown in Table 4.1. It is well-known that use of an STO-4.31G basis set tends to over-estimate the absolute values of the binding energy, since the magnitude of the relaxation energy is under-estimated. That this is still the case for cationic species was confirmed by performing ΔSCF calculations for methyl and ethyl cation using a Slater

TABLE 4.1 Calculated Binding Energies and Relaxation Energies (in eV) of Simple Carbocations.

Molecule		ΔSCF		Koopmans'			
		B.E.	ΔB.E.	B.E.	ΔB.E.	R.E	ΔR.E.
Methyl cation	C	309.04	(0)	317.99	(0)	8.96	(0)
Ethyl cation	$C1^+$	306.22	-2.82	316.62	-1.38	10.40	+1.44
	C2	301.78	-7.26	312.74	-5.25	10.96	+2.01
Bridged ethyl cation		304.06	-4.98	314.98	-3.02	10.92	+1.96
n-Propyl cation	$C1^+$	304.87	-4.16	316.09	-1.90	11.22	+2.26
	C2	301.01	-8.03	312.47	-5.52	11.46	+2.51
	C3	299.98	-9.06	311.63	-6.36	11.65	+2.70
"Bent" propyl cation	$C1^+$	304.06	-4.98	315.41	-2.58	11.35	+2.39
	C2	300.98	-8.06	312.84	-5.19	11.83	+2.87
	C3	300.31	-8.72	312.43	-5.56	12.12	+3.16
Corner-protonated cyclopropane	C1,C2	302.36	-6.67	313.97	-4.02	11.61	+2.66
	C3	301.03	-8.01	312.85	-5.15	11.82	+2.86
Iso-propyl cation	C1,C3	300.86	-8.17	312.11	-5.88	11.25	+2.29
	$C2^+$	304.94	-4.10	315.93	-2.07	10.99	+2.03
n-Butyl cation	$C1^+$	304.59	-4.45	316.09	-1.90	11.50	+2.54
	C2	300.64	-8.40	312.16	-5.83	11.52	+2.56
	C3	299.42	-9.62	311.31	-6.68	11.89	+2.93
	C4	298.20	-10.84	309.81	-8.18	11.60	+2.64
t-Butyl cation	C1,C2,C3	300.23	-8.81	311.62	-6.37	11.39	+2.44
	$C2^+$	303.98	-5.06	315.35	-2.64	11.37	+2.41

Double Zeta basis set[235] with Clementi's exponents;[32] a comparison of the results for the two basis sets is given below in Table 4.2. However, it is clear from this table

TABLE 4.2 BE and RE (in eV) for methyl and ethyl cation, using different basis sets.

Molecule	Slater Double Zeta				STO-4.31G			
	BE	ΔBE	RE	ΔRE	BE	ΔBE	RE	ΔRE
Methyl	306.21	(0)	12.05	(0)	309.04	(0)	8.96	(0)
Ethyl C1$^+$	303.58	-2.63	13.39	1.34	306.22	-2.83	10.40	1.44
C2	299.18	-7.03	13.87	1.83	301.78	-7.26	10.96	2.01

that shifts in binding energy and changes in relaxation energy are well-described even at the STO-4.31G level.

As a preliminary investigation on the effect of angle-strain on binding and relaxation energies of bridge-head carbons in species such as the 2-norbornyl cation, an angle-deformation study on methyl cation was undertaken, Figure 4.1. As the molecule is deformed from the planar equilibrium geometry, there is a slight increase in the binding energy (less than 0.2 eV, even for severe deformations). The concomitant relaxation energy change, however, is an order of magnitude smaller, and may therefore be neglected. This is an indirect confirmation of the conclusion reached in the previous chapter, in which bending modes in methane and ethane were not considered in the study of vibrational fine-structure; if such modes were significant, it might be anticipated that significant changes in binding energy would be observed during angle deformation. This topic is presently being analyzed in some detail, with an investigation of the stretching and bending

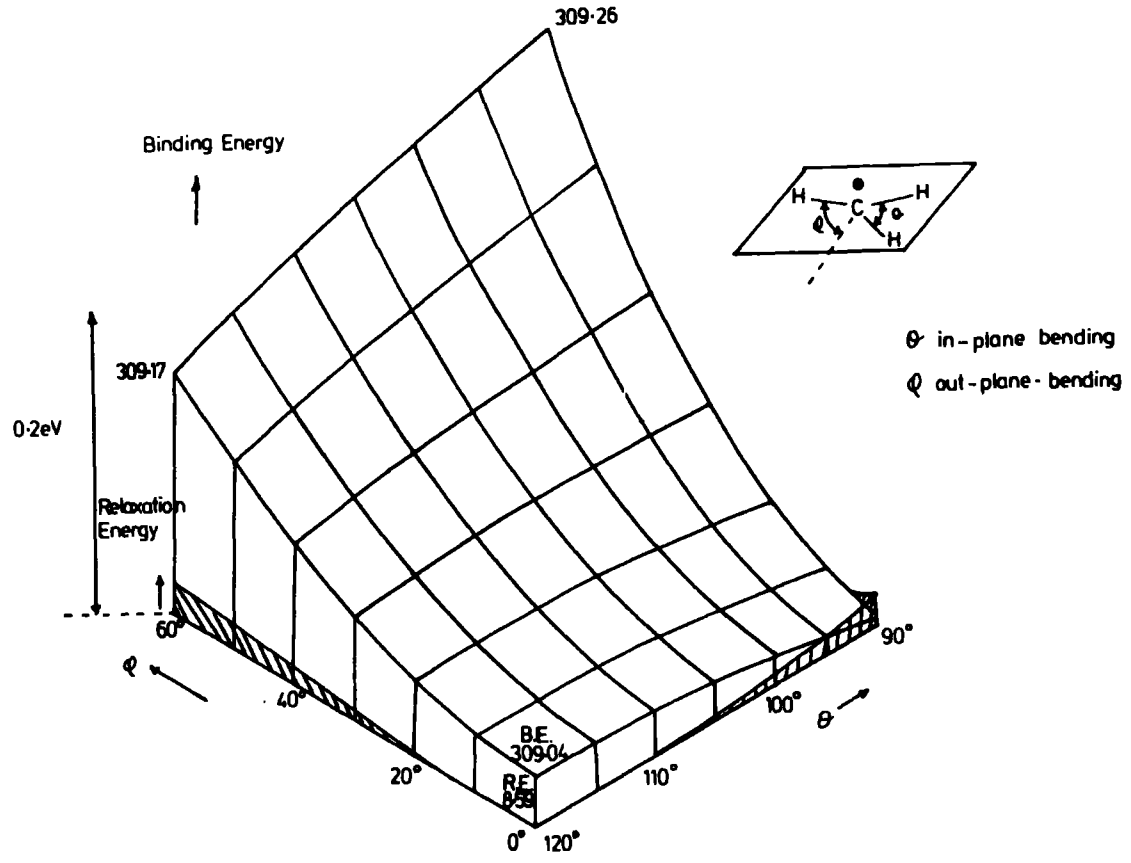

Fig. (4.1) Effect of angle-deformation on BE and RE of methyl cation.

modes in both singlet and triplet methylene, and its corresponding core hole states.

Figure 4.2 shows a plot of the calculated C_{1s} binding energy shift and change in relaxation energy (as compared with methyl cation) for the series methyl, ethyl, isopropyl and t-butyl cation (a), and methyl, ethyl, n-propyl, n-butyl cation (b). The circles o show the changes for the carbon atom bearing the positive charge in the cation, whilst the crosses x show the changes for the methylene carbon atom adjacent to this positive charge.

For the linear carbocations, Figure 4.2(b), there is a pronounced decrease in binding energy for the $-\underline{C}H_2^+$ carbon

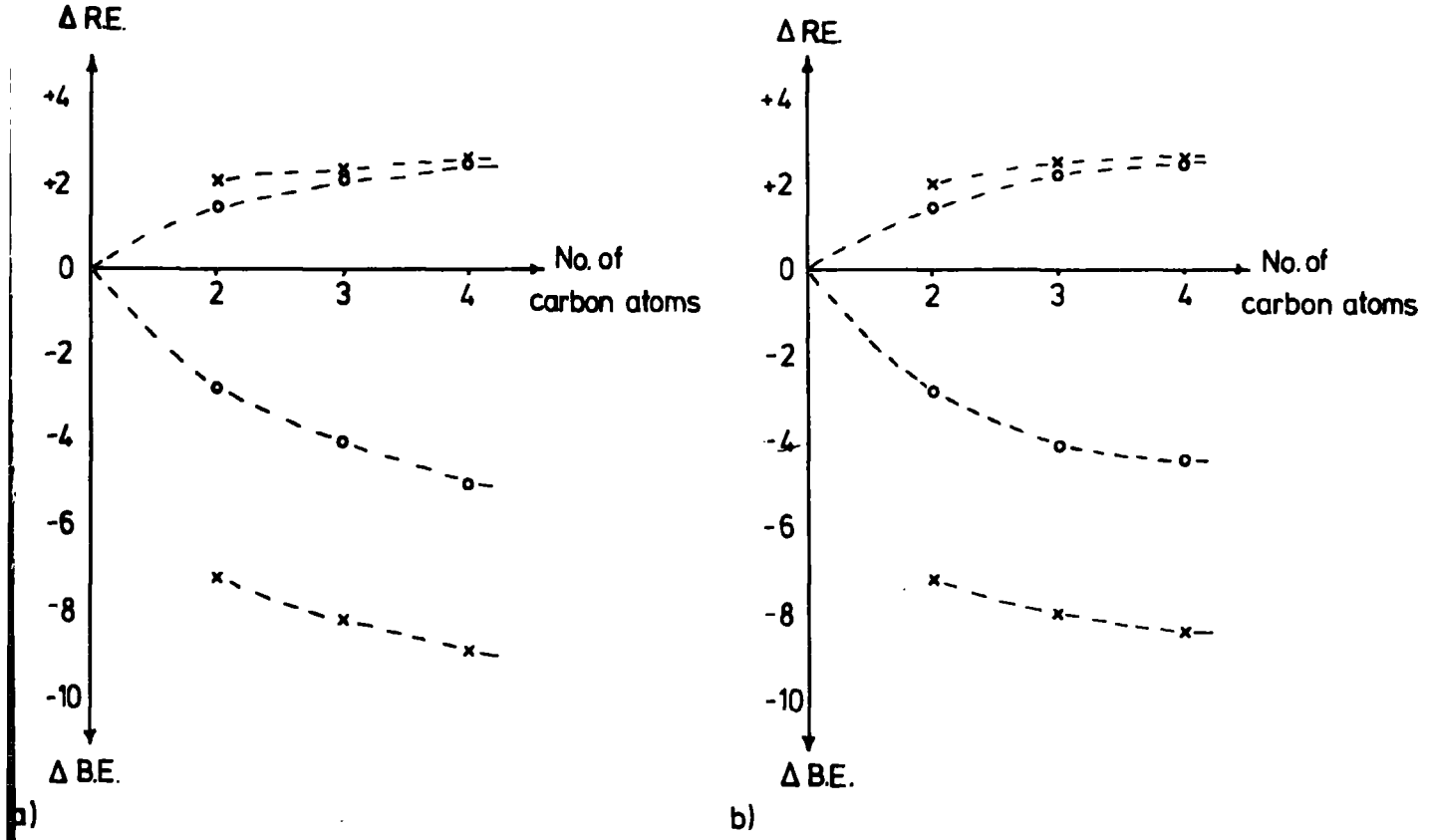

Fig.(4.2) Δ SCF BE and RE as a function of the number of carbon atoms in:

(a) branched-chain carbocations;

(b) linear carbocations.

atom (o), which seems to level off at a value of ∿-4.5 eV. Although there is a corresponding increase in relaxation energy, this does not account for all of the shift in the binding energy, increasing only to a value of ∿2.5 eV. This contrasts with the situation for the C_{1s} binding-energies of the corresponding hydrocarbons, where almost the entire shift in binding energy could be ascribed to changes in relaxation energy. The situation is even worse for the adjacent methylene carbon atoms, $-\underline{C}H_2 - CH^+_2$, (x); here, the value of the binding energy shift decreases only by about 1 eV from the value of ∿-7.3 eV in ethyl cation, whilst the relaxation energy remains fairly constant at ∿2 eV.

The situation is somewhat similar in the case of the branched-chain carbocations, Figure 4.2(a). In this case, the binding energy decreases do not level off as in the case of the linear carbocations; the relaxation energy increase, however, is much the same as for the linear carbocations, being much less in magnitude than the shifts in binding energy.

Previous calculations have shown that a slightly bent, methyl-eclipsed 1-propyl cation is energetically preferred to the methyl-staggered 1-propyl cation.[236] It was therefore of interest to compare the calculated C_{1s} ΔSCF binding energies in these species, together with the values for the limiting form of "bent" propyl cation, corner-protonated cyclopropane, as shown in Figure 4.3. The ground-state energies of all three species fall within 1.6 kcal mol^{-1}; the changes in binding energies along the series are much more dramatic, however. In going from the n-propyl to the "bent" propyl cation, the C1 binding energy decreases whilst the C3 binding energy increases, leading to a decrease in the internal chemical shift (as indicated by the line-diagrams in Figure 4.3) of 1.15 eV (equivalent to $\sim$26.5 kcal mol^{-1}). On going to corner-protonated cyclopropane, there is a significant decrease in the binding energy, leading to a further decrease in the chemical shift of 2.42 eV. The changes in relaxation energies in this series are much less marked. This is a good illustration of the fact that although the ground-state energies are very similar, the core-electron binding energies are very sensitive to these structural changes. This will be discussed in more detail in section 4.3.

Figure 4.4 shows a plot of binding energy against

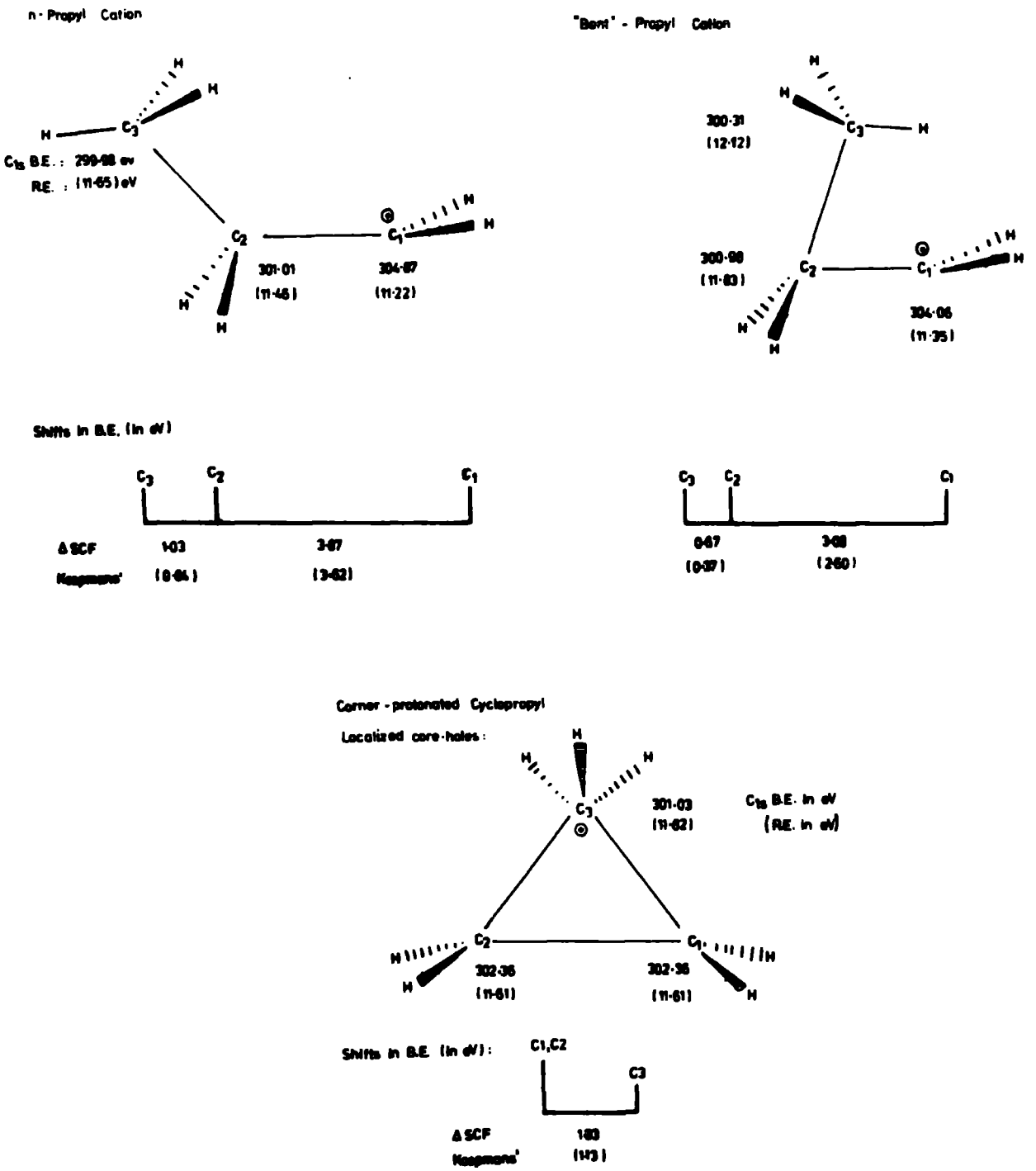

Fig. (4.3) ΔSCF BE and RE for various propyl cationic species.

relaxation energy for the simple carbocation systems. In common with the results obtained from a study of the C_{1s} binding energies in a series of neutral molecules,[149] the span in binding energies is greater than the span in relaxation energies. Clear trends are discernible: for the carbon-atoms bearing the positive charge in the cation, there are almost linear trends

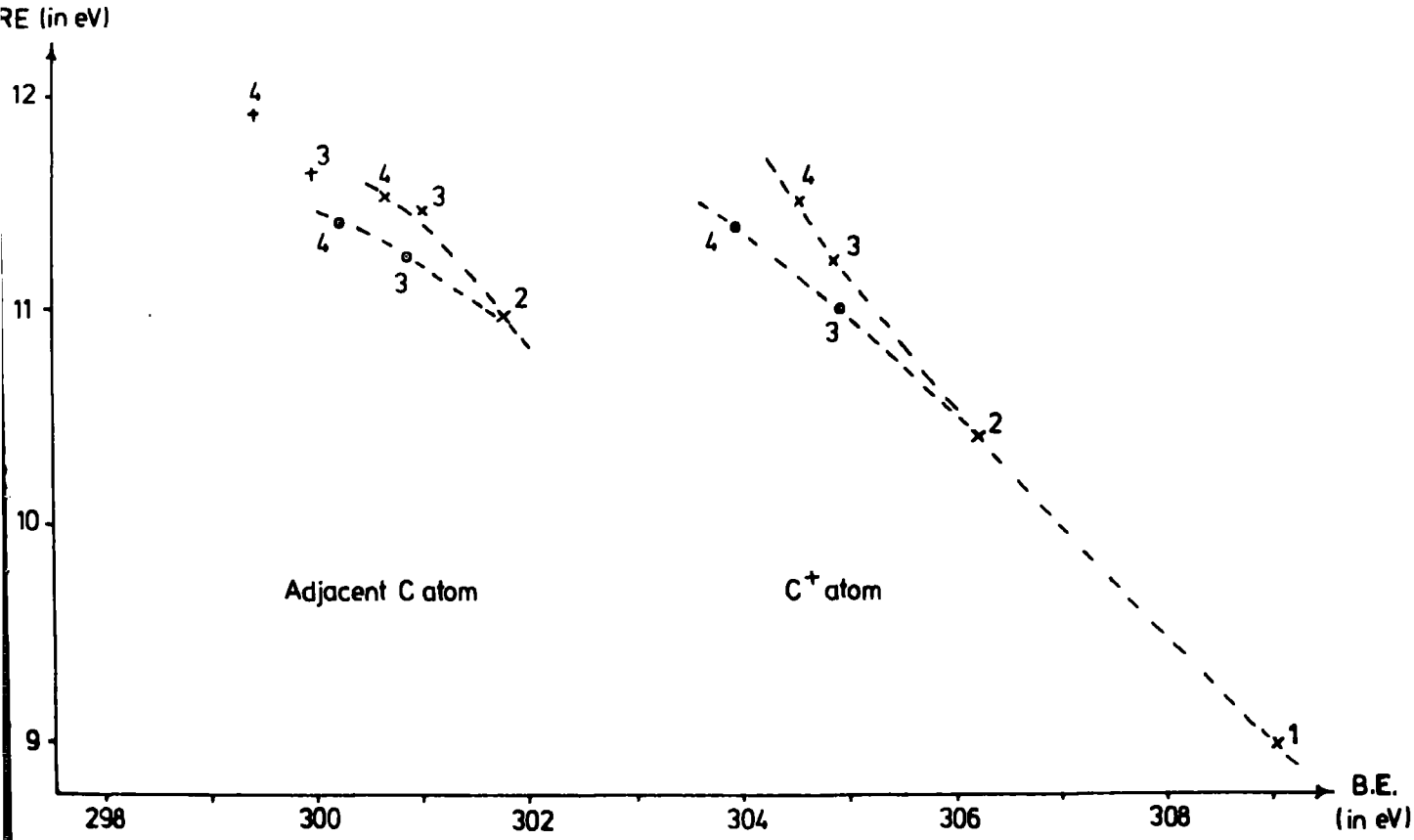

Fig. (4.4) BE vs. RE for carbocation systems. The numbers by each point indicate the number of carbon atoms in the carbocation.

for both the linear carbocations (x) and the branched-chain carbocations (o). This may be qualitatively understood as follows: on going from methyl cation to t-butyl cation, the charge on the positive site is progressively stabilized by the methyl groups. On simple electronegativity grounds, this would lead to a decrease in binding energy. Coupled with this, however, is the expectation that the increasingly more polarisable electron-cloud would lead to a greater relaxation energy. This is exactly what is observed for the central carbon atom in the branched-chain alkanes.

The methylene carbon atoms adjacent to the positive charge are grouped well to the low binding energy side of the

carbon atoms bearing the positive charge. Here, also, a trend seems to be observable between the binding energy and relaxation energy.

A comparison of Figure 4.4 with the corresponding plot for the C_{1s} binding and relaxation energies of the parent alkanes, Figure 3.5, clearly shows the greater span in energies for the carbocations. This is graphically illustrated in Figure 4.5, which shows the calculated ΔSCF binding energy

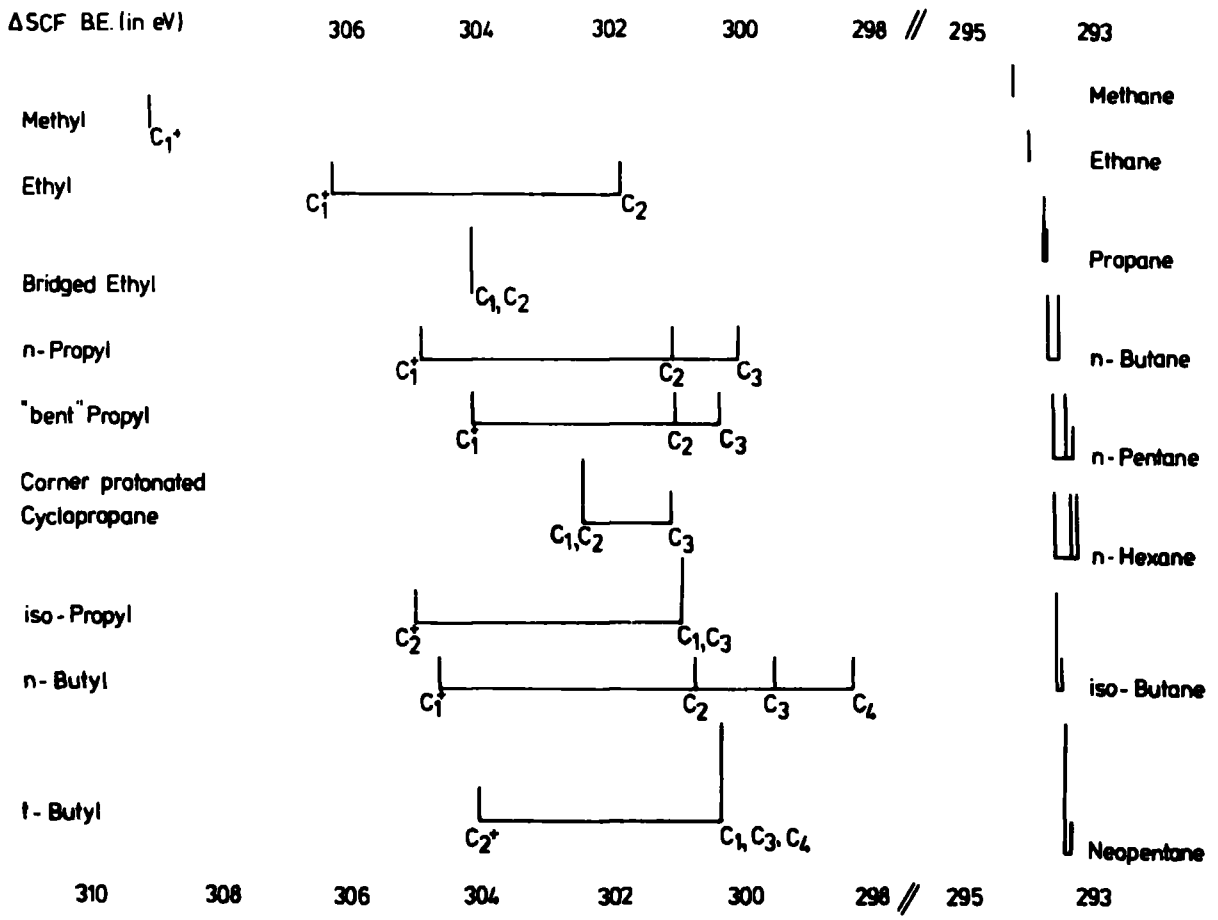

Fig. (4.5) Calculated ΔSCF C_{1s} BE shifts for carbocations and alkanes.

shifts as line-diagrams for both the carbocations and the parent alkanes, on the same scale. Not only are the cation binding energies well-separated from those of the alkanes, but also the internal chemical shifts are much greater than in the

alkanes. This provides strong support for the suggestions that XPS would be an eminently suitable technique for the study of such species; this will be discussed in more detail in section 4.2.

The valence-electron flow accompanying core-ionization in these carbocations, as revealed by Mulliken population analyses, is shown in Figure 4.6. Comparison with Figure 3.3 reveals that the valence-electron flow from each hydrogen decreases from 0.265 in methane to 0.231 in methyl

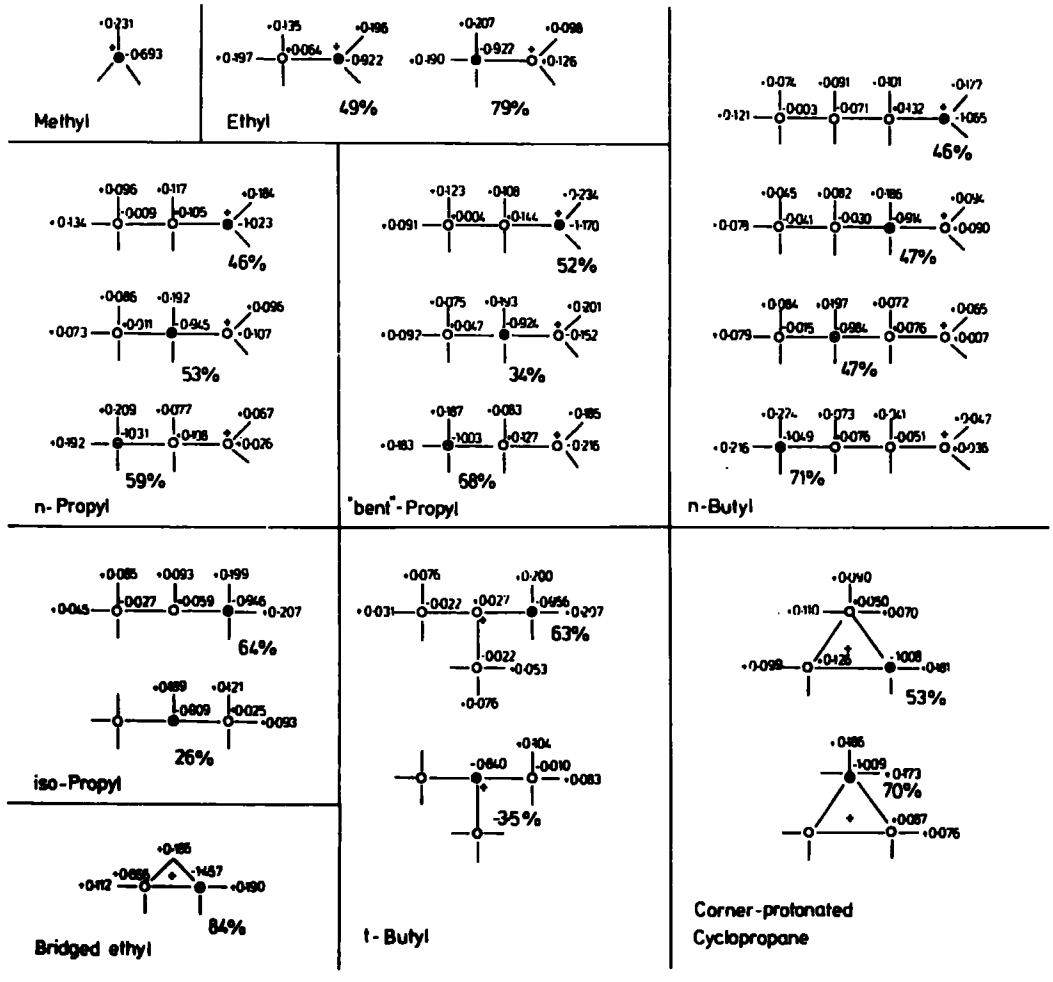

Fig. (4.6) Mulliken valence-electron flow accompanying core-ionization in simple carbocations.

cation. This may be naively rationalized on the grounds that the electron-cloud in the cation is already somewhat contracted

due to the positive charge, making further contraction consequent on core-ionization more difficult than in the case of the neutral molecule. On this basis, it would be expected that for the anion, there should be a larger flow from each hydrogen atom; this is indeed found to be the case (0.287 electrons). This conclusion is reinforced by a consideration of the relaxation energies, which are 8.96 eV, 10.96 eV and 11.32 eV for methyl cation, methane and methyl anion, respectively.

The percentages shown in Figure 4.6 are the nearest neighbour contributions to the total valence-electron flow to the core-ionized carbon. As in the case of the alkanes, the majority of the flow arises from the hydrogen atoms; thus in the linear carbocations, core-ionization of the carbon atom bearing the positive charge results in a contribution of 46-49%. This value decreases to 26% for isopropyl cation, and for t-butyl cation, there is in fact no flow to the central carbon atom on core-ionization from the nearest neighbours. Similar considerations hold for core-ionization of the carbon atom adjacent to the positive charge; this is 79% in ethyl cation, ~64% for the branched-chain carbocations, and ~50% for methylene carbon atoms in the linear carbocations.

One interesting difference from the alkanes is that there is considerably greater flow from the carbon chain in the carbocations. For example, core-ionization in ethane leads to a contribution of +0.020 electrons to the core-hole from the neighbouring carbon atom. In ethyl cation, however, if the core-hole is created on the carbon already bearing the positive charge (CH_3-$\underline{C}H_2^+$), there is a flow of +0.064 electrons from the other carbon, whilst if the methyl carbon in ethyl

cation ($\underline{C}H_3$-CH_2^+) is core-ionized, there is a contribution of +0.126 electrons from a formally positively-charged carbon atom.

4.2 A Theoretical Investigation of the Core Hole States of the 2-Norbornyl Cation

4.2.1 Introduction

Despite the intense research activity into the classical or non-classical nature of the 2-norbornyl system, opinion is still as diverse as ever.[223-226] Theoretical calculations at various levels of sophistication agree in that the energy difference for isolated systems between the classical and non-classical formulations is small.[241] It would, therefore, seem reasonable to focus attention on properties of the system which would provide a direct means of distinguishing between the two, and accordingly a whole host of spectroscopic techniques has been applied to this problem. However, the only such technique which would *a priori* appear capable of effecting this distinction is XPS, for which the time-scale precludes any ambiguities arising from rapidly equilibrating structures. Unfortunately, the issue has been clouded by technical difficulties in obtaining appropriate core-level spectra, and the available data[227,231,232] have been interpreted as supporting both possibilities. Comparison must eventually be made with model systems, from which inferences are then drawn concerning the interpretation of the experimental data. A fundamental difficulty has been the lack of suitable models for comparison; in this section, an attempt is made to rectify this situation.

4.2.2 Computational Details

Theoretical studies previously reported[135,149,188] indicate that relaxation energies accompanying core-ionization are dependent on electronic structure, and differences in relaxation energies can contribute significantly to binding energy shifts, particularly for systems with considerable valence-electron asymmetry.[210] Electronic reorganization accompanying core-ionization should, therefore, be taken into account; the most straightforward means accomplishing this is by the ΔSCF method.[136,137] An alternative method involves the equivalent cores concept,[167,168] whereby binding energy shifts are computed from the heats of reaction of the appropriate isodesmic process. Previous calculations have indicated that shifts are accurately described at the ΔSCF STO-4.31G level, whilst for the less basis set dependent equivalent cores approach, calculations at the STO-3G level are generally adequate.

Allen and Goetz[242] have detailed an extensive non-empirical LCAO MO SCF investigation at both the STO-3G and STO-4.31G level on the electronic structures of classical and non-classical 2-norbornyl cation. As a basis for the detailed interpretation of the experimental XPS data, the core-hole spectra at the ΔSCF STO-4.31G and equivalent cores STO-3G level have been calculated, employing the optimized geometries obtained by Allen and Goetz. The numbering convention used for the classical and non-classical forms of the 2-norbornyl cation is illustrated in Figure 4.7. In addition, an "optimized" STO-3G basis set has also been used, since it is known that absolute binding energies are well-reproduced by this method.

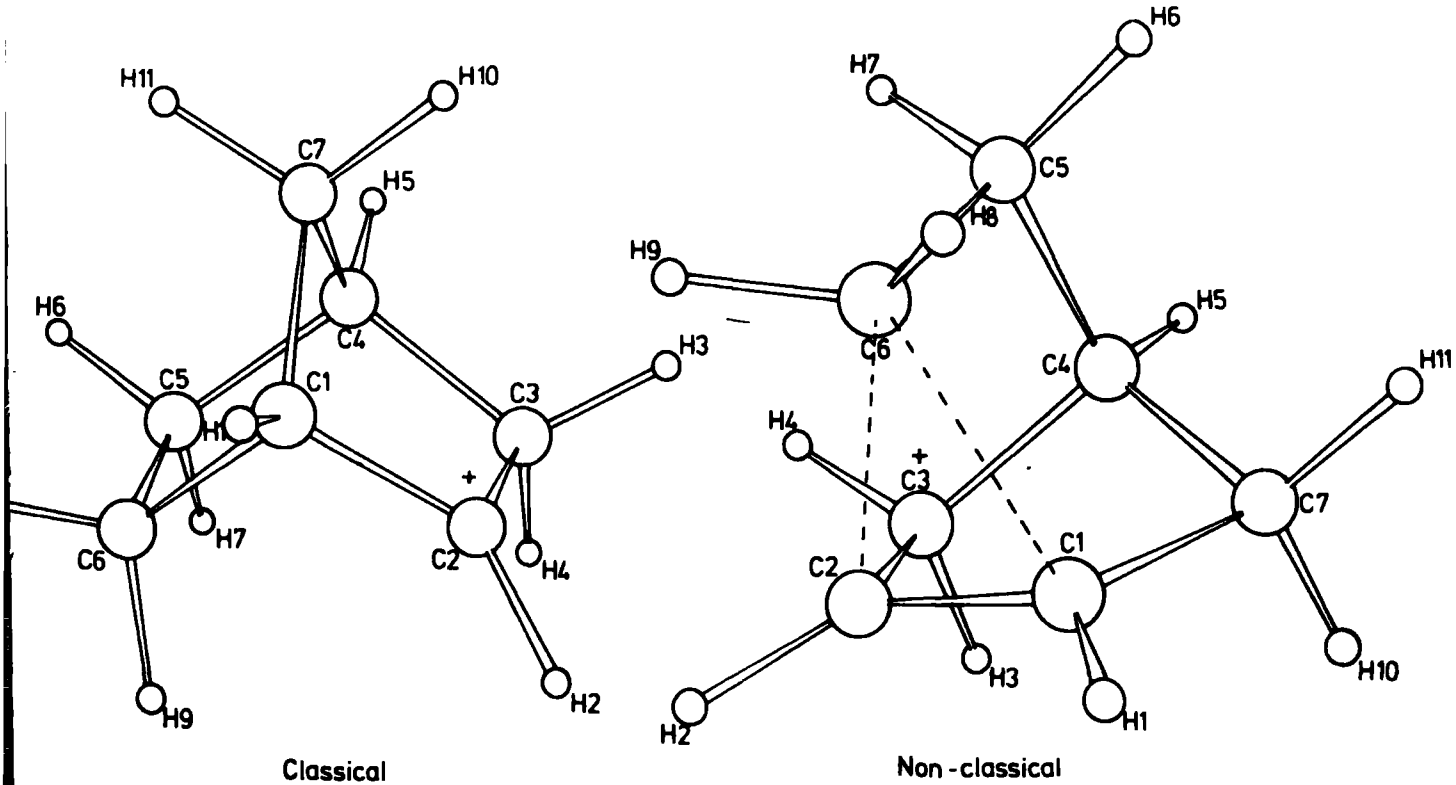

Fig. (4.7) Perspective representations of the classical and non-classical forms of the 2-norbornyl cation.

4.2.3 Results and Discussion

To illustrate the importance of relaxation, Table 4.3 shows the calculated binding energy shift for ethyl cation.

TABLE 4.3 BE shifts for ethyl cation (in eV)

	Double Zeta		STO-4.31G		STO-3G	
	ΔSCF	Koopmans'	ΔSCF	Koopmans'	ΔSCF	"Optimized"
Ethyl Cation	4.40	3.92	4.44	3.87	4.90	4.19

At the Slater Double Zeta level, neglect of relaxation effects leads to an underestimation of the shift of ∿0.5 eV. Previous studies have shown that for first-row atoms, shifts and indeed absolute binding energies are well-reproduced at this level, calculations at this level for large systems such as the 2-norbornyl

cation would, however, be prohibitive both in terms of computer resources and expense. As far as binding energy shifts and differences in relaxation energy are concerned, the ΔSCF method at the STO-4.31G level is perfectly adequate. Furthermore, use of the "optimized" STO-3G basis set is found to give reasonable agreement with the Slater Double Zeta basis, whilst the normal STO-3G ΔSCF result is only in poor agreement.

Before considering the results for the 2-norbornyl cation, comparison may be made with experiment for the t-butyl cation, Table 4.4, for which there is no dispute concerning its "classical" nature. The reported core-level spectrum[227]

TABLE 4.4 BE Shifts for t-Butyl (in eV)

	STO-4.31G		STO-3G				
	Δ SCF	Koop-mans	ΔSCF	Koop-mans	Equiv-alent Cores	"Opti-mized"	Equivalent Cores MINDO/3
t-Butyl cation	3.75	3.73	4.13	4.67	3.72	4.19	3.40[a]

(a) Ref. 244

consists of a doublet structure (intensity ratio 1:3), with a C_{1s} binding energy shift of 3.9 ± 0.2 eV. Clearly, the STO-4.31G ΔSCF and equivalent cores STO-3G results are in excellent agreement with experiment, in contrast to the Koopmans' value using a small basis set (STO-3G), which greatly over-estimates the binding energy shift. The MINDO/3 method,[243] which has been extensively parametrized to reproduce thermodynamic data, does relatively poorly.

The good agreement between theory and experiment is significant, since although the mode of sample preparation used for the XPS investigations involves a relatively uncharacterized system, possibly involving ion-pairs in a frozen

solvent matrix, it is almost inconceivable that agreement could be entirely fortuitous. Previous work,[245,246] however, suggests that shifts (but not absolute binding energies) computed for an isolated ion should correlate directly with experimental data pertaining to the solid state.

The computed shifts and assignments for the C_{1s} binding energies of the classical and non-classical 2-norbornyl cation are shown in Table 4.5. The main feature evident from this is that the span in binding energies for the classical ion is much larger than for the non-classical ion (4.4 eV compared with 2.1 eV, respectively, for the ΔSCF STO-4.31G basis). The STO-3G (Koopmans' and ΔSCF) calculations seem to overestimate the binding energy shifts, whilst the ΔSCF STO-4.31G, the STO-3G equivalent cores, and the "optimized" STO-3G calculations are in excellent overall agreement with one-another with regard to both shifts in binding energies, and relative ordering. This contrasts strikingly with the MINDO/3 equivalent cores calculations of Dewar.[244] This may be attributable to the different geometries obtained by the MINDO/3 optimization:[244] for example, in the classical ion, the C6-$\hat{C}$1-C2 angle is 8.5° greater than in the STO-4.31G geometry,[242] whilst in the non-classical ion, the C6-C1 (C6-C2) and C1-C2 bond-lengths are 0.2 and 0.05Å shorter and longer, respectively, than the STO-4.31G geometry. It seems more likely, however, that the discrepancy is due to the inadequacy of the MINDO/3 method for calculating heats of reaction for the isodesmic core-exchange processes involved in the equivalent cores concept. Indeed, previously published equivalent cores MINDO/3 calculations of XPS shifts[247] gave only reasonable agreement with experiment - for example, the internal C_{1s}

TABLE 4.5 Binding Energy Shifts (in eV)

		STO-3G		STO-4.31G		"Optimized"	Equivalent Cores	
		Koopmans'	ΔSCF	Koopmans'	ΔSCF	STO-3G	STO-3G	MINDO/3[a]
2-Norbornyl cation								
Classical	C2	5.61	5.15	4.40	4.44	4.89	4.44	1.79
	C3	1.88	1.91	1.32	1.45	1.64	1.58	0.57
	C1	2.07	1.68	1.45	1.28	1.68	1.58	0.96
	C6	1.02	0.68	1.08	0.80	0.89	0.86	0.39
	C4	0.85	0.40	0.51	0.27	0.54	0.54	0.80
	C7	0.51	0.42	0.38	0.31	0.43	0.39	-0.13
	C5	O(309.30)[b]	O(299.56)	O(310.13)	O(298.11)	O(292.28)	O	O(295.34)
Non-Classical	C1,C2	3.20	2.59	2.43	2.01	2.49	2.17	1.00
	C6	1.71	0.89	1.84	1.25	1.79	1.57	0.85
	C3,C7	0.56	0.52	0.38	0.33	0.41	0.49	-0.08
	C4	0.39	-0.09	0.19	-0.12	0.17	0.15	0.53
	C5	O(309.78)	O(300.06)	O(310.44)	O(298.47)	O(292.69)	O	O(295.55)

(a) Ref. 244

(b) Figures in brackets give the absolute binding energy

chemical shift in acetone is given as 3.5 eV (ΔSCF STO-4.31G gives 2.6 eV;[193] experiment 2.6 eV); the CH_4 to CF_4 C_{1s} shift is quoted as 14.5 eV (12.9 eV, 11.0 eV for equivalent cores STO-4.31G[135] and experiment, respectively); and the ordering for the O_{1s} levels in formic acid is incorrect, whereas ΔSCF STO-4.31G predicts the correct ordering.[193] Furthermore, a recent publication demonstrates that MINDO/3 is not suited to treat four-electron, three-centre bonds, since thermodynamic data for such compounds are both rare and unreliable, and thus not included in the determination of the MINDO/3 parameters.

The computed STO-4.31G differences in relaxation energy span ranges of 0.31 eV and 0.59 eV for the classical and non-classical ions, respectively. The slightly less adequate treatment of relaxation phenomena at the ΔSCF "optimized" and equivalent cores STO-3G is manifest in the slight difference in ordering for the C4 and C7 hole-states in the classical ion, and the C4 and C5 hole-states for the non-classical ion.

The differences in electronic relaxation accompanying core-ionization are best illustrated by means of density-difference contour plots. Figure 4.8 shows such plots for both the classical and non-classical forms of the 2-norbornyl cation. In all cases, the plane shown contains atoms C2, C1 and C6, with C6 at the top of the plot. An area of 14 x 14 bohr is shown. Negative contours (dashed lines) indicate an increase in electron-density consequent on core-ionization. Core-ionization at C6 leads to a similar reorganization pattern for both the classical and non-classical species: there is a build-up of electron density in the C1-C2 bonding region as

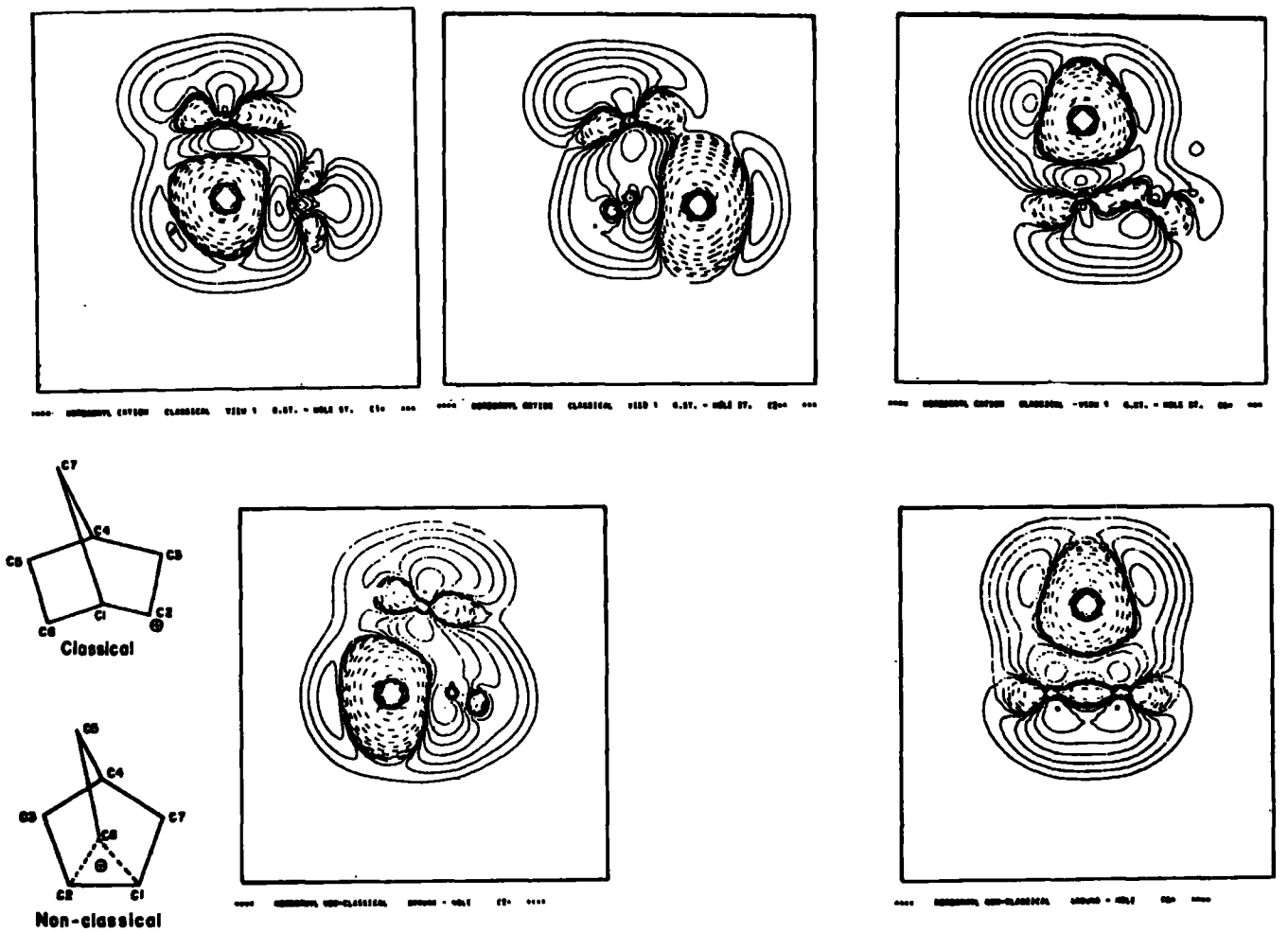

Fig. (4.8) Density difference contour plots for the 2-norbornyl system.

well as in the immediate vicinity of the core-hole in both cases. Core-ionization at C2 (or C1) in the non-classical cation shows some electron-density increase in the C6 region; for the classical cation, however, there is also a build-up of electron density in the C6-$C2^{+}$ bonding region. This is not seen if C1 in the classical case is core-ionized.

The core hole state spectra may be synthesized by taking components of appropriate line-shape (gaussian) and line-width. The band-profiles obtained with the different non-empirical methods used here all give very similar results; Figure 4.9 shows the simulated core-level spectra obtained

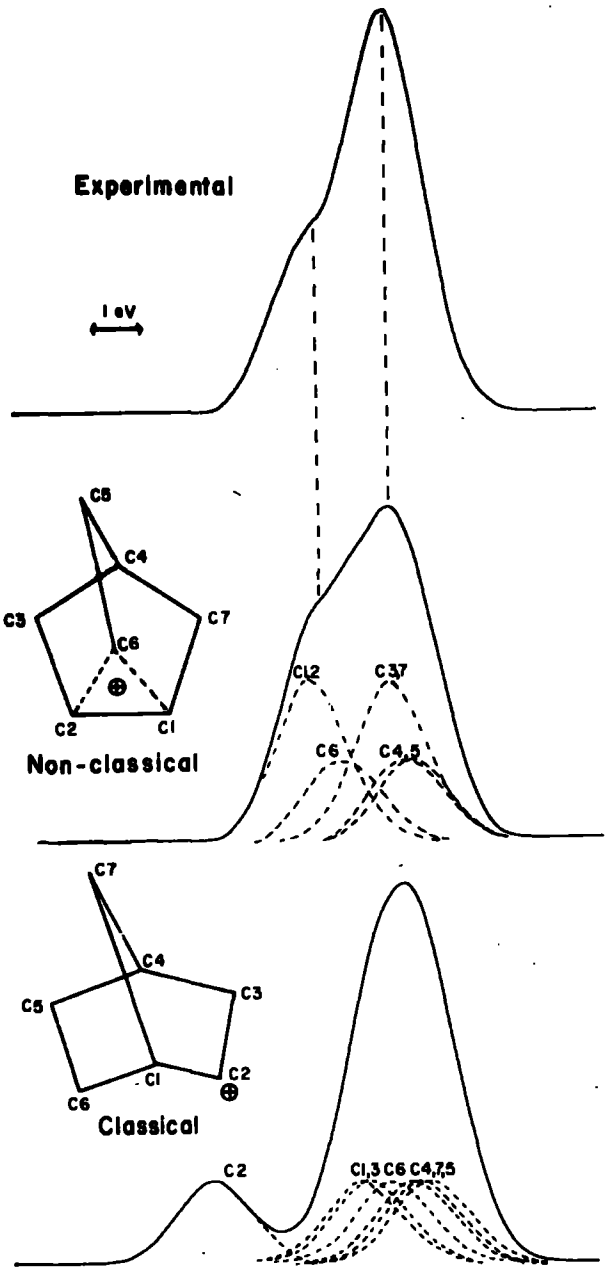

Fig. (4.9) C_{1s} spectra for the classical and non-classical 2-norbornyl cation.

from the ΔSCF STO-4.31G calculations, with component FWHM of 1.8 eV. Even with such relatively poor resolution, a clear-cut distinction between the classical and non-classical species is apparent. An interesting feature of the non-classical spectrum is the intermediate binding energy calculated for C6,

which falls midway between the two major components attributable to C1(C2) and C3(C7), C4 and C5. This would imply that any attempt to deconvolute the experimental spectrum into just two components is untenable.[229,232] For the classical ion, the large shift to high binding energy of C2 leads to a well-resolved spectrum, with an intensity ratio of 1:6.

When considering the experimental data, contamination problems suggest that emphasis should be placed on shifts rather than relative intensities.[224] Even a cursory perusal of the synthesized spectra suggests that the experimental data are not interpretable in terms of a classical 2-norbornyl cation. Comparison between the calculated non-classical spectrum and a smoothed version (normalized to a flat base-line) of the experimental data, however, is quite striking. The most logical conclusion to draw is that the published spectrum pertains to a non-classical 2-norbornyl cation, for which the surface has been contaminated by extraneous hydrocarbon. Such contamination is known to be a major problem in recording XPS spectra, and it is not unreasonable to expect that during the time-scale of the experiment, at the low temperature employed, such a contaminant layer would remain essentially inert. With a knowledge of electron mean free paths [249] ($\sim$20 Å for kinetic energies appropriate to the experimental data) and taking a monolayer as $\sim$5 Å thick, the experimental data would be quantatively described in terms of the calculated line-profile for the non-classical ion with a fractional ($\sim$0.6) monolayer coverage of hydrocarbon contamination. To this extent, the calculations outlined here resolve experimental ambiguities.

It is worth emphasizing that the energy difference between the classical and non-classical structures is so small

(less than 0.2 kcal mol^{-1} at the STO-4.31G level) that minor electronic perturbations would be expected to have quite a profound effect. The efficiency of a methyl substituent in stabilizing a positive charge is well-known, and it might therefore be anticipated that the 2-methylnorbornyl cation would prefer a classical structure. The expense and computer resources required preclude a full theoretical study of this system; however, on the basis of the results presented in section 4.1, where it was found that on going from 2-propyl to t-butyl cation, the central carbon binding energy decreases by $\sim$0.9 eV, it might be anticipated that the span of 4.4 eV in binding energy for the classical 2-norbornyl cation would be reduced to $\sim$3.5 eV on going to the methyl-substituted species. This is, in fact, in very good agreement with the reported shift of $\sim$3.7 eV[229,232] for 2-methylnorbornyl cation.

4.3 On the Relative Energies of the Ground and Core Hole States of Ethyl, 1-Propyl and 2-Norbornyl Carbocations

4.3.1 Introduction

It has become increasingly apparent over the past few years that the electronic reorganization accompanying core-ionization can substantially modify the potential energy surface with respect to the ground-state.[170] Despite the fact, therefore, that core-electrons contribute insignificantly to bonding, core-ionization is sufficiently strong a perturbation, as far as the valence-electrons are concerned, to provide a monitor of overall valence-electron distributions. One manifestation of the changes in potential energy surface consequent on core-ionization is the recent observation of vibrational fine-structure accompanying core-ionization in simple molecules.[150,199,200] A particularly striking example

of the changes in bonding accompanying core-ionization arises for hydrogen-bonded dimers,[250] which will be discussed in the following chapter. For the water dimer, removal of a core-electron from the monomer providing the hydrogen for the hydrogen-bond increases the hydrogen-bond strength, compared with the ground-state system, by some 40 kcal mol^{-1}. Core-ionization can, therefore, considerably enhance comparitively weak interactions in appropriate systems and hence magnify energy differences which may be quite small for the ground-state system.

The electronic structure of isomeric classical and non-classical carbocations constitutes an area of intense research activity on both an experimental and theoretical front.[219,220] In this section, it will be shown how a theoretical consideration of the ground and core hole states can provide some insight into the structure and bonding in these systems. Non-empirical LCAO MO SCF computations on the ground-state and localized C_{1s} hole-states have been carried out at the STO-4.31G level employing appropriate optimized geometries[236,245] for the classical and non-classical forms of ethyl cation, 1-propyl cation, and 2-norbornyl cation, as described in sections 4.1.2 and 4.2.2. The characteristic nature of the core-level spectrum of 2-norbornyl cation has already been discussed in section 4.2; in this section, the energetic perferences of the core-ionized species will be considered.

4.3.2 Results and Discussion

(a) Ethyl cation

The structure of the ethyl cation has been studied in great detail. The first full geometrical optimization[251] (at the STO-3G level) gave the classical (eclipsed)

ion as the most stable form, some 11.4 kcal mol^{-1} lower in energy than the bridged (non-classical) form. This energy is reduced to 7.3 kcal mol^{-1} at the STO-4.31G level however, the addition of d-functions (as in the STO-6.31G* basis set)[252] further favouring the bridged structure. Introduction of p-functions on hydrogen (STO-6.31G**) suggests the non-classical structure is the more favourable, and calculations including correlation[253] furthers this notion, favouring the bridged structure by 8 kcal mol^{-1}.

Differential solvation effects have been investigated theoretically by Jorgensen,[239] using a semi-empirical computation scheme. Employing five HCl molecules as a representative electron-donating solvent, the classical cation was favoured by ∿14 kcal mol^{-1} over the non-classical conformation. Estimates of differential solvation energies have also been made using a simple model[228] in which only the isotropic charge, dipole, or dipole-dipole interactions are considered. Using this model, the differential solvation between the classical and non-classical forms of ethyl cation is computed to be much less (∿2.4 kcal mol^{-1}).[240] Investigations of solvent effects should clearly be repeated with *ab initio* wavefunctions; and it should be noted that solvents which are poor electron-donors (such as superacids) may produce considerably smaller differential solvation effects.

Figure 4.10 shows the STO-4.31G results obtained for the ground and core hole states of the classical and non-classical forms of the ethyl cation. In accord with the published data, this basis set favours a classical ground-state for the ethyl cation, by ∿7 kcal mol^{-1}. The effect of core-ionization is dramatic, however; a core-hole on Cl (bearing

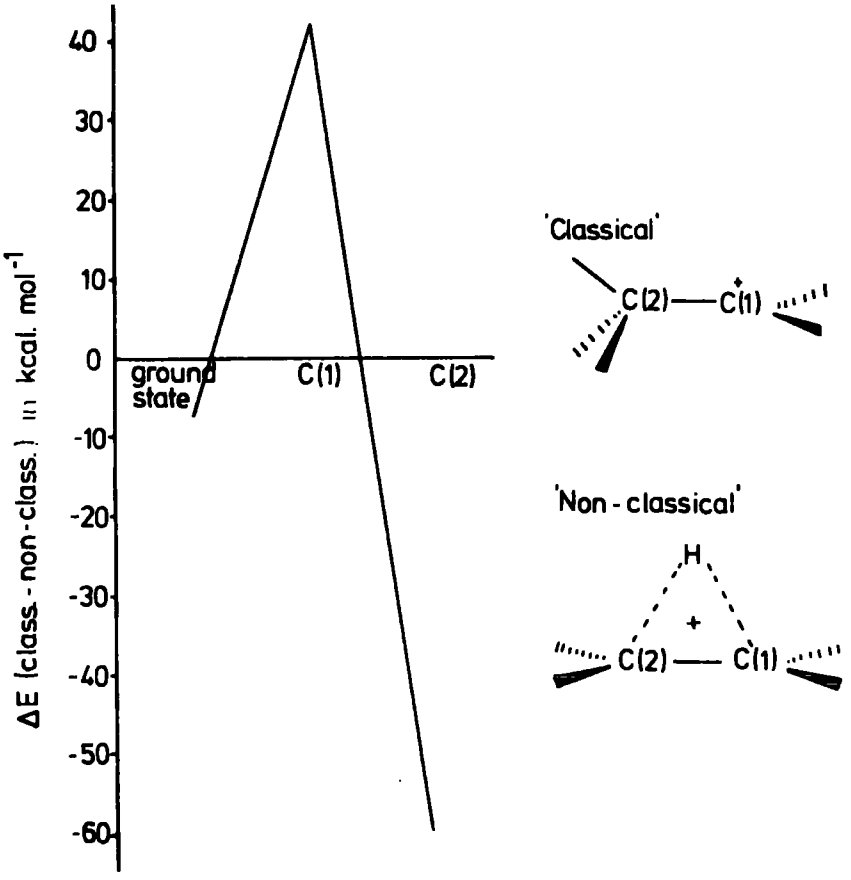

Fig. (4.10) Relative energy differences between the classical and non-classical forms of ethyl cation.

the positive charge in the classical species) favours a non-classical cation by ∿42 kcal mol^{-1}, whilst a core-hole on C2 favours the classical cation by ∿60 kcal mol^{-1}.

(b) 1-Propyl cation

The isopropyl (2-propyl) cation is by far the most stable form on the $C_3H_7^+$ energy surface; however, the nature of the second possible minimum energy form of $C_3H_7^+$ has received considerable attention.[254,236] Three types of 1-propyl structure have been considered in particular: corner-protonated cyclopropane; a similar structure in which one of the methyl-group hydrogens lies in the plane of the three carbons rather than perpendicular to it, "bent" propyl cation; and n-propyl cation. The relative energies of these species

are given in Table 4.6. Other species which have been studied all have higher energies than these. The STO-6.31G* is the highest level of theory used to date, and gives corner-protonated cyclopropane as the second stable form of $C_3H_7^+$.[251]

TABLE 4.6 Relative energies of $C_3H_7^+$ ground state structures (in kcal mol^{-1})[a].

	STO-3G	STO-4.31G	STO-6.41G*
2-propyl	0	0	0
n-propyl	19.7	17.4	17.0
"bent" propyl	20.5	16.9	14.1
corner-protonated cyclopropane	22.8	17.3	13.0

(a) Ref. 251

The results obtained for 1-propyl cation are shown in Figure 4.11. The computed energy-difference between n-propyl cation and corner-protonated cyclopropane is 0.7 kcal mol^{-1} for the ground-state, the range in ground state-energies for the three species being similar to that quoted at the STO-4.31G level in Table 4.6. The dotted line shows the relative energy-difference between the "classical" (n-propyl) and "bent" 1-propyl species; it is apparent that creation of a core-hole, and hence increased valence-electron demand, on C1 favours the bent form by some 20 kcal mol^{-1}. By contrast, creating a core-hole on C3 slightly favours the classical form, which again may be taken as evidence for slight electronic interaction between C3 and C1 in the bent form of the 1-propyl cation. For the creation of a core-hole on C2, however, the energetic preference essentially remains the same. Considering now the "bent" and "non-classical" (corner-protonated

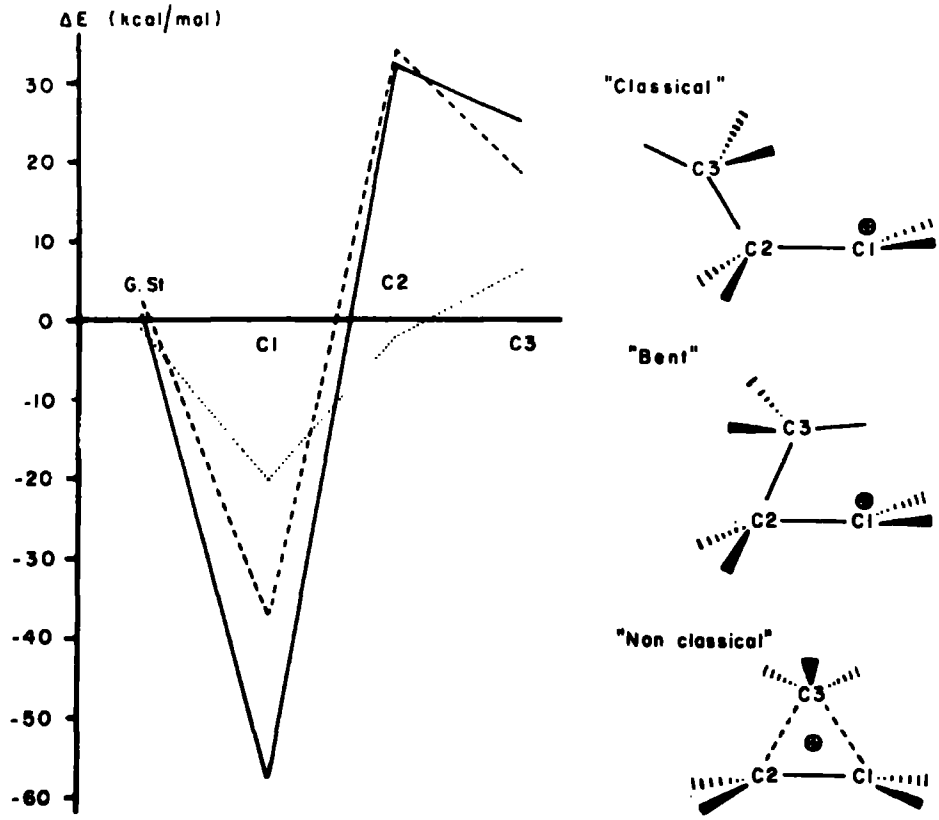

Fig. (4.11) Relative energy differences between the various forms of 1-propyl cation.

cyclopropane) forms, from the results indicated by the dashed line it is apparent that the creation of a core-hole on C1 markedly favours participation with C3, whereas a core-hole on the other carbons obviates such an effect, favouring instead the "bent" structure. The solid line, pertaining to the energy difference between the "classical" and "non-classical" forms of the 1-propyl cation, is effectively the sum of the former two lines, and shows that creation of a core-hole at C1 now greatly favours the latter (by $\sim$57 kcal mol^{-1}) whereas a core-hole on either C2 or C3 favours the "classical" structure by $\sim$32 and 25 kcal mol^{-1} respectively.

(c) 2-Norbornyl Cation

Similar trends are shown in Figure 4.12 for

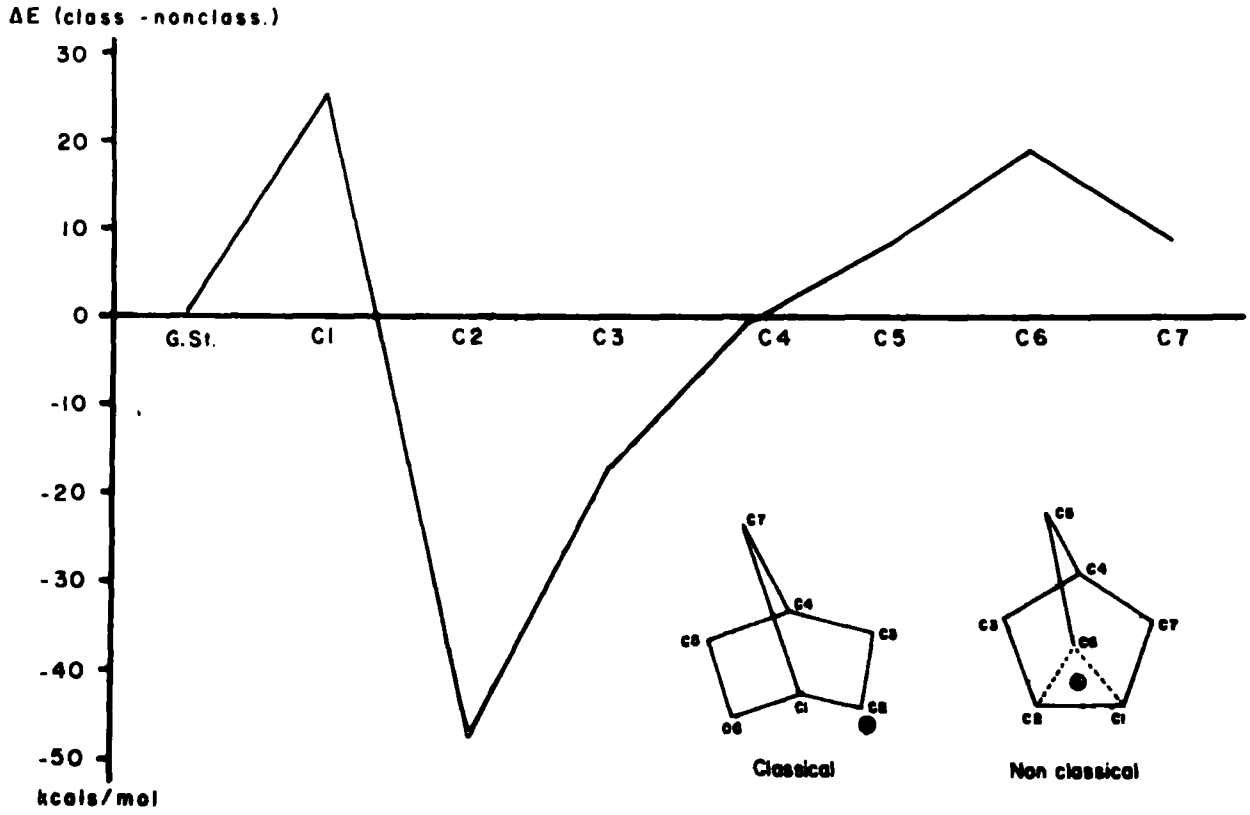

Fig. (4.12) Relative energy-differences between the classical and non-classical forms of 2-norbornyl cation.

the 2-norbornyl system. The recent study of Allen et al.[242] gives the energy of the non-classical ion as 5.2 kcal mol^{-1} higher than the classical conformation at the STO-3G level; this difference is reduced to only 0.2 kcal mol^{-1} at the STO-4.31G level. However, the formation of a core-hole on C2 enhances participation from C6, with the result that the non-classical species is favoured by $\sim$48 kcal mol^{-1}. On the other hand, creation of a core-hole at C1 or C6 (i.e., atoms which in the non-classical case are donors to C2) leads to the classical cation being favoured by $\sim$ 25 and 19 kcal mol^{-1} respectively.

The manifestation of these results is that the core hole state spectra are highly characteristic for the

isomeric species and differ quite significantly for systems which on an absolute energy scale are closely similar.

The lifetimes of the hole-states are typically expected to be in the range 10^{-11} - 10^{-14} sec.; the manifestation of the substantial changes in potential energy surface in going from the ground-state to core hole state, therefore, is likely to be small asymmetries of the core hole state spectra, arising from vibrational excitation accompanying core-ionization. Such excitations are difficult to detect even for small molecules studied in the gas phase; for carbocations studied in the condensed phase they would almost certainly remain undetected.

The effect of different substituents in a molecule, creating either electron demand at, or donating electron density to, a given atom, is well-known in physical organic chemistry, having significant consequences on reactivity and rates of reaction. The creation of a core-hole may be regarded as an extreme case of such electron demand at an atomic centre, and it is hoped that the study of core hole states may provide some insight into electronic reorganizations upon electron demand and donation within a molecule.

CHAPTER FIVE

A THEORETICAL INVESTIGATION OF ELECTRONIC REORGANIZATIONS ACCOMPANYING CORE AND VALENCE IONIZATION IN SOME SIMPLE HYDROGEN-BONDED SYSTEMS

Non-empirical LCAO MO SCF calculations have been carried out on the ground-state and core-ionized states of some hydrogen-bonded dimers. In the particular case of H_2O, the trimer has also been investigated. Comparison of absolute and relative binding energies and relaxation energies with respect to the corresponding monomers reveals that substantial changes occur in going to the associated species. The relaxation energies for a given core-hole are shown to increase on going from monomer to dimer, indicating that intermolecular contributions to relaxation energies are of the same sign, irrespective of the sign for the shift in core binding energy. Creation of a core-hole in the dimer species is shown to give rise to substantial changes in hydrogen-bond energies compared with the neutral species. In the case of valence holes dominantly of 2s and 2p character, it is shown that trends in shifts and relaxation energies parallel those for the core hole states.

5.1 Introduction

There is considerable current interest in the theoretical examination of hydrogen-bonding; recent advances are well-reviewed in Schuster's comprehensive treatise,[256] and by Kollman.[257] Some recent approaches worthy of note are:

(i) the physical model of the hydrogen-bond deduced from *ab initio* MO wavefunctions by Allen;[258-261]

(ii) the energy decomposition analysis of Morokuma,[262] extended and developed to calculate separately the charge-transfer and higher-order effects,[263,266]

and (iii) the attempt by Kollman to organize all the types of noncovalent intermolecular complexes into a single framework.[267,268]

Some headway has also been made in the problem of the solvation of molecules;[269-273] and there have been a number of large-scale CI studies to determine the contribution of correlation energy to the dimerization energy.[274,275]

Whilst most of the studies reported to date refer to what might be termed "normal" hydrogen-bonded systems, there has also been considerable interest in strongly hydrogen-bonded systems, the most comprehensively studied being the HF_2^- system.[276,277] In a recent publication some aspects of the potential energy surfaces of the bichloride ion and radical have been investigated.[278] This ion constitutes a strongly hydrogen-bonded system for which experimental data is available for both symmetric and unsymmetric systems. For the corresponding radical $HCl_2^{\cdot}$, the theoretical calculations have clarified the interpretation of experimental data and shown unambiguously that by contrast with the anion, the hydrogen-bond strength is quite small. A recent study by Emsley[279] suggests that the hydrogen-bond between the fluoride anion and formic acid, $HCO_2H.....F^-$, is stronger than that in bifluoride anion, $F\text{-}H....F^-$, previously believed to be the upper limit of hydrogen-bond strength.

The electronic relaxation accompanying core-ionization has

been systematically investigated as a function of electronic environment. In the previous two chapters, the changes in binding energy shifts and differences in relaxation energy have been studied for a series of neutral alkanes, and simple carbocations; an extended series of oxygen-containing compounds has also been investigated.[193] Such studies have revealed significant variations in interatomic contributions to relaxation energies; in continuance of this, prototype systems for assessing the importance and absolute magnitude of intermolecular contributions to relaxations accompanying core-ionizations have been considered. Such an investigation is particularly apposite at this time, since a considerable body of evidence is accumulating from studies of adsorbed molecules at surfaces that in the condensed phase there are significant intermolecular (extra molecular) contributions to relaxation energies.[103,280] As prototype systems which may be studied theoretically at relatively modest computational expense, simple hydrogen-bonded dimers and trimers have some considerable merit, since they represent systems intermediate between isolated molecules, for which only intramolecular relaxations are feasible, and the condensed phase, for which intermolecular contributions may well be of importance.

In this chapter, a non-empirical LCAO MO SCF investigation of core and valence ionizations for a series of hydrogen-bonded dimers involving H_2O, NH_3 and HF is described. For comparison, the corresponding monomers have also been investigated, and for water, the trimer is also studied. Such simple systems may be regarded as prototypes for the investigation of the importance of relaxation phenomena as a function of association. This forms a logical extension to the previous chapters.

Furthermore, the available data, both theory and experiment, for normal and strongly hydrogen-bonded systems, taken in conjunction with the equivalent cores concept, suggest that there may well be interesting changes in hydrogen-bond strengths in going from the neutral to core-ionized hydrogen-bonded systems.

5.2 Computational Details

The calculations were performed using the ATMOL3[72,73] system of programs, implemented on an IBM 370/195. It was of interest to compare basis sets; consequently, the calculations were performed using the following:

(a) an STO-4.31G[7] basis set, using Raimondi and Clementi's[30] best-atom exponents;

(b) an STO-4.31G basis set, using "optimized" exponents[169,170]; and

(c) a Slater Double Zeta basis set,[235] using Clementi's[32] exponents.

A considerable volume of literature exists concerning the geometry optimizations for simple hydrogen-bonded systems. At the time at which these calculations were commenced, Pople's geometries[219] for the water-ammonia systems, optimized at the STO-3G level, were used. For the water dimer and trimer, geometries given by Johnson, Herman and Kjellander[281] were used. These dimer geometries are in fact very similar to those optimized at the STO-4.31G level by Allen.[258] For the water-hydrogen fluoride system, Allen's STO-6.31G optimizations were available.[260]

The details of the geometries used are given in Table 5.1 and Figure 5.1.

TABLE 5.1 Geometries of monomers, dimers and trimers

	R in Å [a]	θ in deg. [b]	Reference
NH_3	1.033	106.2	46a
OH_2	0.957	104.54	281
FH	0.917	-	260
H_3N ...H-OH	2.91	4.0b	46a
H_2O ...H-OH	2.85	54.7	281
HF ....H-OH	3.11	69.8	260
H_2O ...H-NH_2	2.89	60.9	46a
H_2O ...H-F	2.74	40.4	260
$(H_2O)_3$ [c]	2.85	54.7	281

a) For monomers, R is the X-H distance
θ is the $H\hat{X}H$ angle

For dimers R is the heavy-atom separation
θ is defined in Figure 5.1.

b) This is the calculated angle between the N-acceptor axis and the centre-of-gravity axis of NH_3 (see Figure 5.1).

c) See Figure 5.1b.

It should be noted that for the dimer geometry optimizations:

(i) all monomer units are held at the previously quoted values;

(ii) all hydrogen-bonds are assumed to be linear.

Neither of these assumptions is likely to be in serious error, since the published work shows relatively minor changes in terminal bond-length and bond-angles consequent upon formation of a given dimer from the relevant monomers.[282]

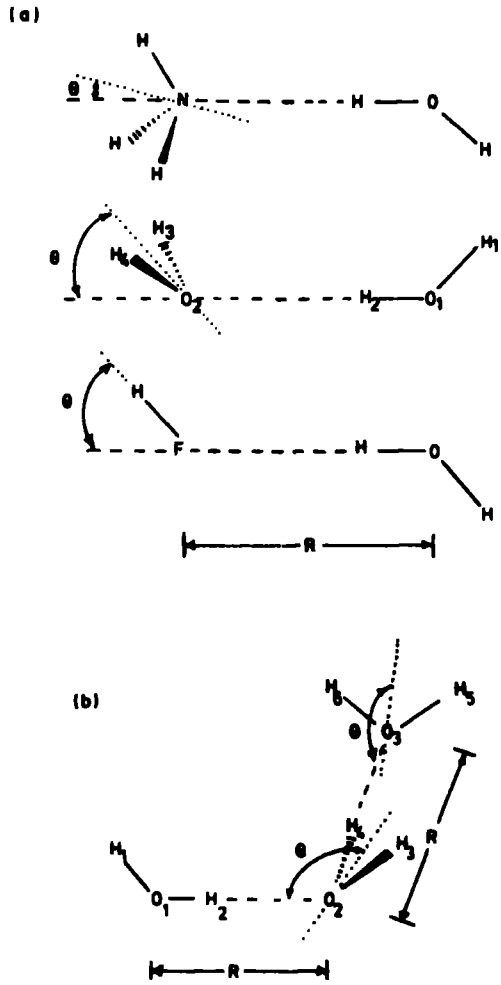

Fig.5.1 Definitions of R and θ. The dotted line is the centre-of-gravity axis of the acceptor.

Calculations for the dimers were performed in the configurations shown.

5.3 Results and Discussion

5.3.1 Core and Valence Ionizations for Water, Water Dimer and Water Trimer

(a) Binding Energies

The changes in absolute and relative binding energies for the O_{1s} level in going from water monomer to dimer to trimer as a function of basis set are shown in Table 5.2. As expected on the basis of previous work, whilst the Slater Double Zeta and "optimized" STO-4.31G basis set calculations

TABLE 5.2 Absolute and Relative Binding Energies for the O_{1s} levels in Water, Water Dimer, and Water Trimer (in eV).

Molecule (a)	Slater Double Zeta		STO - 4.31G		"Optimized" STO - 4.31G	
	B.E.	ΔB.E.	B.E.	ΔB.E.	B.E.	ΔB.E.
Water Monomer O 1s	539.75	(0)	545.49	(0)	539.12	(0)
Water Dimer O1 1s	538.42	-1.33	544.11	-1.38	537.85	-1.27
O2 1s	540.51	+0.76	546.39	+0.90	539.98	+0.86
Water Trimer O1 1s	538.03	-1.72	543.72	-1.77	537.46	-1.66
O2 1s	539.21	-0.55	545.04	-0.45	538.73	-0.39
O3 1s	540.86	+1.10	546.74	+1.25	540.24	+1.21

a) For details of numbering, see Fig.5.1b.

are in excellent agreement with the experimentally determined binding energy for H_2O (539.88 eV), the straightforward STO-4.31G basis set calculation considerably overestimates the binding energy. This largely arises from an underestimate of the relaxation energy, as will be discussed in the next section.

Also displayed in Table 5.2 are the calculated shifts in binding energies for the O_{1s} levels in going from monomer to dimer to trimer. Although the hydrogen-bond strengths for the neutral systems are quite small (<0.02 eV), the shifts in core binding energies are substantial. Thus in going from the monomer to the dimer, the O_{1s} level of the component providing the hydrogen for hydrogen-bond formation (O1) decreases in binding energy, whilst the other component (O2) increases, such that the computed shift is in excess of 2 eV. Although the small 'unoptimized' STO-4.31G basis overestimates absolute binding energies, the computed differences are closely similar

to those for the "optimized" and Double Zeta basis. A similar picture emerges for the trimer: O3, which acts as an electron donor, is calculated to shift to higher binding energy, with respect to the monomer, whilst O1 shifts to lower binding energy. The central oxygen (O2) of the water molecule, which acts as both a donor and acceptor, is calculated to decrease in binding energy. Comparison with the dimer suggests that a simple additive model is applicable. Thus, consideration of the shifts in binding energy for the O_{1s} levels of a water molecule either providing the hydrogen, or the lone-pair, for bonding to the hydrogen of the hydrogen-bond suggests a shift with respect to the monomer for the central oxygen of the trimer that is in excellent agreement with that computed directly (viz., the O1, O2 shift for the dimer compared with the shift with respect to the monomer, for O2 in the trimer). The span in binding energies for the trimer is calculated to be substantially ($\sim$0.7 eV) larger than for the dimer. With the development of Molecular Beam Techniques for producing such species in the gas phase, and with the advent of XPS instrumentation requiring extremely small partial pressures for the production of high resolution spectra of adequate signal to noise ratio, it will be of interest to see if these predictions are verified. As a corollary to this, it seems likely that in going from the gas phase monomer to the condensed phase (physically adsorbed at a surface for example) at sub-monolayer coverage, where association might produce a range of hydrogen-bonded species (dimers, trimers, etc.), there would be a considerable variation in line-width as a function of degree of association at the surface. The literature data refer either to mono- or multi-layer coverage[280,283] so that there is no

data currently available pertinent to this point.

For the monomer and dimer, it is possible to identify unambiguously the O_{2s} levels, which are somewhat core-like in character. This also proved to be the case for the trimer; however, with the Double Zeta basis set, there were convergence problems, in that it was difficult to converge on the O_{2s} levels localized on the individual oxygen atoms. For all three systems it proved possible to identify valence-ionized states dominantly of O_{2p} character; however, there were again convergence problems for the Double Zeta basis set. It is of interest to compare the shifts with those for the O_{1s} levels shown in Table 5.2. The absolute binding energies computed for the O_{2s} and O_{2p} valence-levels of the water monomer are shown in Table 5.9. The extensive calculations of Meyer[140] indicate that correlation energy corrections are opposite in sign for the 2s and 2p levels and this is clear from the present data, for which the ΔSCF calculations overestimate the binding energy for the former and underestimate for the latter. Since the orbitals are relatively localized however, it may reasonably be expected that correlation energy terms would tend to cancel in comparing *shifts* in binding energies.

The data in Table 5.3 clearly demonstrate that both in terms of magnitude and sign the shifts for the valence O_{2s} and O_{2p} levels are closely similar to those for the core-levels, despite the fact that the absolute binding energies differ substantially. Although convergence problems prevent a detailed comparison of the computed shifts as a function of basis set, the shifts computed for the trimer using Koopmans' Theorem are closely similar for the Double Zeta and STO-4.31G basis sets. This is not unexpected on the basis of the ΔSCF shifts for the dimer shown in Table 5.2.

TABLE 5.3 Changes in Valence Binding Energies on Association (in eV).

	STO - 4.31G		Double Zeta	
	ΔBE (ΔSCF)	ΔBE (Koopmans')	ΔBE (ΔSCF)	ΔBE (Koopmans')
(i) Oxygen 2s [a]				
Monomer	(0)	(0)	(0)	(0)
Dimer 01	-1.16	-1.05	-1.16	-1.05
02	+0.98	+1.25	+0.86	+1.14
Trimer 01	-1.55	-1.42		-1.42
02	+0.21	+0.21		+0.11
03	+1.32	+1.62		+1.51
(ii) Oxygen 2p [a]				
Monomer	(0)	(0)	(0)	(0)
Dimer 01	-1.12	-1.05	-1.12	-1.04
02	+0.96	+1.53	+0.53	+1.42
Trimer 01	-1.12	-1.40		-1.40
02	-0.11	-0.23		+0.52
03	+1.34	+1.30		

a) Absolute binding energies are quoted in Table 5.9.

(b) Relaxation Energies

The calculated relaxation energies and differences in going from monomer to dimer to trimer for the O_{1s} levels are shown in Table 5.4. As has been previously noted, the particular features of interest in this investigation are the intermolecular contributions to relaxation energies as a function of association.

TABLE 5.4 Changes in O_{1s} Relaxation Energies on Association of Water.

Molecule	Double Zeta	STO-4.31G	"Optimized" STO-4.31G (a)	(b)
Monomer O $1s^c$	(0)	(0)	(0)	(0)
Dimer O1 $1s$	+0.11	+0.16	+0.06	+0.06
O2 $1s$	+0.37	+0.38	+0.42	+0.66
Trimer O1 $1s$	+0.13	+0.20	+0.08	+0.08
O2 $1s$	+0.51	+0.57	+0.51	+0.75
O3 $1s$	+0.37	+0.41	+0.45	+0.99

a) The reference for the relaxation energy corresponds to Koopmans' Theorem for the unoptimized STO-4.31G basis set.

b) The reference for the relaxation energy corresponds to the average of the negative of the Fock eigenvalue for the ground-state molecule in the "optimized" and unoptimized STO-4.31G basis sets.

c) Absolute values of R.E. are quoted in Table 5.9.

Whilst the absolute magnitudes of the relaxation energies are underestimated by the calculations at the STO-4.31G level, the differences are in excellent agreement with those obtained for the Double Zeta basis set. Comparison with the shifts in binding energies recorded in Table 5.2 reveals that irrespective of whether the binding energy of a given O_{1s} core-level increases or decreases in going from monomer to dimer to trimer, the relaxation energies are always larger for the associated species. Furthermore, the relaxation energy change is largest for O2 of the trimer, which involves the central of the three units. This increase in relaxation in going to the

associated systems is in agreement with experimental data on physisorbed species at surfaces[280,283] where the difference in energy scales (when due allowance has been made for the work function) has been attributed to this source. An interesting feature arising from these experimental data is that the so-called "relaxation shift" is observed to be virtually the same for both core and valence levels. This might at first sight seem a little surprising, since the absolute magnitudes of the relaxation energies themselves are so different. By contrast, for chemisorbed species in which there is substantial perturbation of certain valence-levels (and hence indirectly core-levels), the contributions to shifts arising from changes in relaxation energies are difficult to unravel.

It is clear that hydrogen-bond formation involves a substantial perturbation of the valence-electron distribution. Although the relaxation energies for the core-levels increase on association, matters are not so clear-cut for the valence-levels. This is indicated in Table 5.5. For the essentially core-like O_{2s} levels, the relaxation energies for dimer and trimer hole-states are larger than for the monomer, and it is significant that the magnitudes of these differences are comparable with those for the O_{1s} core-levels, despite the large difference in absolute magnitude for the relevant relaxation energies.

(c) Population Analysis

Although a Mulliken population analysis provides only a crude indication of the electron distribution in a molecule, it is nonetheless useful in outlining broad features of charge migrations. For the ground-state species, the changes

TABLE 5.5 Changes in O_{2s} and O_{2p} Relaxation Energies on Association of Water

		STO-4.31G	Double Zeta
(i) Oxygen 2s [a]			
Monomer		(0)	(0)
Dimer	01	+0.11	+0.10
	02	+0.27	+0.28
Trimer	01	+0.13	
	02	+0.38	
	03	+0.30	
(ii) Oxygen 2p [a]			
Monomer		(0)	(0)
Dimer	01	+0.07	+0.07
	02	+0.56	+0.50
Trimer	01	+0.09	
	02	-0.12	
	03	-0.04	

a) Absolute values of the relaxation energy are quoted in Table 5.9.

in total population for a given water molecule as a function of association are given in Table 5.6. In going from the monomer to dimer, electron density is transferred from the water molecule containing 02 to that containing 01. The calculated changes in population for the two units are 0.039 and 0.108 electrons, respectively, for the Double Zeta and STO-4.31G basis sets. In going from the dimer to trimer, considering firstly hydrogen-bonding the monomer unit containing 03 to that containing 02, the change in population on the former is 0.043 (0.116) electrons for the two basis sets, i.e. almost the same

TABLE 5.6 Charge-transfer from monomer units

	Charge Transfer [a]		Bond Overlap Population
	Double Zeta	STO-4.31G	STO-4.31G
$HO - H \ldots OH_2$	0.039	0.108	0.165
$HO^*-H \ldots OH_2$	0.104	0.191	0.255
$HO-H \ldots O^*H_2$	-0.008	0.042	0.053
$HO-H \ldots OH_2OH_2$	0.045	0.114	
$HO^*-H \ldots OH_2OH_2$	0.117	0.206	
$HO-H \ldots O^*H_2OH_2$	-0.008	0.044	
$H_2OHO-H \ldots OH_2$	0.043	0.116	
$H_2OHO^*-H \ldots OH_2$	0.108	0.200	
$H_2OHO-H \ldots O^*H_2$	-0.007	0.047	

a) The sense $H_nB \rightarrow HAH_m$ is taken as positive.

*) Indicates the core-ionized atom.

charge transfer as computed for the dimer. The concomitant modification of charge transfer involving the other hydrogen-bond is extremely small (0.006 electrons for both basis sets). The trimer may alternatively be viewed as being formed from hydrogen-bonding the monomer unit containing O1 to the dimer, with the monomer providing the hydrogen of the hydrogen-bond. The charge migration from dimer to monomer then amounts to 0.045 and 0.114 electrons for the two basis sets, comparable to those discussed above. The change in population for the monomer unit containing O3 is again very small (0.008, 0.004 electrons).

For the particular case of the STO-4.31G basis set, the bond overlap population of the dimer has been calculated.

This is quite close in magnitude to the calculated change in population for the monomer units on forming the dimer, implying not unreasonably that charge transfer is dominantly into the hydrogen-bonding region.

For the core-ionized species, it is of interest to compare the overall transfer in charge from a given monomer as a function of association, and compare these with the corresponding figures for the ground-states. For the dimer, formation from the monomers is accompanied by electron transfer to the molecule providing the hydrogen for hydrogen-bond formation. Creation of a core-hole on O1 in the dimer considerably enhances this electron drift from one unit to the other, the computed increase in population for the monomer unit containing O1 compared with the neutral system being 0.065e and 0.083e for the Double Zeta and STO-4.31G basis sets, respectively. By contrast, creation of a core-hole on O2 drastically reduces the capabilities of the monomer unit for electron transfer for hydrogen-bond formation, and the computed reductions in electron transfer compared with the ground-state are 0.047e and 0.066e for the two basis sets. The population analysis with the Double Zeta basis set even suggests that the overall electron transfer is very small and in the opposite sense to that for the ground-state.

A similar picture emerges for the trimer. Creation of a core-hole on O1 is accompanied by an increase in electron transfer from the dimer of 0.072e (0.092e); there is a concomitant increase of 0.013e (0.019e) in electron donation from the monomer containing O3. It will become clear that this is related to the computed change in hydrogen-bond

strength for the core-ionized species. By contrast, creation of a core-hole on O3 causes a significant reduction in electron transfer to the dimer of 0.050e (0.069e), and indeed for the Double Zeta basis set, the monomer unit in the core-ionized species becomes very weakly electron accepting. The core-ionization of the central monomer unit (O2) is accompanied by a considerable increase in valence-electron population of 0.118e (0.152e). This arises in the following way: in the ground-state, O2 receives 0.043e (0.116e) from O3; however, this is accompanied by a charge transfer of 0.045e (0.114e) from O2 to O1, leaving a net charge of -0.002e (0.002e). O_n core-ionization of O2, the donation from the O3 monomer unit increases by 0.065 (0.004e), whereas the donation from O2 to O1 decreases by 0.053 (0.070e), leaving a net charge on the O2 unit of 0.116e (0.156e).

The changes in valence-electron populations (the electronic charge-flow from each atom) on going from the ground-state to core-ionized species are shown in Table 5.7. Certain trends are clearly discernible. For the water monomer, creation of a core-hole on oxygen results in a substantial increase in valence-electron population on oxygen at the expense of the two hydrogens; whilst the absolute magnitudes of electron populations depend very markedly on the basis set, the differences reported in Table 5.7 are remarkably similar. For the dimer and trimer, there is again a substantial increase in valence-electron population on the atom on which the core-hole is located, largely at the expense of the directly-bonded hydrogens. If the directly-bonded hydrogen is involved in hydrogen-bonding, the charge flow is highly asymmetric, a much greater proportion of the overall increase in electron population

TABLE 5.7 Changes in Valence Population on Core-Ionization of Water Species

		Double Zeta	STO - 4.31G			Double Zeta	STO - 4.31G
Monomer [a]	O*	-0.528	-0.556	Trimer [a]	O1*	-0.500	-0.522
	H1	+0.264	+0.278		H1	+0.279	+0.292
	H2	+0.264	+0.278		H2	+0.149	+0.139
					O2	-0.019	-0.009
					H3	+0.049	+0.054
					H4	+0.030	+0.028
Dimer [a]	O1*	-0.503	-0.524		O3	-0.018	-0.017
	H1	+0.277	+0.289		H5	+0.024	+0.027
	H2	+0.161	+0.152		H6	+0.005	+0.008
	O2	-0.027	-0.019				
	H3	+0.046	+0.051		O1	+0.072	+0.079
	H4	+0.046	+0.051		H1	+0.038	+0.041
					H2	-0.058	-0.049
	O1	+0.075	+0.082		O2*	-0.526	-0.559
	H1	+0.039	+0.041		H3	+0.261	+0.270
	H2	-0.067	+0.058		H4	+0.148	+0.135
	O2*	-0.547	-0.587		O3	-0.023	-0.015
	H3	+0.250	+0.261		H5	+0.044	+0.049
	H4	+0.250	+0.261		H6	+0.044	+0.049
					O1	+0.022	+0.025
					H1	+0.006	+0.007
					H2	-0.015	-0.014
					O2	+0.069	+0.072
					H3	+0.034	+0.035
					H4	-0.065	-0.056
					O3*	-0.546	-0.587
					H5	+0.247	+0.259
					H6	+0.248	+0.259

a) For details of numbering, see Figure 5.1

* indicates core-ionized atom

on oxygen coming at the expense of electron migration from the other directly-bonded hydrogen.

(d) Changes in Hydrogen-bond strength accompanying core-ionization.

The substantial reorganization of valence-electron distribution concomitant with core-ionization inferred from the population analyses would suggest significant changes in the energetics of hydrogen-bond formation.

For the dimer, the calculated hydrogen-bond energy of 4.8 kcal mol^{-1} for the Double Zeta basis set is in good agreement with experiment ($5.2\pm$ 1.5 kcal mol^{-1}),[284] whilst the smaller basis set tends to overestimate the bond strength (11.9 kcal mol^{-1}). Comparison of the dimer with the trimer provides a hydrogen-bond energy of 6.5 kcal mol^{-1} (14.1 kcal mol^{-1}), whilst for dissociation of the trimer into three monomer units, an average bond energy of 5.7 kcal mol^{-1} (12.9 kcal mol^{-1}) is obtained, where the figures in brackets refer to the STO-4.31G basis. Both of these values are significantly higher than for the dimer itself. The effect of creating a core-hole in the dimer and trimer is dramatic in terms of the computed changes in hydrogen-bond strength; this is indicated in Table 5.8.

Considering the dimer, creation of a core-hole on O1, for which the population analysis indicates an increase in electron donation from the monomer containing O2, is accompanied by a large increase in hydrogen-bond strength, such that it is now comparable with typical hydrogen-bond strengths for such species as HF_2^- and HCl_2^-.[285] By contrast, the hydrogen-bond strength for the species with the core-hole located on O2 is very substantially less than for the neutral

TABLE 5.8 Changes in Hydrogen-Bond Strengths on Core-Ionization (in kcal mol^{-1}).

Molecule	Core-Hole	Hydrogen Bond	Double Zeta	STO-4.31G
Dimer [a]	01	01 02	+30.66	+31.77
	02	01 02	-17.42	-20.74
Trimer [b]	01	01 02	+40.57	+41.98
		02 03	+ 9.95	+10.17
	02	01 02	-17.16	-20.27
		02 03	+30.90	+32.25
	03	01 02	- 7.19	- 7.03
		02 03	-24.63	-27.74

a) Relative to the ground-state hydrogen-bond strength.

b) Relative to the average ground-state hydrogen-bond strength.

(A positive sign indicates an *increase* in hydrogen-bond energy).

system. The changes in hydrogen-bond energy are closely similar for the two basis sets.

From the data in Table 5.8 (and Fig.5.4), it should be noted that the 'vertical' binding energies referred to here are associated with a repulsive part of the potential energy surface for the core-ionized species (as opposed to the attractive part for the O1 core-ionized system), and represent lower bounds to the hydrogen-bond strength. This does not necessarily imply that the surface for this core-ionized state does not have a minimum which is lower in energy than the dissociation limit.

For the trimer, creation of a core-hole on O1 is again accompanied by a very large increase in hydrogen-bond

energy; this effect is relayed to the other hydrogen-bond. These changes are again qualitatively in line with those expected on the basis of the population analysis. Creation of a core-hole on O2 increases the hydrogen-bond strength with respect to the monomer unit containing O3, and causes a decrease with respect to O1. Finally for a core-hole on O3 in the trimer, both hydrogen-bond energies decrease with respect to the neutral system.

It should be emphasized that these energies refer to vertical processes, and represent lower bounds to the adiabatic processes. Thus it seems likely that the large increase in hydrogen-bond strength in certain cases will be accompanied by a decrease in hydrogen-bond length; for those systems in which there is a decrease in hydrogen-bond strength, the equilibrium geometries may well involve an increase in hydrogen-bond length. The lifetimes of the core-hole states, however, are determined by de-excitation predominantly by the Auger process, and are likely to be in the range of 10^{-13} sec. This is several orders of magnitude too short to be of any chemical significance, and since the transitions from the ground-state are vertical, a discussion of hydrogen-bond energies in terms of vertical processes seems eminently reasonable. The large calculated changes in hydrogen-bond energies and the implication of substantial changes in equilibrium geometries for the core-ionized species does, however, have important ramifications with respect to vibrational fine-structure accompanying core-ionization, a field of considerable current interest from both an experimental and theoretical standpoint.

5.3.2 Core- and valence-ionization for hydrogen-bonded dimers involving H_2O with H_2O, NH_3 and HF.

(a) Binding Energies

The calculated absolute binding energies for the monomers are shown in Table 5.9, for the core-levels and for valence orbitals. For the N_{1s}, O_{1s} and F_{1s} levels, the calculations are in excellent agreement with experiment for the Double Zeta and optimized STO-4.31G basis sets. For the STO-4.31G basis set however, the relaxation energies are underestimated and consequently the calculated absolute binding energies are too large. For the valence-levels, the calculated binding energies are overestimated (2s) or underestimated (2p) compared with experiment; this is attributable not only to deficiencies in the basis sets, but more importantly to the neglect of correlation energy changes, which are opposite in sign for the two levels. The changes in core binding energies with respect to the appropriate monomer are shown for all of the dimer species studied in Figure 5.2.

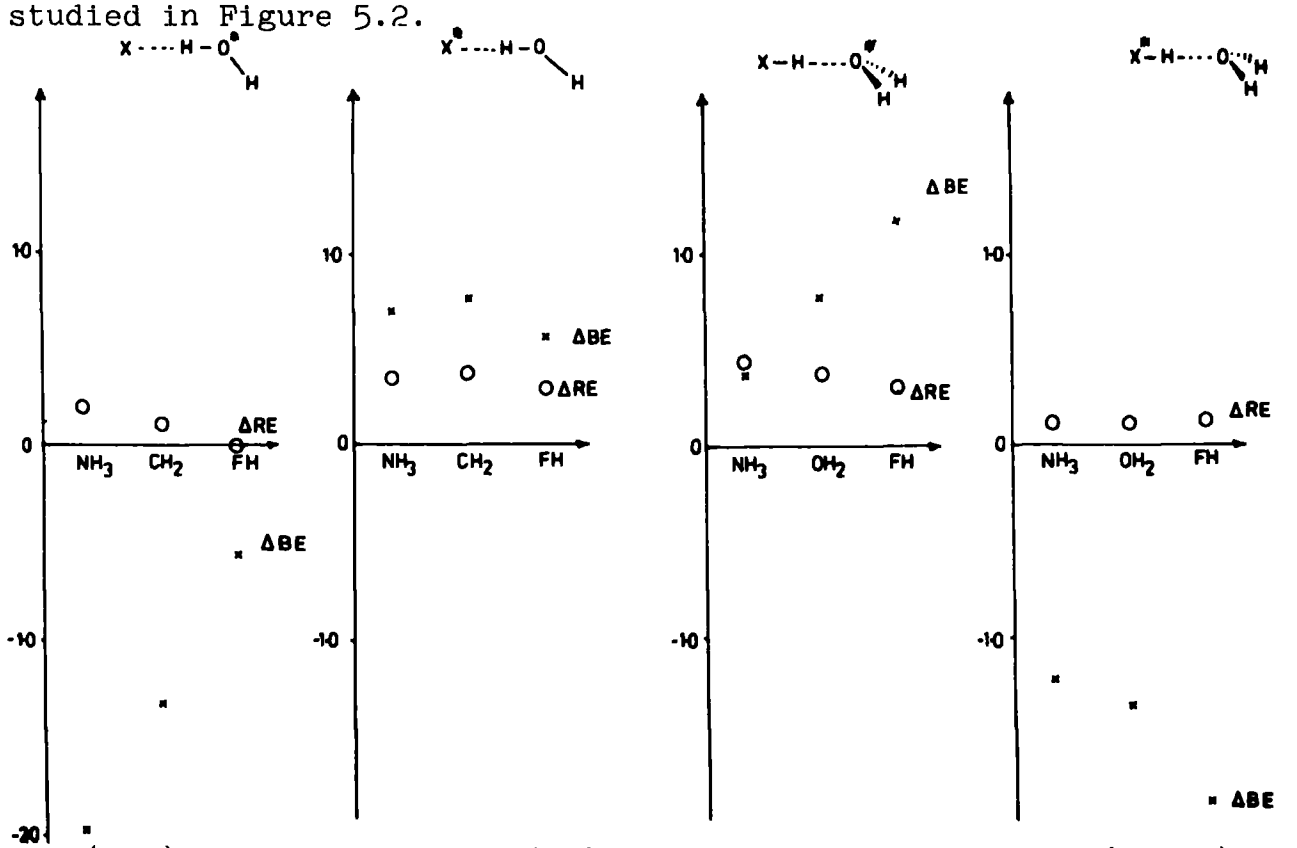

Fig.(5.2) Changes in core (1s) BE and RE on association (in eV)

TABLE 5.9 Absolute Binding Energies and Relaxation Energies of Monomer Units (in eV)

Molecule	Level	Double Zeta B.E.	Double Zeta R.E.	STO - 4.31G. B.E.	STO - 4.31G. R.E.	"OPTIMIZED" STO-4.31G B.E.	"OPTIMIZED" STO-4.31G R.E. a	EXPERIMENTAL B.E.	EXPERIMENTAL Reference
NH_3	N 1s	405.76	16.82	409.91	13.68	405.73	17.83 16.56	405.58	141
	2s	29.20	1.63	29.15	1.82			~27	208
	2p (lone pair)	9.09	2.10	8.46	2.14			10.85	82
HF	F 1s	693.94	20.91	701.27	16.22	692.25	25.24 22.15	694.22	141
	2s	41.18	2.06	40.26	2.36			39.65	285
	2p (lone pair)	14.81	2.44	12.01	2.67			16.12	285
H_2O	O 1s	539.75	19.16	545.49	15.35	539.12	21.71 19.55	539.7 539.88	82 141
	2s	34.82	1.87	34.45	2.16			~32 32.2	208 82
	2p (lone pair)	11.19	2.43	9.55	2.58			12.61	82

a, Upper R.E. value obtained from (g.st. Koopmans' - ΔSCF B.E.);

Lower R.E. value obtained from (av. Koopmans- ΔSCF B.E.)

Since the shifts in binding energies and changes in relaxation energies are virtually the same for all three basis sets employed, only the results for the Double Zeta basis set are presented.

For the O_{1s} core-ionized species, the shifts with respect to the water monomer are in the opposite sense, depending on whether the hydrogen is provided by X or by the water monomer under consideration. For either situation, the magnitude and direction of the shifts are qualitatively in agreement with simple electronegativity considerations. Thus, with water providing the hydrogen for the hydrogen-bond, the effect of this hydrogen-bonding on the O_{1s} level is a shift to lower binding energy, being largest for the best donor: viz., the shifts are in the order $NH_3>H_2O>HF$. Conversely, if a core-hole is created on the oxygen of a water monomer not providing the hydrogen for the hydrogen-bond, the reduced efficiency as a donor is manifest in a shift to higher binding energy which increases in the order $NH_3<H_2O<HF$.

The picture which emerges when a core-hole is created on X is slightly more complicated. Thus, when X provides the hydrogen for hydrogen-bond formation, the increased electron donation from water lowers the core binding energies, the shifts being in the order $NH_3<H_2O<HF$. When the hydrogen for hydrogen-bond formation is provided by the water monomer and the core-hole is created on X, the shifts are small and to higher binding energy, and are comparable for $X=NH_3, H_2O$ and HF. Although superficially this may seem surprising, the previous discussion on the water dimer and changes in populations accompanying core-ionization provides a straightforward rationalization. In comparing the populations for the core-ionized dimers with those for the monomers from which they may be

constructed, the calculated changes are extremely small, and indeed for the Double Zeta basis set, the overall electron transfer is to the core-ionized monomer. In the particular case of a neutral water monomer X, the electronic environment is not too dissimilar to the isolated core-ionized species.

For the dimers involving core-holes located on the water monomer, the "internal" shift in the O_{1s} binding energy for the two distinct hydrogen-bonding situations shows a smooth decrease in the series $NH_3 > H_2O > HF$, the shifts being 2.35, 2.08, 1.73 eV respectively. Defining the centroid of the shift as the average of the O_{1s} shifts, with respect to the water monomer, for the two hydrogen-bonding situations HX ... H - O^*H and X-H ... O^*H_2, it is found that the centroid is at a lower binding energy for X = NH_3 and H_2O, and higher binding energy for X = HF.

For the dimers, hole-states corresponding approximately to removal of valence 2s and 2p electrons may be identified from the manifold of valence-ionized states. These behave in an analogous manner to the core hole states. This is shown in Figure 5.3; comparison with Figure 5.2 is quite striking, both in respect of the signs and magnitudes of the calculated shifts.

(b) Relaxation energies

One of the prime motivations for this study was to investigate changes in relaxation energies as a function of association. The absolute magnitudes of the computed relaxation energies for the monomers, for both the core and valence 2s and 2p levels, are given in Table 5.9. In defining relaxation energies computed from the "optimized" STO-4.31G

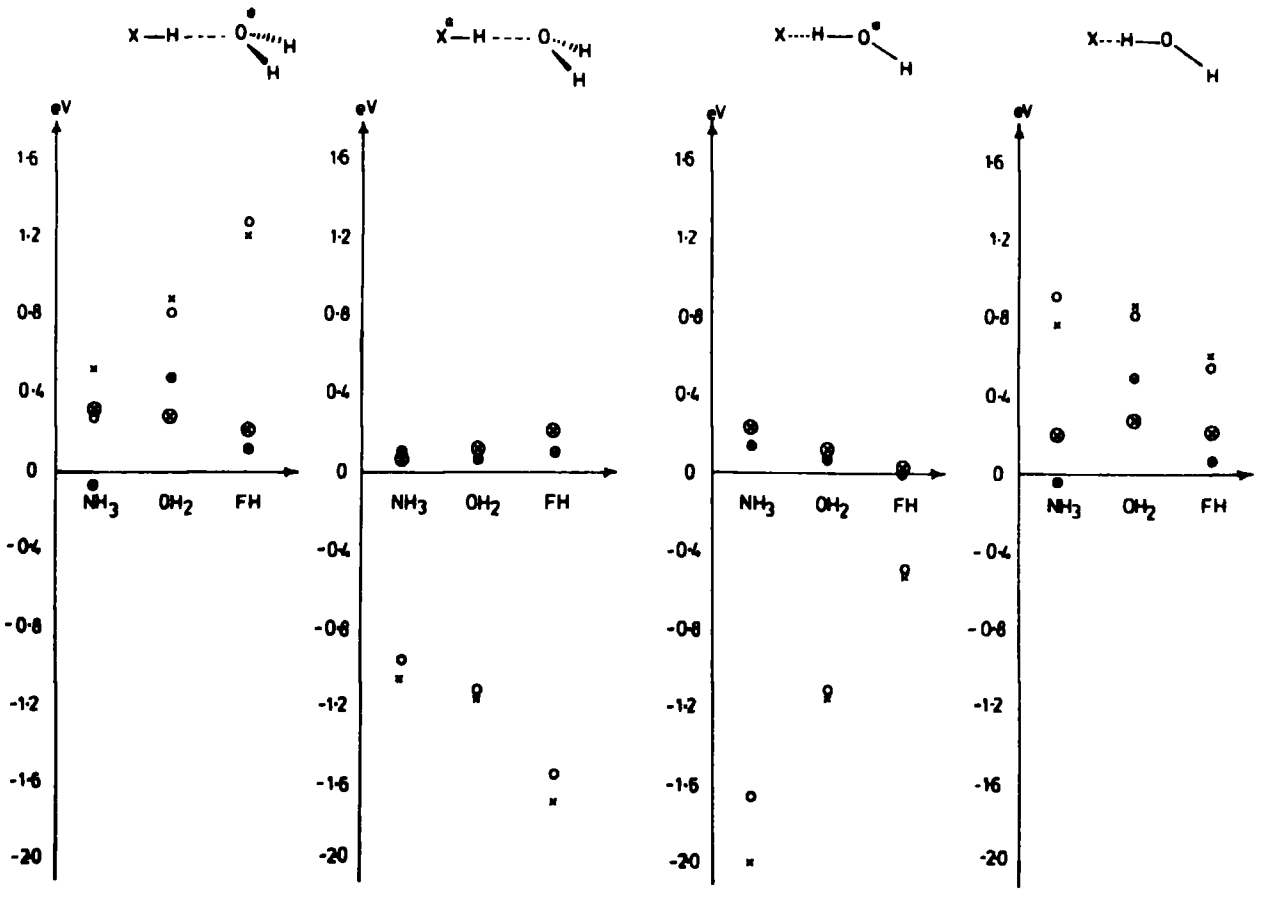

Fig. (5.3) Changes in valence (2s and 2p) BE and RE on association (in eV). × and ● refer to the 2s BE and RE, respectively; o and ⊙ to the 2p BE and RE.

basis set, two possibilities present themselves. Firstly, the reference for the unrelaxed system can be taken as the negative of the Fock eigenvalue for the neutral molecule using the "unoptimized" STO-4.31G basis set; alternatively, this may be averaged with the corresponding Fock eigenvalue for the neutral molecule using the optimized basis. Comparison with the relaxation energies based on the "optimized" STO-4.31G calculations for the hole-state species are in much better agreement than those computed directly for the standard STO-4.31G basis. The absolute magnitudes of the relaxation energies computed from the "optimized" STO-4.31G basis are closer to

those for the Double Zeta basis when the reference for the "unrelaxed" system is taken as the average over the Fock eigenvalues. Similar treatments have been carried out for all of the dimers and relevant hole-states; the trends and differences for the relaxation energies are in good agreement with those calculated with the Double Zeta basis set. However, the differences are rather closer to those calculated using the Double Zeta basis set when the reference for the relaxation energies corresponds to Koopmans' Theorem for the unoptimized STO-4.31G basis set calculations for the neutral molecule, as may be seen, for example, in Table 5.4. The changes in relaxation energy on going from monomer to dimer for a given core-hole are shown in Figure 5.2. Considering firstly hydrogen-bonded dimers involving a core-hole on oxygen, it is clear that although there are substantial shifts to lower binding energies when water provides the hydrogen for the hydrogen-bond, and substantial increases in binding energy when the hydrogen-bond is provided by X, the relaxation energy change with respect to the monomer is always positive. That is, in going to the associated system, the relaxation energy increases, irrespective of whether the binding energy for the core-level increases or decreases. A similar situation obtains for dimers involving a core-hole located on X. In all cases the increase in relaxation energy in going from monomer to dimer is relatively small, being in the range 0 to 0.42 eV. For the valence hole-states, the changes in relaxation energy are shown in Figure 5.3. For the 2s levels, the magnitudes of the changes in relaxation energy are closely similar to those for the core-levels. This is interesting, since the absolute magnitudes of the relaxation energies differ by a factor of ten. The changes in relaxation

energy on association are therefore proportionately larger for the valence 2s levels.

(c) Population analysis

Formation of a given hydrogen-bonded dimer is accompanied by electron transfer to the monomer providing the hydrogen for hydrogen-bond formation. The relative magnitudes of the electron transfer are consistent with a qualitative picture based on electronegativity considerations, as shown in Table 5.10.

TABLE 5.10 Charge transfer from monomer units

	Charge Transfer [a]		Bond Overlap Population
	Double Zeta	STO-4.31G	STO-4.31G
H_2N-H .... OH_2	0.042	0.136	0.218
HO-H .... OH_2	0.040	0.108	0.165
F-H .... OH_2	0.042	0.094	0.143
H_3N .... H-OH	0.060	0.110	0.143
H_2O .... H-OH	0.040	0.108	0.165
HF .... H-OH	0.016	0.061	0.086

a) The sense $H_nB \rightarrow HAH_m$ is taken as positive

Thus for H_2O acting as the acceptor, the increase in electron population compared with the monomer is in the order $NH_3 > H_2O > HF$. For the water monomer acting as a donor, the dependence on the acceptor providing the hydrogen for hydrogen-bond formation is somewhat less marked.

Considering now the hole-state species, the calculated changes in electron population in terms of electron density transferred from one monomer unit to another are shown

in Figure 5.4 for the Double Zeta basis set. The corresponding figures for the STO-4.31G basis are in excellent overall agreement with these, as might have been anticipated from the results previously discussed for water, water dimer and trimer.

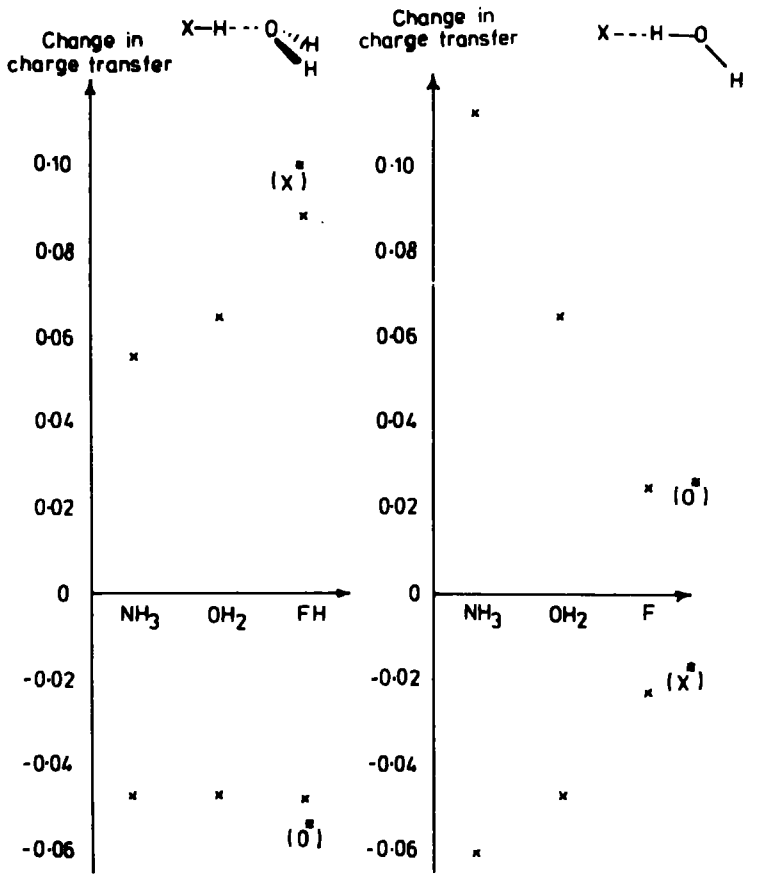

Fig. (5.4) Changes in charge transfer from monomer units on core-ionization, relative to the ground-state dimers.

Creation of a core-hole on X, when X provides the hydrogen for hydrogen-bond formation to water, is accompanied by increased electron donation from the water molecule in the order $X=HF>H_2O>NH_3$. These increases exactly parallel the change in bond overlap population between oxygen and the hydrogen involved in hydrogen-bonding, as shown in Table 5.11. An increased hydrogen-bond energy for such core-ionized species might therefore be anticipated. With X acting as a donor to a core-ionized water molecule (which provides the hydrogen for

TABLE 5.11 Change in bond overlap population (STO-4.31G) between monomers on core-ionization

	X *	O *
X-H ... OH_2		
H_2N - H ... OH_2	+0.086	-0.149
HO - H ... OH_2	+0.090	-0.111
F - H ... OH_2	+0.101	-0.094
X ... H - OH		
H_3N ... H - OH	-0.102	+0.162
H_2O ... H - OH	-0.111	+0.090
HF ... H - OH	-0.060	+0.033

hydrogen-bond formation), there is again an increase in valence-electron population on the core-ionized monomer compared with the ground-state, in the order $NH_3 > H_2O > HF$. The changes in population are again largely accounted for by an increase in overlap population in the hydrogen-bond region.

Creation of a core-hole on the monomer unit not providing the hydrogen for hydrogen-bond formation results in all cases in a reduction of valence-electron population transfer with respect to the neutral dimers. For H_2O providing the hydrogen for hydrogen-bond formation, the changes in electron population are least for X=HF and largest for $X=NH_3$, whilst if X provides the hydrogen for hydrogen-bond formation, the reduction in population is closely similar for $X=NH_3$, H_2O and HF. The changes in bond overlap populations for the hydrogen-bonds again follow these trends.

(d) Changes in Hydrogen-bond strengths accompanying core-ionizations

The population analyses, showing substantial electronic reorganizations on the creation of core-holes in the dimer species, suggest that the hydrogen-bond strengths in these species may be considerably different than for the neutral molecules. The calculated hydrogen-bond strengths for the ground-state dimers are shown in Table 5.12.

TABLE 5.12 Hydrogen-bond strengths (in kcal mol^{-1})

	Double Zeta	STO-4.31G
H_2N - H ... OH_2	1.54	10.74
HO - H ... OH_2	4.82	11.94
F - H ... OH_2	12.45	15.72
H_3N ... H - OH	9.20	10.94
H_2O ... H - OH	4.82	11.94
HF ... H - OH	4.00	10.38

The calculated changes in hydrogen-bond energies with respect to the neutral dimers are shown in Figure 5.5 for the Double Zeta basis set; those for the STO-4.31G basis are closely similar. The computed changes are substantial and in a direction that might have been anticipated from the population analysis. Thus, creation of a core-hole on a monomer which provides the hydrogen for hydrogen-bond formation substantially increases the hydrogen-bond energy such that the species may be classified as a strongly hydrogen-bonded system. By contrast, creation of a core-hole on the other monomer unit leads to a substantial decrease in hydrogen-bond strength. From this it is clear that core-ionization can considerably enhance

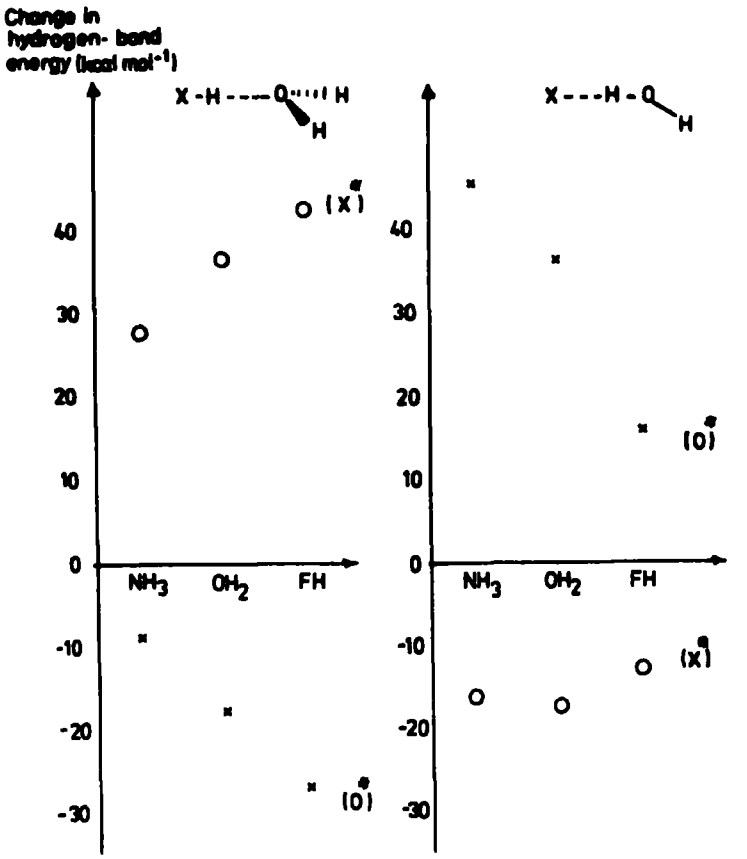

Fig.(5.5) Change in hydrogen-bond strength on core-ionization (in kcal mol^{-1}). o refers to core-ionization on X; x refers to core-ionization on H_2O.

weak interactions in appropriate systems, and hence magnify energy differences which may be quite small for the ground-state system.

As noted previously, the lifetimes for such core-ionized species before undergoing de-excitation by the Auger process are such that the chemistry which might be exhibited is not available for direct investigation. However, the drastic changes in potential surfaces, compared with the neutral dimers, implied by these results suggest that core-ionizations should be accompanied by considerable vibrational fine-structure. With the advent of high-resolution instrumentation, the direct

study of such species in molecular beams at relatively modest partial pressures becomes a feasibility, and it will then be of some interest to compare the theoretical predictions reported here with the experimental data.

CHAPTER SIX

SINGLE ORBITAL RELAXATION ACCOMPANYING CORE-IONIZATION

A method is presented for the calculation of the individual contributions from each occupied orbital to the total relaxation energy accompanying core-ionization, within the ΔSCF formalism. The magnitude and sign of the contributions are shown to depend quite markedly on the localization and bonding characteristics of the orbitals concerned, but are in accord with chemical intuition. The basis set dependence of the single orbital contributions to the total relaxation energy accompanying C_{1s} and O_{1s} core-ionization in carbon monoxide has been investigated.

Single orbital relaxation energies accompanying core-ionization in the first-row atoms have been investigated; the diatomic molecules CO and N_2 have also been studied. Single orbital relaxation energies for C_{1s} and O_{1s} core-ionization in CO, and N_{1s} core-ionization in N_2, have been calculated. For CO, comparison with individual orbital Mulliken population analyses, and density difference contour plots is made. Variation of single orbital relaxation energies as a function of bond-length has been studied for both CO and N_2. Considerable insight into the relaxation process accompanying core-ionization may be gained from such an analysis.

The influence of an applied electric field on core binding and relaxation energies accompanying core-ionization has been theoretically investigated by means of non-empirical LCAO MO SCF calculations within the ΔSCF formalism, on simple prototype

molecules (CO and N_2). Single orbital contributions to the total relaxation energies, together with Mulliken population analyses and density difference contours for CO, are presented. Investigations of the effect of an electric field on potential energy surfaces, as evidenced by band-profile analysis, are also considered.

6.1 A Method for Obtaining Single Orbital Contributions to the Total Relaxation Energy Accompanying Core-Ionization

6.1.1 Introduction

The topic of interest in the previous three chapters has been the electronic relaxation accompanying both core and valence ionization, studied within the ΔSCF formalism. One aspect of considerable current interest is the change in computed bond-lengths in going from the ground to core hole states in simple molecules, the main point of interest being focussed on the interpretation of the vibrational fine-structure apparent in high-resolution XPS data. This has recently been studied both theoretically[197-200] and experimentally[287] with a good degree of success. The emphasis to date has been on the *total* relaxation energy accompanying core-ionization. In the case of carbon monoxide, for example, it has been shown that the total relaxation energy accompanying C_{1s} core-ionization is not strongly dependent on bond-length, which contrasts with the situation for the O_{1s} core-ionized system[170,288]. To gain further insight into this reorganization process, it was felt appropriate to investigate the different components of this total process; accordingly, in this chapter it is shown how it is possible to discuss this phenomenon in terms of the individual molecular orbital relaxation effects accompanying core-ionization.

6.1.2 Method

The approach adopted is illustrated schematically in Figure 6.1.

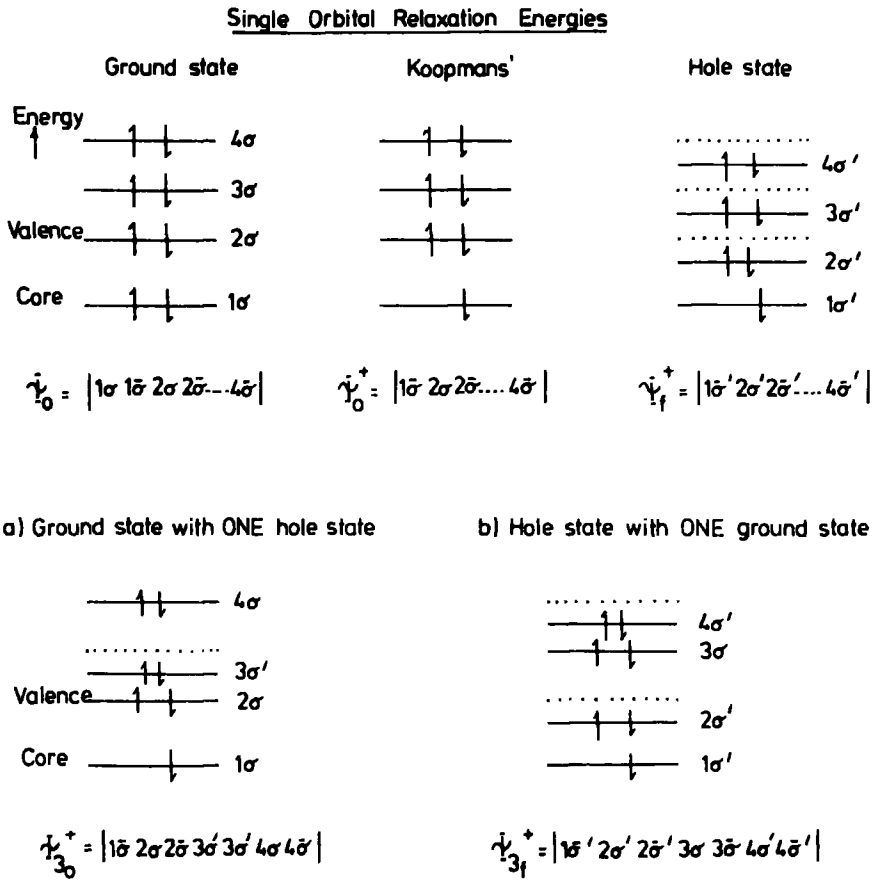

Fig. (6.1) A schematic illustration of the method for obtaining single orbital relaxation energies

The total relaxation energy accompanying core-ionization in a molecule may be obtained from non-empirical LCAO MO SCF calculations within the ΔSCF formalism. This may be illustrated as in Figure 6.1, where Ψ_o refers to the ground-state, and Ψ_o^+ and Ψ_f^+ to the "Koopmans'" and hole-state wavefunction. The relaxation process is illustrated by the use of dotted lines to show the unrelaxed orbital energies; hole-state spin-orbitals are indicated with a prime. The vectors computed in this way for the ground and core hole state molecular orbitals may be used to determine the single orbital relaxation energies; the approach

involves two distinct but complementary calculations, which give upper and lower bounds to the single orbital relaxation energy:

(a) the total energy of a hypothetical state for the core-ionized species in which all the orbitals are "frozen", save that orbital under study, which is "relaxed", is calculated. For example, if MO 3 is of interest, then the wavefunction Ψ_{3o}^{+} is used in Figure 6.1. A comparison of the binding energy obtained from this hypothetical state with that obtained from the completely "frozen" system (corresponding to the Koopmans' binding energy), gives a value for the single orbital relaxation energy.

(b) the converse situation, where a hypothetical state for the core-ionized species is now constructed corresponding to all "relaxed" orbitals, save that orbital under study, which is "frozen": this corresponds to Ψ_{3f}^{+} in Figure 6.1. The binding energy appropriate to this state is compared with that for the completely "relaxed" system (corresponding to the ΔSCF binding energy) to give a value for the single orbital relaxation energy.

The value obtained from calculation (a) provides an upper, and that from (b) a lower, bound to the single orbital relaxation energy. This may be understood naively as follows: if all the orbitals save one are frozen, then that orbital will attempt to "relax" as much as possible; conversely, if all orbitals are relaxed save one, then that orbital cannot relax as much as it would do in a normal ΔSCF calculation. Taking the simple average of the two calculations (a) and (b) gives a value for the single orbital relaxation energy. It is found that the sum of all the

single orbital relaxation energies in a molecule corresponds exactly to the total relaxation energy for that molecule calculated directly.

It is necessary at this point to consider the method in more detail. The hole-state computations involve the minimization of one-component energy expressions of the form (1.161):

$$< \Psi|\hat{H}|\Psi >/< \Psi|\Psi >$$

where the single determinantal wavefunctions Ψ involve both doubly-occupied valence- and core-orbitals, as well as the singly-occupied orbital corresponding to the core-ionized system. If the unnormalized form of the single determinantal wavefunction corresponding to the neutral molecule (2n electrons) is written as:

$$\Psi_o = |\psi_1\bar{\psi}_1 \text{ ---- } \psi_n\bar{\psi}_n| \qquad (6.1)$$

with corresponding expectation value E_o, then the binding energy in the absence of relaxation, corresponding to removal of an electron from ψ_i, is given by:

$$E^K_{BE_i} = (E^+_{oi} - E_o) \qquad (6.2)$$

Here, E^+_{oi} corresponds to the expectation value for the determinantal wavefunction:

$$\Psi^+_{oi} = |\psi_1\bar{\psi}_1 \text{ --- } \psi_i \text{ --- } \psi_n\bar{\psi}_n| \qquad (6.3)$$

In the ΔSCF formalism, the corresponding binding energy including relaxation effects, $E^R_{BE_i}$, is given by:

$$E^R_{BE_i} = (E^+_{fi} - E_o) \qquad (6.4)$$

E^+_{fi} corresponds to the expectation value for the determinantal

wavefunction

$$\Psi^{+}_{fi} = |\psi_1'\bar{\psi}_1' \text{ --- } \psi_i' \text{ --- } \psi_n'\bar{\psi}_n'| \qquad (6.5)$$

where the prime indicates inclusion of relaxation effects in the wavefunction. The total relaxation energy is therefore defined from (2.16) as:

$$E_{Ri} = (E^{+}_{oi}-E_o) - (E^{+}_{fi}-E_o) \qquad (6.6)$$

In practice, the unrelaxed binding energy (6.2) may be obtained directly from Koopmans' Theorem for systems involving only a single open shell; however, in general the expectation values would be required as defined in (6.6).

Consider now the definition of a single orbital relaxation energy ${}_jE_{Ri}$ for the orbital ψ_j, consequent upon core-ionization from orbital ψ_i. In terms of the method outlined above, this would be given as the average of the relaxation energies calculated according to calculations (a) and (b):

$$\begin{aligned} {}_jE_{Ri} &= \tfrac{1}{2}(\text{RE from (a)} + \text{RE from (b)}) \\ &= \tfrac{1}{2}[(E^{+}_{oi} - {}_j'E^{+}_{oi}) + ({}_jE^{+}_{fi} - E^{+}_{fi})] \end{aligned} \qquad (6.7)$$

Here, ${}_j'E^{+}_{oi}$ and ${}_jE^{+}_{fi}$ correspond to the expectation values for the determinantal wavefunctions:

$${}_j'\Psi^{+}_{oi} = |\psi_1\bar{\psi}_1 \text{ --- } \psi_i \text{ --- } \psi_j'\bar{\psi}_j' \text{ --- } \psi_n\bar{\psi}_n| \quad \text{and}$$

$${}_j\Psi^{+}_{fi} = |\psi_1'\bar{\psi}_1' \text{ --- } \psi_i' \text{ --- } \psi_j\bar{\psi}_j \text{ --- } \psi_n'\bar{\psi}_n'| \text{ respectively.}$$

The first term in (6.7) corresponds to the relaxation energy for the single relaxed orbital ψ_j' in the field of unrelaxed orbitals, whilst the second term corresponds to the single unrelaxed orbital ψ_j in the field of relaxed orbitals. The total relaxation energy in this definition is therefore the sum of components from each doubly-occupied orbital, plus a contribution from the singly-occupied

core-orbital, as shown in (6.8), where E'_{Ri} is for the time being distinguished from E_{Ri} in (6.6):

$$E'_{Ri} = \sum_{\text{occupied orbitals}} \tfrac{1}{2}[(E^{+}_{oi} - {}_{j'}E_{oi}) + ({}_{j}E^{+}_{fi} - E_{fi})] \qquad (6.8)$$

It will be shown that the energy expressions (6.6) and (6.8) are equivalent.

The general energy expressions for the component energy terms involved in (6.8) are similar to (1.40) and may be written as:

$$E^{+}_{oi} = h_i + \sum_{p\neq i} 2h_{pp} + \sum_{p\neq i}\sum_{q\neq i} 2(J_{pq} - K_{pq}) + \sum_{q}(J_{iq} - K_{iq}) \qquad (6.9)$$

$${}_{j'}E^{+}_{oi} = h_i + \sum_{\substack{p\neq i\\ p\neq j}} 2h_{pp} + 2h'_{jj} + \sum_{\substack{p\neq i\\ p\neq j}}\sum_{\substack{q\neq i\\ q\neq j}} 2(J_{pq} - K_{pq}) + \sum_{q}(J_{iq} - K_{iq}) + \sum_{q} 2(J'_{jq} - K'_{jq}) \qquad (6.10)$$

$$E^{+}_{fi} = h'_i + \sum_{p\neq i} 2h'_{pp} + \sum_{p\neq i}\sum_{q\neq i} 2(J''_{pq} - K''_{pq}) + \sum_{q}(J''_{iq} - K''_{iq}) \qquad (6.11)$$

$${}_{j}E^{+}_{fi} = h'_i + \sum_{\substack{p\neq i\\ p\neq j}} 2h'_{pp} + 2h_{jj} + \sum_{\substack{p\neq i\\ p\neq j}}\sum_{\substack{q\neq i\\ q\neq j}} 2(J''_{pq} - K''_{pq}) + \sum_{q}(J''_{iq} - K''_{iq}) + \sum_{q} 2(J'_{jq} - K'_{jq}) \qquad (6.12)$$

In these equations, unprimed h, J and K integrals involve the unrelaxed orbitals, singly-primed h, J and K integrals involve both relaxed and unrelaxed cross-terms, and doubly-primed J and K integrals involve only relaxed orbitals. Then:

$$(E^{+}_{oi} - {}_{j'}E^{+}_{oi}) = 2h_{jj} - 2h'_{jj} - \sum_{q} 2(J_{jq} - K_{jq}) - \sum_{q} 2(J'_{jq} - K'_{jq})$$

$$({}_{j}E^{+}_{fi} - E^{+}_{fi}) = -2h'_{jj} + 2h_{jj} + \sum_{q} 2(J''_{jq} - K''_{jq}) + \sum_{q} 2(J'_{jq} - K'_{jq})$$

Substituting into (6.8) leads to a cancellation of cross-terms involving integrals with both relaxed and unrelaxed functions. The overall expression simplifies to terms involving either the final-state relaxed eigenfunctions, or the unrelaxed ground-state neutral molecule functions. Introducing n_j as the orbital occupancy of MO ψ_j then gives:

$$E'_{Ri} = \sum_j [(n_j h_{jj} + \sum_q n_j (J_{jq} - K_{jq})) - (n_j h'_{jj} + \sum_q n_j (J''_{jq} - K''_{jq}))] \qquad (6.13)$$

This, however, is merely:

$$E'_{Ri} = E^+_{oi} - E^+_{fi}$$

which is the relaxation energy defined in (6.6).

Nuclear repulsion terms in the energy expressions have been neglected, since they will cancel. The energy expressions given here imply that the general single determinantal wavefunction

$$\Psi = |\psi_1\bar{\psi}_1 \text{ --- } \psi_i \text{ --- } \psi_j'\bar{\psi}_j' \text{ --- } \psi_n\bar{\psi}_n|$$

involving both relaxed and unrelaxed eigenvectors is orthonormalized. With either a single unrelaxed orbital in a field of relaxed orbitals, or a single relaxed orbital in the field of frozen orbitals, this is found to be the case to a very good degree of approximation (better than 0.001). Finally, although core-ionization from a closed-shell species was explicitly considered here, (6.13) is perfectly general, and single orbital relaxation accompanying core-ionization from open-shell systems may also be calculated using this approach.

6.2 Carbon Monoxide - An Investigation of the Basis Set Dependence of Single Orbital Relaxation

6.2.1 Introduction

Before commencing a systematic study of single orbital

relaxation energies accompanying core-ionization in a series of small molecules, a preliminary investigation was undertaken. Since a wealth of data exists for carbon monoxide, this molecule was chosen to exemplify the method. The emphasis of this preliminary investigation was two-fold: to see if the results obtained are physically in accord with chemical intuition; and to investigate the basis set to be used for a systematic study. Accordingly, calculations were performed using the experimental bond-length (2.132 au) of CO for both the ground and core hole state species, implementing the method described in the previous section over a range of basis sets.

6.2.2 Results and Discussion

(a) Single Orbital Relaxation Energies

To put the results in context, it is useful to consider the localization characteristics of the occupied MO in carbon monoxide; this may be best illustrated by means of density contour maps, shown in Figure 6.2 for C-O (in that molecular orientation), over an area of 10 x 10 au. The 5σ orbital may thus loosely be described as a lone pair on carbon. The degenerate 1π orbitals are essentially p-orbitals; 24% of the Mulliken gross population is located on carbon, with a bond overlap population of 0.116. The 4σ orbital is predominantly of oxygen lone pair character, whilst the 3σ orbital may be described as a strongly bonding MO, with considerable O 2s character. The 2σ and 1σ orbitals (not shown in Figure 6.2) are the carbon and oxygen 1s orbitals, respectively.

The single orbital relaxation energies accompanying core-ionization are shown in Table 6.1 for an STO-6.33G plus polarization basis set. As anticipated from the previous section,

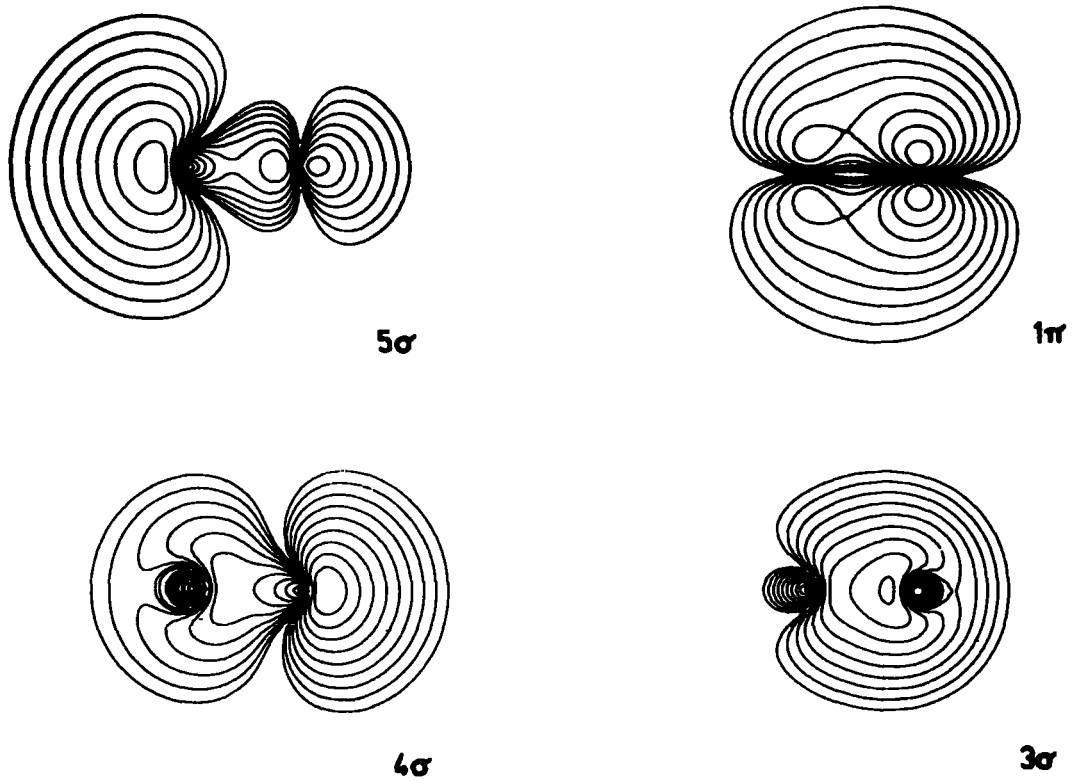

Fig.(6.2) Electron density contour plots for the valence-orbitals of CO.

the sums of the single orbital relaxation energies (i.e., the average of calculations (a) and (b)) agree exactly with those calculated directly. Furthermore, Table 6.1 illustrates that the two types of calculation, (a) and (b), respectively over- and underestimate the single orbital relaxation energies. The results are also in accord with chemical intuition. Clearly, the contribution from the localized core-orbitals in CO to the total relaxation energy would be expected to be negligible; this is found to be the case. The relative contribution from the 3σ orbital is essentially the same (15%, 13% of the total) for both carbon and oxygen core-ionization; this is not surprising, since this orbital is the most bonding of the σ-orbitals, and contributions to the relaxation

TABLE 6.1 Single Orbital Relaxation Energies for CO (in eV)

Molecular Orbitals	C_{1s} Relaxation Energy			O_{1s} Relaxation Energy		
	Calculation (a)	Calculation (b)	Average	Calculation (a)	Calculation (b)	Average
5σ	4.25	2.74	3.49	-0.97	-0.10	-0.54
1π[a]	3.36	1.24	2.30	9.40	3.60	6.50
4σ	1.91	0.00	0.95	7.21	1.87	4.54
3σ	2.60	0.71	1.66	3.97	1.35	2.66
2σ	0.09	0.08	0.09	0.00	0.00	0.00
1σ	0.00	0.00	0.00	0.27	0.22	0.25
Sum	15.57	6.01	10.79	29.28	10.54	19.91
Directly Calculated			10.79			19.91

[a] The figures quoted here refer to one of the two degenerate orbitals only.

energy might therefore have been anticipated to be small and similar for core-ionization on either atom. The situation for the 4σ and 5σ orbitals is more complex. On the basis of the localization characteristics, since the 4σ orbital is a lone pair on oxygen, and the 5σ orbital a lone pair on carbon, a large contribution to the total relaxation energy from these orbitals on core-ionization of oxygen and carbon, respectively, might be expected. This is found to be the case (23%, 32%); the contribution to relaxation on core-ionization of the atom with no lone pair (carbon for the 4σ orbital, oxygen for the 5σ orbital) is expected to be small; again, this is borne out by the results in Table 6.1, with contributions corresponding to 9% and -3% of the total, respectively. Finally, the degenerate π-orbitals would be expected to give the most significant contribution to the total relaxation energy, that contribution on oxygen core-ionization being somewhat greater. This is also found to be the case (21%, 33% from each π-orbital, on carbon and oxygen core-ionization, respectively).

A more detailed analysis of the results for CO will be presented in a later section; at this point, however, it is clear that the method of determining the single orbital contributions to the total relaxation energy used here gives results in good accord with what one might have anticipated on intuitive grounds, and that this approach shows considerable potential for furthering the understanding of the electronic reorganization process.

(b) Basis set Dependence

Before a detailed, systematic study of a series of molecules is undertaken, it is of considerable importance to choose

a good basis set for the particular property of interest. Accordingly, the total energies, ΔSCF binding energies, and relaxation energies of CO, for a range of different basis sets, are presented in Table 6.2, calculated at the experimental equilibrium bond-length. The STO-4.31G basis set has been described previously. 3d Polarization functions were added to each atom, with exponents of 0.938 and 0.990 for carbon and oxygen, taken from Yoshimine and McLean,[35] to give an STO-4.31G + P basis set. For the STO-6.33G basis set, double zeta functions in bases of contracted GTF were used, with the expansion parameters determined by a least-squares fit to STO at the STO-3G level; exponents were taken from Clementi.[32] The same polarization functions were used to give an STO-6.33G + P basis set. Dunning's[49] (9s 5p/4s 2p) contraction of Huzinaga's[50] primitive set, with the same set of polarization functions, was also employed, as was a Slater Double Zeta basis set.

From Table 6.2, it is clear that Dunning's contraction gives an excellent value for the total energy of CO; however, of prime interest in this investigation is the relaxation energy accompanying core-ionization. Here, Dunning's contraction compares only poorly with the Slater Double Zeta basis set, whilst the STO-6.33G + P basis set, although energetically not as good as Dunning's contraction, provides a much better description of the relaxation process. Since a study of a variety of molecules was envisaged, including fluorine-containing molecules, and possibly elements even higher in the Periodic Table, it was felt desirable to use a basis set with polarization functions. A Slater Double Zeta basis set with polarization would be prohibitively time-consuming; in this event, although the Dunning contraction was quicker

TABLE 6.2 Total Energies (in au), ΔSCF BE and RE (in eV), for CO

Basis Set	Total Energy	C_{1s}		O_{1s}	
		ΔSCF BE	RE	ΔSCF BE	RE
STO-4.31G	-112.093258	300.80	8.31	548.47	16.06
STO-4.31G, plus polarization	-112.134108	300.83	8.47	548.53	16.15
STO-6.33G	-112.555484	299.81	10.77	543.83	19.80
STO-6.33G, plus polarization	-112.580713	299.64	10.79	543.71	19.91
Dunning (9s5p/4s2p), plus polarization	-112.758174	299.07	10.45	543.51	18.90
Slater Double Zeta	112.675813	299.63	11.37	543.31	20.44

computationally, the STO-6.33G + P basis set was chosen, since it gave relaxation energies of essentially Slater Double Zeta quality.

The single orbital relaxation energies accompanying C_{1s} and O_{1s} core-ionization in CO for some of these basis sets are given in Table 6.3. As might have been anticipated from Section 6.1, in all cases, the sum of the single orbital relaxation energies exactly equals the directly computed value. For the core-orbitals (1σ, 2σ), the STO basis sets all under-estimate the single orbital relaxation energy, whilst the Dunning contraction does not. Of more importance, however, is the fact that for the valence orbitals, the STO-6.33G + P basis set performs consistently better than Dunning's contraction, and much better than the STO-4.31G basis sets. This validates the choice of this basis set for further studies. The general features of the single orbital relaxation energies accompanying core-ionization are, however, retained irrespective of the basis set employed. For example, for the relaxation accompanying O_{1s} core-ionization in CO, the contribution from the 5σ orbital is always small and negative, whilst the dominant contribution comes from the 1π orbitals.

6.3 Single Orbital Relaxation Energies Accompanying Core-Ionization in the First-Row Free Atoms

6.3.1 Introduction

Having made a preliminary investigation of the method for determining single orbital relaxation energies, and having chosen a basis set (STO-6.33G + P) for subsequent studies, a suitable starting point is a consideration of the first-row atoms, B to Ne. These systems have been well-studied theoretically, and provide a suitable background for the subsequent discussions of molecular systems.

TABLE 6.3 Single Orbital Relaxation Energies (in eV) Accompanying C_{1s} and O_{1s} Core Ionization in CO

		STO-4.31G	STO-4.31G + P	Dunning + P	STO-6.33G + P	Slater Double Zeta
O_{1s}	$1\pi^a$	5.27	5.26	5.97	6.50	6.51
	5σ	-0.73	-0.77	-0.74	-0.54	-0.56
	4σ	3.61	3.73	4.35	4.54	4.72
	3σ	2.56	2.58	2.61	2.66	2.54
	2σ	0.00	0.00	0.00	0.00	0.00
	1σ	0.08	0.08	0.74	0.24	0.70
	Sum	16.06	16.15	18.90	19.91	20.44
C_{1s}	$1\pi^a$	1.89	1.92	2.18	2.30	2.32
	5σ	2.04	2.03	2.84	3.49	3.39
	4σ	0.84	0.89	0.77	0.95	1.04
	3σ	1.58	1.64	1.71	1.66	1.60
	2σ	0.07	0.07	0.77	0.09	0.69
	1σ	0.00	0.00	0.00	0.00	0.00
	Sum	8.31	8.47	10.45	10.79	11.37

[a] This figure refers to one of the degenerate orbitals.

6.3.2 Results and Discussion

The total energies and ΔSCF binding energies obtained in this study are shown in Table 6.4, together with the Hartree-Fock Energies, neutral-atom electron binding energies from relaxed orbital relativistic HF-Slater calculations, and experimental binding energies. The basis set is clearly adequate, the total energies being approximately 0.1% less than the HF energies. The calculated binding energies at the ΔSCF level compare reasonably with the ΔSCF relativistic calculations; neither of these allow for correlation effects, however.

The total relaxation energies accompanying core-ionization, together with the single orbital contributions to the total relaxation energy, are shown in Figure 6.3. In going from B to Ne, there is a steady increase in the total relaxation energy

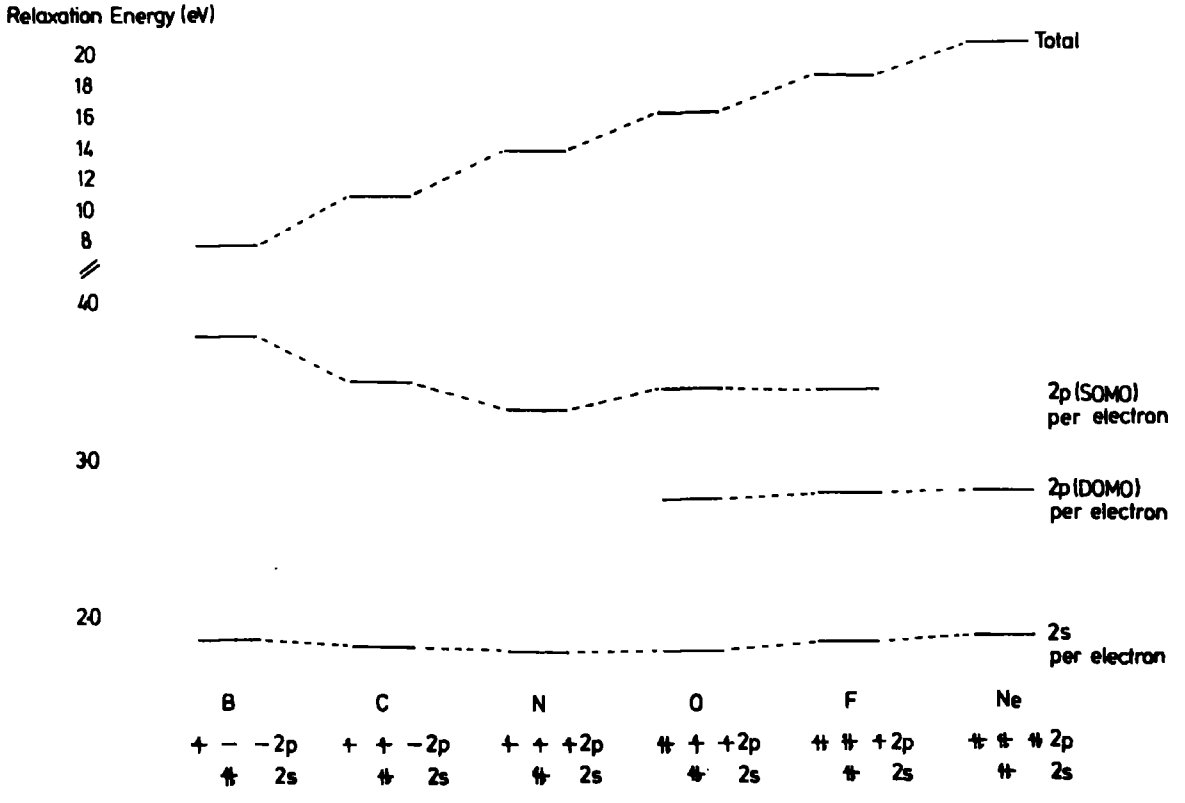

Fig. (6.3) RE accompanying core-ionization in first-row atoms.

TABLE 6.4 Total Energy (in au) and ΔSCF BE (in eV)

	Total Energy	HF Energy[a]	ΔSCF BE	Theoretical BE[b]	Experimental BE[c]
B	-24.5032	-24.5290	201.2	200.8	194
C	-37.6488	-37.6886	296.4	296.9	289.3
N	-54.3417	-54.4009	409.9	411.9	409.93
O	-74.7236	-74.8093	544.9	545.3	543.1
F	-99.2877	-99.4093	698.3	697.6	696.71
Ne	-128.3801	-128.5470	870.8	869.1	870.37

[a] Ref. 288.

[b] Ref. 52.

[c] Ref. 117. B and Ne values are free atom; all others are standard state.

from 7.8 eV for B to 20.6 eV for Ne. The contribution from the 2s orbitals remains essentially constant across the series at 1.84 ± 0.05 eV per electron; the situation for the 2p orbitals is more complex. The contribution from the singly-occupied 2p orbitals decreases from 3.8 to 3.5 to 3.3 eV per electron. For the O, F and Ne atoms, the contribution from the doubly-occupied 2p orbitals (per electron) is virtually constant at 2.77 ± 0.02 eV; the remaining singly-occupied 2p orbital contribution increases slightly in O and F to 3.44 eV. Overall, then, the 2s contribution per electron remains constant across the series, whilst the average (DOMO and SOMO) 2p contribution per electron decreases across the series, although the total 2p contribution is responsible for the steady increase in relaxation energy across the series.

6.4 Single Orbital Relaxation Energies Accompanying Core-Ionization in Some First-Row Diatomic Molecules

6.4.1 Introduction

A preliminary account of the variation in core binding and relaxation energy as a function of geometry has been presented in Chapter 4, and a detailed analysis for the singlet and triplet states of CH_2 and CF_2 is being undertaken at present. In a recent paper, Goscinski and Palma[289] have investigated the relative importance of changes in total relaxation energy as a function of bond-length, in determining whether the equilibrium geometry for a core-ionized species corresponds to an increase or decrease in bond-length (with respect to the neutral molecule). The particular systems of interest were nitrogen and carbon monoxide, for which the gradients of relaxation energies as a function of bond-length have previously been established.[170]

The total relaxation energy (primarily associated with the valence-electrons) arises from contributions from each of the occupied valence-levels. The results presented so far in this chapter have shown that contributions from individual orbitals depend quite strikingly both on the location of the core-hole and on the localization characteristics of the valence-orbital. To investigate this in more detail, the results of non-empirical LCAO MO SCF computations of approximately Double Zeta quality on individual orbital relaxations accompanying core-ionization in carbon monoxide are presented here. The study covers:

i) single orbital relaxation energies, and their variation with bond-length;

ii) Mulliken population analyses of the individual molecular orbitals as a preliminary indication of charge variation accompanying core-ionization;

iii) density difference contours as a more detailed pictorial representation of individual orbital relaxations.

Taken in conjunction, these methods provide a very adequate description of single orbital relaxation.

The variation of binding energy and relaxation energy consequent upon core-ionization as a function of bond-length for the nitrogen molecule has also been investigated, together with the single orbital relaxation energies. Comparison is made with the isoelectronic CO molecule.

6.4.2 Computational Details

The basis set used and method of obtaining single orbital relaxation energies have been adequately described in a previous section. Density difference contours for the total

relaxation process have previously been presented for CO;[170] in this study, the density difference contours appropriate to each individual molecular orbital have been constructed. The areas studied were in each case divided into a mesh of 97 x 97 points. The same geometry (viz. the equilibrium geometry of the neutral molecule) was used for both the ground and core-ionized states, and the planes studied were the molecular plane (10 x 10 au) and a plane perpendicular to this, bisecting the bond (8 x 8 au). Contours are drawn from 0.0004 au, each contour successively doubling in value until a maximum of 0.8 au is reached. Positive values are represented by solid lines; corresponding negative values by dashed lines. All difference plots are of the ground-state minus the hole-state; thus, dashed lines indicate an *increase* in electron density subsequent on core-ionization. The valence orbital plots are all to the same scale; those for the core-orbitals, however, are a factor of approximately three larger.

In some senses, the nitrogen molecule is considerably more difficult to treat theoretically within the formalism previously described, in that the computation of the individual valence-orbital contributions to the total relaxation energy requires the appropriate localized vectors for the neutral molecule (since in the ΔSCF RHF formalism, the hole-state is described in localized terms). One way to obtain localized vectors is by the application of a perturbation to the system. In this particular case, an electric field across the molecule was applied to remove the symmetry of the system and thereby localize the vectors. This will be discussed in more detail in a subsequent section.

6.4.3 Carbon Monoxide

a) Introduction

The basis set employed for this investigation was chosen as a reasonable compromise between cost effectiveness from the computing standpoint and accuracy. Table 6.5 shows the computed equilibrium bond-lengths for the neutral molecule and core-ionized species, together with the calculated absolute binding and relaxation energies. For comparison, data is also included for computations employing basis sets of Slater Double Zeta functions, and Slater Double Zeta plus polarization functions, denoted Triple Zeta. The slightly poorer description of the core-orbitals gives a significantly higher total energy for the neutral molecule; however, the good description of the valence-levels required for the adequate description of relaxation and binding energies is clearly evident, since the basis set chosen approaches the accuracy of that for the Slater Double Zeta set. This is also found to be the case for the computed bond-lengths. Overall, therefore, the basis provides a good description of the ground and hole-states as a function of internuclear separation. Figure 6.4 shows the change in binding energy (vertical), relaxation energies and Koopmans' energies for the C_{1s} (solid line) and O_{1s} (dotted line) hole-states as a function of bond extension or compression in carbon monoxide. The gradients for the relaxation energies are essentially the same as those previously reported[170] using the Slater Double Zeta basis set (0.27 and 2.42 eV au^{-1} for C_{1s}, O_{1s} respectively, compared with 0.26 and 2.40 eV au^{-1}). It is clear from a comparison with the change in core orbital energies that the substantial lengthening of the bond associated

TABLE 6.5 Equilibrium Bond-Lengths, Binding Energies and Relaxation Energies for CO

Basis Set	Calculated Equilibrium Bond-Length[a] (in au)			Total Ground State Energy (in au)	Vertical[c] Binding Energy (in eV)[b]		Relaxation Energy (in eV)	
	CO	C*O	CO*		C_{1s}	O_{1s}	C_{1s}	O_{1s}
STO-6.33G + P	2.171	2.056	-[d]	-112.5816	299.6	543.7	10.8	19.9
Double Zeta[e]	2.155	2.052	2.324	-112.6762	299.6	543.3	11.4	20.4
Triple Zeta[e]	2.123	2.010	2.230	-112.7098	298.1	542.0	11.9	20.8

a The experimental bond-length for CO is 2.132.[214]

b Experimental values for C_{1s} and O_{1s} holes in CO are 296.2 eV and 542.3 eV respectively.[170]

c The vertical binding energies reported refer to the experimental ground-state geometry.

d The equilibrium bond-length for CO* was not explicitly calculated, but could be estimated to be greater than 2.28 au.

e These values taken from ref. 170.

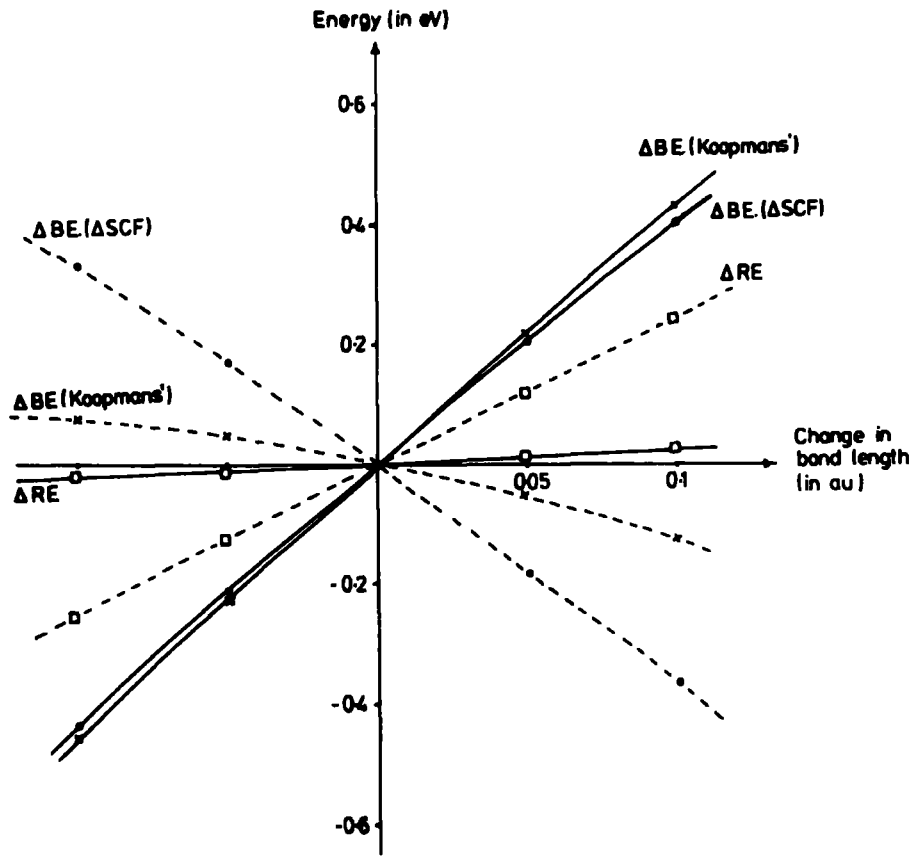

Fig.(6.4) Variation of ΔSCF BE, Koopmans' BE and total RE as a function of bond-length.

with O_{1s} core-ionization is largely associated with the strong change in relaxation energy as a function of bond-length; this contrasts with the situation for the C_{1s} core-ionized species, for which the equilibrium bond-length is somewhat shorter than the neutral molecule. This point has been considered in some detail recently by Goscinski and Palma from the standpoint of the transition formalism.[289]

b) Single Orbital Relaxation Energies

Individual orbital relaxation energies have been given in Table 6.1 for C_{1s} and O_{1s} core-ionization of CO at the experimental bond-length. The salient features of that table will be

briefly recapitulated here to provide the necessary background for subsequent discussion. For the C_{1s} levels, the large contribution to the relaxation energy comes from the 5σ (lone pair on C) orbital; for O_{1s} core-ionization, the contribution from this orbital is small and negative. The degenerate 1π orbitals contribute substantially to the relaxation accompanying C_{1s} ionization, and represent the dominant contribution to the total relaxation energy for the O_{1s} hole-state. The 4σ (lone pair on O) orbital contributes substantially to O_{1s} relaxation, but not to C_{1s} relaxation; and the 3σ orbital contribution is small and similar for both O_{1s} and C_{1s} core-ionization.

The different contributions to the total relaxation energy from each of the occupied valence-orbitals in CO, as a function of the hole-state, is dramatically shown in Figure 6.5, where comparison is also made with the orbital relaxations accompanying core-ionization of C and O atoms.

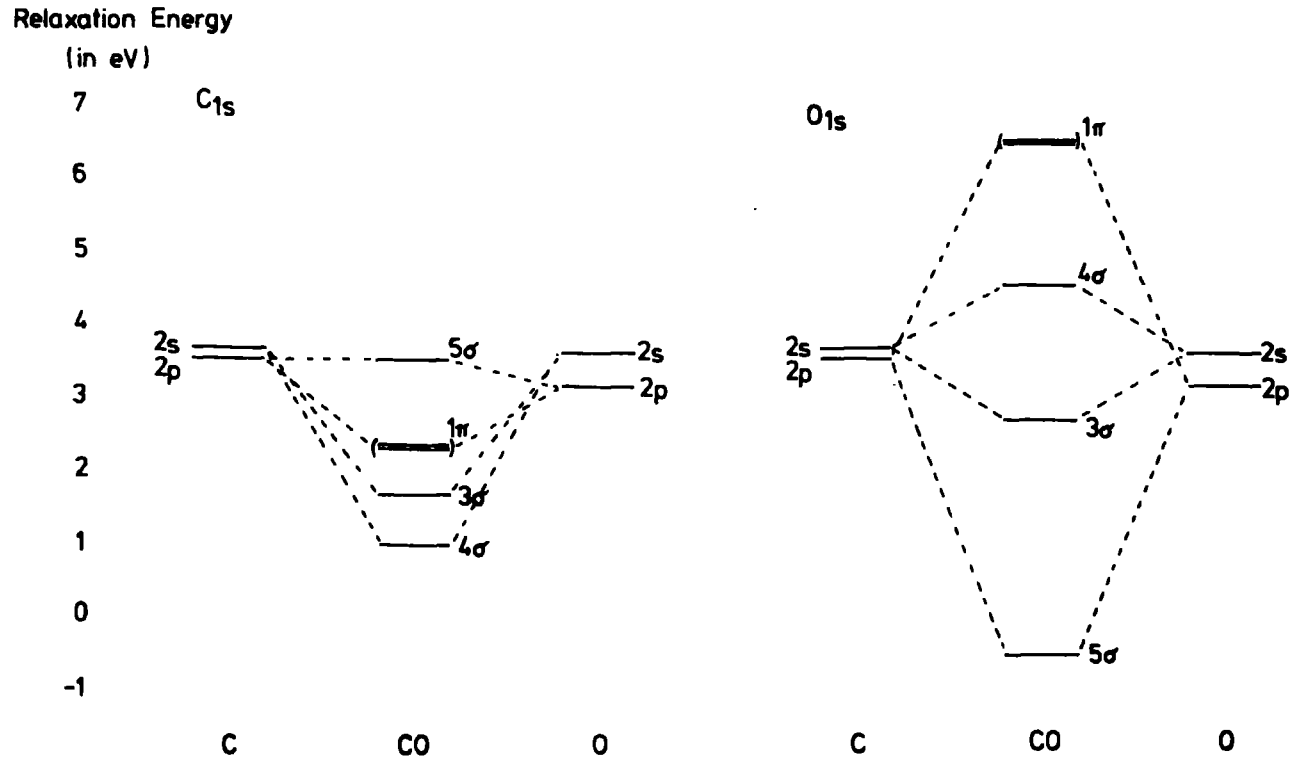

Fig. (6.5) Single orbital relaxation energies accompanying C_{1s} and O_{1s} core-ionization in CO.

c) Mulliken Population Analysis

The Mulliken population analyses for both the neutral molecule and core-ionized species are displayed in Table 6.6. However, such an analysis can at best provide only a crude rationale for the trends in relaxation energies. Thus for the 5σ orbital, the overall electron transfer accompanying core-ionization is away from the atom on which the core-hole is created, which might *a priori* suggest that the orbital relaxation energies should both be small. The orbital relaxation energy for the C_{1s} core-ionized species, however, receives its largest contribution from the 5σ orbital, whilst for the O_{1s} core-ionized species, the relaxation energy contribution is actually small and negative. This can be rationalized in terms of the fine details of electronic reorganization as evidenced from the density contour maps. The nature of the gross electron transfers that occur may be understood however in terms of the relative orbital energy mismatch between valence 2s and 2p orbitals on carbon and oxygen as a function of the location of the core-hole. Thus, in going from the neutral molecule to the C_{1s} core-ionized system, the energy mismatch decreases, such that the percentage s character of the 5σ orbital, as far as carbon is concerned, decreases. Since the negative bond overlap population between carbon and oxygen for this orbital originates in the C_{2s} - O_{2p_x} interaction, on going from the ground-state to core-ionized state, the antibonding interaction decreases. For the O_{1s} hole-state however, the increased C_{2s} character of the 5σ orbital leads to a considerably increased antibonding interaction. With the exception of the 3σ orbital for the O_{1s} core-ionized case, the electronic reorganization accompanying core-ionization follows the expected trend on the basis of the positive contributions to the individual relaxation energies (viz. creation

TABLE 6.6 Mulliken Population Analyses for the Ground and Core Hole States of CO

Molecular Orbital	Ground State			C_{1s} Hole State			O_{1s} Hole State		
	Gross Atomic Population		Overlap Population	Gross Atomic Population		Overlap Population	Gross Atomic Population		Overlap Population
	C	O		C*	O		C	O*	
5σ	0.934	0.066	−0.114	0.879	0.121	−0.099	0.985	0.015	−0.131
1π	0.244	0.756	0.116	0.322	0.678	0.111	0.085	0.915	0.050
4σ	0.168	0.832	−0.072	0.233	0.767	−0.161	0.106	0.894	−0.042
3σ	0.120	0.880	0.075	0.197	0.803	0.106	0.151	0.849	0.101
2σ	1.002	−0.002	−0.003	0.999	0.001	0.001	1.002	−0.002	−0.002
1σ	0.002	0.998	0.002	0.002	0.998	0.002	−0.009	1.009	−0.014
Total	5.431	8.569	+0.243	4.910	8.090	0.141	4.817	8.183	0.038

of a core-hole on one atom results in electron transfer from the other). For the 3σ orbital, the net population on oxygen increases; however, since the overlap density is quite substantial as an artefact of the equal apportionment to both nuclei, the gross atomic population on oxygen is actually calculated to decrease on O_{1s} core-ionization. This again can be discussed in somewhat more detail on the basis of the density difference contours, as can the electronic reorganizations in the core-orbitals accompanying core-ionization, which are found to be negligible as far as the Mulliken analysis is concerned.

d) Density Difference Contours

Since accurate density contours for the valence-orbitals of CO have been extensively documented[290] (Figure 6.2), the discussion here is centred on density difference contours for the neutral molecule and core-ionized species. The total electronic relaxation accompanying core-ionization in CO by means of total density difference plots computed in the molecular plane and in a plane perpendicular to the molecular axis bisecting the bond has previously been investigated.[170] Such plots are most revealing of the changes in total electron distribution accompanying core-ionization. It is found that whilst in going to the C_{1s} core hole state, there is a build up of density in the inter-bond region, for the O_{1s} core hole state there is a decrease; this provides a rationale for the results obtained by direct computation that the equilibrium bond-lengths are respectively shorter and larger for the C_{1s} and O_{1s} core-ionized species compared with the neutral molecule. In the light of the considerable differences in orbital relaxation energies, it is clear that orbital density

difference plots should provide considerable insight into the component terms of the total relaxation energy.

The relaxation for the core-orbitals is very small. This is reflected by the density difference contours. To emphasize reorganization of core-orbitals, therefore, the density difference contours shown in Figure 6.6 correspond to those appropriate for

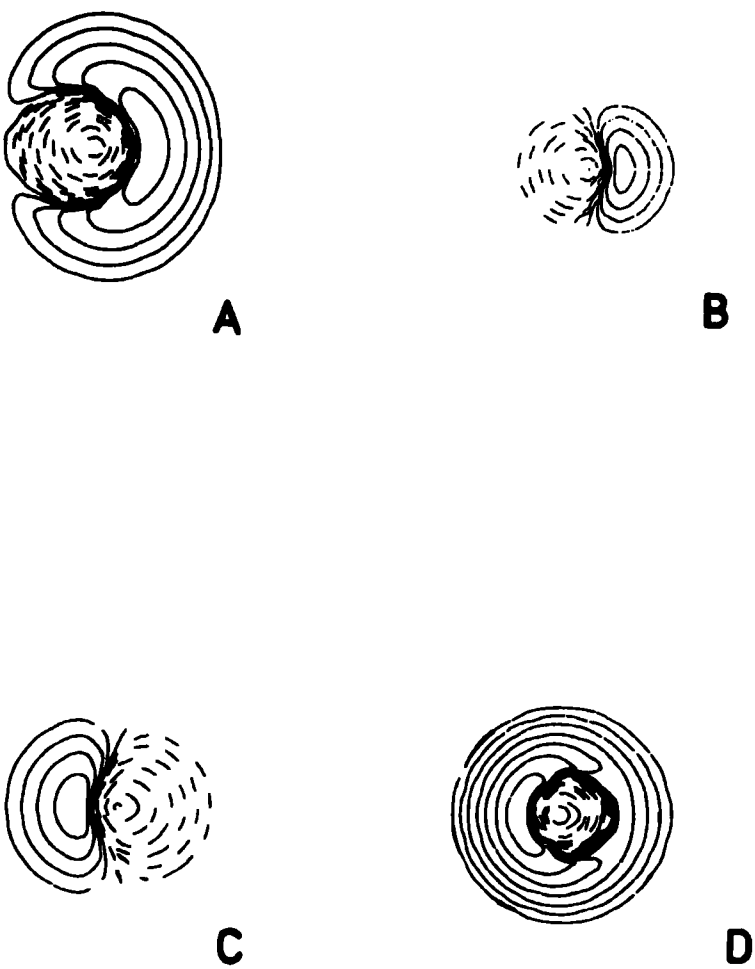

Fig.(6.6) Density difference contours in the molecular plane showing the electronic reorganization accompanying core-ionization for the 1σ and 2σ orbitals of CO.

a single electron in both the relaxed and unrelaxed orbital. The complete density difference for these orbitals involves a doubly-occupied ground-state with the appropriate hole-state being

singly-occupied. The net effect of this would be to produce a somewhat asymmetric density difference plot with all of the contours positive. This makes it difficult to appreciate the distortion of the orbitals, and it is therefore preferable to present the density difference for equal population. Considering firstly creation of a core-hole on carbon (A and B) it is clear that for the 2σ orbital (centred on carbon, A), the asymmetry of electron flow (from the valence-electrons) is manifest in the ground-state; the decrease in electron density is largely in the sector in the opposite direction to the lone pair 5σ orbital providing the largest single contribution to the relaxation energy. The polarization of the 1σ orbital (centred on oxygen, B) is also clear from this, since although the population is essentially the same as for the neutral molecule, the contour is asymmetric in the same sense as that for the 2σ orbital. This is readily understandable in terms of the overall electronic migration towards the carbon atom on creation of the core-hole. Considering now creation of a core-hole on oxygen (C and D), it is found that the density difference plot for the 1σ orbital (D) is fairly symmetrical, showing little polarization from valence-orbitals. For the 2σ orbital (C), the contour plot is asymmetric in the sense of the oxygen hole; viz., electron density is transferred onto the side towards the core-hole. This polarization is analogous to that found in the 1σ orbital when a core-hole is created on carbon. The situation for the valence orbitals is considerably more complex. Figure 6.7 displays the data for the 5σ orbital. The orientation of the molecule and the lettering is consistent for Figures 6.7 to 6.10. Thus, A and B represent the molecular plane, the carbon atom being located on the left; C and D show contours in a plane

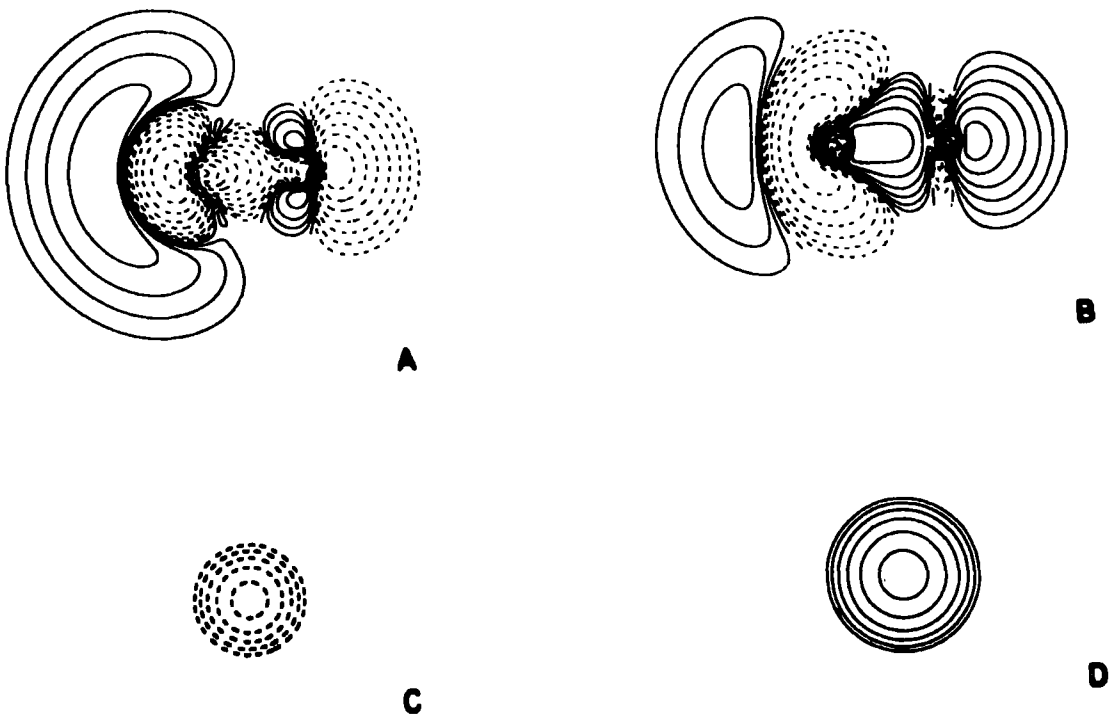

Fig.(6.7) Density difference contours for the 5σ orbital in CO. through the molecular axis, bisecting the bond. A and C show C_{1s} core-ionization, B and C show O_{1s} core-ionization. For the C_{1s} core-ionized system, which has a large, positive orbital relaxation energy, the contours taken in the plane perpendicular to the internuclear axis show an increase in density on going to the core-ionized species. This corresponds with the increased bond overlap population revealed by the Mulliken population analysis, suggesting that the relaxation energy contribution might increase with a decrease in bond-length. The electronic reorganization revealed by the computed in-plane density difference contours for the 5σ orbital is quite complex. The Mulliken population analysis suggests overall electron transfer from carbon to oxygen. The contours reveal, however, that in the immediate vicinity of the nuclei and in the interatomic region there is a significant increase in electron density in going to the core-ionized

species. Electron transfer from carbon to oxygen is therefore predominantly associated with the regions directed away from the termini of the bond. This can be rationalized on the basis of the increased interaction between the component orbitals located on a core-ionized carbon and on oxygen, compared with the situation in the neutral molecule. For O_{1s} core-ionization, the contour taken perpendicular to the internuclear axis shows a decrease in population on core-ionization, whilst the in-plane contour reveals an overall decrease in population around the oxygen. This provides a rationale for the computed negative orbital relaxation energy.

The density difference contours for the 1π orbitals are shown in Figure 6.8. For the contour perpendicular to the molecular axis, the behaviour with respect to O_{1s} and C_{1s} core-ionization is considerably different. For O_{1s} core-ionization the density decreases, whilst in the bonding region close to the internuclear axis the population increases for C_{1s} core-ionization. The corresponding in-plane contours are also shown, revealing a straightforward electron transfer to the atom on which the core-hole is created, consistent with the positive contribution to the relaxation energy for core-ionization from either core-orbital.

For the 4σ orbital, the contours taken perpendicular to the molecular axis differ quite strikingly for O_{1s} and C_{1s} core-ionization (Figure 6.9). For the former, there is an increase in density in the bonding region, whilst for the latter there is a decrease in density, which is relatively diffuse in character. This reflects the relative changes in bond overlap populations

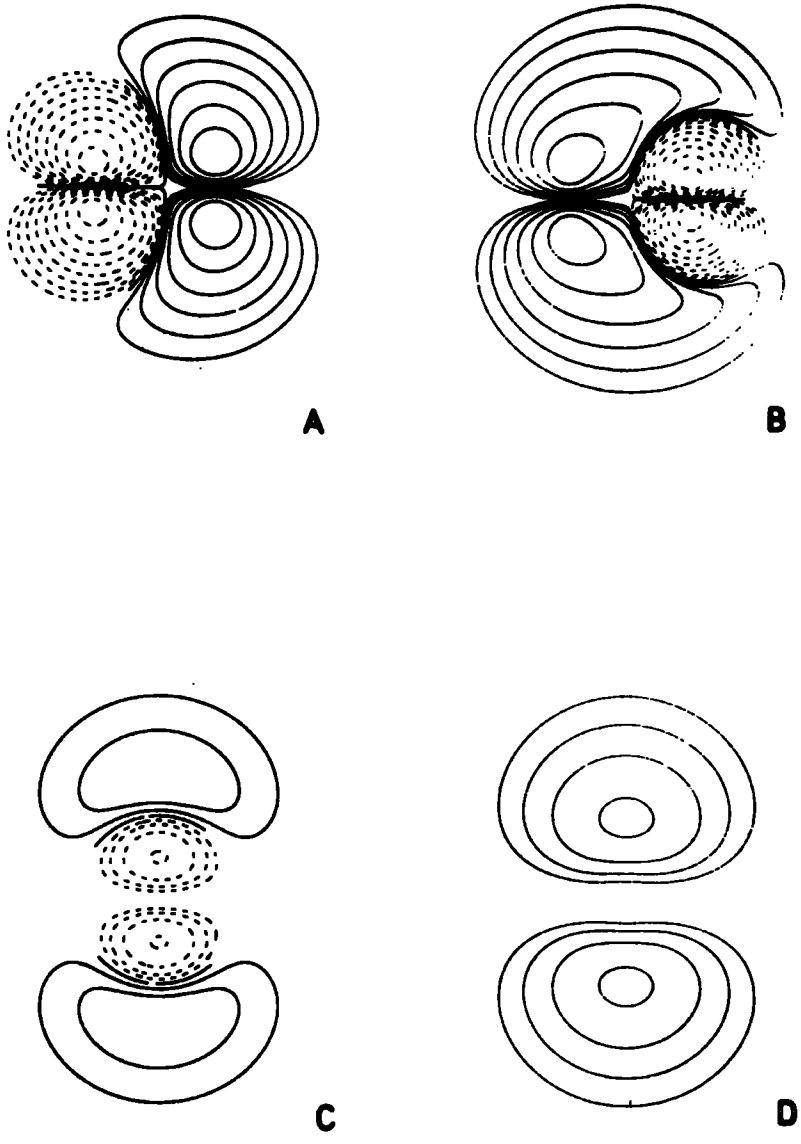

Fig.(6.8) Density difference contours for the 1π orbitals in CO.

as deduced from the Mulliken population analysis. The in-plane contours reveal an overall electron transfer from oxygen to carbon accompanying C_{1s} core-ionization; however, this is largely associated with the non-bonding regions, and in consequence the orbital relaxation energy is quite small. For O_{1s} core-ionization on the other hand, there is a substantial build-up of electron density, both on the oxygen and in the internuclear region. This is predominantly at the expense of the non-bonding regions, and

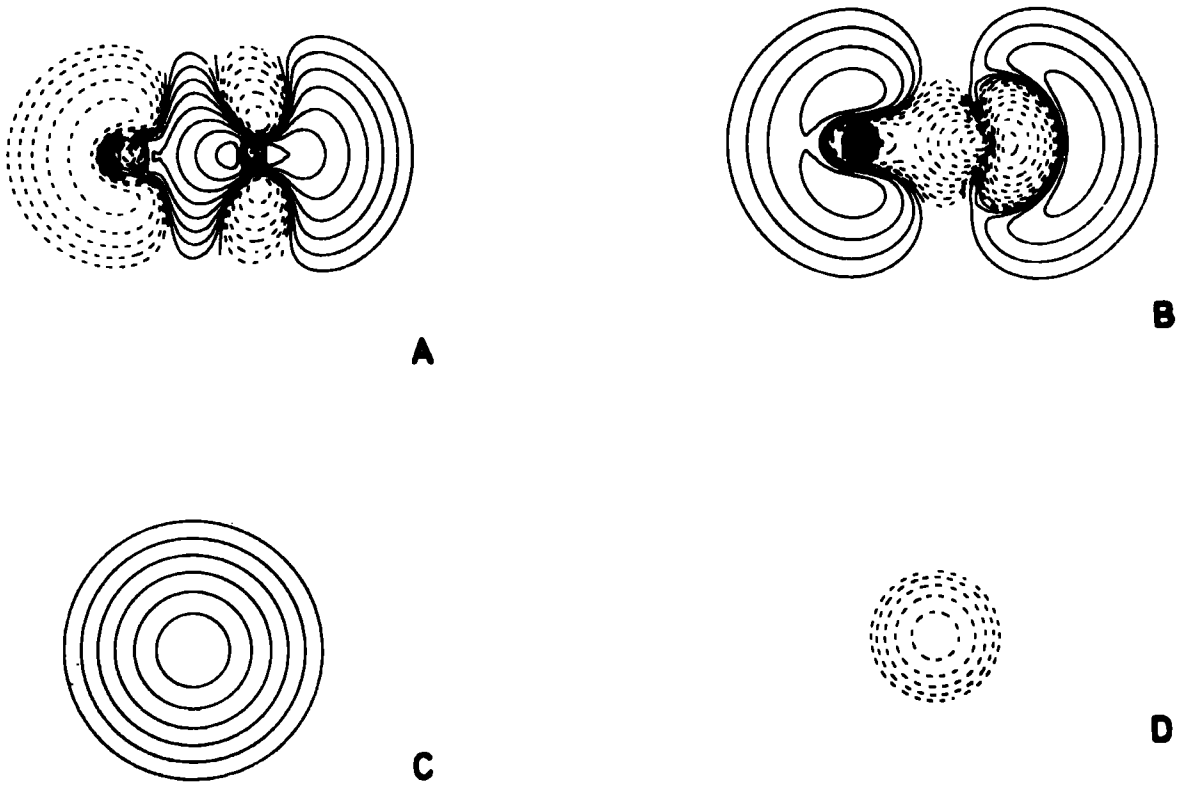

Fig.(6.9) Density difference contours for the 4σ orbital in CO.

the contribution to the total relaxation energy for O_{1s} core-ionization is substantial. For the 3σ orbital (Figure 6.10), the contour plots taken perpendicular to the molecular axis are significantly different; that for C_{1s} ionization exhibits an increase in density which is somewhat extended in space, whilst although that for the O_{1s} ionization also exhibits an increase in the region close to the molecular axis, it shows a decrease at larger distances. The crude overall picture provided by the Mulliken population analysis therefore receives some support from the more detailed picture provided by the contour plots. For the C_{1s} hole-state, there is a build up of electron density around the carbon, largely at the expense of the non-bonding region about oxygen; whilst for the O_{1s} hole-state, the corresponding increase in density on oxygen originates mainly from the bonding region. The

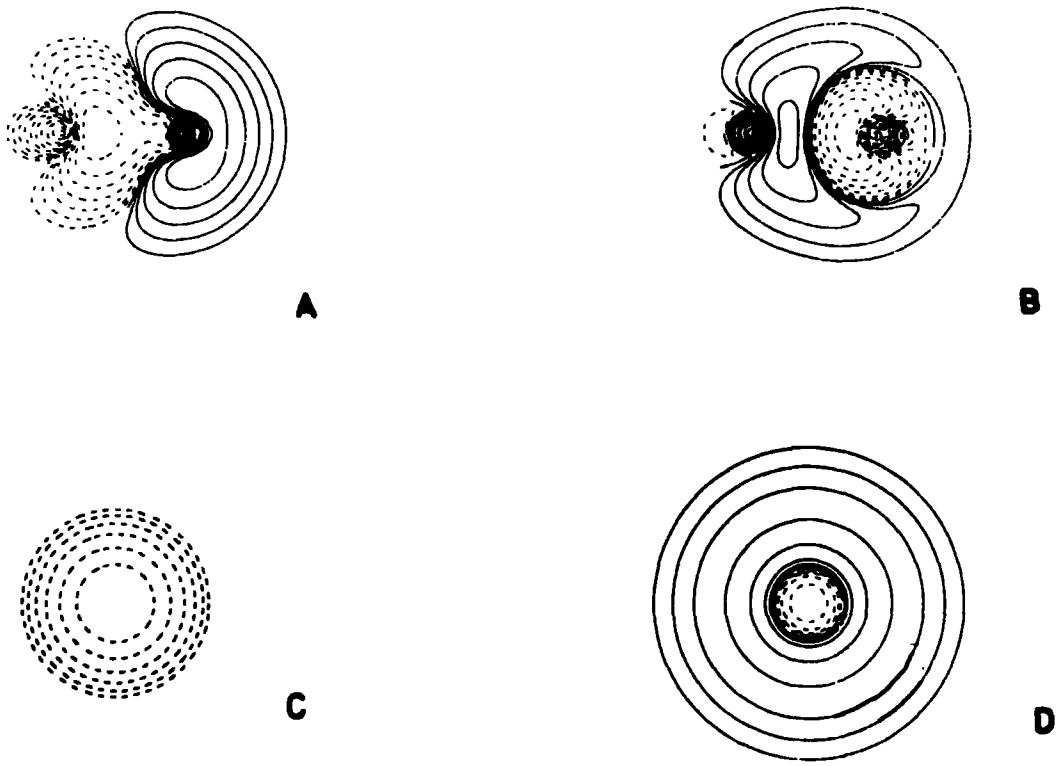

Fig. (6.10) Density difference contours for the 3σ orbital in CO.

calculated orbital relaxation energies are in both cases quite substantial and positive.

e) Orbital Relaxation Energies as a Function of Bond-Length

Previous theoretical studies on CO and the core-ionized species indicated that the total relaxation energies associated with C_{1s} and O_{1s} core-ionization increase as a function of bond-length in an approximately linear manner,[170] at least over realistic ranges of bond extensions and compressions about the bond-length appropriate to the neutral system (cf. Figure 6.4). The complex dependence of the individually computed orbital relaxation energies on both the location and localization characteristics of the orbital provides a considerable incentive for investigating the dependence of these orbital relaxation energies

on bond-length. The relevant data are displayed in Figure 6.11, and form an interesting comparison for core-ionization of the C_{1s}

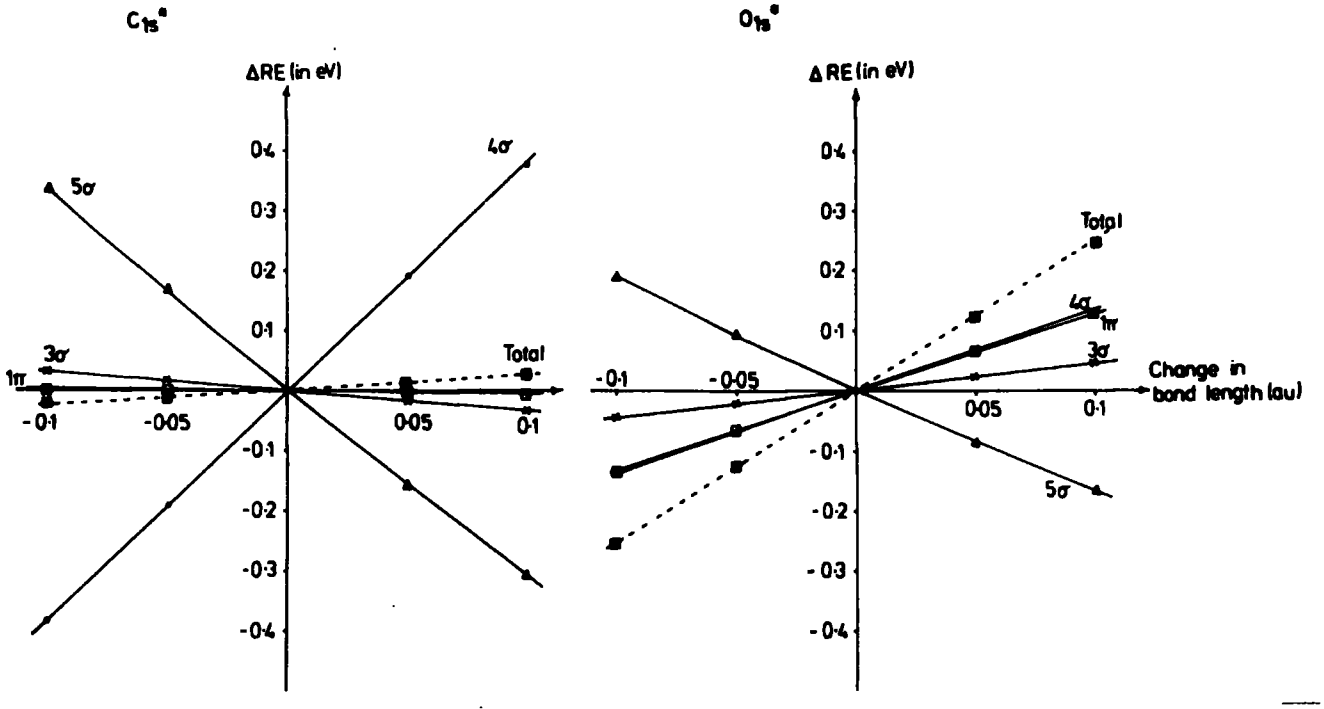

Fig.(6.11) Changes in single orbital relaxation energies as a function of bond-length.

and O_{1s} levels. For the C_{1s} core hole state, the 5σ orbital relaxation is strongly dependent on bond-length, decreasing linearly with increasing bond-length, the slope being -2.8 eV au^{-1}. This may be rationalized pictorially by consideration of the density difference contours previously described (Figure 6.7). For the O_{1s} core hole state, for which the relaxation energy is computed to be negative, the change as a function of bond-length is in the same sense as for the C_{1s} core hole state; however the gradient is ∿ 50% smaller.

The orbital relaxation energies for the degenerate 1π orbitals show negligible dependence on bond-length for the C_{1s} hole-state; however, for the O_{1s} hole-state, the slope is positive. The density contours perpendicular to the molecular plane indicate an overall decrease in population on going from the neutral molecule to the O_{1s} core-ionized system; however, as has been previously

noted, for the C_{1s} core-ionized system, the build-up in electron density in the internuclear region close to the molecular axis is offset by a decrease in the more remote internuclear regions, such that overall there is little change in electron density in this region. For the 4σ orbital, which contributes a large proportion of the relaxation energy for the O_{1s} core-ionized system, the relaxation energy increases as a function of bond-length. This, taken in conjunction with the contributions provided by the 1π orbitals of comparable dependence on bond-length, offsets the negative contribution provided by the 5σ orbital, such that the total relaxation energy increases quite significantly with bond-length. For the C_{1s} core-ionized system however, the relaxation energy for the 4σ orbital shows an even stronger dependence on bond-length, the slope being 3.8 eV au^{-1} compared with 1.3 eV au^{-1} for the O_{1s} hole-state. It is the contribution from this orbital which determines that the overall relaxation energy accompanying C_{1s} ionization increases as a function of bond-length, albeit slightly.

For the 3σ orbital, the dependence of relaxation energy on bond-length is comparatively small and approximately the same magnitude but of the opposite sign for the C_{1s} and O_{1s} hole-states; indeed, the relaxation energies contribute approximately the same proportion of the total relaxation energy in the two cases. The population analysis and density difference contours suggest a comparable build-up of electron density in the internuclear region for the two hole-states, despite the fact that the dependence of relaxation energies on bond-length are opposite in sign. Nonetheless, the changes in gross atomic populations as a function of bond-length for the two core hole states, displayed in Figure 6.12,

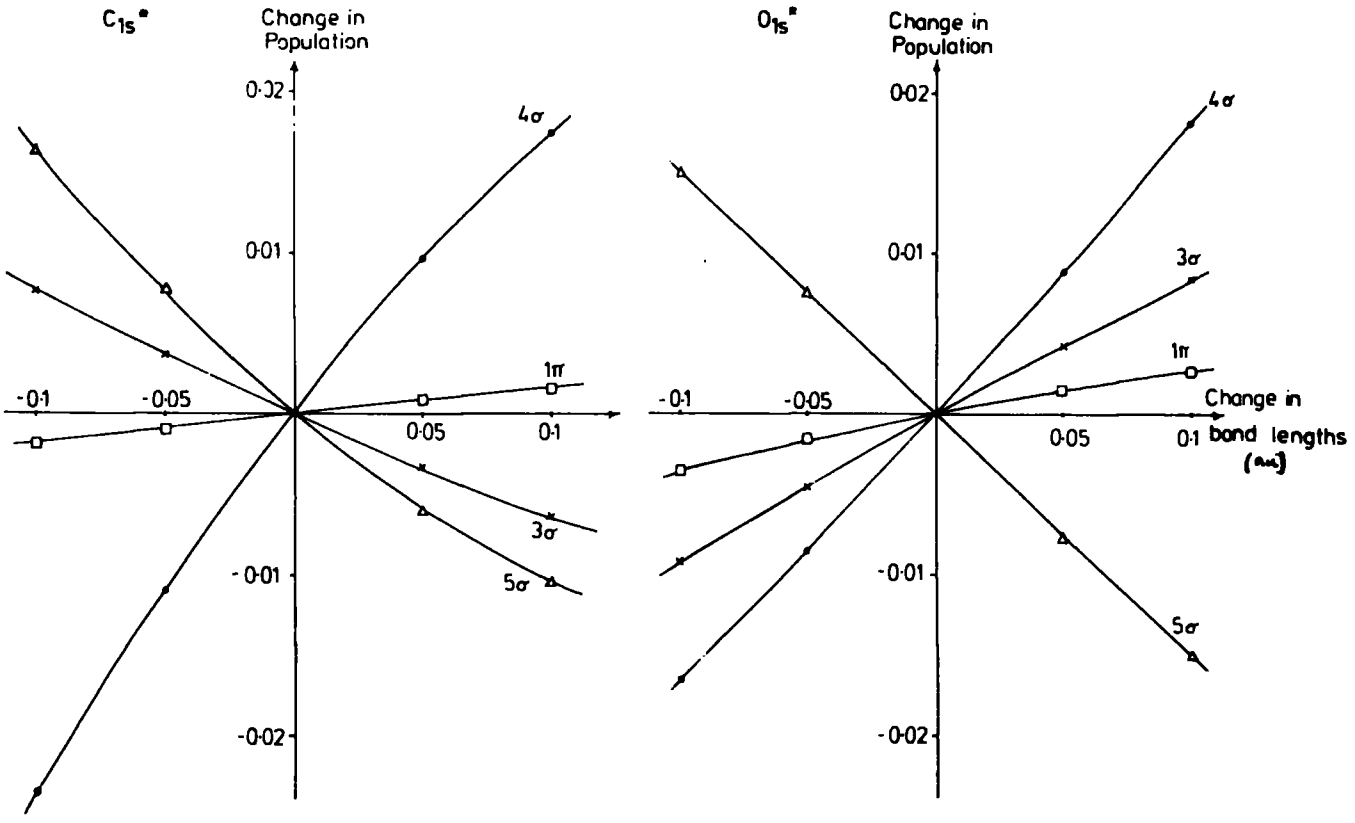

Fig.(6.12) Change in Mulliken gross atomic population of the core-hole atom as a function of bond-length.

show a remarkable correspondence with the changes in relaxation energies.

6.4.4 Nitrogen Molecule

An investigation of the core hole states of N_2, with particular emphasis on vibrational fine-structure accompanying core-ionization, and on the variation of total relaxation energy as a function of bond-length, has previously been described.[170] In this section, the results of an investigation of the individual valence-orbital contributions to the relaxation energy as a function of bond-length are presented. Before considering this data however, it is worthwhile investigating the change in potential energy surface consequent upon core-ionization. It has been shown[170] that the potential energy surface for the localized core hole state of N_2 corresponds to a shorter N-N bond-length than for the neutral molecule. It might be thought that such

changes in potential energy surfaces are solely manifestations of electronic reorganizations accompanying core-ionizations. This is not entirely true, however; it is possible to compute the potential energy surface for the core-ionized state neglecting relaxation effects. As may be seen from Table 6.7, the computed change in bond-length of 0.048 au for nitrogen compares with that computed from the hole-state calculations of 0.018 au; viz., the inclusion of relaxation effects leads to a substantial decrease in the computed bond-length change in this case. Confusion on the role of relaxation effects in changing the potential energy surfaces in going from the neutral molecule to the core hole state stems from two lines of incorrect reasoning:

i) Core-electrons are essentially non-bonding, and therefore in the absense of relaxation effects, it might naively be anticipated that there is little change in potential energy surface in going from the ground to the core hole state. This is not the case however, since even if the density distribution remained essentially the same, its energy would be influenced by the decreased screening originating from the atom on which the core-hole is located, and this will be a function of the bond-length.

ii) Koopmans' Theorem for the core hole state will not in general be a strong function of the bond-length. For a decrease in bond-length of 0.1 au, the Koopmans' Theorem binding energy for the N_{1s} levels changes by $\sim$ 0.01 au; it might therefore be argued that any change in bond-length on ionization is attributable to relaxation effects. The problem here is that Koopmans' Theorem merely provides an energy difference between the ground-state and core hole state in the absence of

TABLE 6.7 Equilibrium Bond-Lengths, Force Constants, Binding Energy and Relaxation Energy for N_2

Nitrogen, N_2	Equilibrium Bond-Length (au)	Force Constant (mdynes. $Å^{-1}$)
Ground-State	2.098	26.30
Hole-State	2.080	25.53
"Koopmans'"	2.050	27.40
Experimental	2.074[a]	22.96[b]

Experimental N_2 bond-length:	eV
ΔSCF Binding Energy	412.88
Koopmans' Binding Energy	428.23
Relaxation Energy	15.35

Single Orbital Contributions to the Relaxation Energy:

Orbital		eV
1π	$(1\pi_u)$	4.37
5σ	$(3\sigma_g)$	0.30
4σ	$(2\sigma_u)$	3.62
3σ	$(2\sigma_g)$	1.90
$1\sigma + 2\sigma$	$(1\sigma_g + 1\sigma_u)$	0.80
Sum		15.36

a Ref. 214

b Ref. 291

relaxation effects, and for individual points on the bond-length coordinate. To construct the *unrelaxed* potential energy surface, however, the variation in energy of the ground-state as a function of bond-length must also be taken into account. When this is carried out, the potential energy surface will inevitably be displaced.

It is thus not in general true to say that changes in equilibrium bond-lengths consequent upon core-ionization are solely attributable to relaxation effects.

The computed individual orbital contributions to the total relaxation energy are displayed in Table 6.7, whilst Figure 6.13 shows the orbital interaction diagram of two N atoms to give N_2, together with the appropriate single orbital relaxation energies. The calculated molecular orbital energy diagram for the N_2 molecule is particularly simple; to provide a ready comparison with CO, the orbital notation 1σ, 2σ, 3σ, ... is used (Table 6.7). On core-ionization, with a localized hole-state, the $1\pi_u$ (1π) orbitals contribute most to the total relaxation. Both of the bonding orbitals, $3\sigma_g$ (5σ) and $2\sigma_g$ (3σ), contribute less than the antisymmetric combination of 2s orbitals, $2\sigma_u$ (4σ).

At the equilibrium geometry of the neutral molecule, the single largest contribution to the relaxation energy originates from the degenerate 1π orbitals; the contribution per orbital of 4.37 eV is almost exactly equal to the average of the 1π relaxation energies computed for the C_{1s} and O_{1s} hole-states of CO (4.40 eV). The contributions fit into a logically consistent pattern; thus, for the C_{1s} and O_{1s} core hole states of CO, the average contributions to the total relaxation energies fall in the order

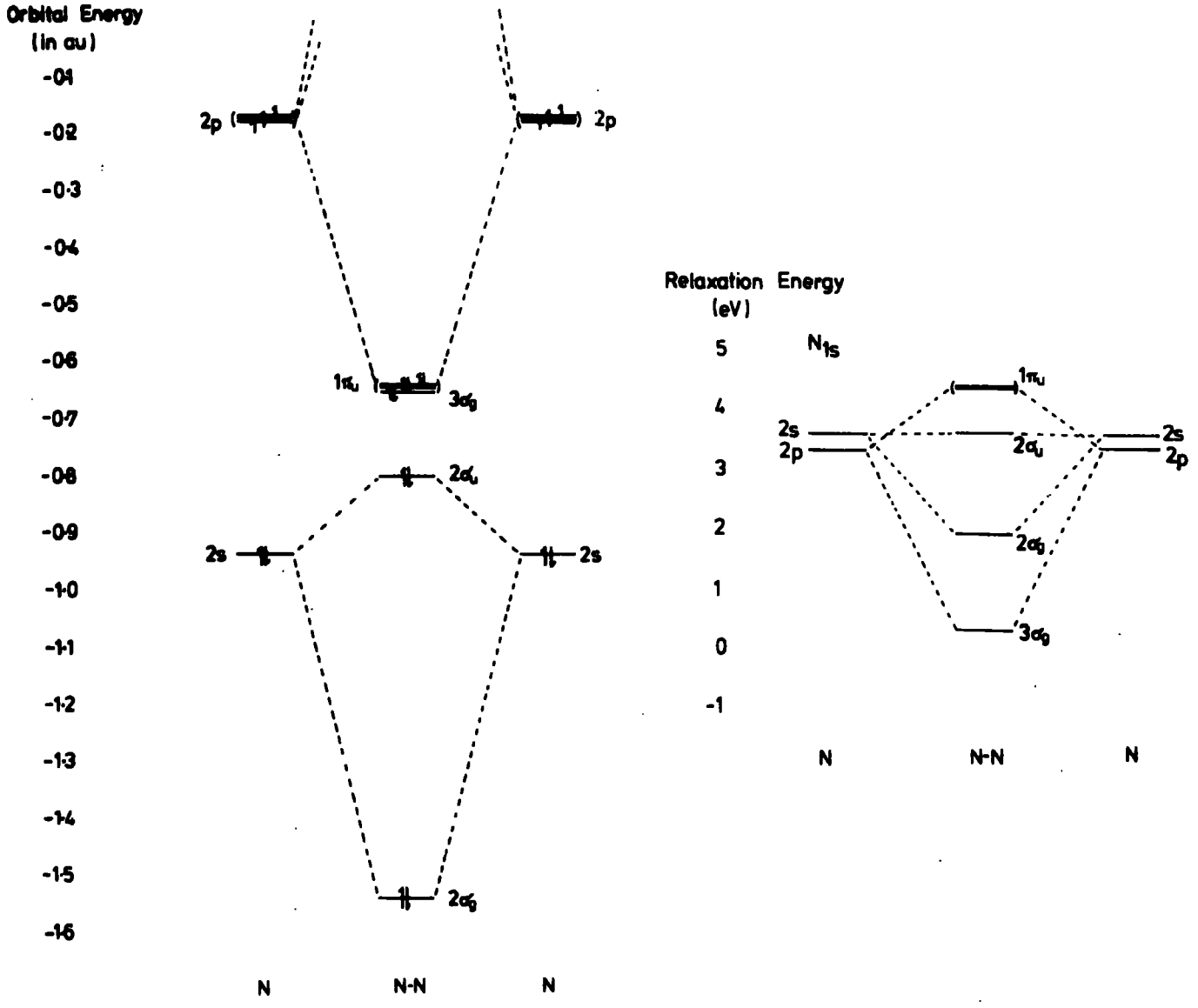

Fig. (6.13) Orbital energies, and single orbital relaxation energies, for N atom and N_2.

$1\pi > 4\sigma > 3\sigma > 5\sigma$, which is also the order computed for the N_{1s} core hole states of N_2.

The theoretically computed total relaxation energy for the N_{1s} core hole state of N_2 is not a strong function of bond-length, having a gradient of $\sim$ 1.8 eV au^{-1}.[170] In the corresponding situation for the core hole states of CO however, the relatively small dependence of relaxation energies on bond-length were attributed to a subtle interplay of the bond-length dependencies for the individual orbital components. These are

shown in Figure 6.14 for the nitrogen molecule. For both the

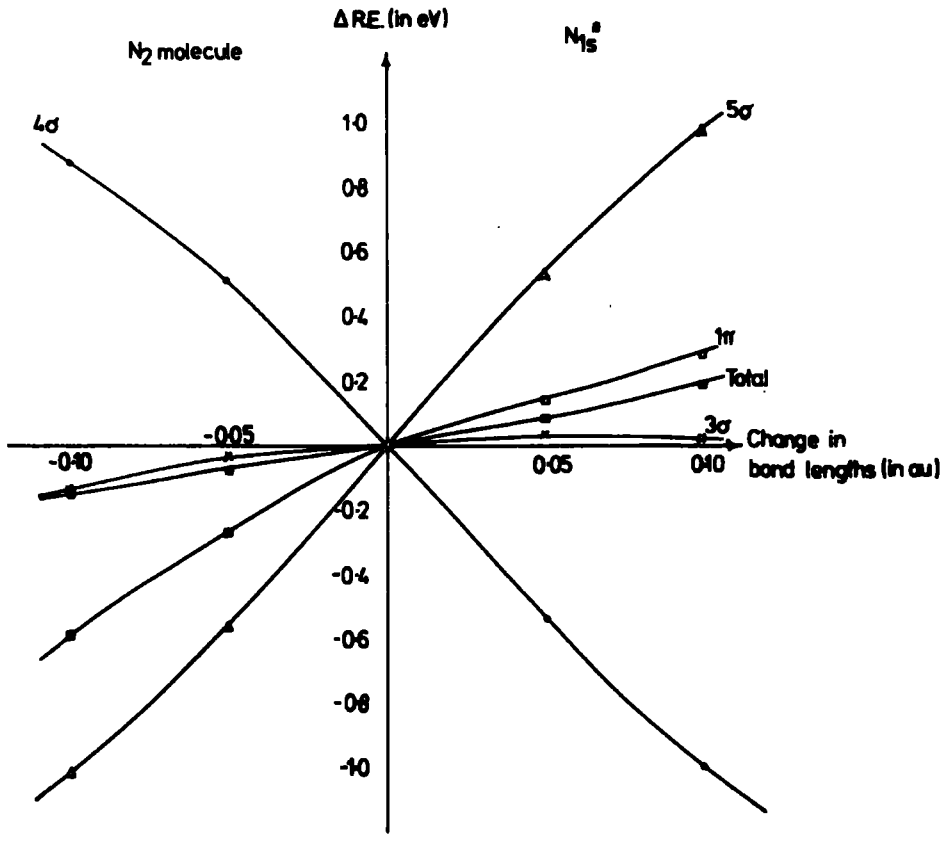

Fig.(6.14) Variation of single orbital relaxation energies as a function of bond-length.

3σ and 1π orbitals, the gradients were small (-0.31 and 0.46, -0.04 and 1.26 eV au^{-1} for the C_{1s} and O_{1s} hole-states respectively); the analysis of N_2 fits into a consistent pattern with this data, as is clear from Figure 6.14. A crude linear correlation provides gradients of 0.6 and 4.1 eV au^{-1} for the 3σ and 1π orbitals respectively. It is somewhat more difficult to correlate the 4σ and 5σ orbitals in N_2 with the corresponding orbitals in CO since the localization characteristics are different; however, the absolute magnitudes of the component relaxation energies fit into a consistent pattern if a direct correlation is assumed.

6.5 A Theoretical Investigation of the Electric Field Dependence of Core-Ionization Phenomena in CO and N_2

6.5.1 Introduction

The anisotropic nature of valence-electron reorganizations accompanying core-ionization might suggest that relaxation energies, and thus core binding energies, should be field dependent. In this section, the changes in binding energies, and in both the total and orbital contributions to the total relaxation energies consequent upon core-ionization have been investigated within the ΔSCF formalism in the presence of a strong electric field. Although of interest from the theoretical viewpoint, there are important parallels to be drawn with experiment. For example, the strong internal fields in ionic solutions, and the increasing interest in the XPS investigations of electrolytes,[292,293] provide a motivation for this study. Indeed, the adsorption of small molecules at insulating surfaces, which under the typical sample charging conditions arising in an XPS experiment might lead to very high electric fields at the interface,[245,294] also provides a likely area in which the results to be described here might be of some interest. It is also possible that with the advent of third-generation XPS instrumentation, characterized by high sensitivity and resolution, appropriate molecular beam experiments could be performed to investigate the field dependence of binding and relaxation energies directly.[295]

6.5.2 Computational Details

Calculations were performed simulating an electric field across the molecule by the appropriate positioning of positive and negative charges along the molecular axis at varying distances

from the geometric centre of the bond. The method employed for obtaining single orbital contributions to the total relaxation energy accompanying core-ionization has been comprehensively described, as has the STO-6.33G + P basis set used.

Density contour plots for the ground and core hole states of CO were generated using a mesh of 97 x 97 points, covering an area of 10 x 10 au for both the molecule with an applied field in both directions (charges situated 5 au from the geometric bond-centre) and the molecule with no applied field, in the molecular plane. Appropriate density difference contours were constructed from these plots.

To investigate changes in band-profile, potential energy surfaces for the ground and core hole states of CO, both with and without the application of a field, were calculated. Band-profiles were then obtained from the Franck-Condon factors, computed using the recurrence relations derived by Ansbacher.[157] Individual component FWHM of 0.54 and 0.58 eV were used for C_{1s} and O_{1s} core-ionization respectively.[170] Energy separations of 0.31 eV and 0.19 eV were used in the absence of field, and 0.31 and 0.22 eV in the presence of an applied field of 4.31 V cm^{-1}, in a sense such that carbon is at the positive pole, for C_{1s} and O_{1s} core-ionization, respectively.

For the nitrogen molecule, potential energy surfaces for the ground and core hole state species were constructed both in the presence and absence of an applied field of 2.68×10^{8} V cm^{-1}. The band-profiles were constructed using the "best fit" individual component FWHM of 0.39 eV obtained in a previous analysis of the nitrogen molecule.[170] Component energy separations of 0.31 eV

and 0.27 eV calculated for the absence and presence of the field respectively, were used. In drawing the difference spectra, allowance has been made for the shifts in binding energy due to the application of the field.

6.5.3 Carbon Monoxide

a) Total relaxation energies and binding energies as a function of the electric field

A preliminary account by Clark[194] showed that for CO, both the absolute binding energies and relaxation energies exhibit field-dependence; the field gradients required for an appreciable effect are understandably large, approaching that required for field ionization. This provided the stimulus for the more detailed investigation reported here. The field dependence of the absolute binding and relaxation energies, for field gradients in the range -4 to +4 V $\mathring{A}^{-1}$, is shown in Figure 6.15. The calculated

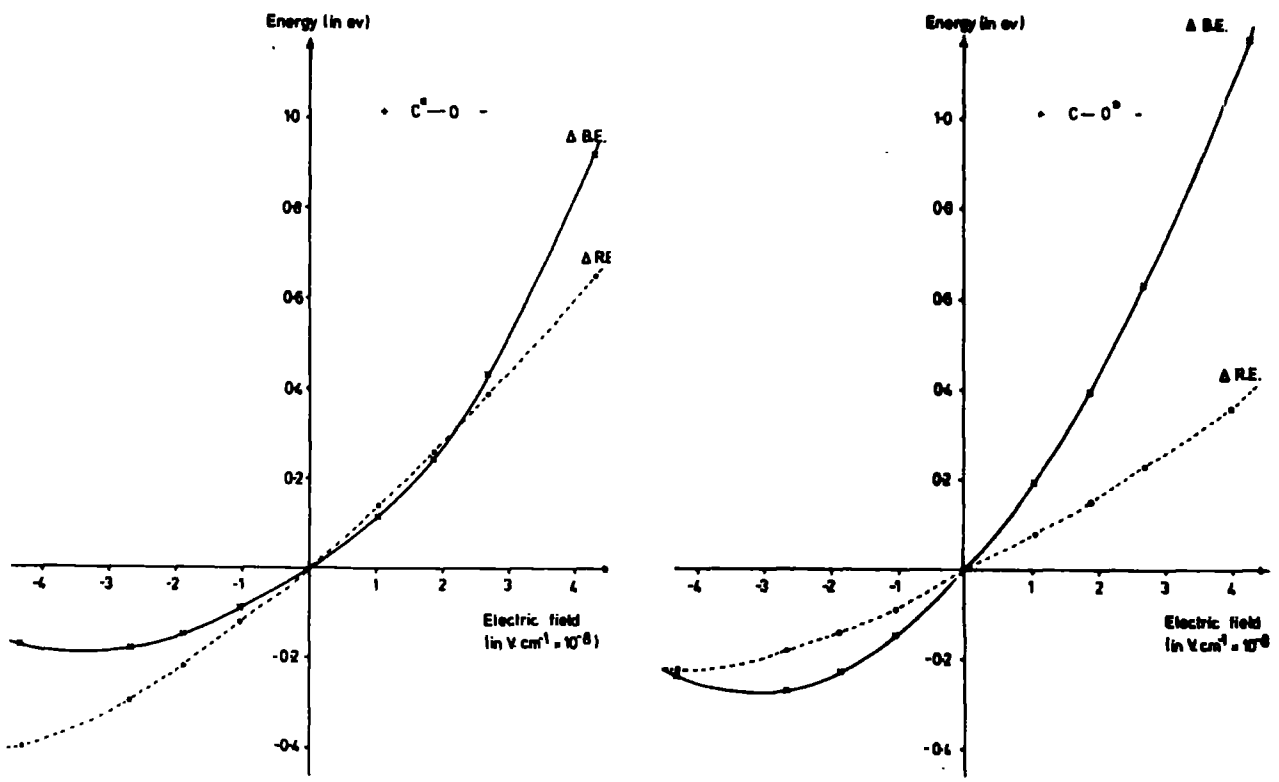

Fig. (6.15) Variation of BE and RE in CO as a function of electric field.

shifts in binding energy are very substantial for these large gradients, ranging over $\sim$ 1.0 eV and $\sim$ 1.5 eV for the C_{1s} and O_{1s} levels respectively. Application of a field in a sense such that carbon is directed towards the positive pole results in an increase in binding energy for both C_{1s} and O_{1s} core-ionization, and in each case the relaxation energy also increases, although the magnitude of such an increase is much smaller for the O_{1s} level than for the C_{1s} level. Indeed, the increases in relaxation energy arising from the application of the electric field substantially reduce the shift in binding energies which might otherwise have been expected on the basis of Koopmans' Theorem. The field dependence in the opposite sense is much less marked, and for both the O_{1s} and C_{1s} levels, the calculated absolute binding energy is somewhat smaller. For the C_{1s} levels, the change in relaxation energy is again significantly larger than for the O_{1s} levels; however, in both cases the contribution reduces the overall shift in binding energy which would have been anticipated on the basis of Koopmans' Theorem.

Since with state-of-the-art instrumentation, absolute binding energies are measurable to within a few tens of millivolts, it is clear that on an absolute scale, field gradients of the order of 10^7 volts cm^{-1} should produce detectable effects. Relative binding energies can probably be determined with substantially higher accuracy; the change in relative binding energies for a field of $\sim 10^7$ volts cm^{-1} applied along the molecular axis for the two distinct polarities would be $\sim$ 10 millivolts, which should be detectable, since with the highest available resolution, it may be anticipated that line-widths would typically be $\sim$ 0.2 eV for individual components of the overall Franck-Condon envelope.

b) Orbital contributions to total relaxation energies as a function of applied field

One of the main conclusions evident from this chapter on simple systems (CO and N_2) is the strong dependence of the individual components on the localization and bonding characteristics of the orbitals. It might, therefore, be anticipated that the total field dependence of both absolute binding energies and relaxation energies should arise from quite differing contributions from individual orbital relaxations. In this section, therefore, an investigation of the field dependence of individual orbital relaxation energies is presented.

The calculated changes in relaxation energy terms as a function of applied field for individual valence-orbitals are displayed in Figure 6.16. For the C_{1s} hole-state, the greatest field dependence is exhibited by the 5σ and 4σ orbitals; this is also the case for the O_{1s} hole-state. Creation of a core-hole on carbon, with the field such that carbon is directed to the positive pole, strongly decreases the contribution to the total relaxation energy provided by the 5σ orbital. This is qualitatively the behaviour which might have been anticipated; for the 5σ orbital (lone pair on carbon), application of a field in this sense will lead to reduced electron migration to the vicinity of the core-hole, and hence reduced contributions to the relaxation energy. This is also the case for the O_{1s} core-hole, with the field in the same sense; however, the relaxation energy contribution, which even in the absence of a field is calculated to be negative, becomes increasingly more negative, the field dependence being even larger than for the C_{1s} hole-state. By contrast, reversing the polarity of the applied field leads to an increase in contribution to the relaxation energies for the 5σ orbital, but with a

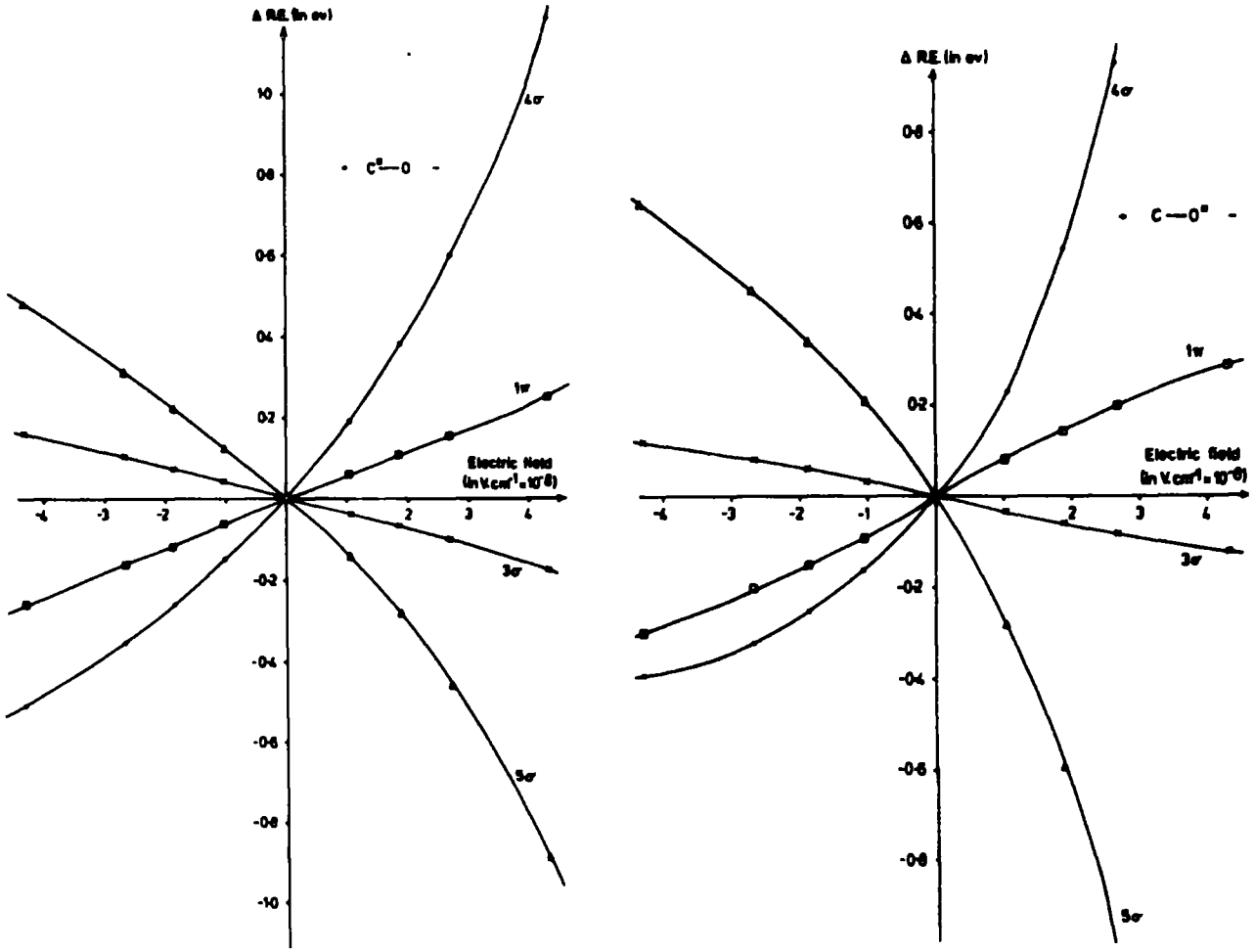

Fig. (6.16) Variation of single orbital relaxation energies in CO as a function of electric field.

somewhat lower field dependence. The situation with regard to the 4σ orbital (lone pair on oxygen) essentially mirrors the behaviour of the 5σ orbital. Thus, the relaxation energy contributions for both C_{1s} and O_{1s} hole-states increase as a function of applied field when the field is with carbon directed to the positive pole. In both cases, however, the field dependence is slightly stronger than for the 5σ orbital, such that the overall contribution from the sum of these two components leads to a small increase in relaxation energy. The field dependence for the 4σ orbital is again somewhat greater for the O_{1s} hole-state. For the reverse polarity, the overall contributions to

the relaxation energies for the 4σ orbital become smaller.

The 1π orbitals, although contributing in absolute terms a substantial proportion of the overall relaxation energies, show much less field dependence than the 5σ and 4σ orbitals. The contributions from the degenerate 1π orbitals, however, more than compensate for the relatively small field dependence of opposite sign exhibited by the 3σ orbital, and since the contributions of opposite sign from the 5σ and 4σ orbitals are closely similar, the variation of the total relaxation energy as a function of field for both the C_{1s} and O_{1s} hole-states may be regarded as being largely provided by the contributions from the 1π orbitals. Indeed, for the O_{1s} core-hole, the change in total relaxation energy closely follows the field dependence for the 1π orbital, since the 5σ and 4σ follow similar but opposite field dependencies, and the contribution from the 3σ orbital is compensated completely by that from one of the degenerate 1π orbitals. The greater field dependence of the total relaxation energy for the C_{1s} hole as compared to the 1π contribution largely arises from the small but significant differences in field dependence for the 5σ and 4σ orbitals, that for the latter being the larger. The clear implication of this work (that orbital contributions to relaxation energies depend markedly on localization and bonding characteristics and that such contributions exhibit significant field dependence) suggests that the experimental study of appropriate model systems should be eminently worthwhile. Thus, changes in relaxation energy will be reflected in changes in binding energy. It may therefore be envisaged that the field dependence of binding energies could reveal information regarding the interaction between a simple molecule and an appropriate surface. For example,

for CO chemisorbed on a metal surface, the orbital contribution to the relaxation energy provided by the 5σ, 4σ and 1π orbitals might be expected to be substantially modified, depending on the bonding mode (viz., terminal with either oxygen up or carbon up; or bridging (doubly or triply); or π-bonded). Since the field dependence of each of the contributions is distinctive, the study of absolute binding energies as a function of field could provide an additional information level as regards the mode of bonding. This particular aspect clearly deserves more detailed consideration and preliminary investigations of appropriate model systems will be detailed in a later chapter.

c) Mulliken population analysis and density difference contours

Changes in Mulliken population analysis and density difference contours as monitors of changes in electron distribution consequent upon core-ionization in CO have been discussed in the previous section. The discussion presented here, therefore, concentrates on the influence of an applied electric field. The polarization of the ground-state electron distribution in the field strength range covered in these investigations is considerable.

The changes in gross atomic populations on the core-ionized atom as a function of applied field are shown in Figure 6.17 for the C_{1s} and O_{1s} hole-states and follow remarkably similar trends to the relaxation energy components illustrated in Figure 6.16. This provides strong evidence that the single largest contribution to the relaxation energy originates in the change in electron density in the immediate vicinity of the atom on which the core-hole is located.

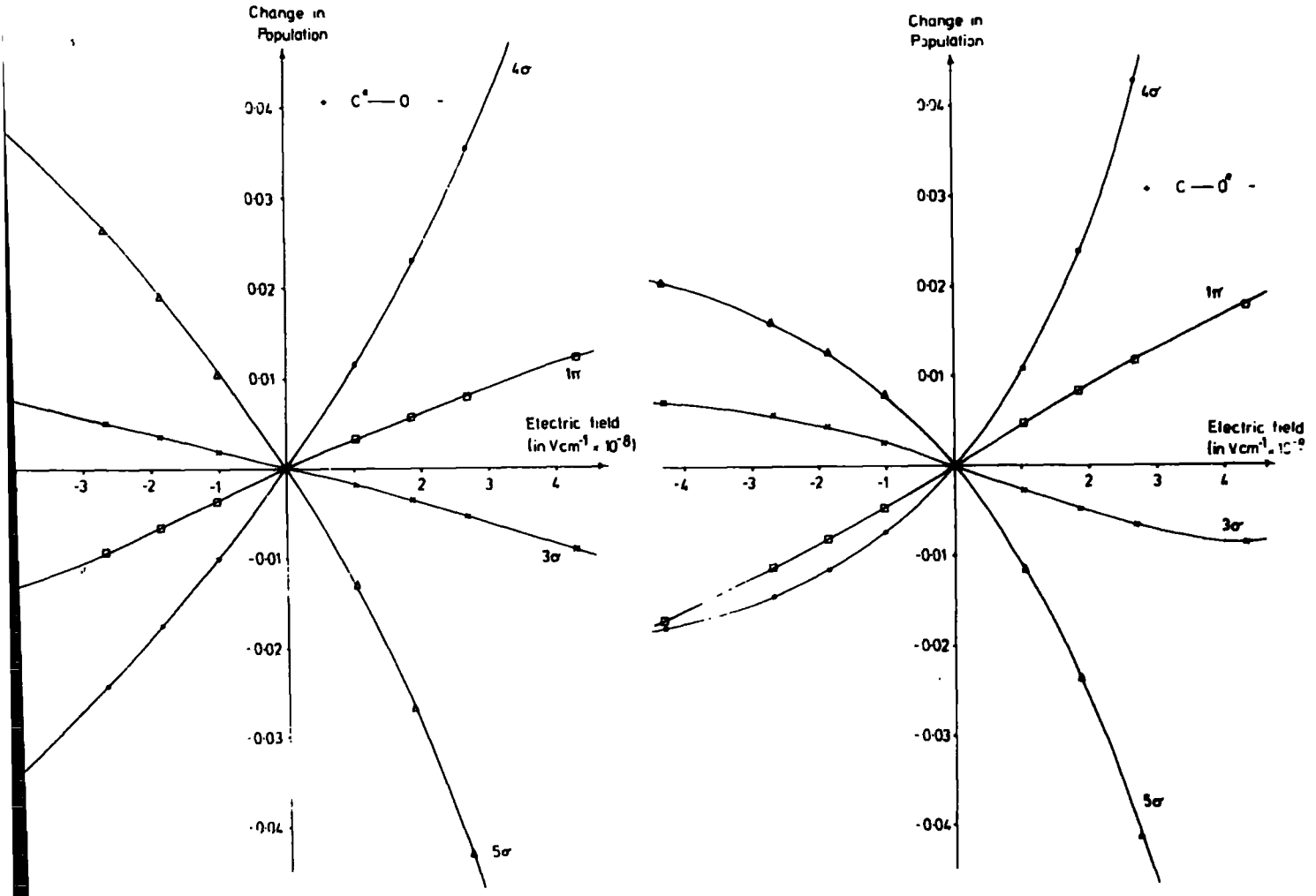

Fig.(6.17) Change in Mulliken gross atomic population of the core-hole atom in CO as a function of applied field.

Density difference contours for both the neutral molecule and core-ionized states in the presence or absence of a field have been computed. The total density difference contours for the ground-state molecule with an applied field in the sense with carbon at the positive pole reveal an overall increase in electron density in the non-bonding (lone pair) region of the carbon and also in the diffuse internuclear region. These increases in electron density are compensated by an overall electron drift from the non-bonding region around oxygen and from the internuclear region close to the molecular axis.

The individual orbital density difference contours displayed in Figure 6.18 illustrate the change in electron density caused by the application of an electric field. In this and

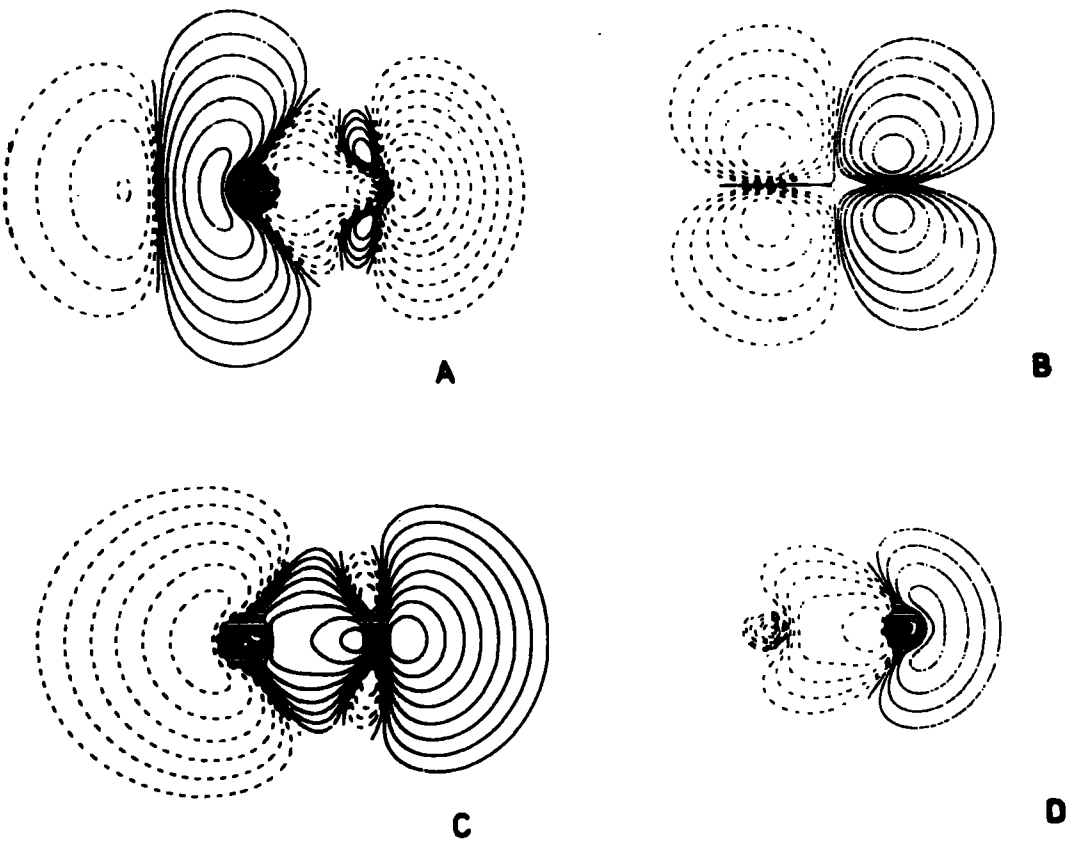

Fig.(6.18) Change in electron density on the application of an electric field.

subsequent contour plots, the orientation of the molecule is + C-O -; A, B, C, D refer to the 5σ, 1π, 4σ and 3σ orbitals, respectively. In this figure, dashed lines indicate an increase in electron density on application of an electric field.

For the 5σ (carbon lone pair) orbital, the applied field (4.31×10^8 V cm^{-1}, carbon at the positive pole), leads to an increase in electron density in the non-bonding region, whilst for the 1π orbitals there is a relatively straightforward transfer of electron density from one end of the molecule to the

other. For both the 3σ and 4σ orbitals, the polarization is such as to increase the electron density in the non-bonding region associated with carbon; however, the fine detail of this overall transfer of electron density is subtlely different for the two orbitals.

In studying the core-ionized species, it is revealing to investigate the changes in density difference in going from the ground-state to core hole state as a function of applied field. Such difference of density difference plots are shown in Figures 6.19 and 6.20 for the C_{1s} and O_{1s} hole states respectively.

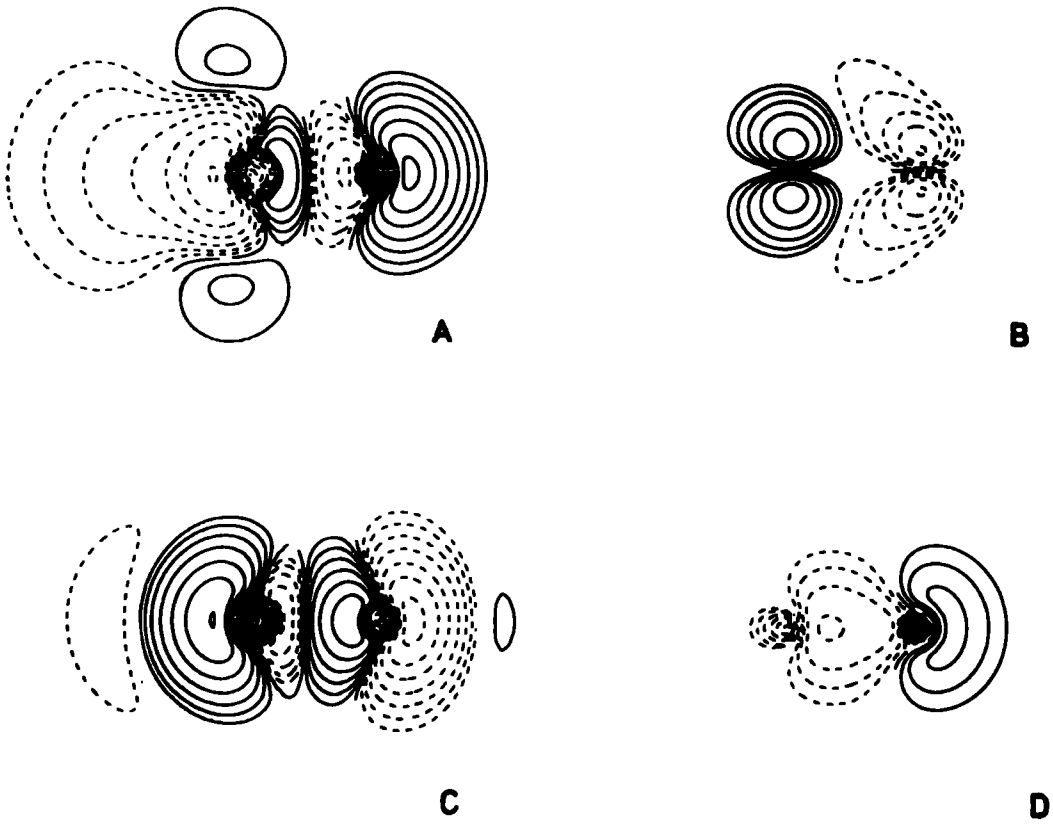

Fig.(6.19) The effect of the application of an electric field on the electron density changes subsequent on C_{1s} core-ionization in CO.

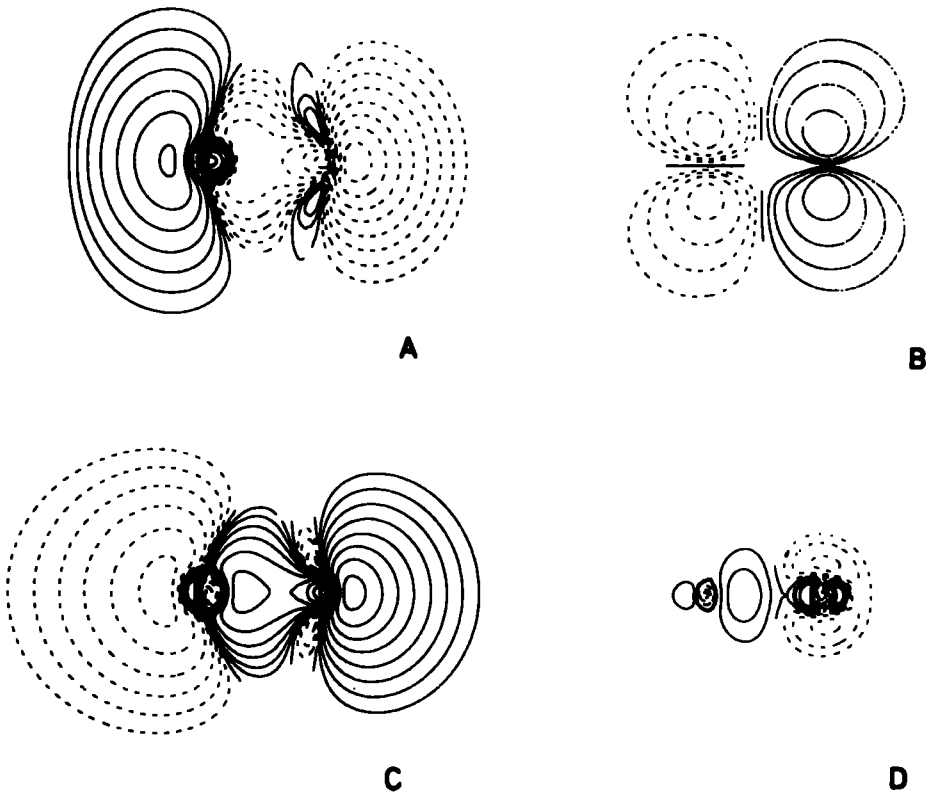

Fig. (6.20) The effect of the application of an electric field on the electron density changes subsequent on O_{1s} core-ionization in CO.

In these two figures, solid lines indicate an increase in electron density on the application of an electric field, since these are now differences of density difference contours, i.e. :

(Ground state - core hole state) - (Ground state - core hole state)
no field field

The data displayed in Figure 6.16 may be rationalized in qualitative terms on the basis of such difference contours. For the C_{1s} hole-state, for example, in the presence of the field the density on carbon increases in the immediate vicinity of the carbon atom for the 1π and for the 4σ orbitals, and decreases for the 5σ and 3σ orbitals, the relaxation energy for the former therefore increasing and the latter decreasing with applied field.

For the O_{1s} hole-state, the behaviour is somewhat analogous; for the 5σ orbital, the density around oxygen decreases in the field, and this is also the case for the 3σ orbital. For both the 1π and 4σ orbitals, which exhibit an increase in relaxation energy in the presence of the applied field, however, there is an increase in density.

d) Vibrational fine-structure accompanying core-ionization as a function of applied field

The changes in equilibrium bond-lengths and in force constants accompanying core-ionization in carbon monoxide have been computed previously.[170] Comparison of theoretically computed and experimentally determined band-profiles for the C_{1s} and O_{1s} levels provides virtually quantitative agreement. The substantial electronic reorganizations accompanying core-ionization of the C_{1s} and O_{1s} levels are manifest in a decrease and increase, respectively, in equilibrium bond-lengths, in going from the neutral molecule to core-ionized species. In the particular case of the C_{1s} core hole state, the decrease in bond-length is accompanied by an increase in force constant , whilst for the O_{1s} core-hole state, the increase in bond-length is accompanied by a decrease in force constant.

The strong field dependence of relaxation energy phenomena suggests that the potential surfaces for both ground and core hole state species may well be modified by application of a strong electric field. In this section, changes in equilibrium bond-lengths and force constants for the ground-state and core hole state species as a function of applied field are considered. Attention has been restricted to a field of 4.31×10^8 V cm^{-1},

with carbon at the positive pole. The computer-intensive nature of such investigations precludes a more extended study over a range of field strengths and molecular orientations.

Comparison is drawn with both the previous theoretical work and available experimental data in Table 6.8. The computed changes in bond-length in going from the neutral molecule to core-ionized species are very similar to those reported previously[170] for a Slater Double Zeta basis set. The force constants are somewhat comparable with those reported for the Triple Zeta basis set, the main difference being that for the C_{1s} core-ionized state, the basis set used in this work suggests a closer comparison with the force constant for the equivalent cores species (NO^+) than is evident from the Triple Zeta calculations. However, the theoretically calculated band-profiles based on the computed Franck-Condon factors are in excellent agreement with the available experimental data for both basis sets. The corresponding data for the molecule and core-ionized species in a field gradient of 4.31×10^8 V/cm. (carbon directed to positive pole) are also shown in Table 6.8.

The application of such a large field has a relatively minor effect on the equilibrium bond-length and force constant of the ground-state molecule; the equilibrium bond-length is calculated to decrease by $\sim$ 0.3% whilst the force constant decreases by $\sim$ 0.4%. However, the substantial changes in valence-electron reorganization accompanying core-ionization previously evidenced by the density difference contours lead to significant changes in equilibrium bond-lengths and force constants in the presence of the field. For the C_{1s} hole-state, the change in bond-length with respect to the system in the absence of an applied field is an increase of

TABLE 6.8 Geometries of CO, C*O, CO* Corresponding to Minimum Energies (in au) and Respective Force Constants (in millidynes per Ångstrom)

	Equilibrium Bond-Length			Force Constant			
	CO	C*O	CO*	CO	C*O	CO*	NO^+
Without field							
STO-6.33G + P	2.168	2.057	2.323	19.4	25.8	10.2	-
Double Zeta[a]	2.155	2.052	2.324	-	-	-	-
Triple Zeta[a]	2.123	2.010	2.230	19.5	28.9	13.1	28.9
Experimental	2.132[b]	-	-	19.0[c]	-	-	24.9[d]
With field							
STO-6.33G + P	2.161	2.063	2.238	19.3	25.3	13.7	

[a] Data taken from ref. 170.

[b] Ref. 214.

[c] Ref. 291.

[d] Ref. 296.

$\sim$ 0.3%, whilst the force constant decreases by $\sim$ 2%. For the O_{1s} hole-state, the changes are much more substantial. Whilst the computed change in equilibrium bond-length in going from the neutral molecule to core-ionized species is 0.155 au in the absence of a field, in the presence of the field the elongation is much smaller (0.077 au). The corresponding force constants also differ significantly, being 10.2 and 13.7 mdynes/Å respectively, compared with the computed force constant of 19.4 mdynes/Å for the neutral molecule in the absence of a field.

Since there is predicted to be a change in absolute binding energy as a result of applying the field, the overall changes in core-level spectra on applying a field are best appreciated in the form of difference spectra. The computed difference spectra for the C_{1s} and O_{1s} hole-states in CO are shown in Figure 6.21. The individual vibrational components are represented by

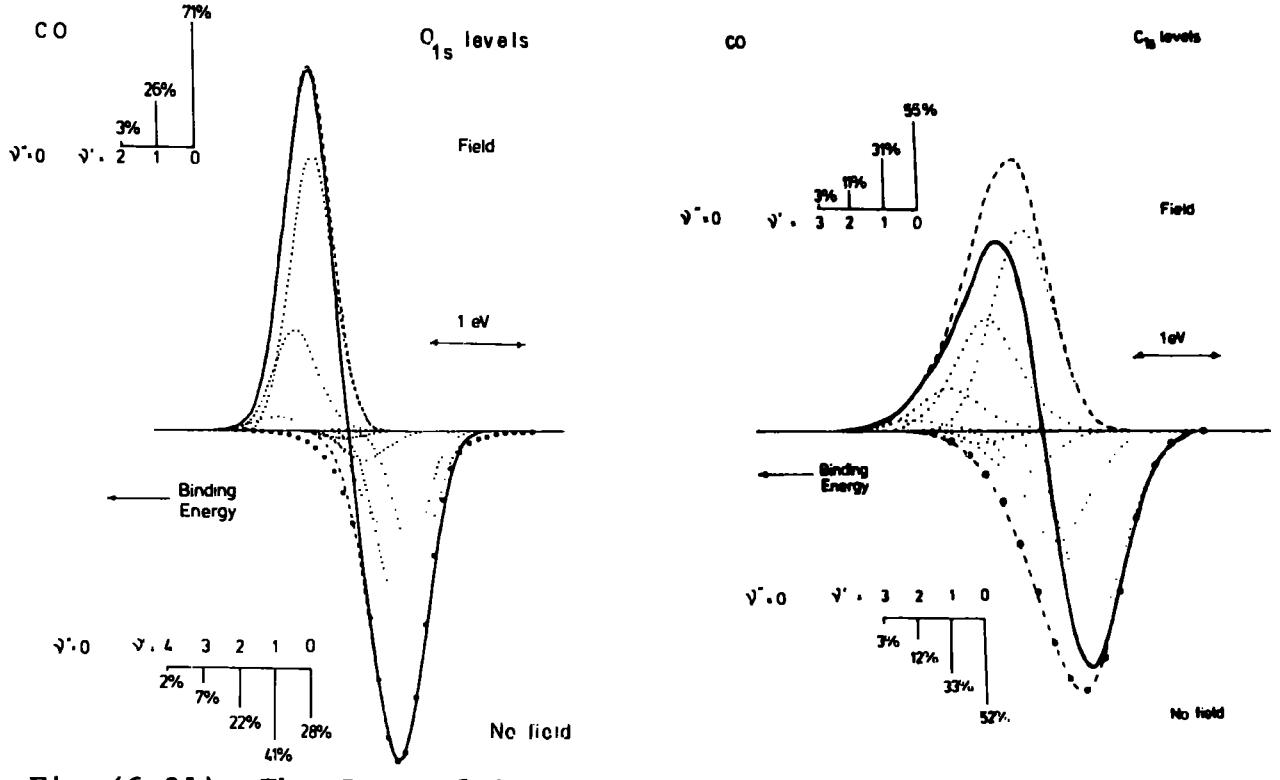

Fig. (6.21) The C_{1s} and O_{1s} spectra and computed Franck-Condon factors for CO in the presence and absence of an applied electric field.

the dotted lines (...) with the theoretical band-profiles shown as the dashed line (---). The solid line represents the difference spectrum (field minus no field). There is only a slight change in the overall band-profile on application of the field; however, the substantial change in binding energy leads to a characteristic profile for the difference spectrum. For comparison purposes, the experimental band-profile at the appropriate resolution is also included, shown as (• •), emphasizing that the basis set employed in this work provides an excellent description for the system in the absence of the field.

The analysis previously published[170] for the O_{1s} core hole state indicates that vibrational excitation accompanying core-ionization is manifest as an overall broadening of the spectrum, since the vibrational quanta are relatively small (0.22 eV). The change in Franck-Condon factors and shift in absolute binding energy on applying a field lead to a quite distinctive difference spectrum, as is evident from the data presented in Figure 6.21. From this, it may be projected that the effects of much weaker fields should be detectable.

6.5.4 Nitrogen Molecule

a) Relaxation energies as a function of applied field

One of the more interesting aspects of the previously presented theoretical studies on carbon monoxide was the prediction that the absolute binding and relaxation energies for the core-ionized species were dependent on the magnitude of an applied field. The field gradients required, however, to demonstrate this phenomenon are considerable ($\sim 10^7$ V cm^{-1}). The field dependence of absolute binding energies depend quite markedly on

relaxation energies and hence on the individual components which contribute to the total. In this section, the effect of an applied field on both binding and relaxation energies for the nitrogen molecule is considered.

Whilst in the RHF formalism, the description of the nitrogen core hole states is in terms of degenerate localized holes, the application of a field removes the degeneracy. From the results displayed in Figure 6.22, it is clear that the application of a very large field results in a substantial shift in

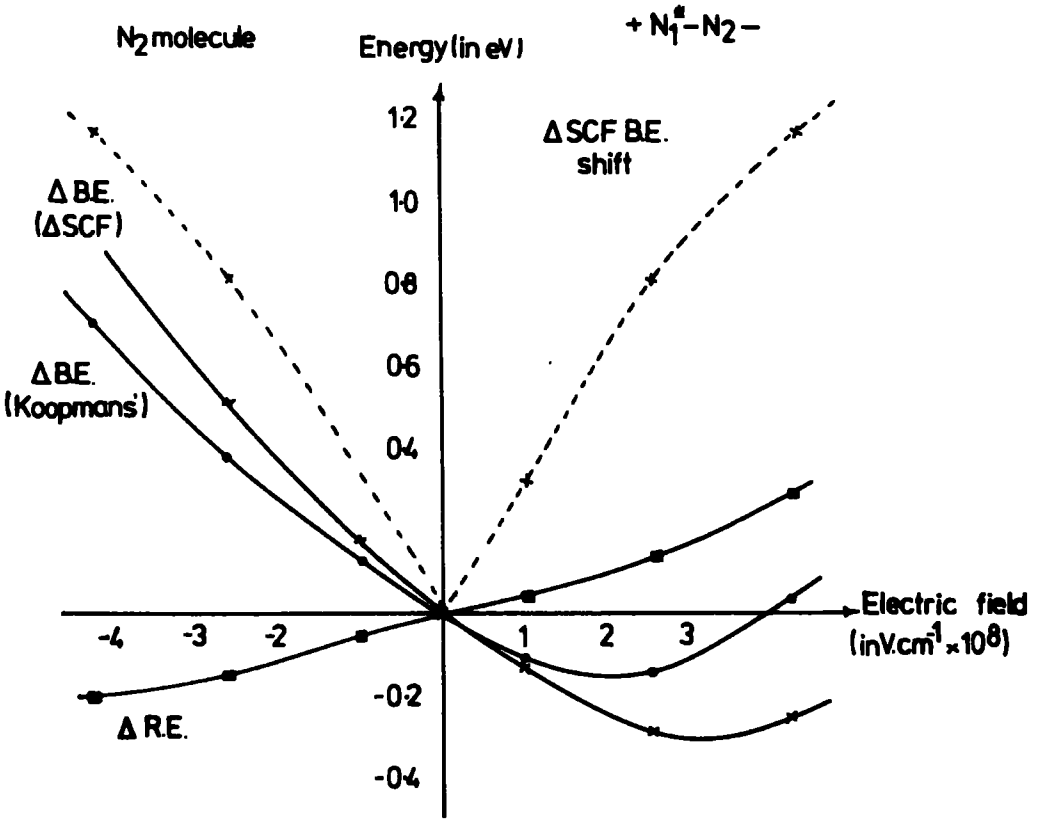

Fig. (6.22) Variation of ΔSCF and Koopmans' BE, and RE in N_2 as a function of electric field.

binding energy between the now inequivalent N_{1s} core-levels; for a field of $\sim 10^8$ V cm^{-1}, the shift between the component peaks, shown by the dashed line (---), is computed to be 0.35 eV, whilst the centroid of the peaks shifts by an insignificant amount

(∿ 0.02 eV) with respect to the molecule in the absence of an applied field. In the absence of relaxation effects, the computed shift between the nitrogens is somewhat smaller (∿ 0.2 eV).

If the field is applied in such a sense that the nitrogen bearing the core-hole is directed towards the positive pole, the computed shift in binding energy with respect to zero field is negative. Thus, for a field of ∿ 4 x 10^8 V cm^{-1}, the computed shift of ∿ -0.25 eV may be compared with that from Koopmans' Theorem of essentially zero. This illustrates the considerable influence of relaxation effects. A similar situation has previously been described for the O_{1s} hole-state of CO. For the reverse polarity, the binding energy of the N_{1s} levels increases as a function of increased field. Thus for the largest applied field, the Koopmans' shift of ∿ 0.7 eV may be compared with that computed including relaxation effects of ∿ 0.9 eV.

The variation of the individual component contributions to the relaxation energies as a function of applied field is illustrated in Figure 6.23. The main feature which emerges is the fact that the contributions from the 1π and 3σ orbitals are not strongly field dependent, whilst the contributions from the 5σ and 4σ orbitals vary in such a manner that the total relaxation energy changes only slightly as a function of applied field. There are some similarities in the computed behaviour of the relaxation energy components for the 4σ and 5σ orbitals with those previously described for carbon monoxide.

For the 4σ orbital, the relaxation energy contribution decreases as a function of the applied field, if this is in a sense such that the nitrogen on which the core-hole is created

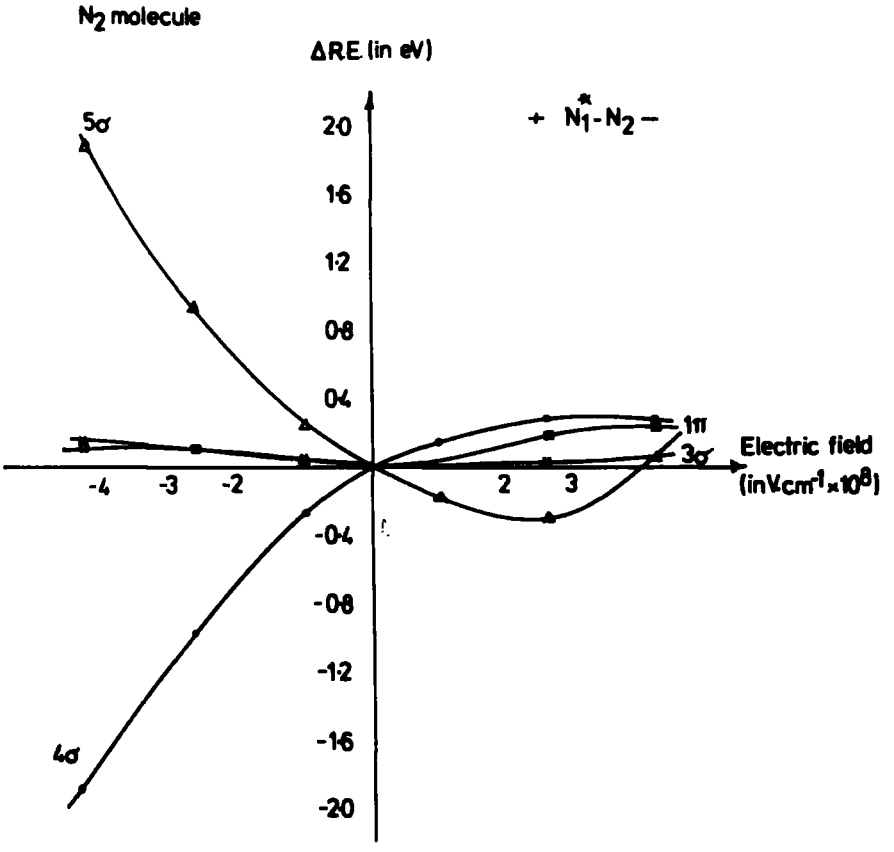

Fig. (6.23) Variation of single orbital relaxation energies in N_2 as a function of electric field.

is directed to the negative pole. The calculations would seem to indicate that for the largest applied field, the contribution from this orbital is some 50% of that appropriate to the system in the absence of a field. For the applied field in the opposite sense, there is a small increase in relaxation energy. The behaviour of the 5σ orbital contribution is almost the mirror image of that for the 4σ; for a large field applied in a sense such that the nitrogen bearing the core-hole is directed towards the negative pole, there is a large computed increase in the relaxation energy. For a field strength of -4×10^8 V cm^{-1}, the increase in contribution is $\sim$ 1.7 eV. This is entirely consistent with the data previously presented for CO. The internal

field at carbon provided by the overall negative charge on oxygen is somewhat analogous to the situation for nitrogen, and the relaxation energy contribution for the 5σ orbital in the particular case of the C_{1s} hole-state is substantial and positive (3.5 eV). For the field in the opposite sense, the relaxation energy contribution for the relevant nitrogen hole-state decreases, and at a field of $\sim 2.5 \times 10^{8}$ V cm^{-1} is essentially zero. This is analogous to the situation arising for the O_{1s} hole-state of CO, where the contribution provided by the 5σ orbitals is actually small and negative (-0.5 eV).

b) Vibrational fine-structure accompanying core-ionization as a function of applied field

The application of large electric field gradients, as well as suggesting a substantial shift in binding energy between the inequivalent nitrogens, also leads to significant computed changes in potential energy surfaces. Table 6.9 shows the computed bond-lengths and force constants for the core-ionized species, both including and in the absence of relaxation effects, in the presence of an applied field. The results obtained with this basis set in the absence of an applied field have been previously discussed (Table 6.7), and are found to agree favourably with the results of Triple Zeta calculations. The calculations here reveal significant changes in both equilibrium bond-lengths and force constants in the presence of a field; the data in Table 6.9 and Figure 6.22 may be used to compute overall band-profiles and a difference spectrum for core-ionized N_2 in the absence and presence of an electric field, as shown in Figure 6.24. The dashed line shows the theoretically calculated band-profiles;

TABLE 6.9 Equilibrium bond-lengths and force constants for N_2 in the presence of an applied field

Nitrogen, N_2	Equilibrium bond-length (au)	Force constant (mdynes/Å)
Applied field (2.68×10^8 V cm^{-1})		
Ground State	2.108	22.26
Hole State		
+ N^*_1-N_2 -	2.110	19.76
+ N_1-N_2^* -	2.063	23.82
"Koopmans'"		
+ N_1^*-N_2 -	2.063	23.74
+ N_1-N_2^* -	2.030	29.35

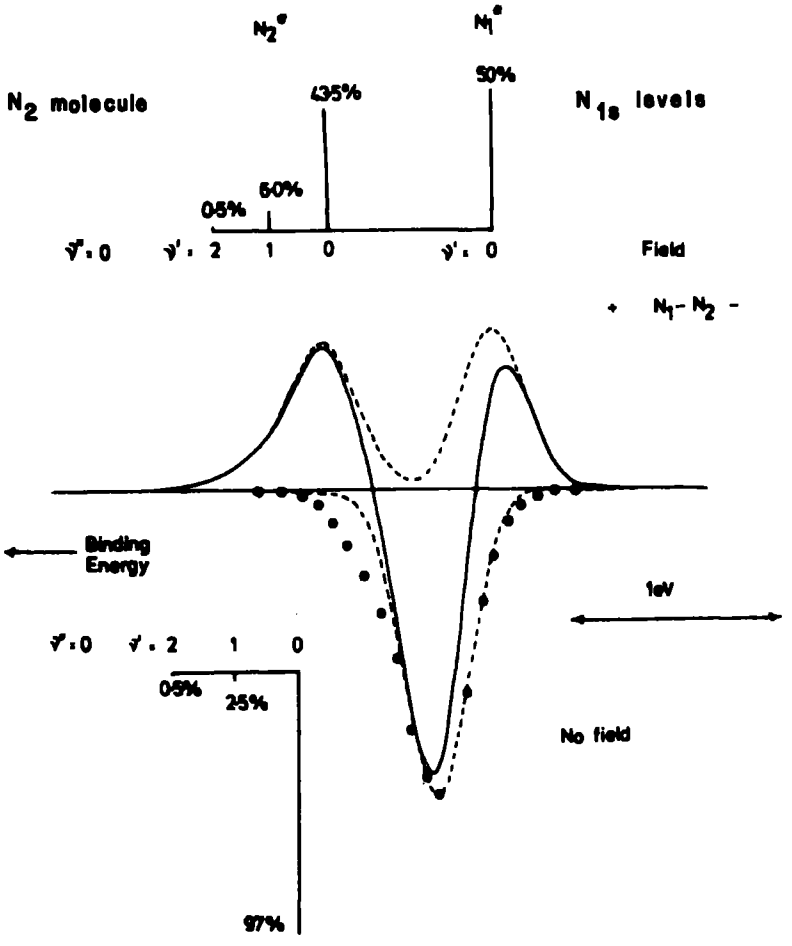

Fig.(6.24) The N_{1s} spectrum and computed Franck-Condon factors for N_2 in the presence and absence of an applied field.

the dotted spectrum is the experimental band-profile; and the solid line represents the calculated difference spectrum.

The difference spectrum is particularaly striking, and suggests that the effect of applying a field might be detectable at more realistic field strengths (i.e., below the field ionization limit). Although the computed band-profile for the system in the absence of a field underestimates the extent of vibrational excitation, it is clear that the two components of the N_{1s} levels for the applied field case differ significantly in FWHM, since the extent of vibrational excitation is different for the inequivalent nitrogens.

The analysis of relaxation energies into components associated with the reorganization of individual orbitals seems to provide some insight into the dependence on electronic structure of the reorganization process. Correlations between related systems may be drawn. The theoretical investigation of the changes in binding and relaxation energies consequent upon applying a strong electric field suggests that appropriate modulation experiments might be worthwhile to provide experimental data for direct comparison with the interesting predictions which have been made. It is not inconceivable that the strong electric fields present at surfaces in appropriate chemisorbed systems could lead to line broadening in a way suggested by the work reported here.

CHAPTER SEVEN

SINGLE ORBITAL RELAXATION ENERGIES ACCOMPANYING CORE-IONIZATION IN SOME POLYATOMIC SYSTEMS

Changes in binding and relaxation energies accompanying core-ionizations are computed within the ΔSCF Hartree-Fock formalism for CO at the equilibrium geometry; CO at the geometries appropriate to COH^+ and HCO^+; COH^+; HCO^+ (linear); HCO^+ (bent); HCO^+ (bent) with geometry appropriate to H_2CO; and H_2CO. Variations in relaxation energies along this series are discussed in terms of the individual valence-orbital contributions to the total relaxation energies. It is found that such an analysis can provide considerable insight into the relationship between electronic structure and electronic reorganizations accompanying core-ionization. Certain aspects of the energetics (protonation and hydrogenation) involved in these systems are also considered.

The two pairs of isomeric molecules HCN, HNC and HNO, HON have also been investigated within the Hartree-Fock formalism for both ground and core-ionized states. Although varying only slightly in total computed energy, it is shown that substantial differences in the core hole state spectra are expected. An analysis of the electronic reorganization processes accompanying core-ionization in these species is given in terms of the single orbital contributions to the total relaxation energies.

Finally, single orbital contributions to the total relaxation energy accompanying core-ionization are computed within the ΔSCF formalism for the isoelectronic series CH_4, NH_3, H_2O, HF and Ne. Individual contributions to the total relaxation energy associated

with the valence-levels of essentially core-like 2s character are also presented.

7.1 Orbital Contributions to Relaxation Energies Accompanying Core-Ionization in the Series CO, COH^+, HCO^+ and H_2CO

7.1.1 Introduction

Carbon monoxide and nitrogen as simple prototype systems have been studied in the previous Chapter. The anisotropic nature of the relaxation phenomena accompanying core-ionizations in these systems suggests that knowledge of the detailed dependence of orbital relaxation energies on bonding characteristics may be extended by relating changes in relaxation energy in the carbon monoxide system, via the intermediacy of the relevant protonated species, to the formaldehyde system. Further, the linear HCO^+ and COH^+ systems provide prototypes for CO terminally bonded to a strong σ-acceptor, and as such might be expected to provide some insight into changes in relaxation energies accompanying coordination. In the particular case of HCO^+, it might be anticipated that orbital contributions to relaxation energies would be strongly dependent on the $\hat{HCO}$ angle, and in the light of the previous investigation of the bond-length dependence, significant variations might be expected as a function of change in bond-lengths for a given $\hat{HCO}$ angle. The investigation of CO, HCO^+, H_2CO, at the appropriate geometries furthermore allows a Born cycle to be constructed.

In this section, therefore, changes in relaxation energy on going from CO at the equilibrium geometry, to the geometries appropriate to the CO fragment in HCO^+ and COH^+, and the changes consequent upon protonation of CO to produce these species are considered. Distortion of HCO^+ to the geometry appropriate to that for production of H_2CO by addition of H^- has also been

investigated from the standpoint of orbital relaxation energies and provides a direct correlation between CO and H_2CO.

7.1.2 Computational Details

Non-empirical LCAO MO SCF calculations were performed within the Hartree-Fock formalism for the ground and O_{1s} and C_{1s} core-ionized species of the title compounds. The basis set employed has been described previously, but may be termed STO-6.33G, with 3d polarization functions for oxygen and carbon, and 2p for hydrogen. Optimized geometries for HCO^+ and COH^+,[297] and an experimental geometry for H_2CO[214] were used. Calculations for CO with geometries appropriate to that in COH^+ and HCO^+ were also performed, as were calculations for HCO^+ with the $\hat{HCO}$ angle and C-H and C-O bond-distances appropriate to H_2CO. The methodology of obtaining single orbital contributions to the total relaxation energy has been documented in the previous Chapter. Density difference contour plots for the molecular plane have also been calculated for this series of molecules, using the same area and contours throughout.

7.1.3 Results and Discussion

a) Energetics of the Born cycle

The calculated total energies allow a relatively complete investigation of the relevant proton and hydride affinities, and heat of hydrogenation, as shown in Figure 7.1. Detailed theoretical investigations of the electronic structures of HCO^+ and COH^+ have previously been described by Bruna, Peyerimhoff and Buenker, including geometry optimizations.[297] The theoretically computed optimized bond-length for CO with the basis set employed in this

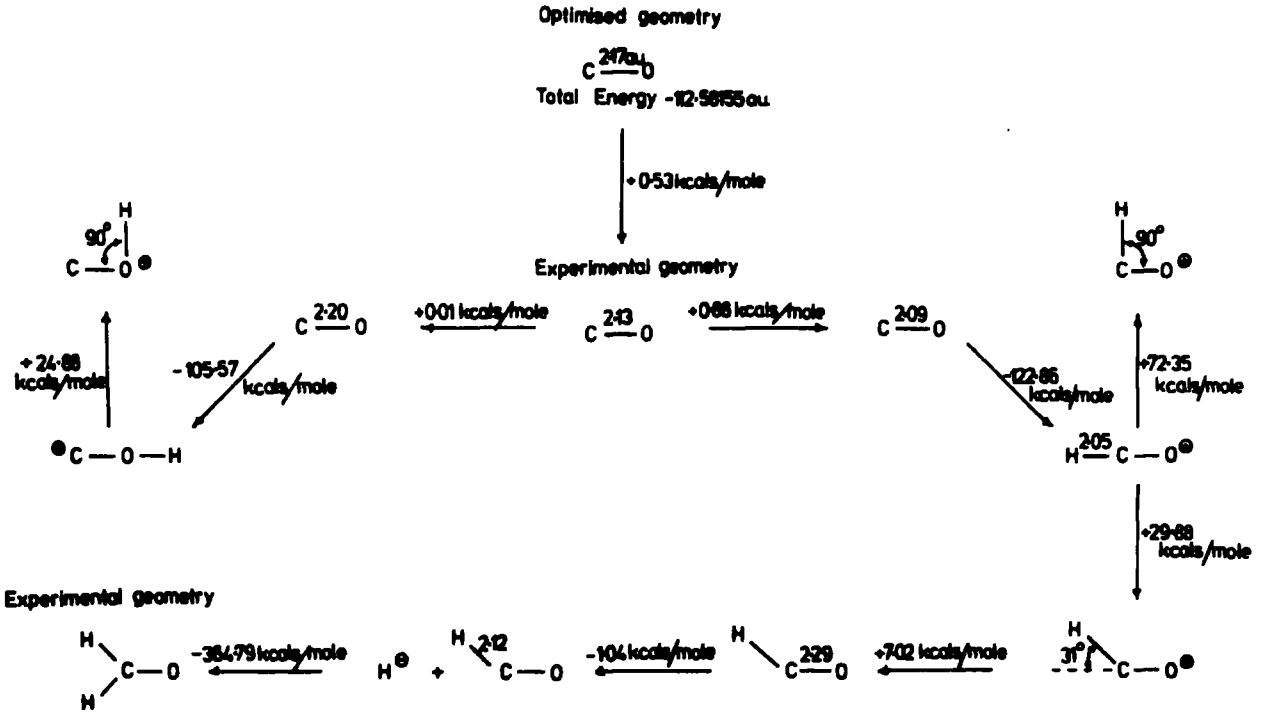

Fig.(7.1) The energetics of protonation of CO

work is some 2% longer than that experimentally determined; for the protonated species, the optimized bond-lengths are ∿ 3% longer and 2% shorter than for CO for the species protonated on carbon and oxygen, respectively. The energies required to elongate or compress the C-O bond-length from that appropriate to the equilibrium for the neutral molecule are small. The proton affinity is considerably higher for protonation on carbon, the energy difference with respect to protonation on oxygen being 16.2 kcal mol^{-1}, with this basis set. This compares with a computed difference of 18.4 kcal mol^{-1} from the work of Bruna and co-workers.[297] The experimentally determined proton affinity of CO (-137 kcal mol^{-1} [298]) is somewhat larger than that calculated with the basis set employed in this work (-121.5 kcal mol^{-1}).

Previous studies[297] have shown that the equilibrium geometry for HCO^+ corresponds to a linear system. The distortion to the bent conformation appropriate in $\hat{HCO}$ angle to that in formaldehyde

is energetically expensive ($\sim$ 30 kcal mol^{-1}) and the considerable increase in C-O bond-length in going to formaldehyde is such that this requires a further 7 kcal mol^{-1}. Lengthening the C-H bond-length to that appropriate to H_2CO, however, leads to a smaller lowering in energy. The computed hydride affinity of HCO^+, with geometry corresponding to that in formaldehyde, of -364.8 kcal mol^{-1} may be compared with that for the equilibrium geometry of HCO^+ (linear) of -328.0 kcal mol^{-1}. It is of interest to investigate the difference in proton affinities for protonation on carbon and oxygen for the π as opposed to the σ system. The calculation on the bent conformation for HCO^+ would suggest that protonation of the π system on carbon would be energetically very unfavourable; by contrast, it might be anticipated that π protonation would be relatively more favourable for oxygen. The computed differences in proton affinities for σ and π protonation of carbon and oxygen confirm this, being 72.4 kcal mol^{-1} and 24.9 kcal mol^{-1} respectively.

The calculations also allow a comparison to be made between the experimentally determined and directly computed heat of hydrogenation of carbon monoxide. The agreement is quite reasonable, as might have been anticipated for an isodesmic process: experimental -1.3 kcal mol^{-1}; theoretical -11.3 kcal mol^{-1}.

b) Core binding energies

The computed ΔSCF binding and relaxation energies (shown in brackets) for C_{1s} and O_{1s} core-ionization of CO are 299.6 eV (10.79 eV) and 543.7 eV (19.91 eV) respectively. With this basis set, therefore, the absolute binding energies are slightly over-estimated, the corresponding experimental values being 296.2 eV and 542.6 eV. As has been previously noted however, relative binding

energies and changes in relaxation energies are well described, and the basis set is therefore particularly suited to the discussion of changes in the orbital contributions to relaxation energies and shifts in binding energies, which are the features of predominant interest in this Chapter. The relevant correlation diagrams for the core binding energies are displayed in Figure 7.2.

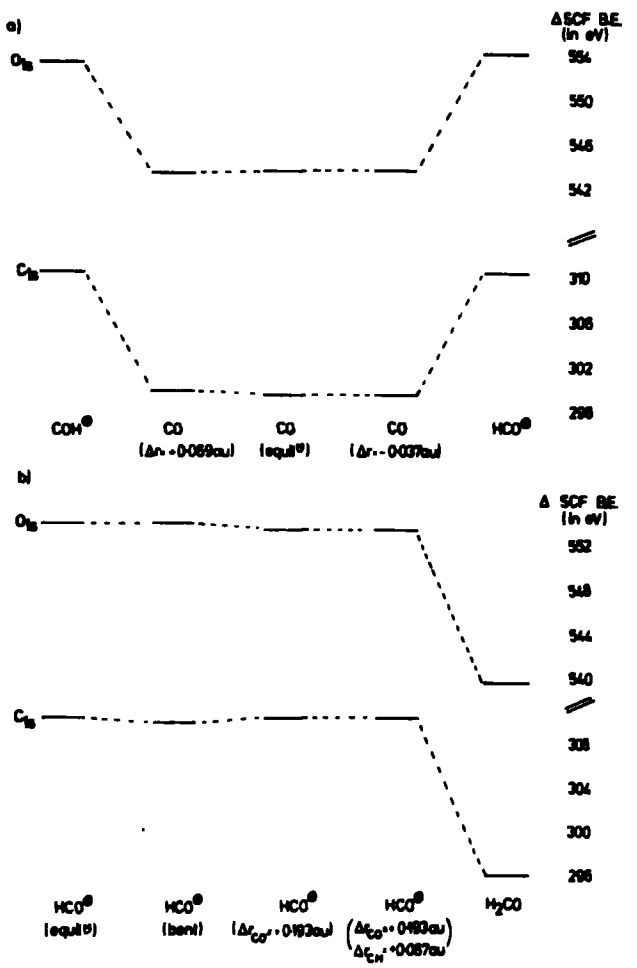

Fig.(7.2) ΔSCF B.E. for a) COH^+, CO, HCO^+ and b) HCO^+ (linear) HCO^+ (bent), H_2CO.

Considering the protonated species, there is a substantial shift to higher binding energy for both the O_{1s} and C_{1s} levels for protonation on either carbon or oxygen. The shifts for both the C_{1s} and O_{1s} levels are computed to be closely similar ($\sim$ 10.8 eV and 10.0 eV, respectively). Also included in Figure 7.2(a) are the

core binding energies for CO at the bond-length appropriate to the protonated species. It has been shown that binding and relaxation energies depend significantly on bond-length, but in a subtle rather than a gross manner. There are similarities that can be noted in the redistribution of valence-electron density consequent upon core-ionization, and protonation of a molecule. For example, the equilibrium bond-length for the C_{1s} hole-state of CO is substantially shorter than for the neutral molecule. Creation of electron demand at carbon by protonation produces a similar change in equilibrium C-O bond-length compared with the neutral molecule. The comparison is reinforced by inspection of appropriate density difference contours. In Figure 7.3, for example, the valence-electron redistribution on C_{1s} and O_{1s} core-ionization in CO is compared with protonation at

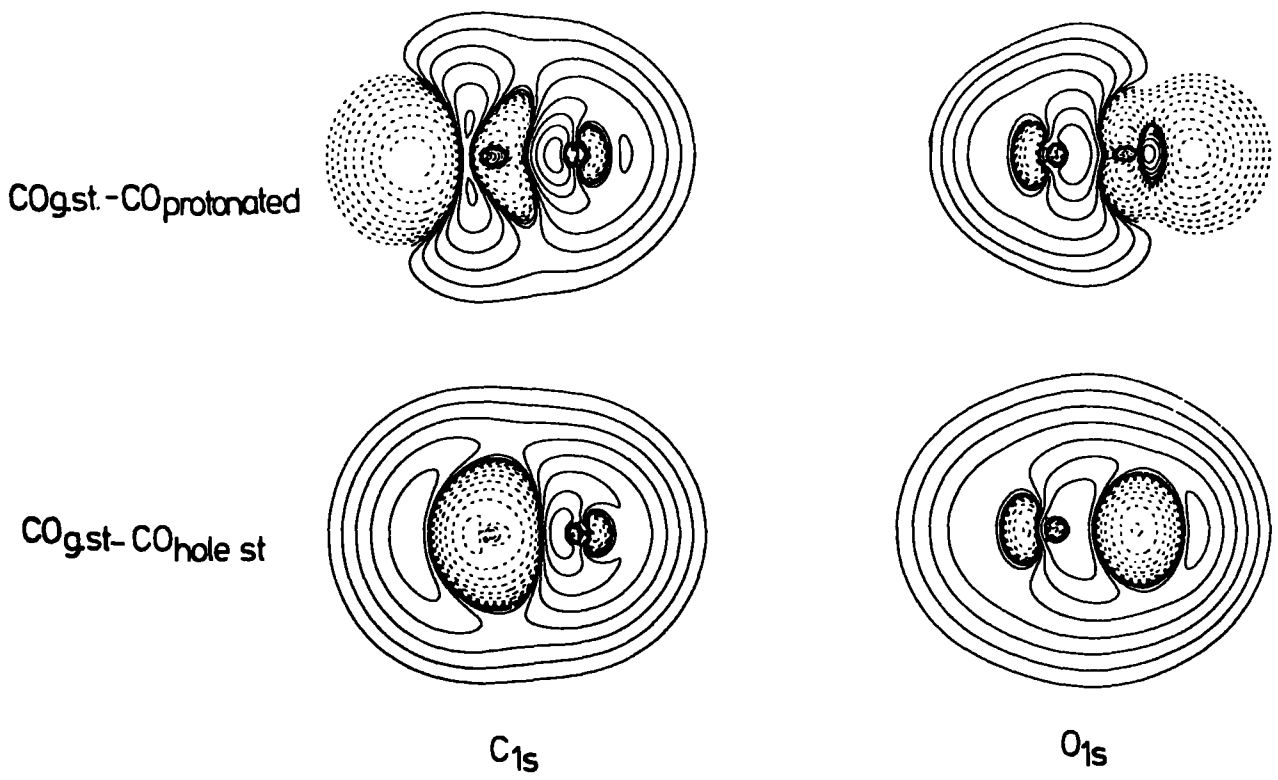

Fig.(7.3) A comparison of changes in valence-electron distribution subsequent on core-ionization, and protonation in CO.

carbon and oxygen to give HCO^+ and COH^+ respectively. When a

core-hole is created on carbon, the change in valence-electron distribution around the oxygen is very similar to the change caused by protonation at carbon; the converse situation for core-ionization at oxygen is also seen. Furthermore, the O_{1s} core-ionized species has a substantially larger equilibrium bond-length, and a comparable situation arises for the oxygen protonated species. The features in common between creation of a core-hole on an atom and protonation of that atom have been developed into a direct relationship between proton affinities and shifts in core binding energies by Shirley.[299]

It is evident from Figure 7.2 that for HCO^+, the C_{1s} binding energy is not a strong function of the $\hat{HCO}$ bond-angle; relaxation energies are also found to be fairly constant. However, individual orbital contributions to relaxation energies are strongly influenced by the molecular geometry. The addition of H^- to HCO^+ to give formaldehyde produces a substantial shift to lower binding energy for both the O_{1s} and C_{1s} core-ionized species.

It is clear from this data that coordination of CO to a strong σ-electron acceptor such as a proton results in a large shift to higher binding energy, which is approximately the same for protonation on either carbon or oxygen. It is of interest to briefly compare the computed shifts for the C_{1s} and O_{1s} levels for HCO^+ with those derived from calculations on CH_3CO^+, where the possibility exists of both σ and π interactions. The computed shifts are some 2 eV to lower binding energy than for the protonated species, as might be anticipated from the synergic effect of σ-donation from CO to CH_3^+ and back-donation via the π system. The shift (with respect to CO) for the C_{1s} levels is however significantly higher than for the O_{1s} levels; this difference is roughly constant

for both of the species studied (HCO^+ and CH_3CO^+). The difference ($\sim$ 0.8 eV) is also that typically measured for transition metal carbonyls in comparison with the free ligand.[300]

c) Relaxation energies

The main purpose of this Chapter is to extend the proposed method of analysis of total relaxation energies into components associated with individual valence-orbital contributions. The points of emphasis therefore are:

(i) how are the component relaxation energy terms changed upon coordination of CO to a strong σ-acceptor (H^+)?

(ii) what changes occur consequent upon the σ-π mixing introduced by altering the $\hat{HCO}$ angle?

(iii) how do the component terms for CO compare with those for H_2CO, which might crudely be taken as a model for a bridge bonded carbonyl?

The results for the series CO, HCO^+ and COH^+ are displayed in Figure 7.4. The total relaxation energies fall within a narrow range; for the C_{1s} levels, the relaxation energies for COH^+, CO and HCO^+ are computed to be 10.3 eV, 10.8 eV and 11.2 eV respectively, whilst for the O_{1s} levels, the corresponding values are 19.9 eV, 19.9 eV and 20.0 eV respectively.

It is convenient to discuss the results for the C_{1s} and O_{1s} core-ionized states separately, where appropriate drawing comparisons between the two sets of data. It is clear, however, from an inspection of Figure 7.4 that there are considerable differences both in terms of sign and magnitude of the individual contributions for ionization of the C_{1s} and O_{1s} levels in the linear series CO, HCO^+, HOC^+. Bond overlap populations reveal that the O-H and C-H

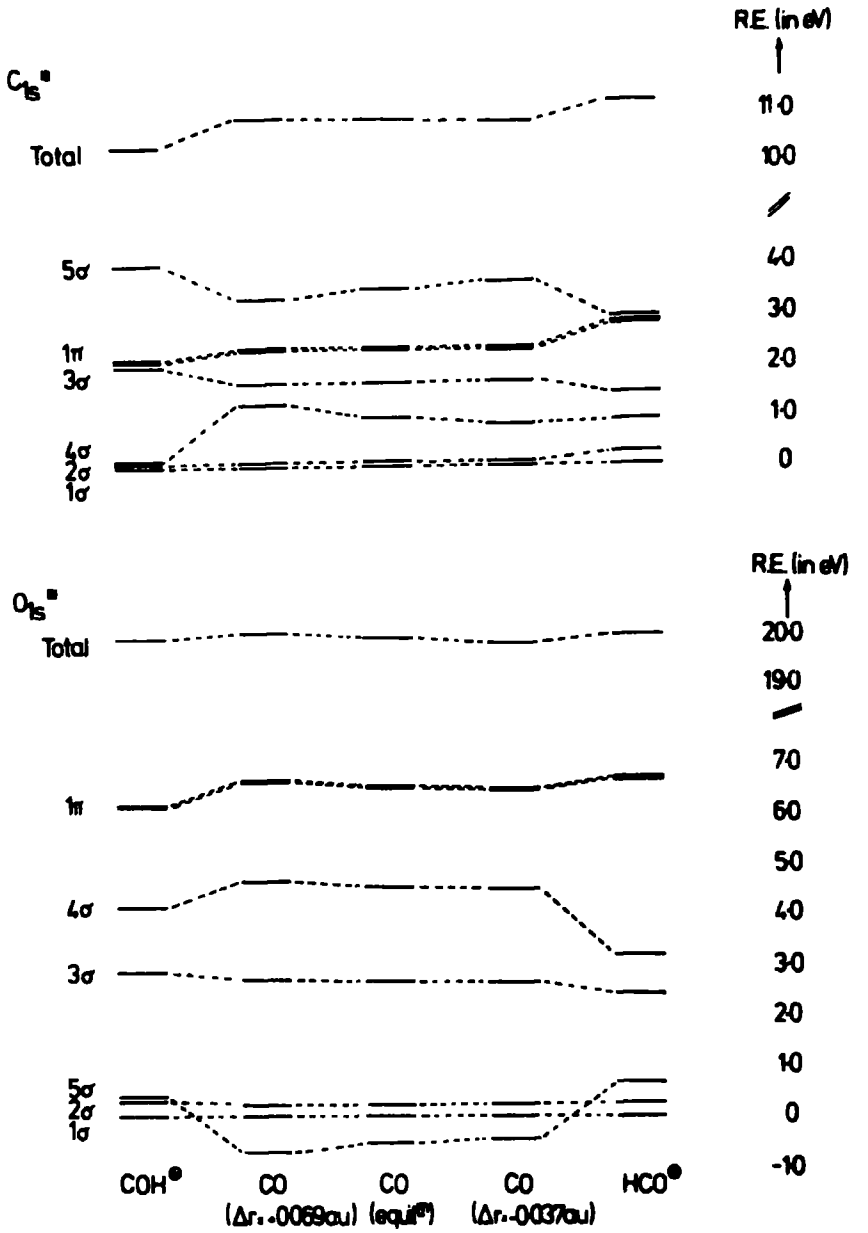

Fig.(7.4) Total R.E. and individual orbital contributions to the total R.E. for the series COH^+, CO and HCO^+, subsequent upon C_{1s} and O_{1s} core-ionization.

bonding interactions are largely associated with the 4σ orbital in COH^+ and HCO^+ respectively and there is, therefore, a tendency for the relaxation energy contributions from this orbital to be somewhat less for the protonated species compared with the neutral molecule.

It was shown in the previous Chapter that whereas for C_{1s} core-ionization, reorganization of the 5σ (carbon lone pair) orbital contributes a significant proportion of the total relaxation energy, the reorganization is such as to contribute a small negative term to the total relaxation energy for the O_{1s} core-ionized species in CO. This situation is considerably modified on going to the protonated species. For the C_{1s} core-ionized species, the protonation on either carbon or oxygen shows the largest changes in contribution to the total relaxation energies for this orbital. Moreover, the data can be interpreted in an entirely consistent manner. For protonation on carbon, the contribution from the 5σ orbital decreases whilst that for the π system (degenerate 1π orbitals) increases. The latter is readily understandable in terms of the decrease in orbital energy mismatch for interaction of the relevant 2p orbitals on carbon and oxygen, giving rise to greater electron transfer on creation of a core-hole on carbon. This is also the case for creation of a core-hole on oxygen for the HCO^+ species, but the situation is reversed for the corresponding oxygen protonated species, which shows a decreased contribution to the total relaxation energy, this being largest for the O_{1s} core-ionized species. The contributions from the core-orbitals themselves are calculated to be small and vary only slightly in going along the series COH^+, CO, HCO^+. One of the more significant features of the data displayed in Figure 7.4 is the computed increase in contribution to the total relaxation energies from the 5σ orbital on going from the neutral molecule to the protonated systems in the particular case of the O_{1s} core-ionized systems. For both HCO^+ and COH^+, the contribution to the relaxation energy is positive, compared with the negative

contribution computed for the neutral molecule.

The data reveal, therefore, that although the total relaxation energies for either C_{1s} or O_{1s} core-ionization in the series COH^+, CO and HCO^+ fall within a narrow range, this arises as a summation of contributions from each of the valence-levels which differ both in sign and magnitude across the series. In all cases, however, the single most important contribution arises from the degenerate 1π orbitals.

This being the case, it is of interest to investigate the changes in contribution arising from bending, and as a convenient link to H_2CO, the relevant data for HCO^+ with an $\hat{HCO}$ bond-angle corresponding to the geometry appropriate to formaldehyde are also considered. The data are displayed in Figure 7.5. The transformation from HCO^+ to H_2CO may be considered in discrete stages, a process of considerable assistance in the construction of the relevant correlation diagrams.

Starting from the theoretically optimized (linear HCO^+) geometry, the $\hat{HCO}$ bond angle is distorted to that appropriate to formaldehyde. The bond-lengths are then subsequently relaxed to the values appropriate to H_2CO.

Considering the extremes of the series, it is a straightforward matter to identify the unique valence-orbital ($2b_2$) for formaldehyde, which in fact corresponds roughly to an antisymmetric combination of the in-plane $2p_y$ orbitals on carbon and oxygen, with the appropriate combinations of H 1s orbitals such that overall the orbital is weakly C-H bonding and C-O antibonding. For the C_{1s} core-ionized state, the distortion from linearity lifts the degeneracy of the π orbitals. The contribution from the remaining π orbital

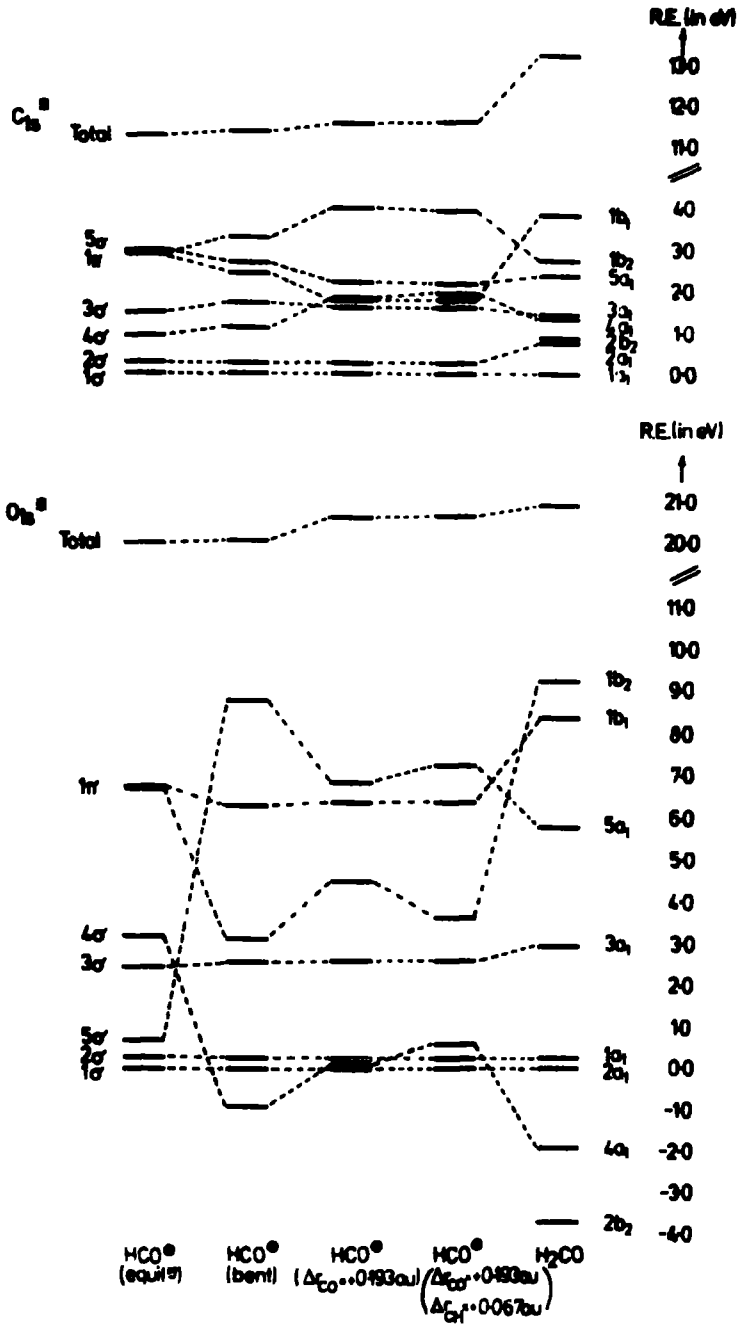

Fig.(7.5) Total R.E. and individual orbital contributions to the total R.E. in the series HCO^+ (linear), HCO^+ (bent) and H_2CO subsequent upon C_{1s} and O_{1s} core-ionization.

decreases, whilst the σ orbital derived from the π orbital provides an increased contribution, such that overall the relaxation energy does not change significantly. In going to formaldehyde, the interaction with the antisymmetric combination of H 1s orbitals

generates an extended in-plane "π-type" orbital, which provides the next-to-largest contribution to the relaxation energy, the largest contribution arising from the π orbital itself. The core-orbital contributions remain roughly constant, and are in all cases small.

For the O_{1s} core-ionized systems, the unique ($2b_2$) orbital actually provides a negative contribution to the total relaxation energy. A negative contribution is also calculated for one of the a_1 σ orbitals. A detailed analysis of the changes in population analysis for the relevant orbitals in going from CO to H_2CO via HCO^+ indicates that this orbital is the $4a_1$ orbital, which in valence-only notoation is the $2a_1$ orbital. These negative contributions are offset by the large positive contributions provided by the in-plane π-type orbital and the π orbital itself. The $5a_1$ orbital, which contributes substantially to the relaxation energy, derives from the interaction of the 5σ orbital of CO with a symmetric combination of the H 1s orbitals. This interaction provides a large increase in relaxation energy for this orbital, which for CO itself provides a small negative contribution for the O_{1s} hole-state. The way in which this orbital evolves to provide such a significant contribution to the relaxation energy is discerned by following the sequence:-

$$CO \rightarrow HCO^+ \text{ (linear)} \rightarrow HCO^+ \text{ (bent)} \rightarrow H_2CO$$

The distortion from linearity causes a substantial reordering of the individual valence-orbital contributions to the relaxation energy. The contribution from the orbital derived from the 5σ orbital in CO increases in magnitude, whilst that from the 4σ is substantially decreased, and finally, in correlating with the $4a_1$ orbital in formaldehyde, there is a further decrease in energy such that the contribution is significantly negative. The variation in

contributions to the total relaxation energies are significantly larger for O_{1s} as compared with C_{1s} core-ionizations. This can be rationalized qualitatively in terms of the difference in electron demands consequent upon creation of a core-hole on carbon in the "centre" of the molecule, compared with creation of a core-hole on the terminal oxygen, where the electron demand in respect of the C-O and C-H bonds will be considerably modified by the overall bonding scheme (viz. H-$\hat{C}$-O). The most profound changes in relaxation energy contributions occur for the 4σ and 5σ orbitals of the linear HCO^+ on bending, in the particular case of the O_{1s} core-ionized species. The 5σ increases its contribution to the total relaxation energy, whilst the 4σ decreases on going from the linear to bent systems. This behaviour can be qualitatively understood in terms of the localization characteristics of the orbitals involved. The 5σ orbital in CO essentially corresponds to a lone pair on carbon with very little contribution on oxygen, such that the relaxation energy contribution is small and negative. For the bent protonated species, however, the component contribution from basis functions on oxygen for this orbital are proportionately bigger, since the orbital energy mismatch is much less. Conversely for the 4σ orbital, (which is predominantly associated with the oxygen for the free ligand) in the bent protonated species, this orbital provides a substantial proportion of the C-H bonding interaction, and protonation leads to an increased contribution from basis functions on carbon, since the orbital energy mismatch is improved compared with the free ligand. In consequence, the contribution provided by this orbital decreases on going from the free ligand to the bent protonated species.

The dependence on bond-length of individual orbital contributions to relaxation energies in the case of CO has been discussed. A similar investigation may be made for the bent protonated species, providing an independent check of the overall validity of the relaxation energy contribution correlation diagram. For the free ligand, the contributions from the 4σ and 5σ orbitals exhibit positive and negative gradients, respectively, for both the C_{1s} and O_{1s} core hole states. A similar pattern is evident from Figure 7.5, extending the C-O bond-length for the bent HCO^+ species. For the π orbital (degenerate in CO), the gradient of the relaxation energy contribution as a function of bond-length is small and negative for the C_{1s}, and small and positive for the O_{1s}, core-ionized states. For the bent protonated species, whilst the contribution for the C_{1s} ionized state follows that for the neutral molecule, for the O_{1s} ionized state, the gradient is essentially zero. For the 3σ orbital, the gradients for the C_{1s} and O_{1s} ionized systems in the free ligands are predicted to be opposite in sign, being positive for the latter. For the bent protonated species the gradients are small and negative for both core-ionized states.

d) Density difference contours

The total density difference contour plots for HCO^+, CO and COH^+ are shown in Figure 7.6, from which it is clear that the overall relaxation process is very similar for all three molecules, as might have been anticipated from Figure 7.4. An analysis of the individual orbital contributions to the total relaxation process has been made. Figure 7.7 shows the variation along this series of the 3σ contribution, those for the 1σ and 2σ orbitals being negligible

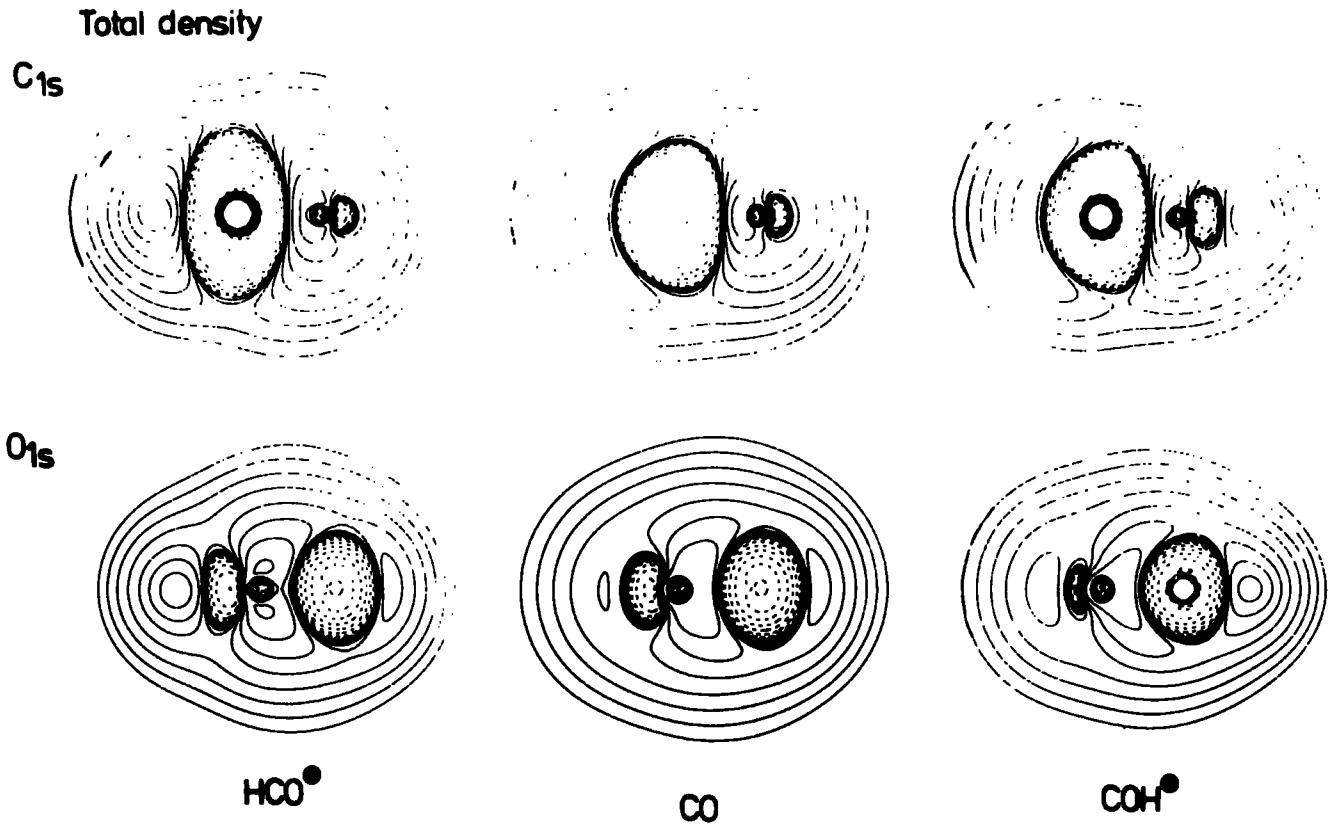

Fig.(7.6) Density difference contour plots for HCO^+, CO and COH^+.

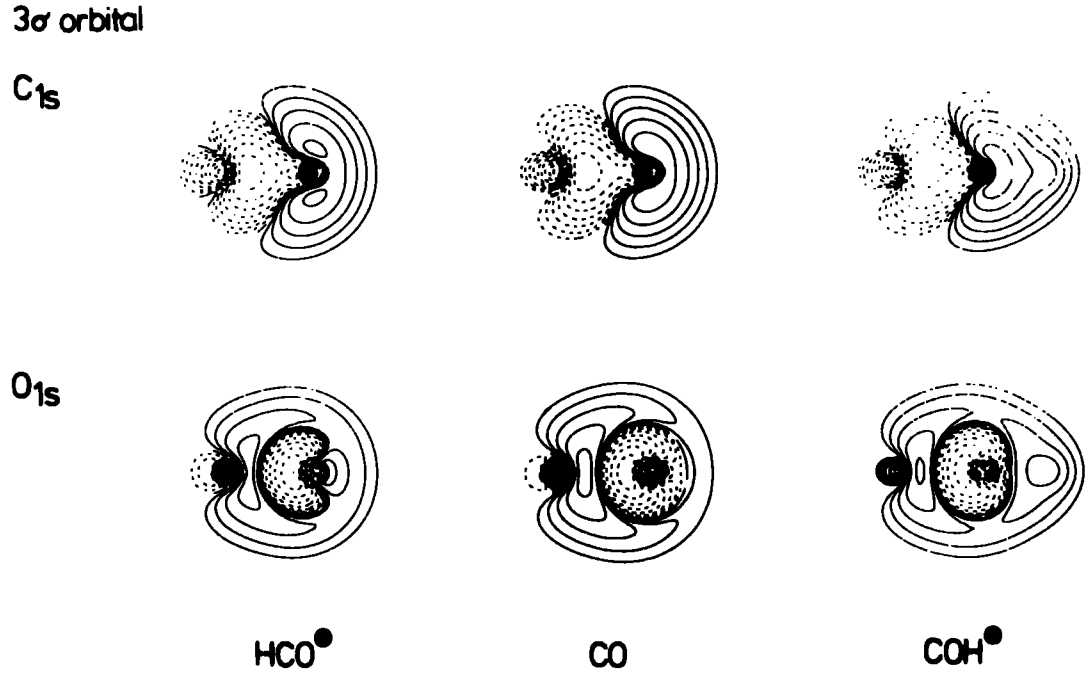

Fig.(7.7) Density difference contour plots for HCO^+, CO and COH^+.

for both O_{1s} and C_{1s} core-ionization. The overall pattern for both C_{1s} and O_{1s} core-ionization is remarkably similar along this series of molecules, giving rise to the virtually constant contribution from this orbital to the total relaxation energy.

The situation for the 4σ orbital (Figure 7.8) is more complex. For C_{1s} core-ionization in CO, there is a build-up in

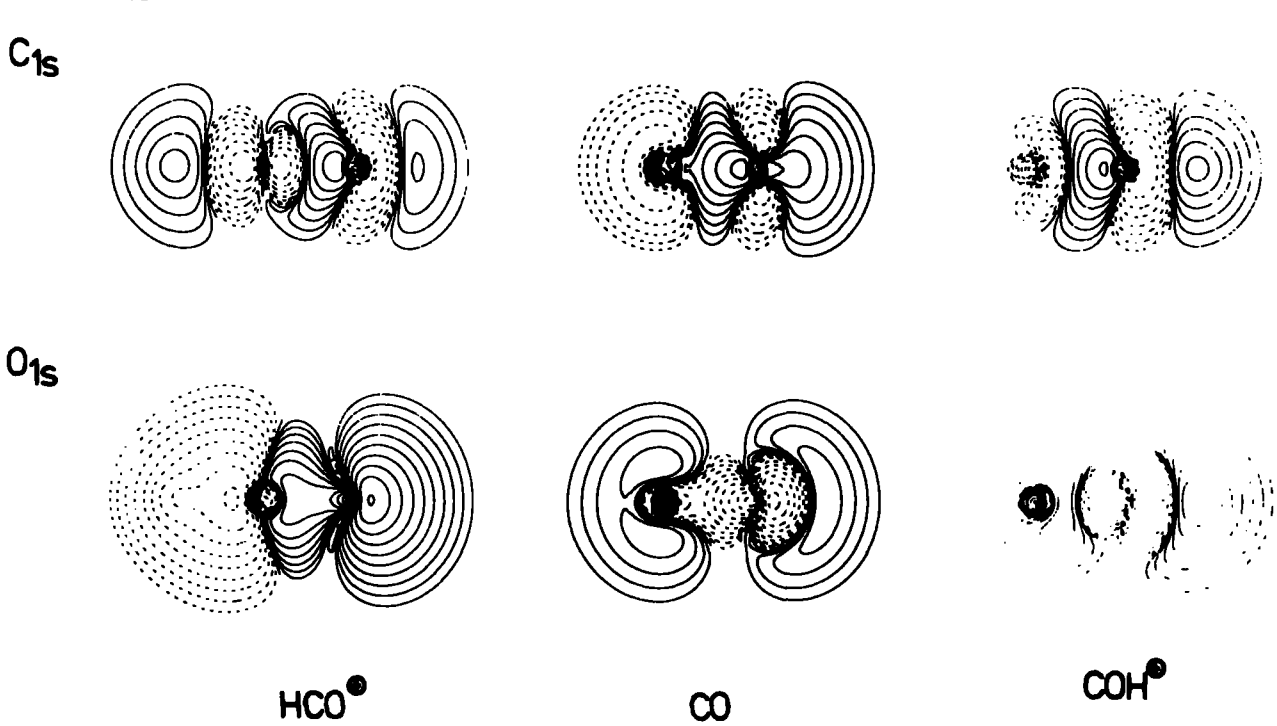

Fig.(7.8) Density difference contour plots for HCO^+, CO and COH^+.

electron density in the region of the carbon atom, at the expense of the oxygen lone pair, and the internuclear bonding region; for COH^+, however, there is an area of electon density increase between the carbon and oxygen atoms. Since less electron density is transferred to the carbon atom, a decrease in single orbital relaxation energy is expected. For HCO^+, there is now less electron-transfer from the oxygen lone pair - rather, some electron density is lost from the hydrogen atom. For O_{1s} core-ionization, the overall pattern of electron flow is fairly similar for CO and COH; however,

the pattern of electron flow is markedly different for HCO^+, in that despite the fact there is a core-hole on oxygen, the electron flow is *to* the C-H region of the molecule. This may account for the decrease of $\sim$ 1.5 eV in the 4σ orbital relaxation energy on going from CO to HCO^+.

The contour plots for the 5σ orbitals are shown in Figure 7.9. For C_{1s} core-ionization, the plots for CO and HCO^+

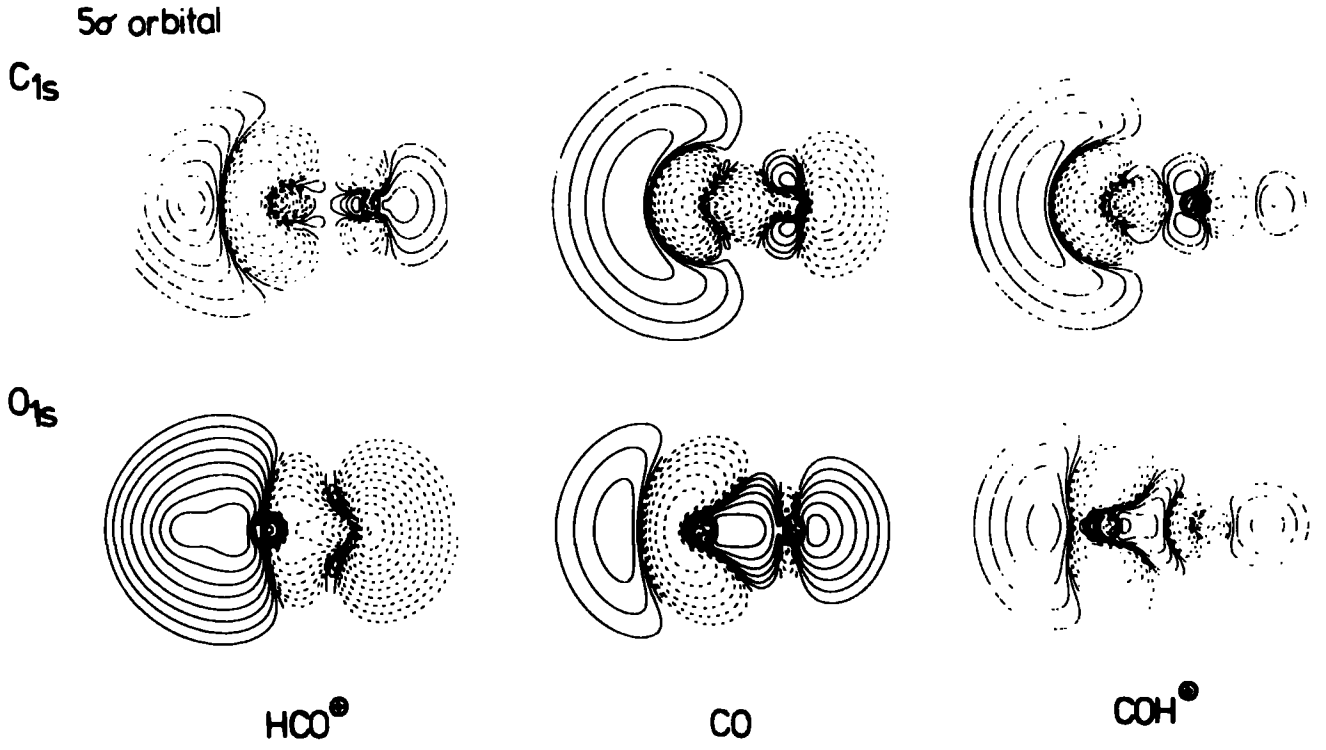

Fig.(7.9) Density difference contour plots for HCO^+, CO and COH^+.

are quite similar, save that less electron-flow to the O-H region in COH^+ occurs than to the O lone pair in CO, resulting in a slightly higher relaxation energy for the 5σ orbital in COH^+. For HCO^+, there is even less transfer of electron density to the oxygen lone pair, but rather more to the C-O bonding region from the hydrogen. For O_{1s} core-ionization, the electron flow for the CO and COH^+ molecules is fairly similar, whilst that for the HCO^+ molecule is again quite distinct, with considerable build-up of

electron density in the C-O bonding and oxygen lone pair regions.

Finally, Figure 7.10 shows the contour plots for the degenerate 1π orbitals. These are extremely similar in appearance.

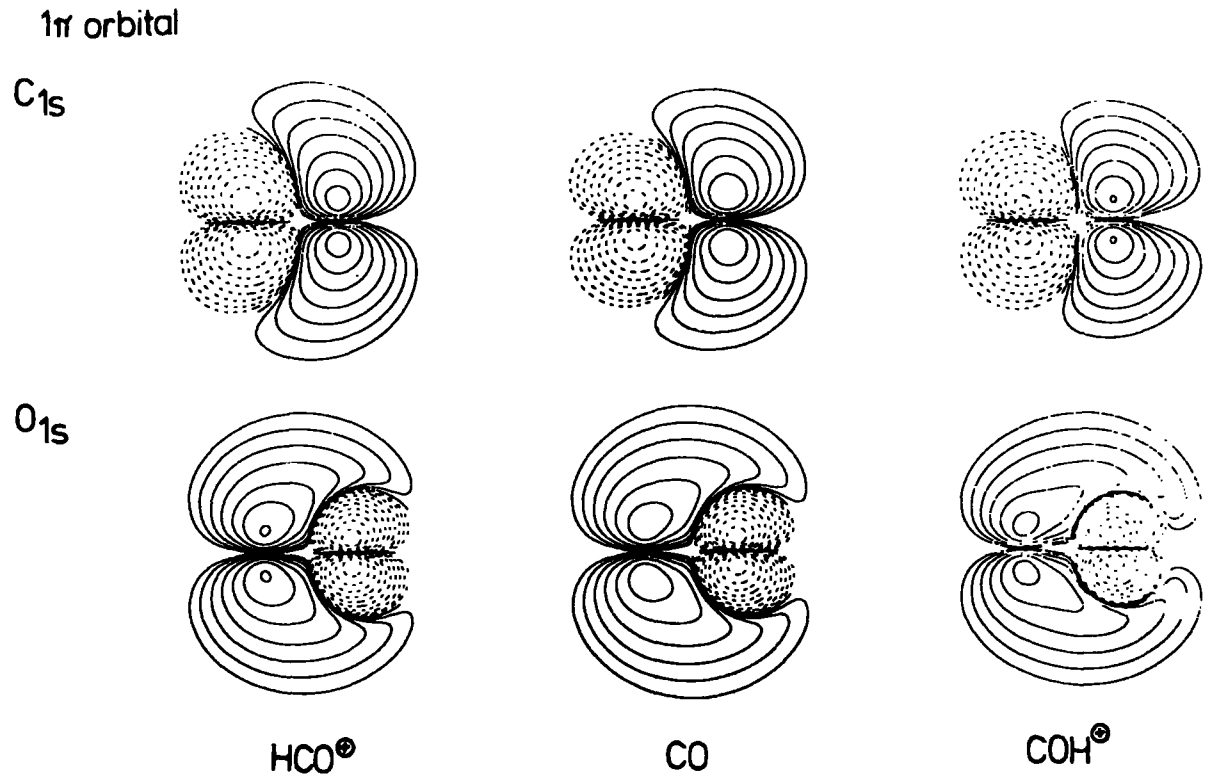

Fig.(7.10) Density difference contour plots for HCO^+, CO and COH^+.

Similar density difference contours may be constructed for the HCO^+ (linear), HCO^+ (bent) and H_2CO molecules, to investigate the effect of σ-π mixing on the valence-electron flow accompanying core-ionization. The total density difference contours are shown in Figure 7.11, and as before, they are quite similar in overall appearance. Again, as perhaps anticipated from the strongly bonding nature of the orbitals, the 3σ orbital relaxation plots, Figure 7.12,are also very similar. For ease of comparison, the orbitals will be referred to by the designation of the CO orbital with which they correspond, even though this orbital, for formaldehyde, is strictly the $3a_1$ orbital.

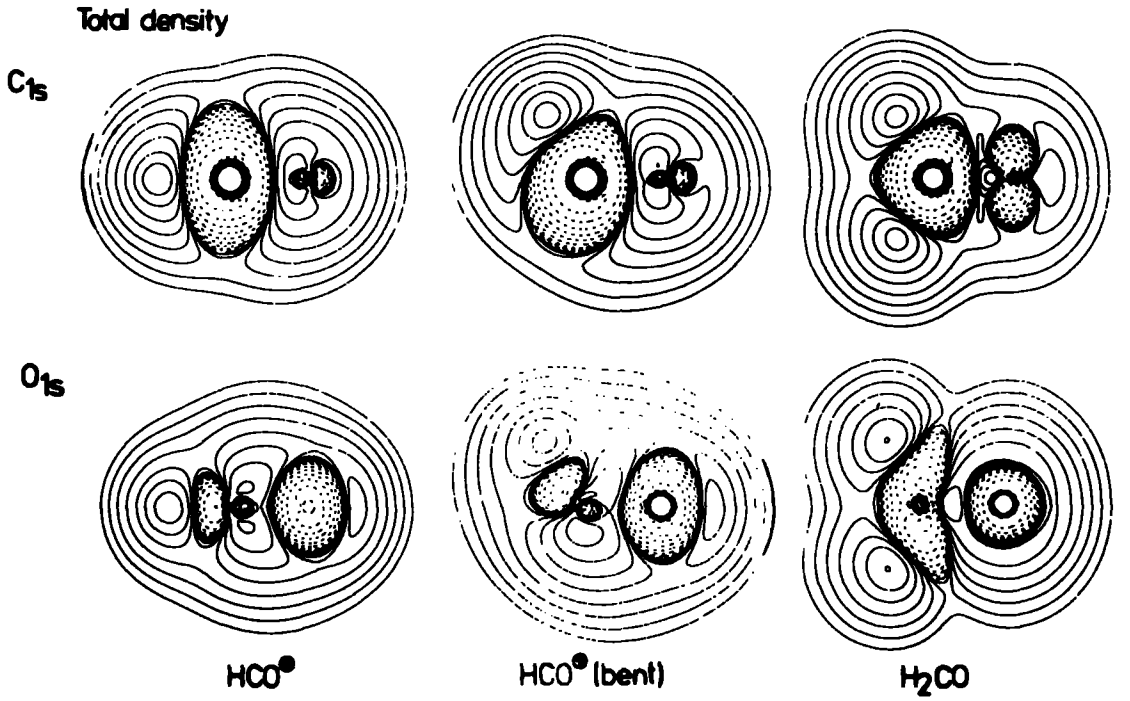

Fig.(7.11) Density difference contour plots for HCO^+ (linear), HCO^+ (bent) and H_2CO.

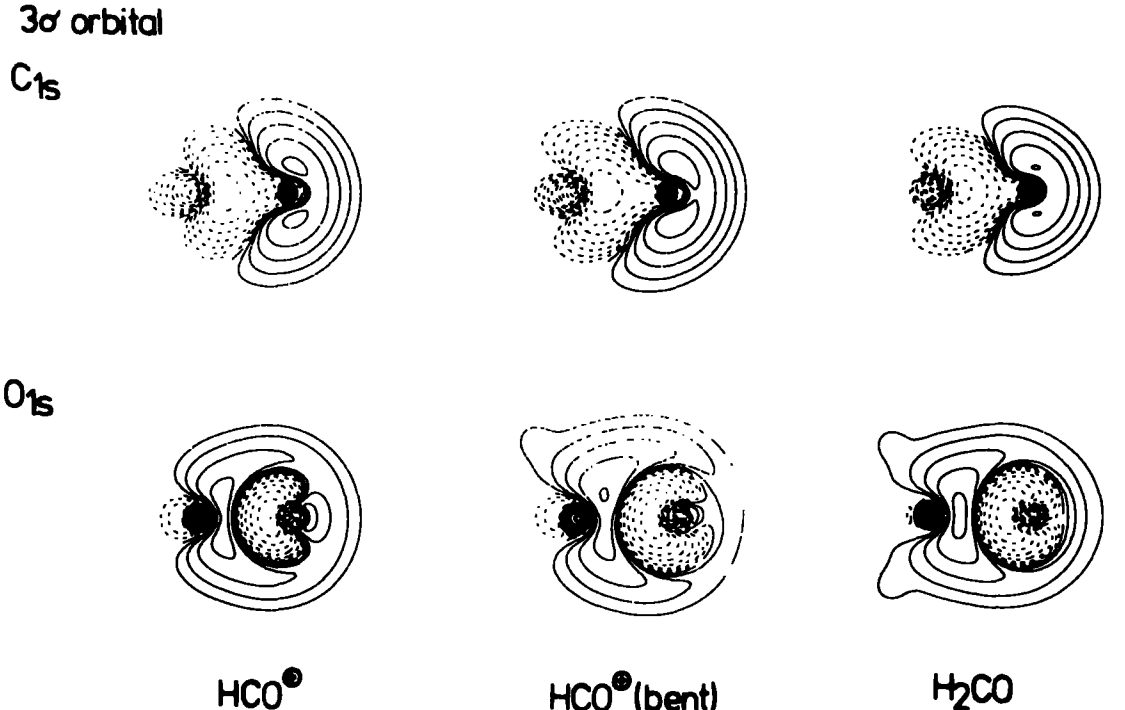

Fig.(7.12) Density difference contour plots for HCO^+ (linear), HCO^+ (bent) and H_2CO.

The 4σ and 5σ orbitals, Figures 7.13 and 7.14, are more complex, but the underlying similarity between the relaxation

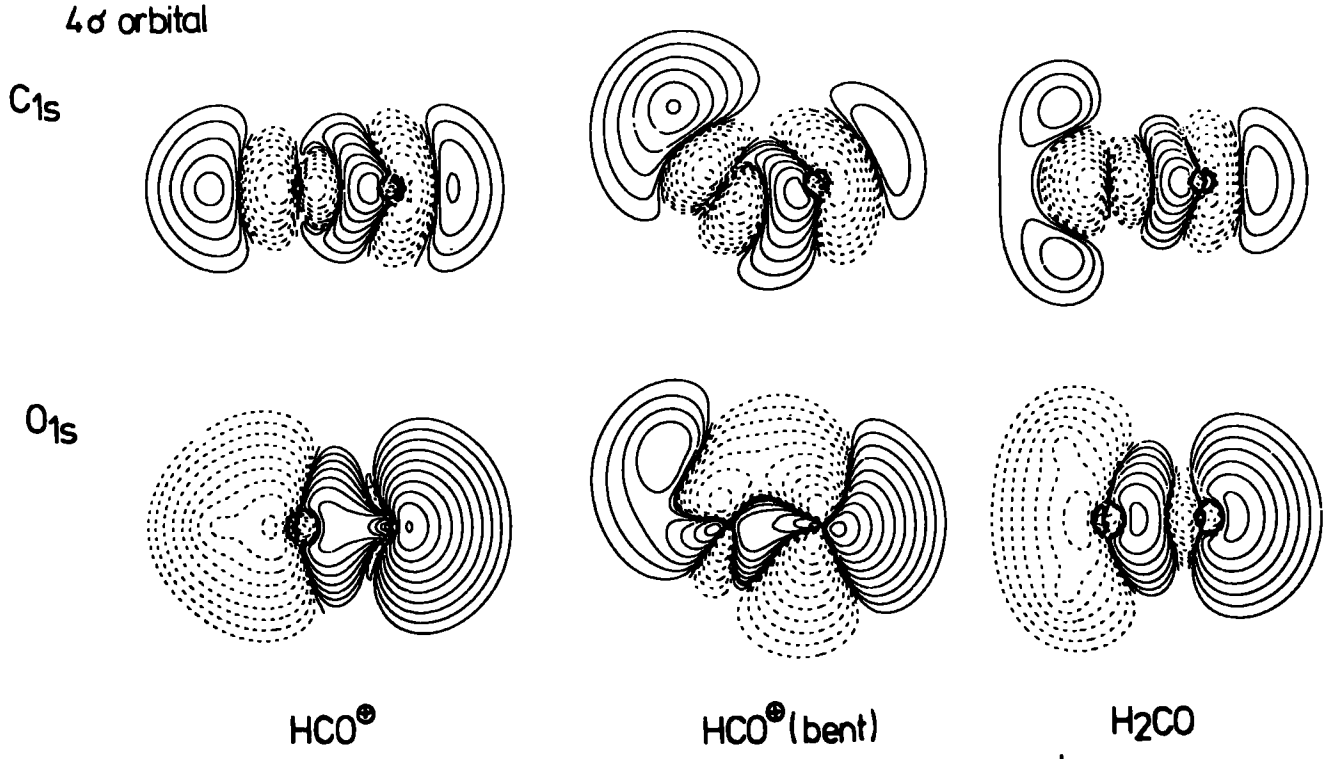

Fig. (7.13) Density difference contour plots for HCO^+ (linear), HCO^+ (bent) and H_2CO.

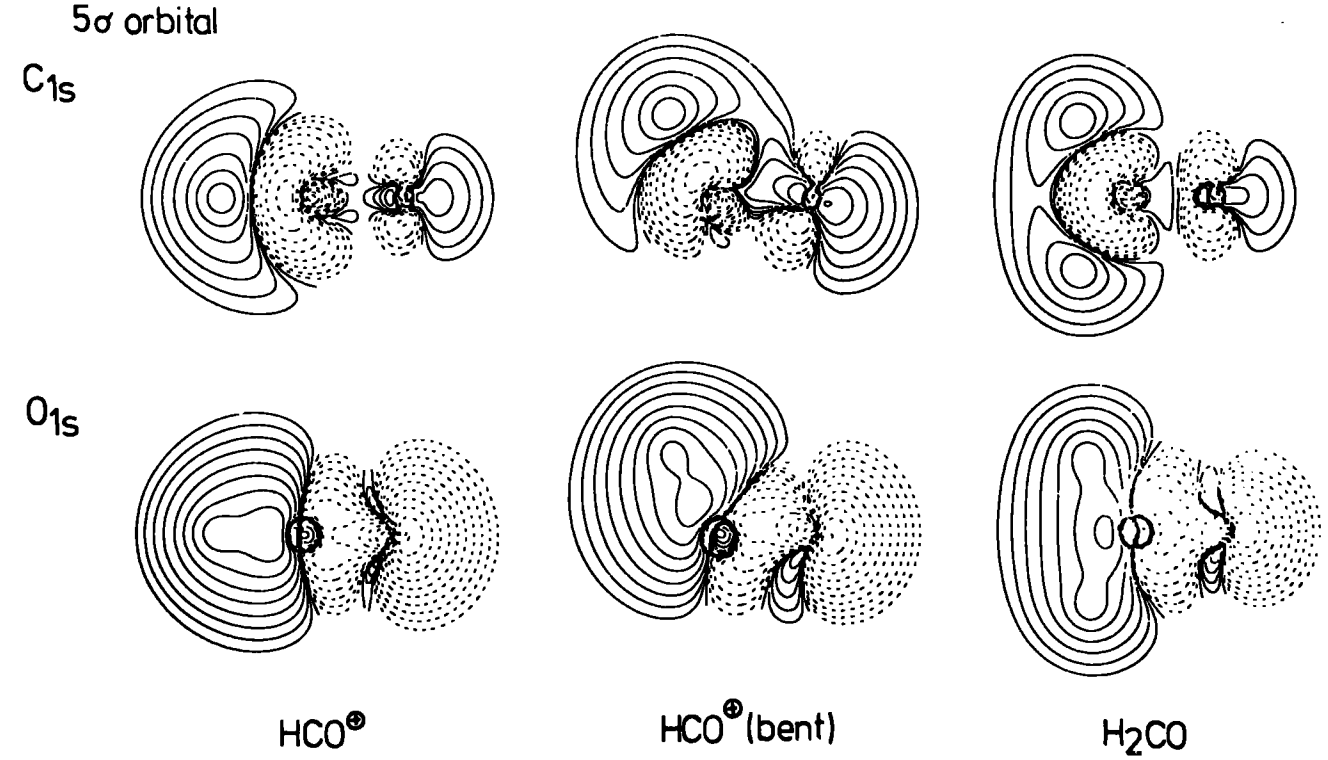

Fig. (7.14) Density difference contour plots for HCO^+ (linear), HCO^+ (bent) and H_2CO.

pattern is apparent. The 1π orbital shown in Figure 7.15 is the in-plane "π-type" orbital of HCO^+ (bent), which becomes the $1b_1$ orbital of formaldehyde.

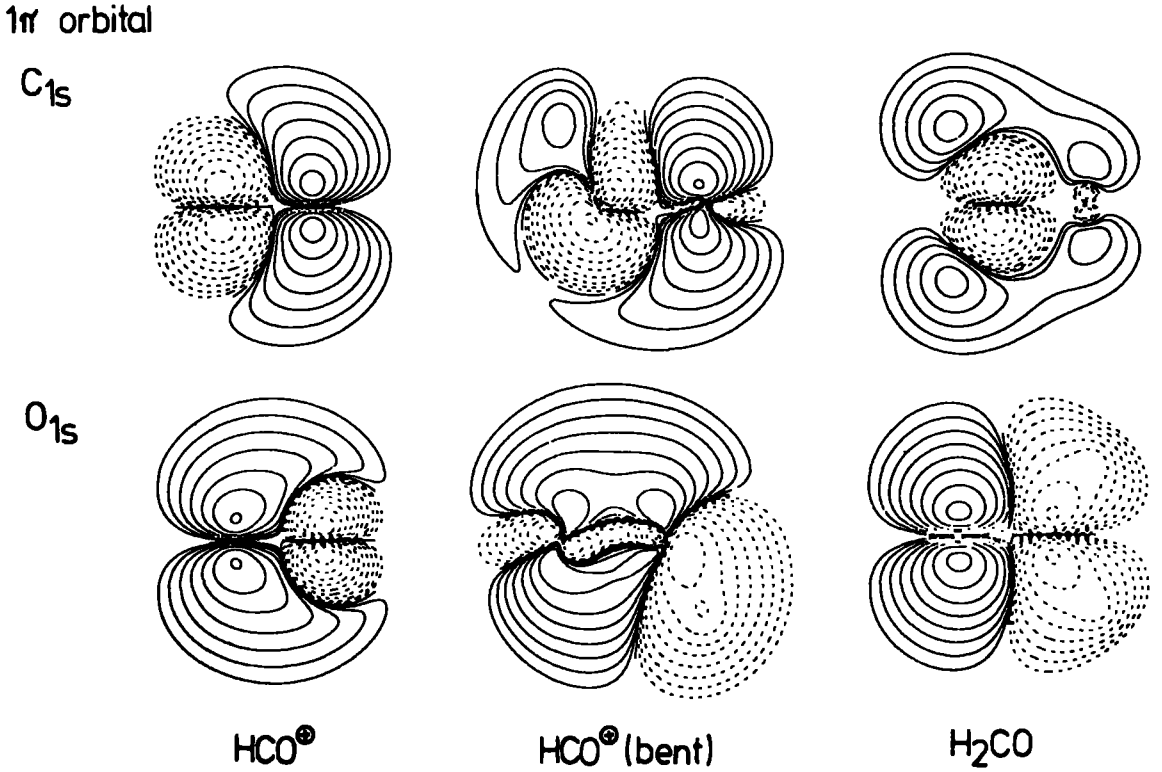

Fig.(7.15) Density difference contour plots for HCO^+ (linear), HCO^+ (bent) and H_2CO.

It should be clear from the foregoing discussion that the analysis of total relaxation energies into individual orbital contributions reveals a striking dependence on the intimate details of the valence-electron distributions. Although it is possible therefore for total relaxation energies to vary by only a small amount in going from one system to another, this arises from a convolution of terms of opposite sign arising from different individual valence-orbitals. It is hoped that an analysis along the lines presented here provides additional insight into the relationship between electronic structure and electronic relaxations accompanying core-ionization.

7.2 Electronic Reorganization Accompanying Core-Ionization in the Isomeric Pairs of Molecules HCN, HNC and HON, HNO

7.2.1 Introduction

In the previous section, an investigation of the changes in orbital contributions to relaxation energies for the series CO → HCO^+ → HOC^+ was given. As an extension of this work, the ground and core hole states of HCN, HNC, HNO and HON were examined. The enthalpies of isomerization for these systems are small in both cases, and it is therefore of interest to investigate the shifts in core binding energies and the contributions originating in differences in relation energies.

Geometries optimized within the SCF approximation were used for HCN, HNC[301] and HON, HNO;[302] comparison with experimental data where possible reveals excellent agreement. For the HON, HNO species, calculations for the ground-state were restricted to the singlet $^1A'$ states. The basis set employed was the STO-6.33G + P previously described.

7.2.2 Results and Discussion

a) Absolute binding energies and shifts

There have been extensive studies of both the ground and excited states of HCN and HNC[301,303] and of HNO and HON,[304-308] and HCN has previously been investigated in some detail with respect to the core hole states,[200] including an analysis of vibrational excitations accompanying core-ionization. There has been no previous investigation of the core hole states for this series of molecules using basis sets of comparable quality. The main emphasis in this section is the interpretation of changes in binding and relaxation energies; however, the computed enthalpies of isomerization may be compared with those previously reported

in the literature. The computed energy difference between HCN and HNC of 5.1 kcal mol^{-1} compares with the value of 9.5 kcal mol^{-1} computed at the SCF level by Schaefer and co-workers,[301] and 14.6 kcal mol^{-1} from an extensive CI investigation. Although the ground-state of HNO is $^1A'$, that for HON is a triplet state ($^3A''$), the singlet $^1A'$ state being $\sim$ 30 kcal mol^{-1} to higher energy.[304] To avoid complications involving multiplet splittings, and to provide a correlation for the individual orbital components, the investigation described in this work has been confined to the $^1A'$ state of HON and the derived O_{1s} and N_{1s} core hole states. The energy difference between HNO and HON of 20.6 kcal mol^{-1} compares favourably with the value of 20 kcal mol^{-1} obtained by Gallup[304] with a gaussian lobe basis set of essentially Double Zeta quality.

The absolute binding and relaxation energies and shifts for the series of molecules are displayed in Table 7.1. For comparison, data for CO and N_2, computed with the same basis set, are also included. The absolute binding energies are typically $\sim$ 2.5 eV too large. Although the energy difference between the tautomers is small, in both cases the shifts in core binding energies within a given pair are quite significant ($\sim \pm$ 0.5 eV). On going from N_2 to HCN, there is a substantial shift to lower binding energy for the N_{1s} levels, partly attributable to the large increase in relaxation energy. The shift to lower binding energy is somewhat reduced for HON however, the relaxation energy contribution to the shift being zero. The computed shift of 2.5 eV in the N_{1s} levels between HON and HCN may be compared with the shift of 3.3 eV in going from HNO to HNC. Although for

TABLE 7.1 ΔSCF B.E. and R.E. (in eV)

Molecule	C_{1s}				N_{1s}				O_{1s}			
	ΔSCF Binding Energy	ΔB.E.	Relaxation Energy	ΔR.E.	ΔSCF Binding Energy	ΔB.E.	Relaxation Energy	ΔR.E.	ΔSCF Binding Energy	ΔB.E.	Relaxation Energy	ΔR.E.
CO	299.6	(0)	10.8	(0)					543.7	(0)	19.9	(0)
N_2					412.9	(0)	15.4	(0)				
HCN	295.4	-4.2	12.6	+1.8	408.5	-4.4	16.8	+1.4				
HNC	296.0	-3.6	12.1	+1.3	408.2	-4.7	17.1	+1.7				
HNO					411.5	-1.4	16.6	+1.2	542.2	-1.5	20.4	+0.5
HON					411.0	-1.9	15.4	0.0	542.8	-0.9	20.6	+0.7
Experimental Data:												
CO	296.2								542.3			
N_2					409.9							
HCN	293.3				406.1							

HCN and HNC, the shifts for the C_{1s} and N_{1s} levels may largely be attributed to changes in relaxation energies, the situation is somewhat more complicated for HNO and HON. The former molecule has the higher N_{1s} binding energy and lower O_{1s} binding energy, despite the fact that the relaxation energy shifts are in a contrary sense. This is almost certainly associated with the fact that for these molecules, the bent conformations correspond to extensive σ-π interaction, compared with a linear conformation. A similar situation in going from the linear to bent conformation for HCO^+ was noted in the previous section.

b) Orbital contributions to relaxation energies

There are significant differences in total relaxation energies for the C_{1s} and N_{1s} hole-states for HCN and HNC. The analysis in terms of individual orbital contributions may provide insight into the origin of such differences. This is shown in Figure 7.16. For the N_{1s} core-ionized systems, the largest contributions to the relaxation energies arise from the degenerate 1π orbitals. The population analysis reveals that on going from the neutral to core-ionized species, there is substantial π-electron transfer from carbon to nitrogen, such that the contributions are comparable for the two systems. The core-levels themselves provide very small contributions overall, and the 3σ orbital, which is predominantly N 2s in character for both HCN and HNC, provides a substantial but essentially invariant contribution to the relaxation energy accompanying N_{1s} core-ionization. An interesting situation is apparent for the 4σ and 5σ orbitals, which for HCN correspond essentially to the C-H bonding and lone pair orbitals on nitrogen respectively. For HNC, the corresponding orbitals are dominantly of N-H bonding and carbon lone pair character.

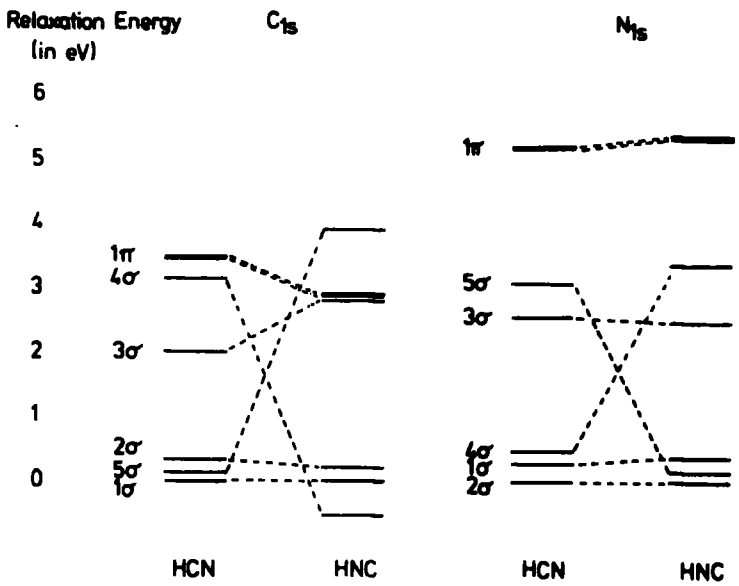

Fig.(7.16) Single orbital relaxation energies accompanying C_{1s} and N_{1s} core-ionization in HCN and HNC.

Considering the lone pair-type 5σ orbitals, creation of a core-hole on nitrogen provides essentially zero contribution to the total relaxation energy in the case of HNC, but a large positive contribution in the case of HCN. This agrees with the analogous situation previously described for CO, where for the 5σ orbital (carbon lone pair), creation of a core-hole on carbon leads to a substantial contribution to the relaxation energy for this orbital, whilst for the O_{1s} core hole state, the contribution is actually negative. This analogy is further strengthened by comparison with the behaviour for the C_{1s} core-ionized systems. Thus for HCN, whereas the 5σ orbital (lone pair on nitrogen) contributes little to the overall relaxation energy, for HNC (largely N-H bonding) the relaxation energy provides the single largest contribution to the overall relaxation energy. This behaviour is mirrored by the 4σ orbitals; for HNC, this orbital (dominantly of N-H bonding character) provides essentially zero

contribution to the relaxation energy for the C_{1s} levels but a large contribution for the N_{1s} levels, whilst for HCN, for which the 4σ orbital is dominantly of C-H bonding character, the reverse situation obtains. It is unfortunately not possible to provide a straightforward pictorial rationalization of the contribution to the relaxation energies provided by the orbitals of predominantly lone pair character on the basis of simple Mulliken population analyses, whereas for the other orbitals an increase in relaxation energy contribution may straightforwardly be associated with an increase in population on the atom on which the core-hole is located. As has been previously noted, in the case of carbon monoxide, for the lone pair orbitals (for which a Mulliken population analysis predicts essentially zero change in going to the core-ionized species) a pictorial representation of the relaxation energy contributions requires density difference contours, which reveal the reorganization of electron density in the vicinity of the atom bearing the core-hole.

The data for HNO and HON are displayed in Figure 7.17. The ground state of HON is a triplet; however, the singlet state is only slightly higher in energy ($\sim$ 1.5 eV) and to avoid complications arising from multiplet effects and to provide a convenient comparison with HNO, the computations refer to the closed-shell systems. In order for a comparison to be drawn with the data for linear HCN and HNC systems, the σ-orbital which arises from the interaction of the H 1s orbital with one of the degenerate (in an RHF formalism) pair of π-orbitals for NO is referred to as the 1π orbital; however, in terms of the symmetry of the bent systems, it should be more correctly denoted as the

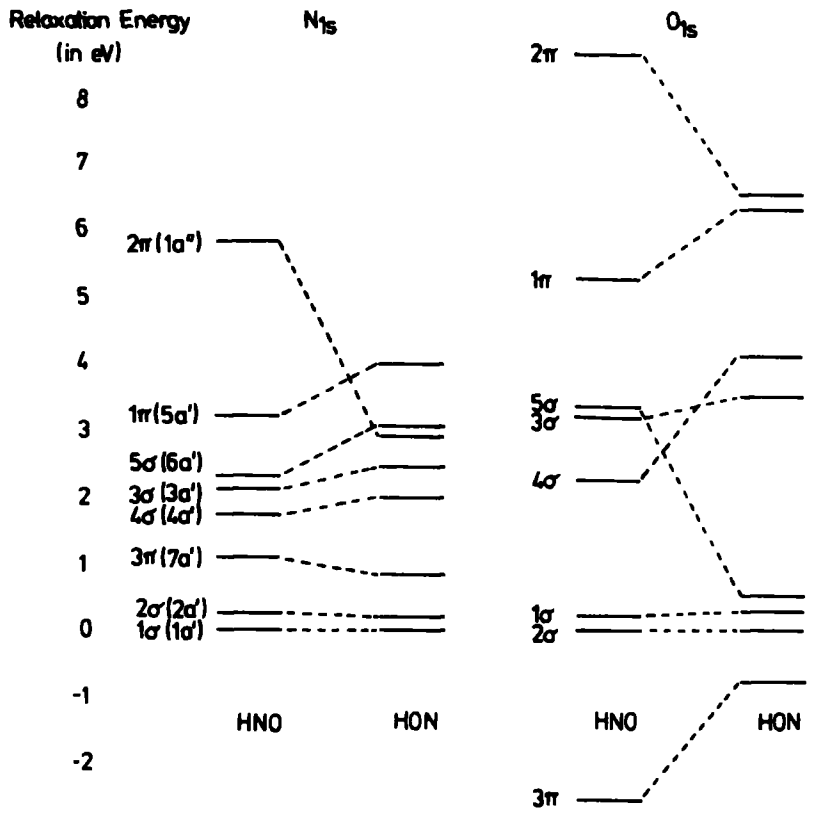

Fig.(7.17) Single orbital relaxation energies accompanying N_{1s} and O_{1s} core-ionization in HNO and NOH.

5a' orbital. For HNO, the largest single contribution to the relaxation energy arises from the strongly bonding N-O π-orbital (2π); the Mulliken population analysis reveals substantial electron transfer to a given atom on creation of the core-hole on that atom. The behaviour of the doubly-occupied antibonding N-O π-orbital (3π) is particularly interesting, in that for the N_{1s} level in HNO it provides a small but significant contribution to the relaxation energy, whilst for the O_{1s} core-ionized species, the contribution is larger in absolute magnitude, but opposite in sign. This may be rationalized in a qualitative manner in terms of the increased (for N_{1s}) or decreased (for O_{1s}) interaction between the orbitals of π-symmetry on nitrogen and oxygen as a function of the effective

orbital energy mismatch between them. The σ-orbital derived from a linear combination of H 1s and in-plane π-orbitals of NO, which has been designated the 1π orbital, contributes substantially to the total relaxation energy for both the N_{1s} and O_{1s} hole-states of HNO. This parallels the behaviour for protonated CO, for which the relaxation energy contribution of the π-orbital, which interacts with the H 1s orbital, decreases only slightly on bending.

The contributions arising from the 4σ, 3σ and 5σ orbitals fall in the same sequence for both the N_{1s} and O_{1s} hole-states of HNO. The 3σ and 4σ orbitals are predominantly of O 2s and N 2s character respectively, and thus have significant lone pair character. The population analysis reveals little overall change in going to the core-ionized species; however, the substantial contributions arise from the local contraction of valence-electon density, which is only readily revealed by density difference contour plots. The 5σ orbital, which is N-O anti-bonding and N-H bonding, provides a significant contribution to the relaxation energy for both core hole states of HNO.

The substantial changes in relaxation energy for both the N_{1s} and O_{1s} levels in going from HNO to HON clearly arise from an interplay of the various contributions from the individual valence orbitals, as evidenced by the data in Figure 7.17. In the absence of relaxation effects, the computed shifts for the N_{1s} and O_{1s} levels in going from HNO to HON would be -1.7 eV and +0.8 eV respectively, compared with the values including relaxation effects of -0.5 eV and +0.6 eV. For HON, the 2π orbital provides a substantial contribution to the relaxation energy for both of the

hole-states. Since the strongly N-O π-bonding orbitals in NO have substantially larger contributions from the oxygen as opposed to the nitrogen π-type orbitals, the interaction with the H 1s orbital on going to the bent HON system is significantly greater, and this is reflected in the somewhat greater contribution of this orbital to the total relaxation energy on going from the HNO to the HON system. For the N_{1s} and O_{1s} hole-states, the contributions provided by the antibonding π-orbital (3π) are smaller in magnitude than for HNO, whilst the contributions from the 3σ and 4σ orbitals increase. An interesting situation arises for the 5σ orbital, which provides a large contribution to the relaxation energy in HNO and for the N_{1s} hole-state in HON; however, the corresponding contribution to the O_{1s} hole-state in HON is very small.

There is no straightforward rationalization for this on the basis of changes in population from a Mulliken analysis. The 5σ orbital, which is N-O antibonding for both HNO and HON, provides an increase in population on the atom bearing the core-hole in the case of the N_{1s} hole-state of HNO; however, there are significant decreases in population for the remaining hole-states. The bond overlap populations reveal the substantial changes in electron distribution in the bonding regions, and it would appear that a Mulliken population analysis provides too crude a picture of the overall electronic reorganization, since it does not allow a ready means of identifying regions close to the nucleus, as opposed to those which are more remote.

7.3 Single Orbital Relaxation Energies Accompanying Core-Ionization in the Isoelectronic Series CH_4, NH_3, H_2O, HF and Ne

7.3.1 Introduction

As a final extension of the method described in the previous Chapter to polyatomic systems, an investigation of the individual orbital contributions to the total relaxation energies accompanying core-ionization in the isoelectric series CH_4, NH_3, H_2O, HF and Ne is presented in this section. This series is of particular interest, since the changes in valence electronic structure may conveniently be discussed in terms of the united atom formalism; indeed Price and Potts have presented an elegantly simple discussion of the valence energy levels for this series based on this concept.[207] Brief consideration is also given to individual orbital contributions to the total relaxation energies associated with the essentially core-like valence 2s levels. As in previous sections, the STO-6.33G + P basis set was used.

7.3.2 Results and Discussion

a) Absolute binding energies and total relaxation energies

The computed absolute binding energies and relaxation energies are displayed in Table 7.2. Comparison with available experimental data reveals excellent overall agreement. The basis set was chosen on the basis of a compromise between flexibility in describing the valence-electron distributions and cost-effectiveness in terms of computing resources. In terms of describing differences in relaxation energies and in assessing the relative importance of contributions arising from individual orbital relaxations, however, the basis should be more than adequate.

b) Orbital relaxation energies accompanying core-ionization

The prime motivation for this work is the direct investigation of the individual orbital contributions to relaxation

TABLE 7.2 Total Calculated and Experimental Binding Energies, and Relaxation Energies (in eV) for Core (1s) and Valence (Dominantly 2s) Ionization of Ne, HF, H_2O, NH_3 and CH_4

Molecule	Core (1s) Ionization			Valence (Dominantly 2s) Ionization		
	ΔSCF Binding Energy	Relaxation Energy	Experimental Binding Energy	ΔSCF Binding Energy	Relaxation Energy	Experimental Binding Energy
Ne	870.76	20.62	870.38[a]	50.03	2.03	48.47[a]
HF	694.61	21.27	694.22[b]	41.21	2.60	40.0[c]
H_2O	540.52	19.37	539.89[b]	34.89	2.23	32.0[c]
NH_3	406.24	16.74	405.58[b]	29.41	1.79	26.7[c]
CH_4	291.35	13.56	290.91[b]	24.32	1.29	22.8[c]

a) Ref. 117.

b) Ref. 141.

c) Estimated from ref. 207.

energies for a simple isoelectronic series. The results are displayed in Figure 7.18, and it is clear from a comparison with

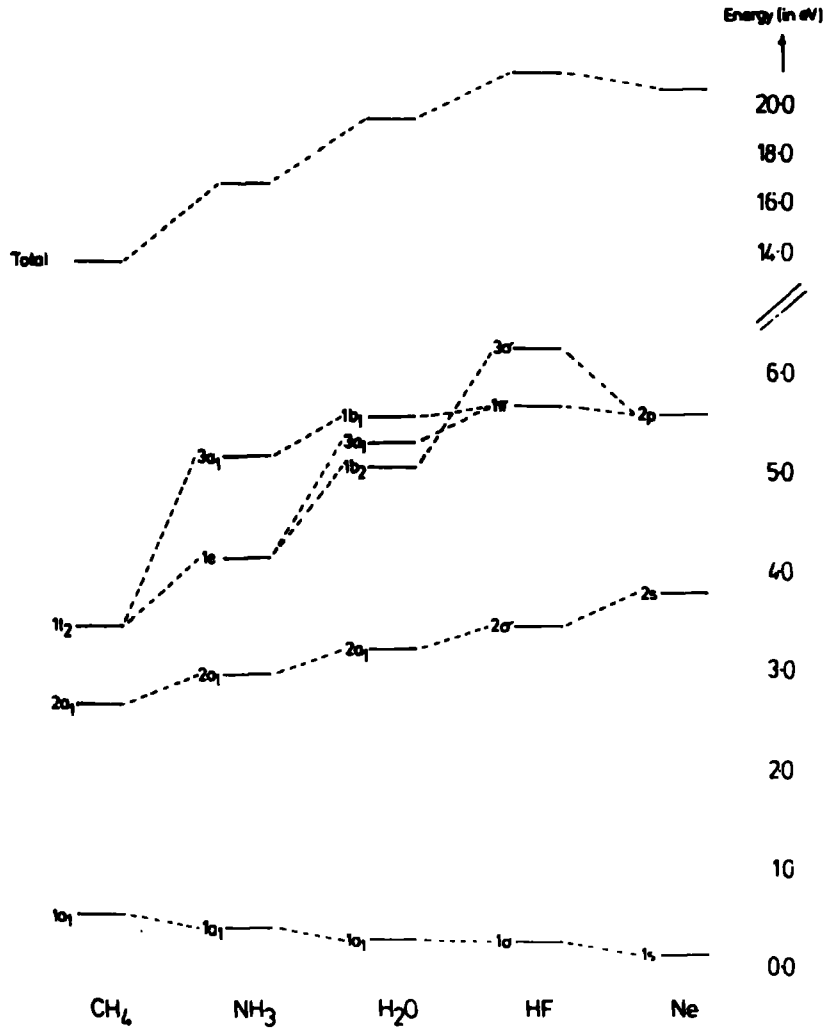

Fig.(7.18) Individual orbital contributions to the total R.E. accompanying core-ionization in the series CH_4, NH_3 H_2O, HF and Ne.

the data in Table 7.2 that the sum of the individual orbital contributions exactly reproduces the total computed relaxation energies. In this figure, the value for a *single* orbital is given in the case of degenerate orbitals.

Considering the two extremes of the series (namely, methane and neon), it is instructive to compare the orbital contributions for the equivalent orbitals. In both cases, the

remaining core-electron (1σ) contributes only a small fraction of the total relaxation energy, which is almost exclusively associated with reorganization of the valence-electron distribution. The $2a_1$ orbital in CH_4 is dominantly of 2s character and the contribution to the total relaxation energy increases in absolute magnitude in going to Ne; however, the percentage contribution of the 2s orbital to the total relaxation energy is approximately constant (16-20%) across the series. The triply-degenerate $1t_2$ orbitals of methane (dominantly of C 2p and H 1s character) correlate with the 2p atomic orbitals of neon, the relaxation energy for the latter being somewhat larger in magnitude than for the former. In both cases, the contribution to the total relaxation energy is considerably larger for the more polarizable orbitals involving valence 2p atomic orbitals, as opposed to the more strongly bound valence 2s levels.

In going from methane to ammonia, the relaxation energy contribution from the $2a_1$ (2s) orbital increases. The $1t_2$ orbitals now correlate with the $3a_1$ (lone pair) and doubly-degenerate 1e N-H bonding orbitals. The contribution to the relaxation energy from the lone pair $3a_1$ orbital is significantly larger than for the 1e orbitals, as might have been anticipated on the basis of their localization characteristics.

The increment in relaxation energy in going from the $2a_1$ orbital of NH_3 to the corresponding orbital in H_2O is almost identical to that in going from CH_4 to NH_3 ($\sim$ 0.26 eV). The orbital relaxation energies for H_2O fall in the order $1b_1 > 3a_1 > 1b_2$, which is also the order of decreasing population on oxygen associated with each of these orbitals, the gross atomic populations on oxygen

for the "half-ionized" states, computed as the average for the ground and core hole states, being 0.96, 0.90 and 0.72 respectively.

In going from water to hydrogen fluoride, there is again a small increase in the relaxation energy associated with the 2σ orbital (F 2s). Since the 3σ (H-F bonding) orbital is strongly polarized with a substantial build-up of negative charge on fluorine, there is a substantial increase in relaxation energy in going from the $1b_2$ orbital in H_2O to the 3σ orbital in HF; indeed, the contribution to the relaxation energy from the bonding orbital is somewhat larger than for the 1π orbitals, which are almost exclusively of F 2p character, there being negligible population of the 2p and 3d polarization functions on hydrogen and fluorine respectively. The contribution to the relaxation energy provided by the degenerate π-orbitals is in fact directly comparable with that calculated for the 2p valence-orbitals of neon.

c) Orbital relaxation energies accompanying dominantly 2s valence ionization

The essentially core-like nature and somewhat similar localization characteristics for the valence-orbitals dominantly of 2s character suggest that correlation energy corrections to computed absolute binding energies should be somewhat similar for the series, and this receives some support from the data presented in Table 7.2. In each case, the ΔSCF technique somewhat over-estimates the absolute binding energies, the correlation energy for the ionic state being somewhat larger for the neutral molecule. The similarity of the correlation energy changes for CH_4 and for Ne are clearly apparent from this data, since the difference between the experimentally determined and theoretically calculated

ΔSCF binding energies is essentially the same (1.6 eV and 1.5 eV respectively). For NH_3 and H_2O, the differences are somewhat larger with respect to Ne; however, the differences are still quite small. Estimates of the correlation energy changes associated with ionization of the 2s orbitals have been reported for both neon and water, being ∿ 0.8 eV[136] and ∿ 1.9 eV[140,309] respectively, with the correlation energy being larger for the ionic species. This difference in correlation energy of 1.1 eV in going from the spherically symmetrical Ne to H_2O largely accounts for the larger energy difference between the experimentally determined and theoretically calculated binding energies, although it is clear that the basis set then still underestimates the total relaxation energies by 0.5 - 1.0 eV. Nonetheless, the small range of correlation energy differences suggests that an analysis of the orbital contributions to the relaxation energies for the 2s levels should allow for a meaningful comparison between these closely related systems. The result of such an analysis is displayed in Table 7.3.

The trends across the series CH_4 to Ne, and relative contributions from each valence-orbital, closely mirror the behaviour for the 1s core-levels; the total relaxation energies, however, are an order of magnitude smaller.

An analysis of contributions to the total relaxation energy accompanying core-ionization has been extended from diatomic molecules in the previous Chapter, to include triatomic and polyatomic molecules in this Chapter. For simple isomeric systems such as COH^+, HCO^+; HNO, HON; and HCN, HNC, where absolute energy differences between isomers may be small, significant differences in core binding energies may be observed; an analysis of the single

TABLE 7.3 Single Orbital Contributions (in eV) to the total Relaxation Energy Accompanying Ionizations of the Dominantly 2s Valence Orbitals in Ne, HF, H_2O, NH_3 and CH_4

	Molecular Orbital	Single Orbital Relaxation Energy (in eV)
Neon	1s	0.00
	2s	0.29
	2p[a]	0.58
	Sum	2.03
Hydrogen Fluoride	1σ	0.00
	2σ	0.34
	3σ	0.76
	1π[a]	0.75
	Sum	2.60
Water	$1a_1$	0.00
	$2a_1$	0.32
	$1b_2$	0.55
	$3a_1$	0.61
	$1b_1$	0.75
	Sum	2.23
Ammonia	$1a_1$	0.00
	$2a_1$	0.25
	1e[a]	0.44
	$3a_1$	0.66
	Sum	1.79
Methane	$1a_1$	0.00
	$2a_1$	0.18
	$1t_2$[a]	0.37
	Sum	1.29

[a] The figures quoted here give the contribution from ONE of the degenerate orbitals.

orbital relaxation energies can shed some light onto the origin of these differences. The isoelectronic series of first-row hydrides shows that a regular trend in single orbital relaxation energies exists across the Periodic Table. Finally, the method of obtaining single orbital relaxation energies has been applied to the valence (2s) levels of a series of molecules.

CHAPTER EIGHT

A THEORETICAL INVESTIGATION OF THE GROUND AND CORE HOLE STATES OF LINEAR AND BENT NiCO AND NiNO: A PROTOTYPE FOR CO AND NO ADSORBED ON NICKEL.

Non-empirical LCAO MO SCF calculations within the Hartree-Fock formalism have been performed on linear and bent conformations of NiCO, for both the $^3\Delta$ and $^1\Sigma$ states arising from the $3d^9 4s^1$ and $3d^{10}$ electronic configurations of Ni, for ground and core-ionized species. Binding and relaxation energies are computed for the nickel atom, the free ligand (CO) and the adsorbed species (NiCO). Comparison with available experimental data reveals good agreement for the shifts in core binding energies for the bent, $3d^9 4s^1$ NiCO system. The main contribution to these binding energy shifts is found to be due to relaxation effects, which may be rationalized in terms of atomic population and bond overlap changes accompanying core-ionization. The relaxation energies accompanying core-ionization are analyzed in terms of the individual orbital contributions. Density difference contour plots are also used to gain a clearer understanding of the processes involved.

A similar analysis is undertaken for the linear and bent conformations of NiNO, for the $^2\Pi$ state arising from the $3d^{10}$ electronic configuration of Ni.

8.1 Carbon Monoxide Adsorbed on Nickel

8.1.1 Introduction

Theoretical and experimental studies of the chemisorption of simple molecules on transition metal surfaces are

of considerable current interest, as evidenced by the ever-increasing literature in this area.[310] The advent of high resolution photoelectron spectroscopy, particularly with the possibility of studying the photon and angular dependent nature of spectra, has provided a wealth of experimental data[311] on what at first sight might be termed simple systems (e.g. CO on Ni), whilst the development of the requisite LEED theory[312] provides a powerful tool for the interrogation of the surface crystallography for such systems. Despite this intense research activity, many of the fundamental questions are surrounded by controversy and remain unanswered.

In the existing theoretical studies on CO adsorbed on Ni surfaces, three kinds of Ni-CO interaction have been proposed:

(a) Blyholder[313] has performed a Complete Neglect of Differential Overlap (CNDO) calculation on CO chemisorbed on a (111) plane group of ten Ni atoms. The bonding of the carbon atom to the nickel atom largely involves Ni s and p orbitals, with little contribution from the d orbitals.

(b) Doyen and Ertl[314] use an Anderson Model Hamiltonian[315] in their approach, including overlap. They consider only the coupling of the $2\pi^*$ and 5σ orbitals of CO to the metal d-band; all other approaches which do not have this restriction predict, however, that the inclusion of the s-p band of nickel is essential for an understanding of the bonding. This model should be extended to include the s-p band and the 4σ and 1π orbitals of CO before it can be used to explain the Ni-CO photoelectron spectrum.

(c) Batra and Bagus[316] considered a model cluser consisting of CO and five nickel atoms, for which they calculated the electronic structure using the spin-unrestricted SCF-statistical-exchange scattered-wave (SCF-Xα-SW) method. They find not only strong interaction between the CO 5σ orbital and an appropriate combination of metal p and d, and also some s, orbitals, but also interaction between the CO 1π orbital with metal p and d orbitals, indicating that CO bonding to nickel involves metal s, p as well as d orbitals.

In all of these calculations, it has been assumed that the molecular axis of the adsorbed CO is perpendicular to the surface, with C pointing to the Ni. Recent angular-resolved UPS measurements,[313,318] combined with a theoretical study of the angular dependence of the UV photoionization cross-sections of gaseous CO,[319] support this assumption.

The comparison of PES data of adsorbed molecules with those of the respective free molecules plays an important role in the study of these systems. From the theoretical standpoint, the major points of issue concern the assignment of valence energy levels for the chemisorbed system and the relationship to the corresponding levels for the free molecule. The question which is most germane to this issue is the role of changes in relaxation energy contributions.

In a recent paper, Bagus and Hermann[320] established with *ab initio* calculations that even for an idealized NiCO molecule, the changes in relaxation energy with respect to the free ligand differed substantially for the various ionized states. They also investigated the shift in core binding energies for the ligand, and found that for the ground-state

of $NiCO(^3\Delta)$, the significant shifts computed without taking relaxation effects into account virtually disappeared when relaxation was included, employing the ΔSCF formalism. Even when they extended the system to a linear Ni-Ni-CO model,[321] only a slight decrease (~0.5 eV) in binding energy was observed. This is in contrast to the experimental data,[280] which reveal substantial shifts to lower binding energy for both the C_{1s} and O_{1s} levels in going from the free ligand to the chemisorbed state, after taking due allowance for the difference in reference levels. A significant feature, however, of the published XPS data for the chemisorption of small molecules on transition metals[310] is the clear indication that shifts for the metal core-levels are small; this has been attributed to the substantial contribution to the relaxation energy provided by the metal lattice.

The LEED studies reported to date[312] have largely been concerned with the restructuring, or lack thereof, in going from a clean surface to the chemisorbed system, and have therefore largely concentrated on changes in interatomic distances within a given surface layer. In particular cases with good experimental data, it is possible to infer the geometric parameters of the chemisorbed species. In a LEED study of CO adsorption on Ni(100), Tracy[322] suggested that the CO molecules occupied four-fold symmetric adsorption sites; most calculations assume the four-fold Ni(100) hollow as the adsorption site. An investigation by Andersson[323] suggested that the CO molecules were linearly bonded to the top sites of the Ni(100) surface net, also obeying four-fold symmetry. A detailed LEED intensity analysis by Pendry and Andersson[324] confirms this suggestion, and furthermore implies that the

vertical spacings between the Ni and C, and the C and O layers, are 1.80 ± 0.10 Å and 0.95 ± 0.10 Å, respectively. To accommodate this, Andersson and Pendry[324] have proposed that for CO chemisorbed on Ni(100), the CO is tipped at an angle of $34^{\circ} \pm 10^{\circ}$ with respect to the surface, the Ni-CO bond-length being essentially the same as in $Ni(CO)_4$.

In the previous two Chapters, it has been shown that the substantial contributions to shifts in core binding energies, which in appropriate systems are attributable largely to relaxation effects, may be partitioned amongst contributions arising from reorganization of the individual valence-orbitals. Extensive studies have been made of the core-ionized states of CO, and for prototype systems in which CO interacts with a σ electron acceptor. As one aspect of this work, the changes in contribution to relaxation energies consequent upon going from CO to HCO^+ in both a linear and bent conformation were studied. The extensive σ-π mixing consequent upon going from a linear to a bent conformation results in significant changes in relaxation energies. This, taken in conjunction with the theoretical results already published on linear NiCO indicating essentially zero shift for the C_{1s} and O_{1s} levels with respect to the free molecule, prompted the investigation of the core hole states of a *bent* NiCO system.

In this section, an account of a theoretical investigation of the neutral molecule and core hole states of a linear and bent NiCO system is presented. The prime focus has been on computing the shifts in core binding energies, and changes in relaxation energies, in going from CO to the NiCO system, and as an ancillary investigation, the energetics of deformation from a linear to bent system have been considered.

8.1.2 Computational Details

Ab initio LCAO MO SCF calculations within the Hartree-Fock formalism were performed for core and selected hole-states of NiCO (linear and bent), Ni (free atom) and CO. The previously discussed STO-6.33G + P basis set was used as before, to enable comparison to be made with the calculations on HCO^+ and CH_3CO^+, discussed in the previous Chapter.

The interatomic distances for the linear Ni-CO system were chosen to be the experimental values for the $Ni(CO)_4$ molecule[325] (Ni-C = 3.477 au, C-O = 2.173 au). For the bent Ni-CO system, bond-distances were kept constant, and an Ni-$\hat{C}$-O angle of 146° was used. Calculations on the free CO molecule were performed at the experimental bond-length (2.131 au).[214]

For the NiCO systems, calculations were performed for the $^3\Delta$ state resulting from a $3d^9\ 4s^1$ electronic structure of the Ni atom, and for the $^1\Sigma$ state arising from a $3d^{10}$ configuration of the Ni atom. The hole-state calculations for the $^3\Delta$ ground-state were all performed for the $^4\Delta$ states, since it is known that the doublet-quartet multiplet splitting is likely to be small, due to the insignificant exchange integrals between the open-shell Ni and CO-like molecular orbitals. In computing the relaxation energies for the open-shell ground-state systems, the "Koopmans'" binding energy was taken as the difference between the energy of the hole-state corresponding to completely frozen orbitals and the energy of the ground-state system.

The single orbital contributions to the total relaxation energy were calculated as described in Chapter 6;

density difference contours for selected orbitals were also performed. In the ground-state of the NiCO systems, the CO-like orbitals retain much of their molecular character, and it is convenient to refer to these levels using the CO notation, with the addition of a tilde: $5\tilde{\sigma}$, $1\tilde{\pi}$, etc.

8.1.3 Results and Discussion

(a) Relative Energies

Previous theoretical investigations of NiCO of comparable quality have been restricted to the $^3\Delta$ ground-state and the derived ionized states of the ligand.[320,321] As a starting point therefore, the relative energies of the linear and bent conformations in both the ground-state $^3\Delta$ and $^1\Sigma$ states are considered. Calculations on the nickel atom and on CO at its equilibrium bond-length also provide an estimate for the bond energy in NiCO; the data are summarized in Table 8.1.

The most interesting and significant feature of the data presented in Table 8.1 is that the energy of the linear and bent conformations for the ground-state of NiCO are closely similar, at least for Ni-C and C-O bond-lengths identical to those in $Ni(CO)_4$. Although these calculations are only likely to provide a crude yardstick of the overall energetics, it would seem to indicate that bent conformations should be included as a starting possibility in any realistic discussion of experimental data relating to the NiCO system. Although the ground-state of the nickel atom (^2F) corresponds to the $3d^8\ 4s^2$ configuration, the energy for the (^3D) $3d^9\ 4s^1$ configuration is only slightly higher (~ 0.09 eV), and since the state for the NiCO system involving a nominal $3d^8\ 4s^2$

TABLE 8.1 Computed Total Energies for NiCO (linear and bent), Ni atom, and free CO

	Total Energy (in au)	Difference (in kcal mol^{-1})
NiCO		
$^3\Delta$ linear	-1616.493755	(0)
bent, 17°	-1616.495044	-0.81
bent, 34°	-1616.495420	-1.04
$^1\Sigma$ linear	-1616.463863	+18.75
bent, 17°	-1616.462695	+19.49
bent, 34°	-1616.458325	+22.23
Ni		
$3d^9\ 4s^1$	-1503.906627	(0)
$3d^{10}$	-1503.798014	+68.15
CO	-112.580713	-
Ni + CO → NiCO (linear)		
$3d^9\ 4s^1$ $^3\Delta$		-4.03
$3d^{10}$ $^1\Sigma$		-53.42

configuration is rather high in the energy manifold, the calculations here have concentrated on the $3d^9\ 4s^1$ and $3d^{10}$ configurations. The energy gap between the $3d^9\ 4s^1$ and $3d^{10}$ configurations for the Ni atom (calculated 2.96 eV; experimental 1.7 eV) decreases in going to both the linear and bent NiCO system (0.81 eV and 1.0 eV respectively), as might have been anticipated on the basis of simple qualitative arguments. The calculations would indicate however, that for the $3d^{10}$ configuration, the linear system is considerably stabilized;

this could have important ramifications with regard to any discussion of vibrational fine-structure accompanying photoionization. The interaction energies of CO with Ni are calculated to be -4.0 kcal mol^{-1} and -53.4 kcal mol^{-1} for the $3d^9\ 4s^1$ and $3d^{10}$ configurations respectively; however, these are for hypothetical processes, and since molecular extra-correlation energies are not included, it is difficult to compare these with any experimental data. One interesting point which does emerge when the data for the core-ionized species are considered, however, is that relatively weak interactions can produce profound changes in ionization and relaxation energies, a feature of XPS which has previously been discussed for other systems.

There has been discussion about whether the order of the 5σ and 1π ionization potentials of CO (in the gas phase the 1π ionization potential is greater than the 5σ) is reversed when this molecule is adsorbed on Ni. Gustafsson *et al.*[326] assign the adsorbed ionization potentials in the same order as observed in the free CO molecule; Brundle and Carley[280] have also used this assignment. Williams *et al.*,[327] however, make the reverse assignment, based on an analysis of angle-resolved UV photoemission studies. Although the inadequancies of the use of Koopmans' Theorem are well-known, Figure 8.1 shows the orbital energies for free CO, $^3\Delta$ linear and bent NiCO, and $^1\Sigma$ linear and bent NiCO. From this, the 5σ and 1π ionization potentials of CO are seen to increase on going to the linear $^3\Delta$ NiCO, the order of the levels changing on adsorption. Bending the NiCO system does not affect the ordering of the levels, though the $5\tilde{\sigma}$-$1\tilde{\pi}$ ordering in both linear and bent NiCO is the same as in the free CO molecule. Clearly,

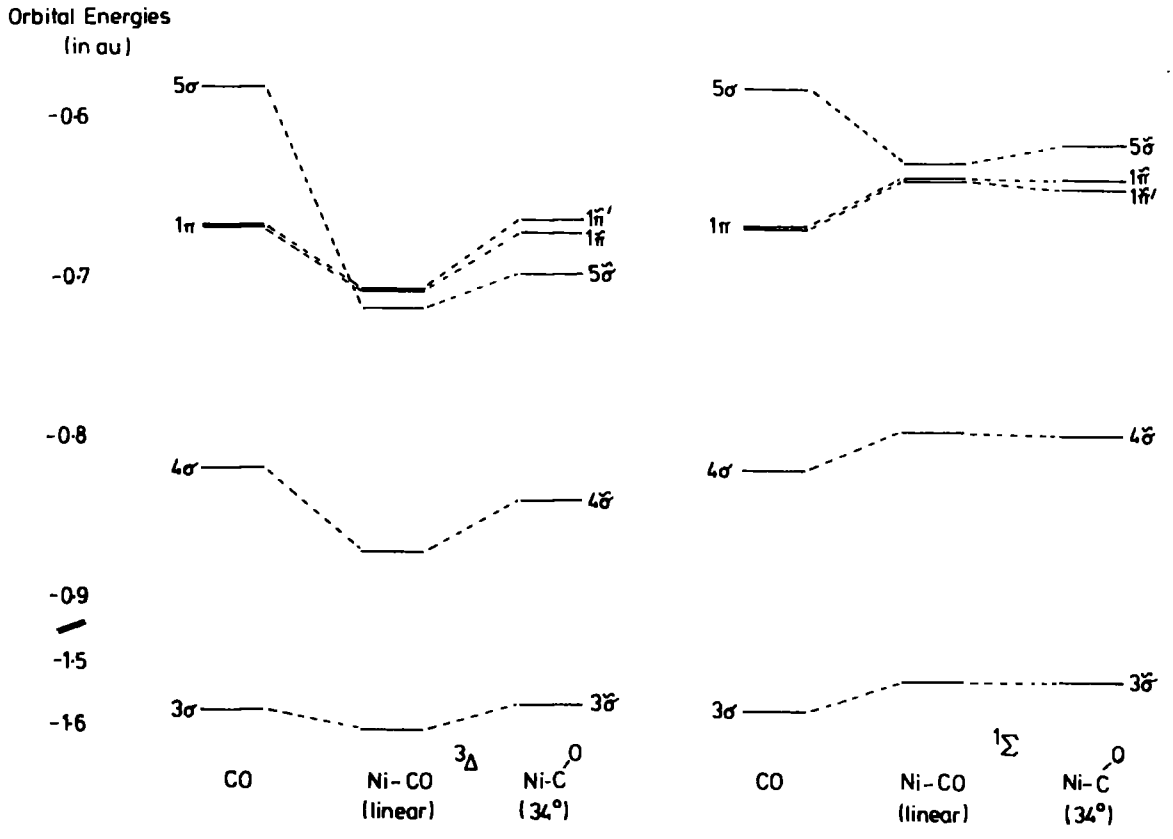

Fig. (8.1) Orbital energies for CO, NiCO (linear) and NiCO (bent).

Koopmans' Theorem is inadequate to discuss these changes in relative ordering, since both relaxation and more importantly, correlation effects are neglected.

(b) Core binding energies and relaxation energies

The prime motivation for this work has been to investigate the at-first-sight rather surprising result that previous theoretical investigations[320,321] have suggested: viz., that for a prototype system for CO chemisorbed on nickel (linear NiCO), there is virtually no shift of the ligand core-levels in going from the free ligand to the complex. The analysis of Bagus and Hermann reveals that this arises from a compensating effect of relaxation phenomena; these will

depend strongly on the geometry, particularly in going from a linear to a bent conformation. The core hole states of linear and bent NiCO for both the $3d^9\ 4s^1$ and $3d^{10}$ configurations have therefore been considered. The results are shown in Table 8.2.

It is immediately evident that bending has a dramatic influence on the core binding energies for the ligand core-levels, and that this is largely attributable to the substantial increases in relaxation energies. The results for the linear NiCO ($^3\Delta$) agree well with those previously reported,[320,321] and confirm the small changes in binding energy for the ligand core-levels. In addition, the calculations reported here show that the shifts for the metal core-levels are also small. For the corresponding bent conformation, the situation is transformed; whereas the metal core-levels are predicted to remain largely unaffected by such a distortion, the ligand core-levels are strongly shifted to lower binding energy, the shifts with respect to the free ligand being $\sim$5 eV and $\sim$6.5 eV for the O_{1s} and C_{1s} levels respectively for angles of 17^o and 34^o. This is in remarkably good agreement with experimental estimates based on data for CO chemisorbed on polycrystalline Ni surfaces for which due allowance has been made for the difference in reference levels,[280] where for the O_{1s} and C_{1s} levels, the estimated experimental shifts are 5.4 eV and 5.1 eV, respectively, to lower binding energy compared with the free ligand. The small shift calculated for the Ni_{2s} levels is also consistent with the available experimental data, particularly since in going from a free NiCO molecule to CO chemisorbed on a Ni surface the extra-molecular

TABLE 8.2 Calculated ΔSCF Binding Energies and Relaxation Energies (in eV)

	Ni_{2s}				O_{1s}				C_{1s}			
	ΔSCF Binding Energy	ΔB.E.	Relaxation Energy	ΔR.E.	ΔSCF Binding Energy	ΔB.E.	Relaxation Energy	ΔR.E.	ΔSCF Binding Energy	ΔB.E.	Relaxation Energy	ΔR.E.
CO					543.71	(0)	19.91	(0)	299.64	(0)	10.79	(0)
$Ni(3d^9 4s^1)$	998.63	(0)	20.25	(0)								
NiCO $^3\Delta$ linear	998.82	0.19	21.66	1.41	544.09	0.38	20.88	0.97	300.21	0.57	11.94	1.15
bent, 17°	998.86	0.23	21.61	1.36	538.72	-4.99	25.80	5.89	293.06	-6.58	18.65	7.86
bent, 34°	998.91	0.28	21.51	1.26	538.75	-4.96	25.05	5.14	293.12	-6.52	17.89	7.10
$Ni(3d^{10})$	991.54	(0)	21.53	(0)								
NiCO $^1\Sigma$ linear	992.96	1.42	23.54	2.01	541.29	-2.42	21.32	1.41	297.42	-2.22	12.72	1.93
bent, 17°	992.97	1.43	23.51	1.98	541.05	-2.66	21.55	1.64	296.55	-3.09	13.56	2.77
bent, 34°	992.98	1.44	23.43	1.90	540.90	-2.81	21.68	1.77	296.28	-3.36	13.75	2.96

contributions to relaxation energies would be expected to reduce the magnitude of this shift with respect to the sub-surface and bulk even further.

The comparable results for the $^1\Sigma$ configuration show a much smaller difference between the linear and bent arrangement, since the relaxation energies are closely similar. This emphasizes the substantial differences in electronic reorganization for differing valence-electron distributions.

(c) Single Orbital Relaxation Energies

An analysis of the relaxation energies accompanying core-ionization along the lines presented in the previous two Chapters has been undertaken for the $^3\Delta$ and $^1\Sigma$ linear and bent NiCO systems. It is gratifying to note that even for such complex systems (in terms of the number of electrons and basis functions), such an analysis is still feasible. Figure 8.2 shows the single orbital contributions to the total relaxation energy accompanying C_{1s} core-ionization in CO, linear and bent NiCO ($^3\Delta$ and $^1\Sigma$). For the $^3\Delta$ NiCO systems, the main change in going from free CO to the linear NiCO is in the 5σ and 4σ contributions, those for 3σ and 1π remaining essentially constant, whilst the 5σ decreases and 4σ increases significantly. This might have been anticipated on the grounds that since the C lone pair orbital (5σ) is now involved in the bonding to Ni, it cannot contribute as much to the relaxation as it did in the free CO molecule; accordingly, a more significant contribution must come from the essentially O lone pair orbital (4σ). On going to the bent NiCO system, the previously degenerate $1\tilde{\pi}$ orbitals now split, the contribution from the remaining $1\tilde{\pi}$ orbital staying effectively the

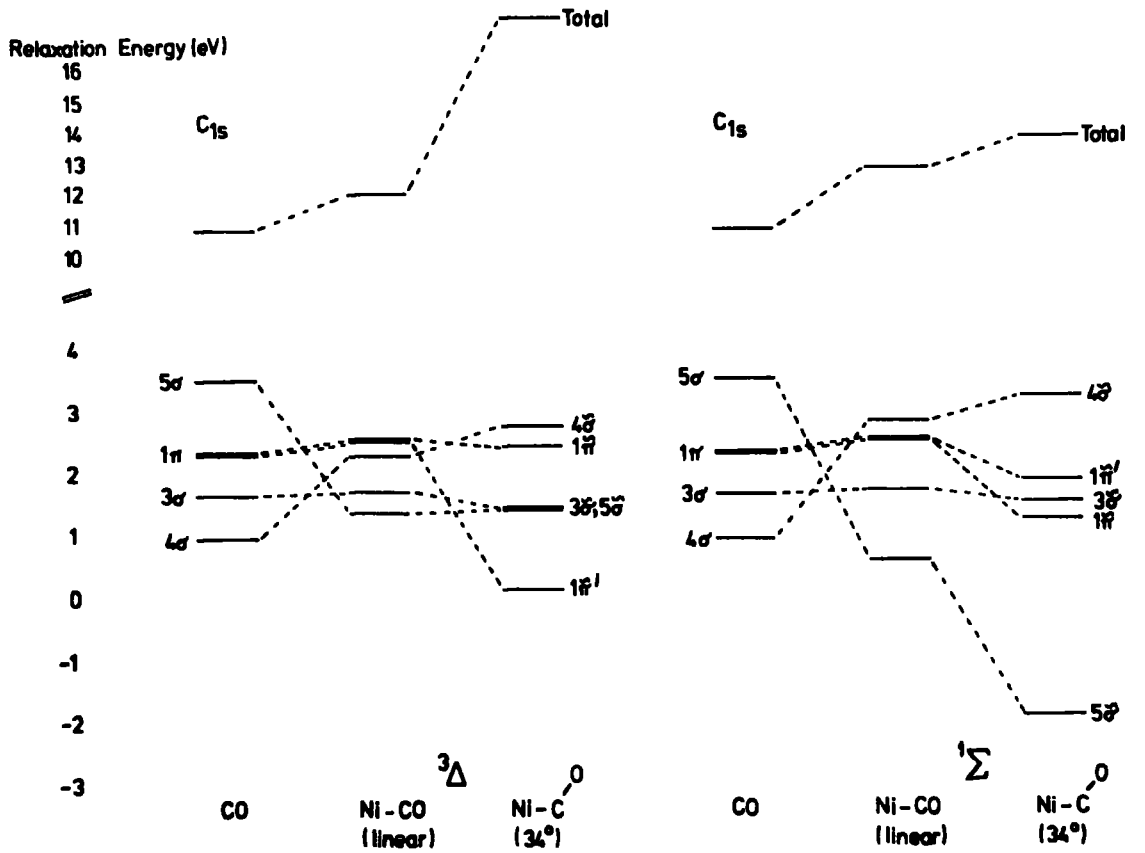

Fig. (8.2) Single orbital relaxation energies accompanying C_{1s} core-ionization.

same as before, whilst the in-plane pseudo π-orbital (designated as $1\tilde{\pi}'$) decreases in its contribution, suggesting that this orbital is now involved in the Ni-CO bonding scheme. The remaining orbitals stay virtually unchanged, save for the $4\tilde{\sigma}$ orbital, which again increases its contribution to the relaxation.

Similar behaviour, in general, is observed for the $^1\Sigma$ NiCO systems. On going from free CO to linear NiCO, the 3σ and 1π orbital contributions remain unchanged, the 5σ decreases and the 4σ increases. The behaviour on bending the NiCO system is somewhat different than that observed in the $^3\Delta$ case, however; now the $1\tilde{\pi}$ and $1\tilde{\pi}'$ orbitals

both contribute less than the previously degenerate $1\tilde{\pi}$ orbitals, but the most dramatic change is a decrease in the $5\tilde{\sigma}$ orbital contribution, making this contribution quite large and negative.

The orbital contributions accompanying O_{1s} core-ionization are shown in Figure 8.3. In this case, the

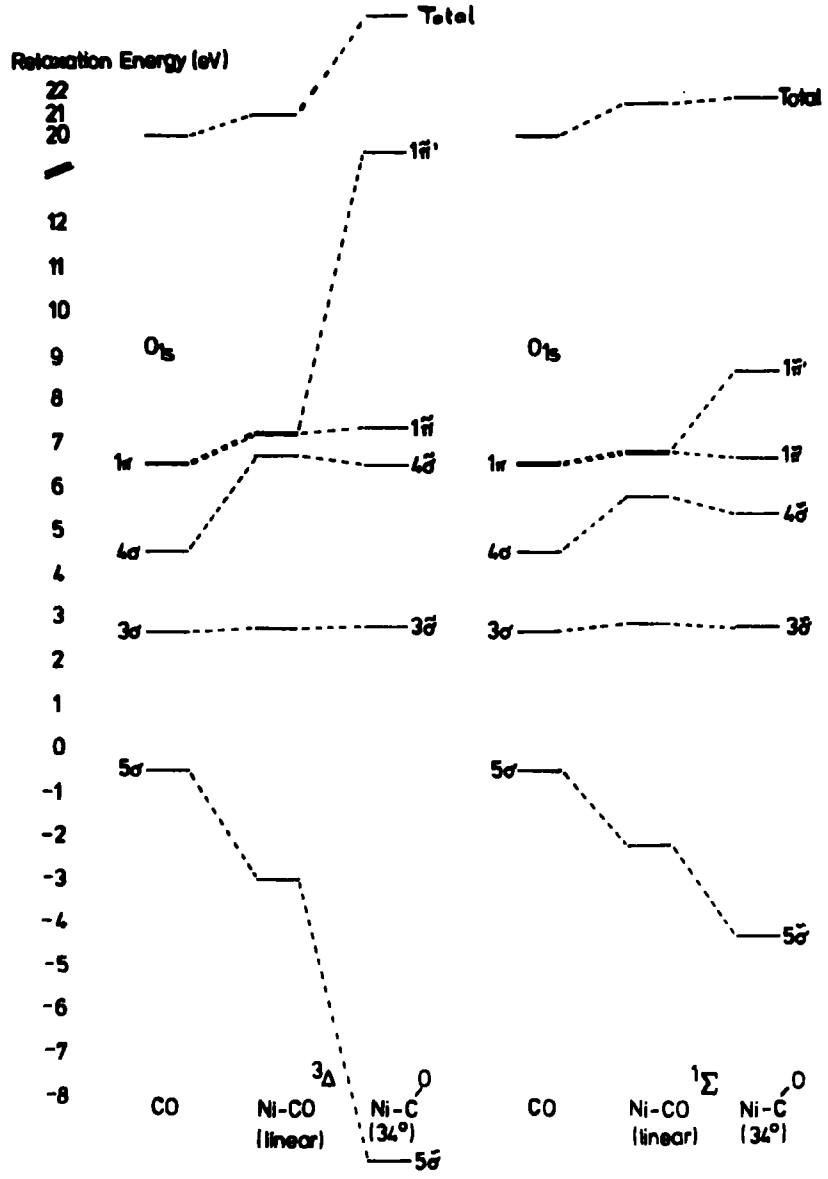

Fig. (8.3) Single orbital relaxation energies accompanying O_{1s} core-ionization.

span in single orbital relaxation energies is much greater than in the case of C_{1s} core-ionization. As expected, on going from free CO to linear NiCO, the 3σ and degenerate 1π

orbital contributions remain much the same, both for the $^3\Delta$ and $^1\Sigma$ cases. As for the C_{1s} core-ionization, the 5σ contribution to the relaxation decreases dramatically to a value of $\sim$-3 eV in the case of $^3\Delta$ NiCO, and $\sim$-2 eV for $^1\Sigma$ NiCO. This is partially offset by the concomitant increase in the 4σ contribution for both $^3\Delta$ and $^1\Sigma$ cases.

On going to the bent NiCO conformations, the degenerate $1\tilde{\pi}$ orbitals split, the $1\tilde{\pi}'$ contribution in this case increasing, as opposed to the C_{1s} core-ionized case, where the $1\tilde{\pi}'$ orbital contributions decreased. This may intuitively be rationalized on the grounds that the portion of the $1\tilde{\pi}'$ orbital nearest the Ni is in the vicinity of the C atom, and thus on C_{1s} core-ionization in the bent species, significant relaxation from the $1\tilde{\pi}'$ orbital in this region is no longer possible. For O_{1s} core-ionization, however, the large portion of the $1\tilde{\pi}'$ in the vicinity of the O atom is not involved in bonding to the Ni atom, and may thus relax to a greater extent than for the C_{1s} case. For the $5\tilde{\sigma}$ orbital, as in the case of C_{1s} core-ionization, this contribution decreases even more on bending the NiCO. It is worth pointing out the similarity in behaviour of the orbital contributions in the $^3\Delta$ and $^1\Sigma$ NiCO systems for both C_{1s} and O_{1s} core-ionization, even though the overall total relaxation energies are significantly greater in the $^3\Delta$ NiCO systems.

The effect of Ni_{2s} core-ionization on the contributions from the CO-like orbitals to the total relaxation energy has also been investigated, as shown in Figure 8.4. For the $^3\Delta$ NiCO configuration, the contributions from all the orbitals save the $4\tilde{\sigma}$ orbital decrease, compared with C_{1s} core-

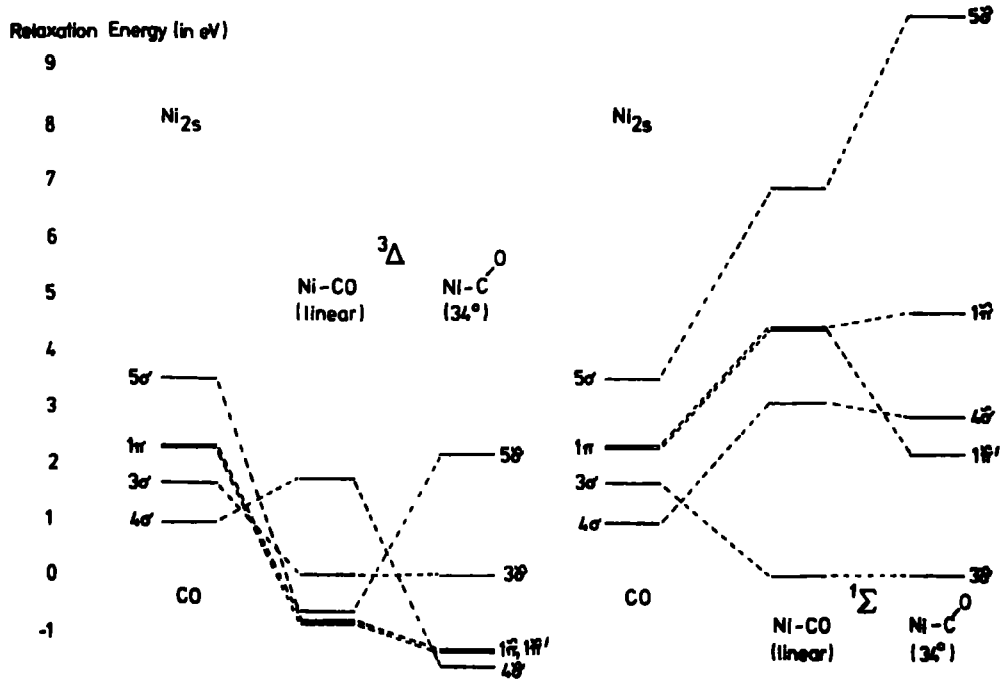

Fig. (8.4) Single orbital relaxation energies accompanying Ni_{2s} core-ionization.

ionization in free CO. In linear NiCO, the $3\tilde{\sigma}$ contribution is essentially zero, whilst the $1\tilde{\pi}$ and $5\tilde{\sigma}$ contributions are small and negative. The main contribution from the CO-type NiCO orbitals comes from the $4\tilde{\sigma}$ orbital. On bending the NiCO, the $3\tilde{\sigma}$ and both the $1\tilde{\pi}$ and $1\tilde{\pi}'$ contributions remain similar in magnitude, but the $4\tilde{\sigma}$ and $5\tilde{\sigma}$ contributions respectively decrease and increase significantly.

Quite a different picture emerges for the $^1\Sigma$ NiCO configurations. Here the $5\tilde{\sigma}$, $1\tilde{\pi}$, and $4\tilde{\sigma}$ orbitals all contribute more to the relaxation accompanying Ni_{2s} core-ionization, compared with C_{1s} core-ionization in free CO. Whilst the $3\tilde{\sigma}$ contribution is virtually zero for the linear NiCO, significant contributions to the relaxation are found for $4\tilde{\sigma}$, $1\tilde{\pi}$ and especially the $5\tilde{\sigma}$ orbitals. Indeed, whilst the $3\tilde{\sigma}$, $4\tilde{\sigma}$ and $1\tilde{\pi}$ orbitals remain much the same on bending

the NiCO, the $5\tilde{\sigma}$ orbital contribution increases even more, whilst the $1\tilde{\pi}'$ contribution decreases.

For the Ni_{2s} core-ionization, a comparison may be made for the Ni-type orbitals, both in free Ni atom, and the NiCO complexes, as shown in Figure 8.5. For the

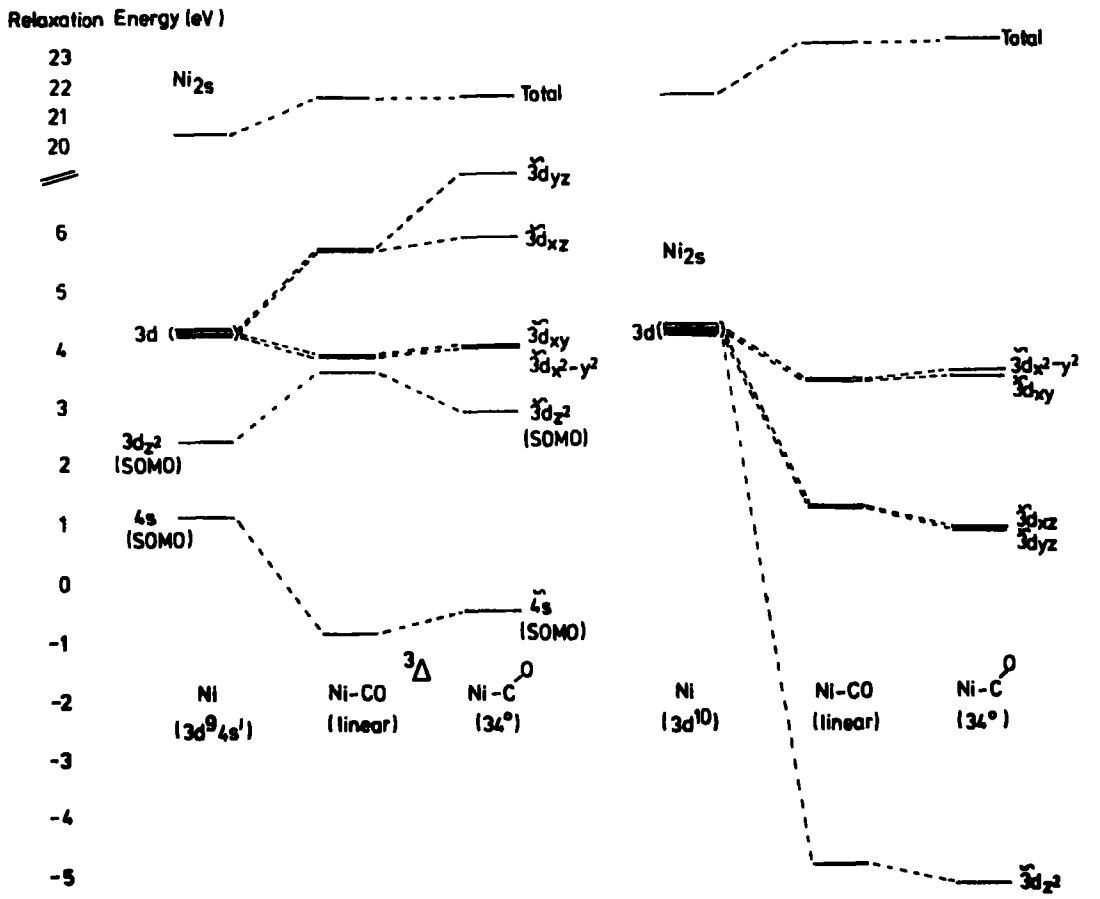

Fig. (8.5) Single orbital relaxation energies accompanying Ni_{2s} core-ionization.

$3d^9\ 4s^1$ configuration of free Ni atom, the contributions to the relaxation energy from the two singly-occupied MO (SOMO), the $3d_{z^2}$ and 4s orbitals, are less than the contributions from the remaining four degenerate 3d doubly-occupied MO (DOMO). On going to the linear NiCO, the $3d_{z^2}$ contribution increases, whilst the 4s contribution decreases; the 3d orbitals are no longer degenerate, but split into two degenerate pairs. The

changes on bending the NiCO system are relatively small, the previously degenerate $3\hat{d}_{yz}$ and $3\hat{d}_{xz}$ contributions splitting.

The pattern obtained for the $^1\Sigma$ NiCO configuration is quite different. In the free $3d^{10}$ atom, the five 3d DOMO are degenerate; on going to the linear NiCO, they split into the $3\hat{d}_{z^2}$, which has a strong negative contribution to the relaxation energy, the $3\hat{d}_{xz}$, $3\hat{d}_{yz}$ orbitals, which have a small contribution, and the $3\hat{d}_{xy}$, $3\hat{d}_{x^2-y^2}$ orbitals. This ordering is reasonable, since the Ni-C-O axis is the z-axis; naively, for this situation uncomplicated by SOMO, the strongly bonding $3\hat{d}_{z^2}$ orbital contributes less than the slightly-bonding $3\hat{d}_{xz}$, $3\hat{d}_{yz}$ orbitals, which in turn contribute less than the $3\hat{d}_{xy}$, $3\hat{d}_{x^2-y^2}$ orbitals which do not interact with the CO system. Indeed, this pattern remains unchanged on going to the bent NiCO system.

(d) Mulliken Population Analysis

The results of Mulliken population analyses for the ground and core hole states of the NiCO systems are displayed in Table 8.3. For the ($^3\Delta$) linear NiCO, the atomic populations on the nickel, carbon and oxygen atoms are 0.12, 0.46 and -0.57 respectively. The net effect of bending the molecule is an overall electron transfer from Ni to C, this arising largely from a change in the σ bond overlap contributions. Indeed, on going from the linear to bent arrangement, there are significant changes in both the Ni-C and C-O bond overlap populations, as might have been naively anticipated on the basis of the lowering in total energy. By contrast, for the $3d^{10}$ configuration, there is a relatively small change in populations in going from the linear to bent arrangement, and

TABLE 8.3 Mulliken Population Analysis

	Gross Atomic Population			Bond Overlap	
	Ni	C	O	Ni-C	C-O
$^3\Delta$ NiCO (linear)					
Ground state	0.1158	0.4589	-0.5747	-0.4836	0.1595
Ni 2s	0.9976	0.4809	-0.4785	-0.7973	0.1734
C 1s	0.2679	0.9310	-0.1983	-0.3737	0.0189
O 1s	0.3505	0.8640	-0.2145	-0.5701	-0.0809
$^3\Delta$ NiCO (bent, 34°)					
Ground state	0.2794	0.3049	-0.5842	-0.2988	0.2014
Ni 2s	1.0947	0.3782	-0.4729	-0.6510	0.2149
C 1s	1.0322	0.3236	-0.3558	-0.1439	0.0274
O 1s	1.1066	0.2116	-0.3181	-0.1996	-0.0681
$^1\Sigma$ NiCo (linear)					
Ground state	0.3100	0.3174	-0.6273	-0.0005	0.1705
Ni 2s	1.1244	0.3876	-0.5120	-0.2557	0.1923
C 1s	0.7635	0.5544	-0.3179	0.0063	0.0298
O 2s	0.7893	0.4881	-0.2774	-0.0549	-0.0719
$^1\Sigma$ NiCO (bent, 34°)					
Ground state	0.3005	0.3038	-0.6044	-0.0003	0.1961
Ni 2s	1.1243	0.3647	-0.4890	-0.2459	0.2257
C 1s	1.0974	0.2599	-0.3573	-0.0437	0.0260
O 1s	0.9566	0.3443	-0.3009	-0.0769	-0.0705

this is consistent with the small differences computed for the binding and relaxation energies. Comparison of the $^3\Delta$ and $^1\Sigma$ states shows an overall increase in electron density on carbon and oxygen at the expense of nickel. A significant feature of the bond overlap terms for the $^1\Sigma$ ($3d^{10}$) configuration is the substantially increased population for the Ni-C bond; this is consistent with the large difference in computed energy of interaction of CO with a nickel atom.

The creation of a core-hole on nickel for the $^3\Delta$ linear state of NiCO gives rise to an almost unit decrease in population on the nickel, the populations on carbon and oxygen decreasing only slightly (<0.1 eV). As might have been anticipated, the creation of a core-hole increases the electron accepting capability of the nickel, whilst decreasing the important bonding interaction provided by reverse π-donation to CO. In consequence, the overall Ni-C bond overlap decreases, whilst that for the C-O bond increases. For the bent arrangement, the changes in electron population are closely similar; this is reflected in the relatively minor changes in both relaxation and binding energies for the Ni_{2s} level in going from the linear to bent system.

The situation for the C_{1s} and O_{1s} levels is considerably different. Thus for the linear NiCO system, creation of a core-hole on carbon leads to substantial valence-electron transfer from oxygen and to a lesser extent nickel, whilst for the O_{1s} core hole state, the electron transfer is largely at the expense of carbon, with again substantially less electron transfer from the nickel. For the bent conformation, electron transfer from the metal is now so effective that for both the

C_{1s} and O_{1s} hole-states, the electron populations on the atoms on which the core-holes are located differ little from those for the neutral molecule, providing a rationale for the substantial increases in relaxation energy on going to the bent species. The bond overlap populations suggest that for both the linear and bent systems, creation of a core-hole on nickel will lead to a longer Ni-C equilibrium bond-length, and correspondingly that the O_{1s} core-ionized species will also give rise to an increased C-O equilibrium bond-length. For the C_{1s} core-ionized states however, the equilibrium bond-lengths for the Ni-C and C-O bonds should be somewhat shorter than for the ground-state. For the $^1\Sigma(3d^{10})$ linear molecule, there is little change in electron populations on Ni, C and O in going to the bent conformation for the Ni_{2s} core hole state. There are, however, differences in the changes in population consequent upon creation of an O_{1s} or C_{1s} core-hole in the linear or bent system, and for the latter this is again manifest in an increased electron migration from the metal.

(e) Density Difference Contours

The reorganization of the valence electron density consequent upon core-ionization may be inferred pictorially from density difference contours. Together with the single orbital relaxation energies and Mulliken population analyses outlined in the previous two sections, this should provide a complete picture of the reorganization processes accompanying core-ionization. In these figures, as before, dashed lines (negative contours) represent an *increase* in electron density in the core-hole state species.

Figure 8.6 shows the reorganization accompanying C_{1s} and O_{1s} core-ionization in CO, linear and bent $^3\Delta$ NiCO for

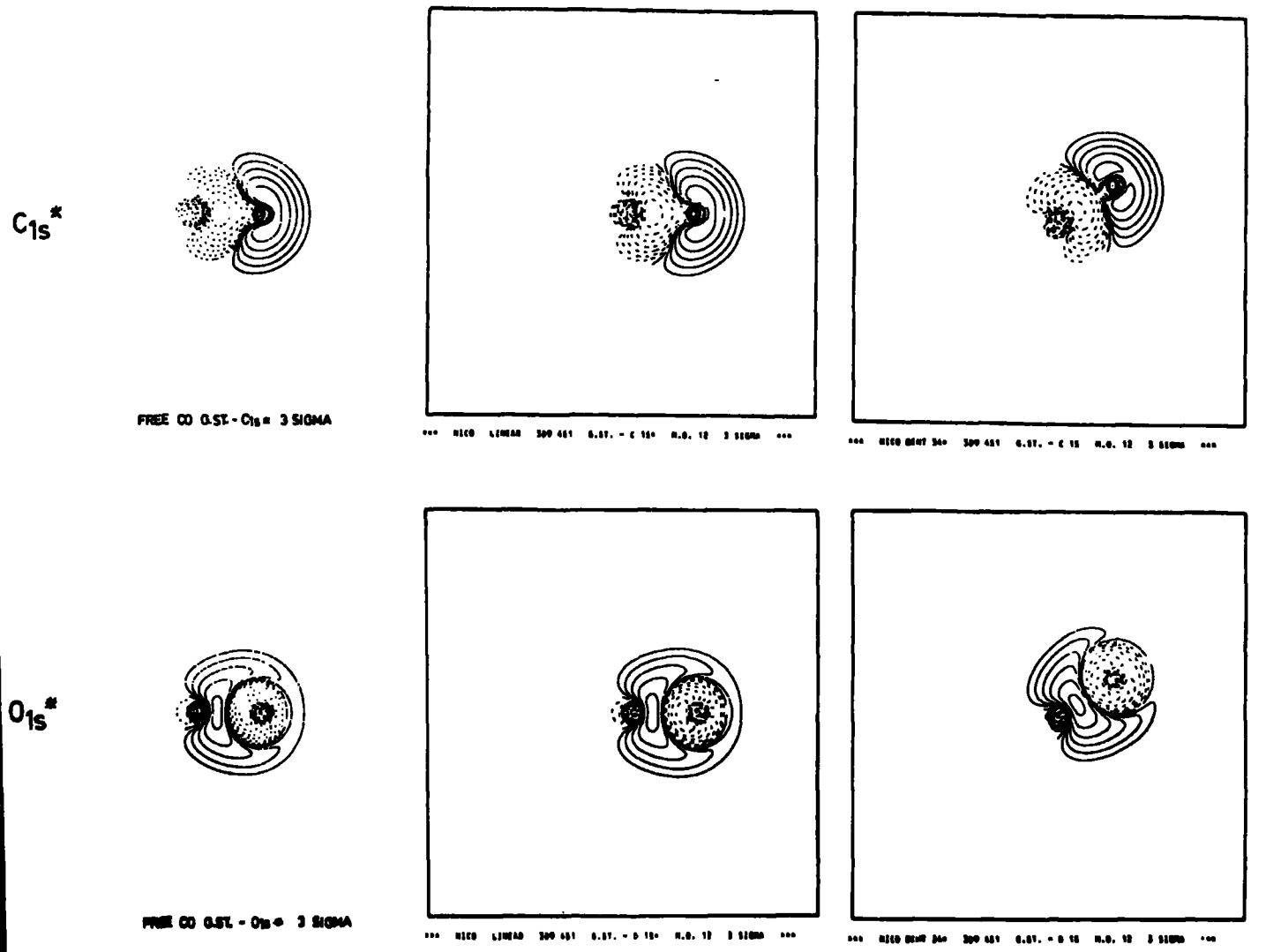

Fig. (8.6) Density difference contours for the 3σ orbital

the 3σ orbital. As anticipated from the single orbital relaxation energies shown in Figures 8.3 and 8.4, the contribution from this orbital is remarkably similar for all three environments, implying that the $3\tilde{\sigma}$ orbital in NiCO is not involved in the Ni-CO bonding.

For the 4σ orbital, shown in Figure 8.7, the overall reorganization pattern in both the linear and bent forms of NiCO is similar to that in the free CO; however, there is now some interaction with the nickel atom, increasing on going from the linear to bent conformation. This results in

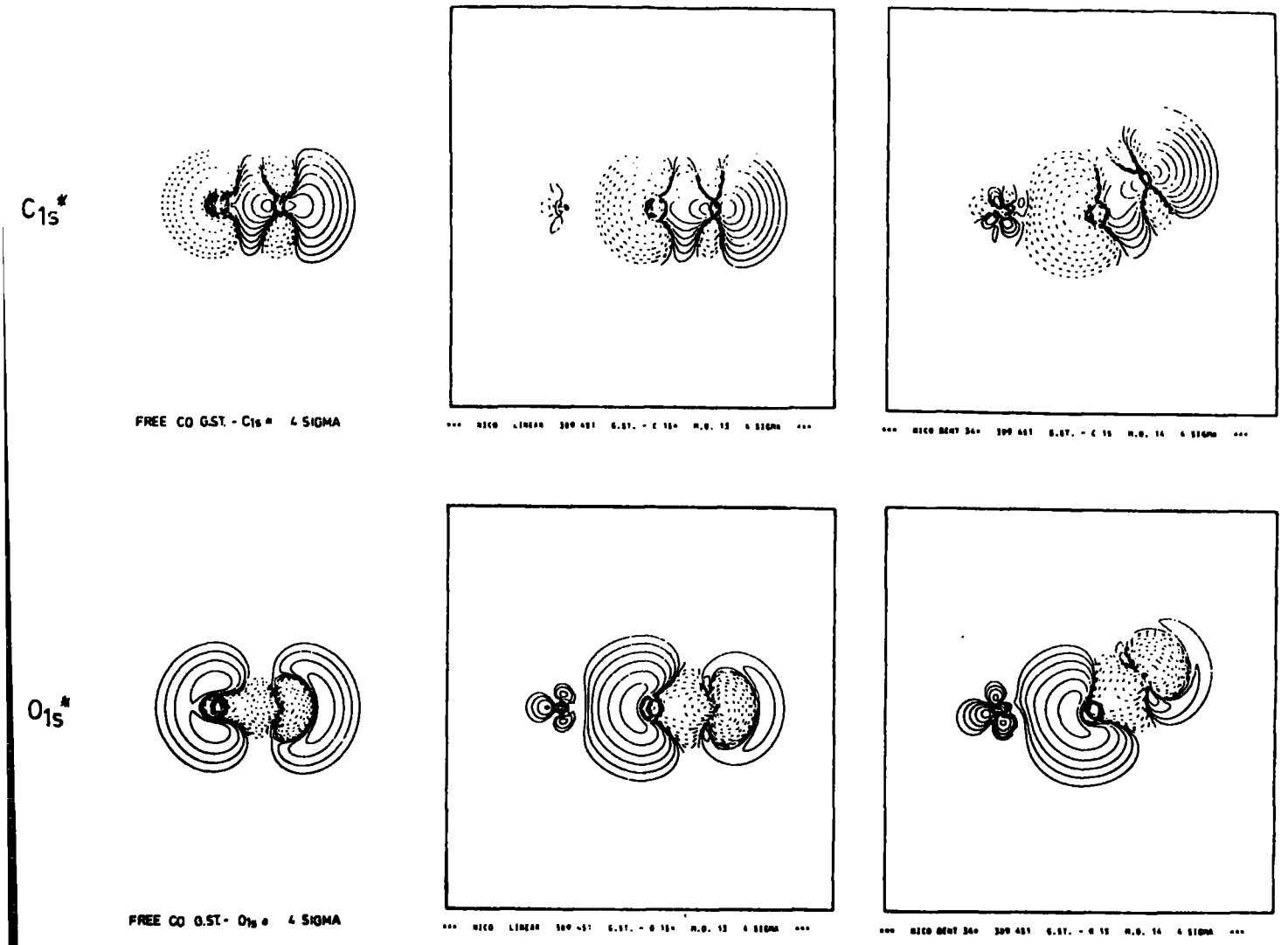

Fig. (8.7) Density difference contours for the 4σ orbital.

an increase in the contribution from the $4\tilde{\sigma}$ orbital to the total C_{1s} and O_{1s} relaxation energies.

Figure 8.8 shows the density difference contours for the 5σ orbital. On going from the free CO to the linear NiCO, it is clear that there is some increase in valence-electron flow from the carbon lone pair, and now also the nickel atom, to the oxygen lone pair, on C_{1s} core-ionization. Similarly, for O_{1s} core-ionization, the electron flow from the carbon lone pair is no longer seen, more electron electron-flow now arising from the oxygen lone pair. This results in the

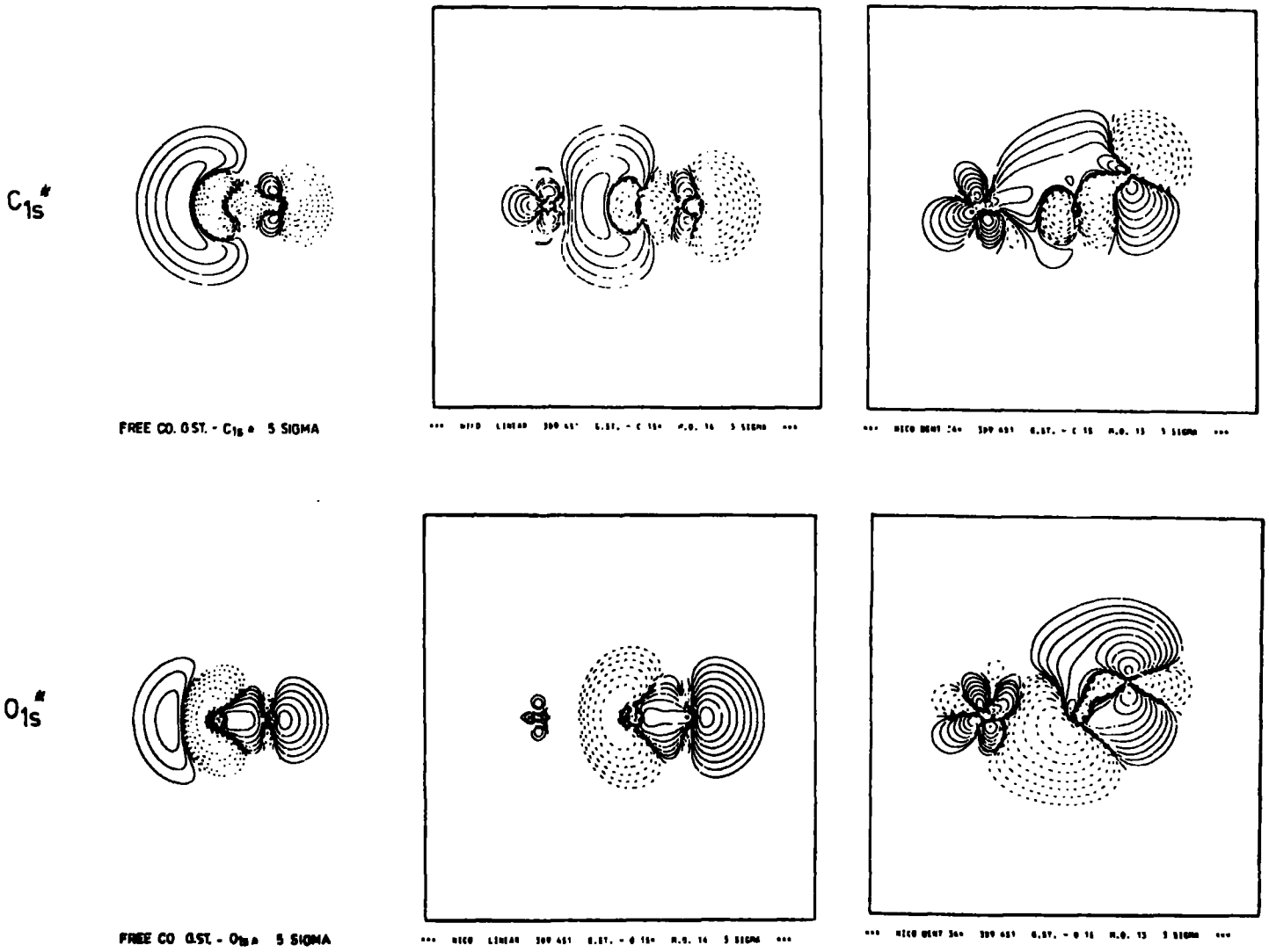

Fig. (8.8) Density difference contours for the 5σ orbital.

dramatic decrease in single orbital relaxation energy observed. On bending the NiCO, greater change in the reorganization pattern is evident for O_{1s} core-ionization, as borne out by the further change in single orbital relaxation energy.

Finally, Figure 8.9 shows the changes in the 1π orbitals. On going to linear NiCO, there is little change. On bending, however, the $1\tilde{\pi}$ to $1\tilde{\pi}'$ orbital changes considerably for both C_{1s} and O_{1s} core-ionization. For the former, the amount of valence-electron density transferred to the carbon atom is considerably decreased, resulting in a decrease in the single orbital relaxation energy accompanying

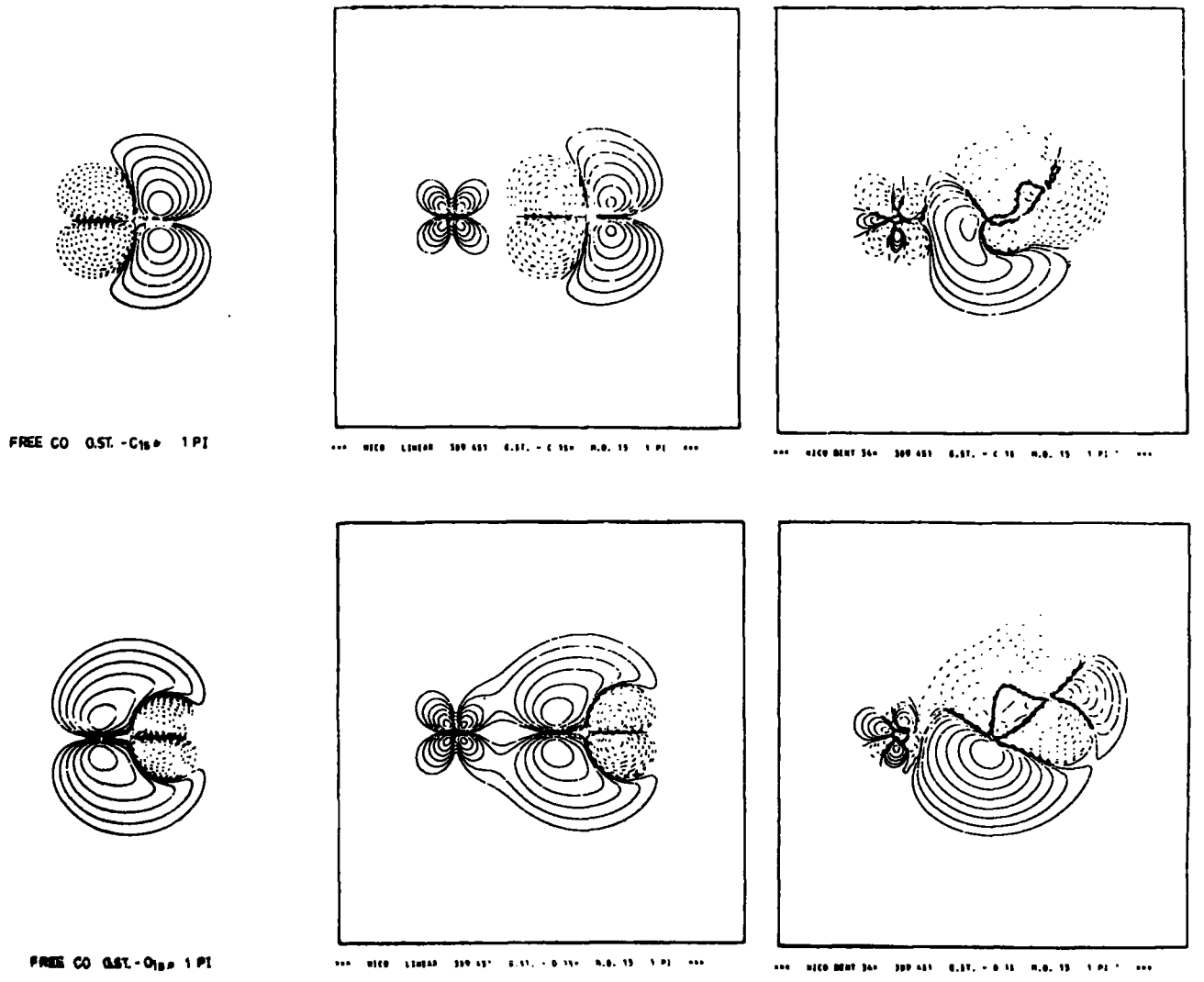

Fig. (8.9) Density difference contours for the 1π orbital.

C_{1s} core-ionization. On the other hand, for O_{1s} core-ionization, there is an increase in the amount of electron density transferred to the oxygen atom, resulting in an increase in the $1\tilde{\pi}'$ orbital contribution to the O_{1s} relaxation energy.

Density difference contour plots for the orbital reorganizations accompanying Ni_{2s} core-ionization have also been considered. Figure 8.10 shows the changes accompanying Ni_{2s} core-ionization in the CO-like orbitals ($4\tilde{\sigma}$, $5\tilde{\sigma}$, $1\tilde{\pi}$) for both linear (upper figure) and bent (lower figure) $^3\Delta$ NiCO. For the $4\tilde{\sigma}$ orbital in the linear NiCO, there is a substantial increase in electron density in the immediate vicinity of the Ni atom. There is a less substantial increase

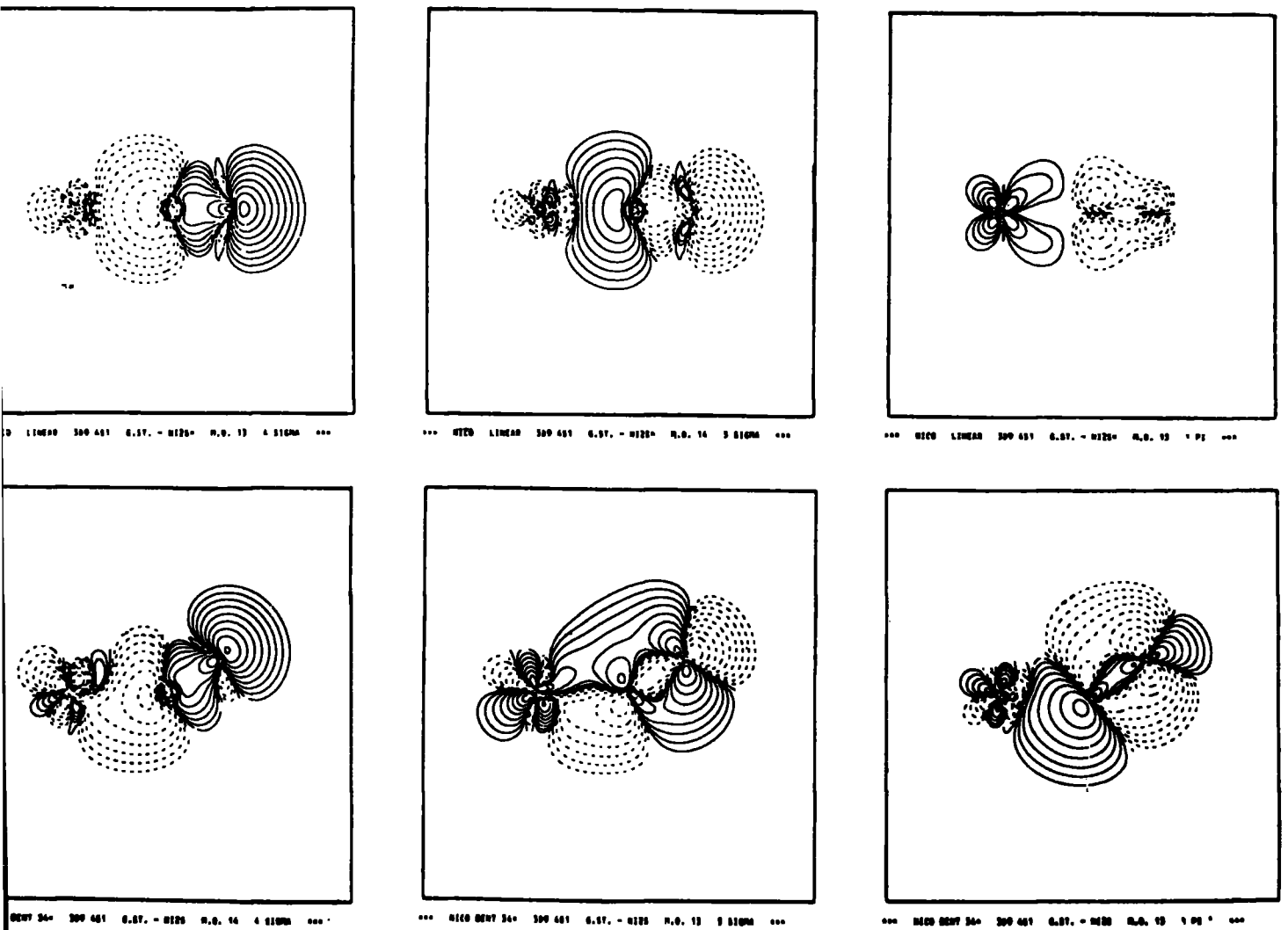

Fig. (8.10) Density difference contours for Ni_{2s} core-ionization.

for the $5\tilde{\sigma}$ orbital, whilst for the $1\tilde{\pi}$ orbitals, there is in fact a decrease in electron density around the nickel atom. In each case, bending the NiCO has a significant effect on the reorganization patterns.

For completeness, Figure 8.11 shows the reorganization of the $3\tilde{d}_{yz}$, $3\tilde{d}_{z^2}$ and $4\tilde{s}$ orbitals in the $^3\Delta$ NiCO systems (linear and bent) accompanying Ni_{2s} core-ionization. Whilst for the $3\tilde{d}_{yz}$ and $3\tilde{d}_{z^2}$ orbitals, there is an increase in the immediate vicinity of the nickel atom, for the $4\tilde{s}$ orbital, there is a decrease in electron density. This seems to account for the negative contribution to the

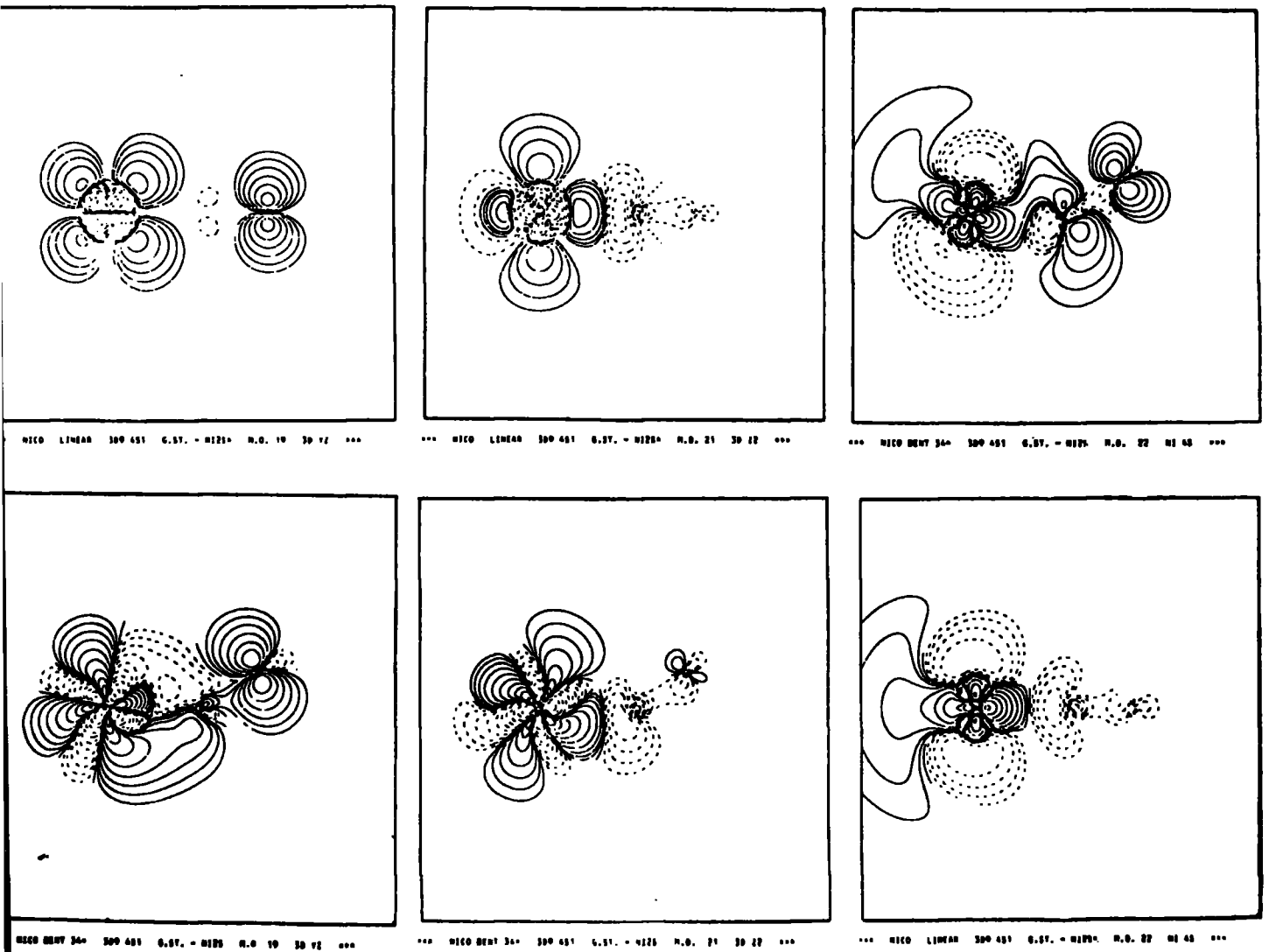

Fig. (8.11) Density difference contour plots for Ni_{2s} core-ionization.

total relaxation energy from this orbital, as shown in Figure 8.5. As in the previous case, bending changes the reorganization patterns, particularly for the $3\hat{d}_{yz}$ orbital.

It seems probable on the basis of the results presented in this Section that a re-examination of the interpretation of the XPS data for CO adsorbed on nickel is required, in terms of simple model systems. It would appear that some features, at least of the core-level spectra, are interpretable in terms of a prototype NiCO molecule in a bent as opposed

to linear arrangement. This provides support for the recently proposed model of Andersson and Pendry.[324] In addition, it is worth emphasizing that this is one more example of the fact that relatively weak interactions in the ground-state can produce profound changes in ionization and relaxation energies.

8.2 Nitric Oxide Adsorbed on Nickel

8.2.1 Introduction

It is of interest to extend the investigation to a different adsorbate system, to see if similar results are obtained on going from a linear to bent conformation. A much less studied system, both experimentally[328] and theoretically,[329] is that of nitric oxide adsorbed on nickel. The bond energy of NO is considerably less than that of CO; due to this, there is an inherent thermodynamic instability of NO, so that the study of the conditions under which adsorbed molecular NO becomes kinetically unstable and dissociates, is of particular interest.[330,331] Although NO is similar to CO in that the initial states have the same symmetry notation, and approximately the same excitation energies, it differs in that it has an unpaired electron in the anti-bonding $2\pi^*$ orbital, which has a low binding energy. A terminally-bonded NO, with an N-O axis angle of between 0° and 60° with respect to the Ni-N axis, has recently been proposed from angular-resolved photoemission spectroscopy.[318] Clearly, the NiNO system would be a good choice for comparison with CO adsorbed on nickel, and an analogous theoretical investigation is presented in this section.

8.2.2 Results and Discussion

(a) Relative Energies, Core Binding Energies and Relaxation Energies

The investigation has been restricted to the ground and core hole states of the linear and bent conformations of NiNO, with $3d^{10}$ Ni parentage; this is the $^2\Pi$ ground state. No account of any multiplet ($^3\Pi$-$^1\Pi$) splitting in the N_{1s} and O_{1s} hole-states either NO or NiNO was taken, the calculations being confined to RHF wavefunctions. The relative energies of the linear and bent conformations, together with the total energy of NO at its equilibrium bond-length of 2.173 au, are shown in Table 8.4. As for the NiCO case, the energies of the linear and bent conformations are very similar.

TABLE 8.4 Computed total energies

		Total Energy (au)	Difference (kcal mol^{-1})
$^2\Pi$NiNO ($3d^{10}$ Ni parentage)			
	linear	-1632.920101	(0)
	bent, 17°	-1632.920556	-0.29
	bent, 34°	-1632.920418	-0.20
Ni	$3d^{10}$	-1503.798014	-
NO		- 129.064453	-
	Ni + NO → NiNO (linear)		
	$3d^{10}$ $^2\Pi$		-36.17

Although only a crude indication of the adsorption energetics may be obtained in this way, it is reassuring to note that the interaction energy of NO with Ni is ∿-36 kcal mol^{-1}.

TABLE 8.5 Calculated ΔSCF B.E. and R.E. (in eV)

	Ni_{2s}				N_{1s}				O_{1s}			
	ΔSCF B.E.	ΔB.E.	R.E.	ΔR.E.	ΔSCF B.E.	ΔB.E.	R.E.	ΔR.E.	ΔSCF B.E.	ΔB.E.	R.E.	ΔR.E.
NO					413.50	(0)	15.07	(0)	544.48	(0)	19.64	(0)
Ni $3d^{10}$	991.54	(0)	21.53	(0)								
NiNO $^2\Pi$ linear	992.46	+0.92	23.77	+2.24	408.62	-4.88	19.36	+4.29	540.04	-4.44	22.91	+3.27
bent, 17°	992.47	+0.93	23.35	+1.82	408.63	-4.87	18.97	+3.90	540.06	-4.42	22.51	+2.87
bent, 34°	992.49	+0.95	23.71	+2.18	405.52	-7.98	22.55	+7.48	537.71	-6.77	25.34	+5.70

The computed binding energies and relaxation energies accompanying N_{1s} and O_{1s} core-ionization, and Ni_{2s} core-ionization, are shown in Table 8.5. In this system, unlike the NiCO system, the most dramatic change in binding energies occurs not in going from the linear to 17° bent conformation; rather the change on increasing the angle-deformation to 34° is far more significant. The estimated experimental shifts for the N_{1s} and O_{1s} levels are 4.9 and 6.9 eV, respectively, to lower binding energy compared with the free ligand, when due allowance has been made for the differences in reference level. For N_{1s} core-ionization, the calculated shifts of ∿4.9 eV for the linear and 17° bent systems are in good agreement with experiment, whereas the value at 34° of ∿ 8 eV is over-estimated. On the other hand, the calculated linear and 17° bent shifts of ∿ 4.4 eV for O_{1s} core-ionization are in poor agreement, whilst the shift at 34° of ∿ 6.8 eV is in excellent agreement with experiment. As in the case of NiCO, these shifts in binding energy may largely be attributed to the relaxation energies. The small calculated shift of less than 1 eV for the Ni_{2s} level in both linear and bent (17° and 34°) NiNO is also consistent with the available experimental data, and is in good agreement with the situation in NiCO.

(b) Single Orbital Relaxation Energies

Before considering the NiNO systems, it is of interest to look at the single orbital relaxation energies in the free NO molecule, as shown in Figure 8.12. For N_{1s} core-ionization, the contributions from the bonding 3σ and oxygen lone pair 4σ orbitals are small, as for C_{1s} core-ionization in CO, and the 1π orbitals contribute significantly; however, in CO, the largest contribution to the C_{1s} relaxation

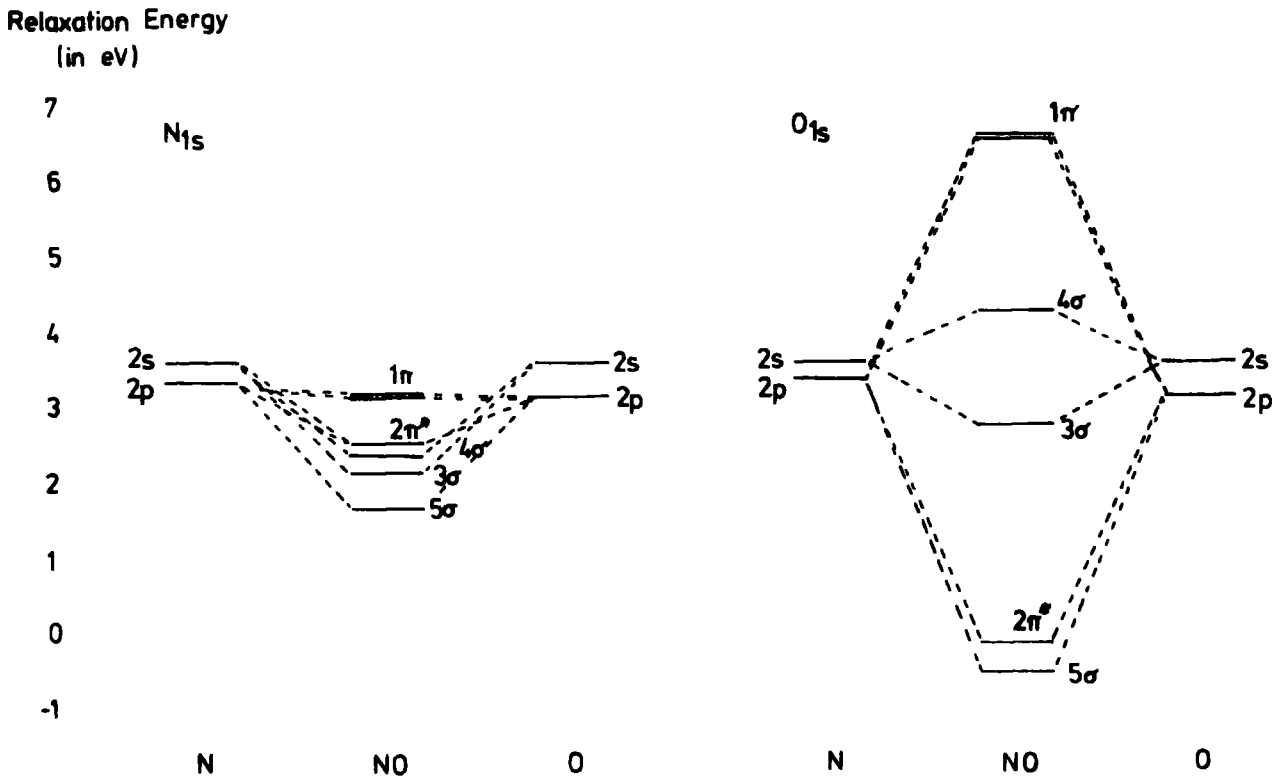

Fig. (8.12) Single orbital contributions to N_{1s} and O_{1s} RE in NO

energy was from the 5σ (lone pair on carbon) orbital, whilst in NO, the 5σ orbital contributes much less, with a slightly greater contribution coming from the anti-bonding $2\pi^*$ orbital. The contributions accompanying O_{1s} core-ionization in NO are strikingly similar to those accompanying O_{1s} core-ionization in CO, with a virtually zero contribution from the $2\pi^*$ orbital.

The changes in these contributions to the O_{1s} and N_{1s} relaxation energies on going to linear and bent (34^o) $^2\pi$ NINO are shown in Figure 8.13. For N_{1s} core-ionization, on going from the free NO molecule to the linear conformation of NiNO, the 3σ and 4σ orbitals remain virtually constant in contribution. The 5σ orbital, however, decreases dramatically, as does the anti-bonding $2\pi^*$ contribution, whilst the 1π orbitals increase their contribution. This would suggest that as in

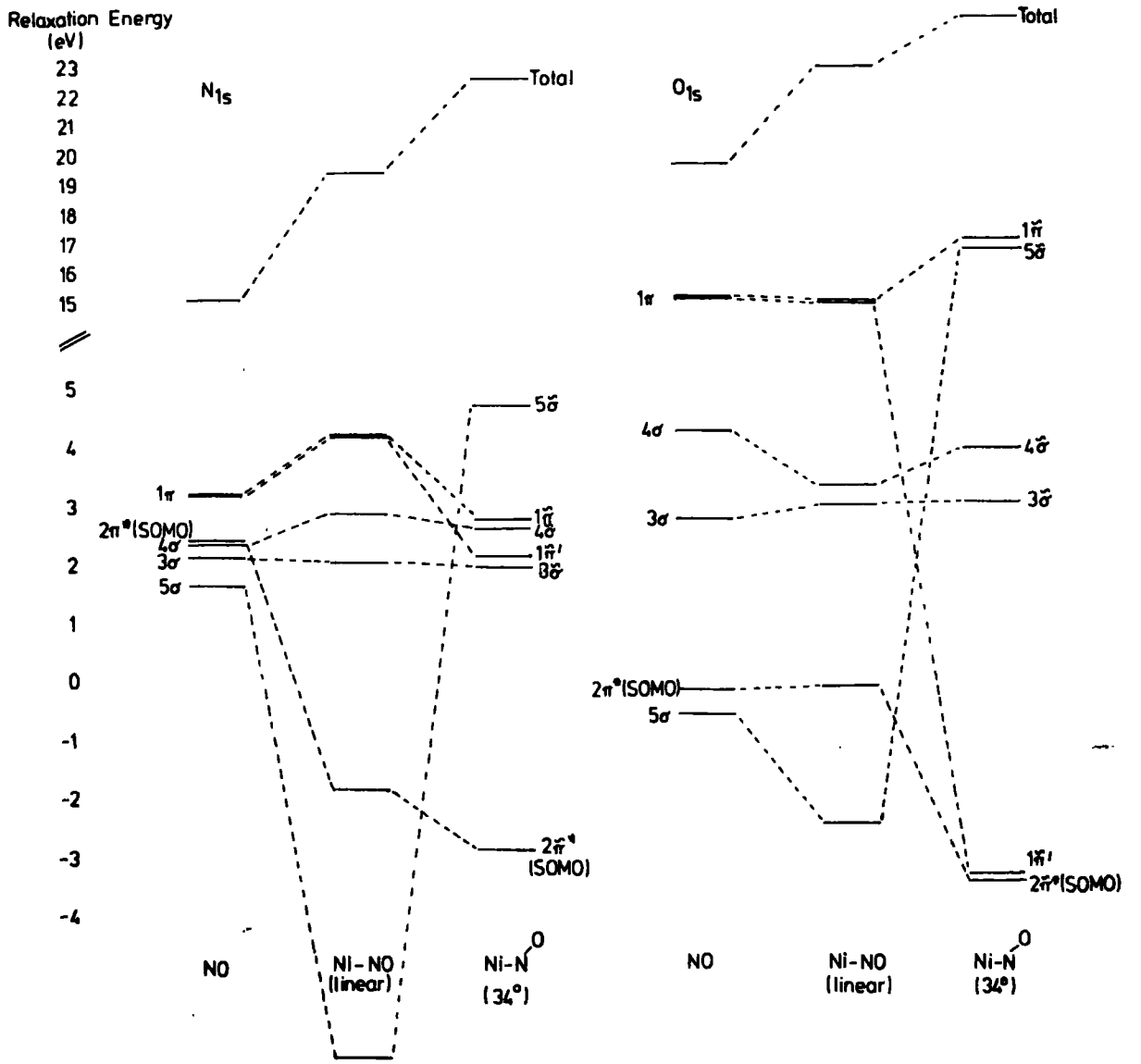

Fig. (8.13) Single orbital relaxation energies accompanying N_{1s} and O_{1s} core-ionization.

linear NiCO, it is the $5\tilde{\sigma}$ and in NiNO, also the $2\tilde{\pi}^*$ orbitals which are strongly involved in the bonding to the nickel atom. The situation changes on bending the NiNO system. The $3\tilde{\sigma}$ and $4\tilde{\sigma}$ orbitals remain very much the same, whilst the previously degenerate $1\tilde{\pi}$ orbitals now split, both decreasing in contribution, the $1\tilde{\pi}'$ more than the $1\tilde{\pi}$. However, for the $5\tilde{\sigma}$ orbital, there is a very substantial increase in contribution, such that it now becomes the largest single component of the total N_{1s} relaxation energy.

For O_{1s} core-ionization, the changes on going from free NO to linear NiNO are a decrease in both 4σ and 5σ contributions, the remainder staying essentially constant. Again on bending, there is a large change in the relative orbital contributions. The in-plane π-orbital ($1\tilde{\pi}$) contribution decreases, whilst the $5\tilde{\sigma}$ increases, by some 10 eV. The $2\tilde{\pi}^*$ contribution also decreases somewhat.

The changes in orbital contributions accompanying Ni_{2s} core-ionization are shown in Figure 8.14, both for the NO-like and Ni-like orbitals. On Ni_{2s} core-ionization

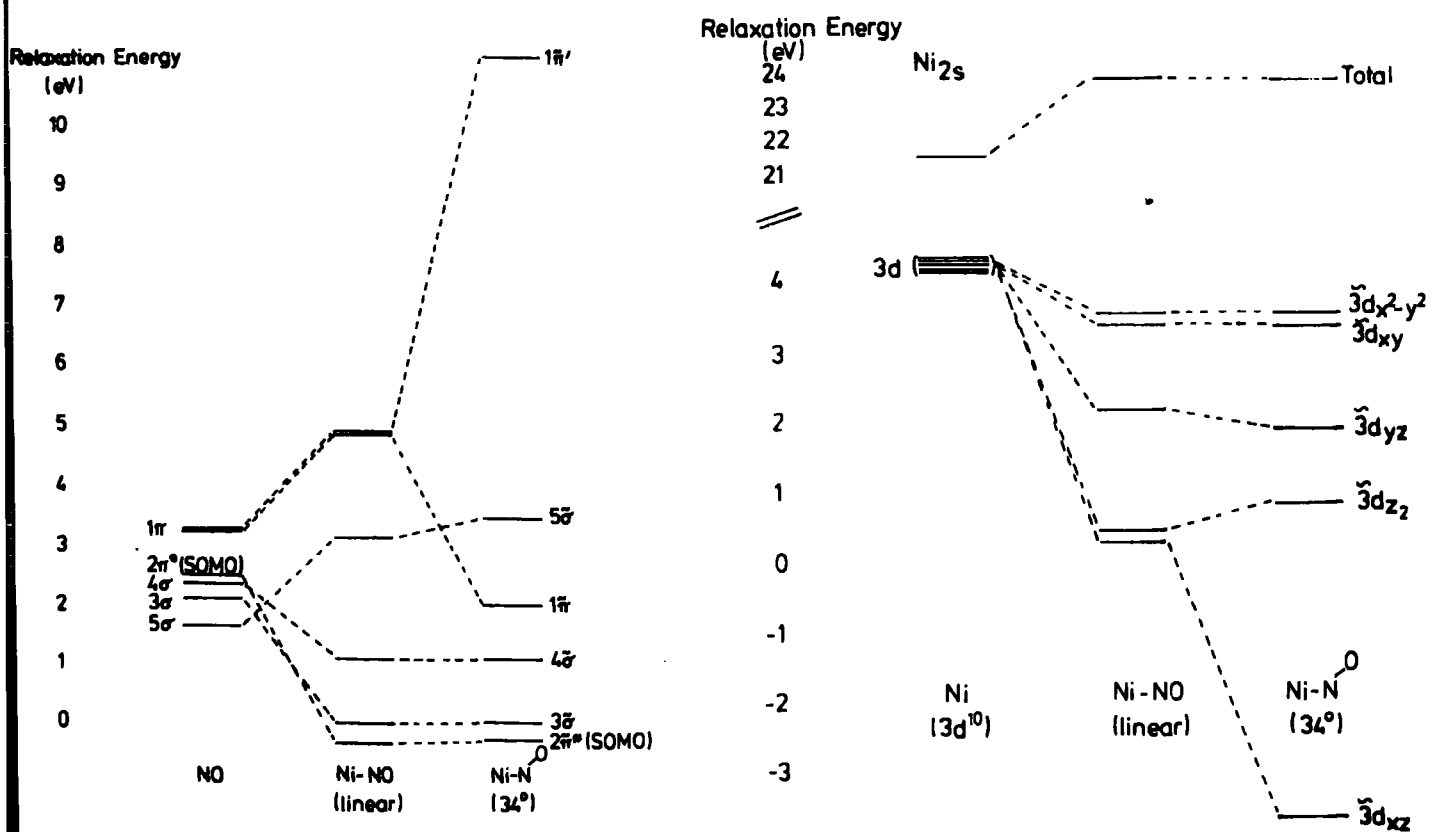

Fig. (8.14) Single orbital relaxation energies accompanying Ni_{2s} core-ionization.

there are zero contributions to the relaxation energy from the $3\tilde{\sigma}$ and $2\tilde{\pi}^*$ orbitals, with increasing contributions from the $4\tilde{\sigma}$, $5\tilde{\sigma}$ and $1\tilde{\pi}$ orbitals. The only significant change on going to the bent NiNO is the splitting of the $1\tilde{\pi}$ orbitals, the $1\tilde{\pi}'$

contribution increasing dramatically, suggesting that this may now interact more strongly with Ni than in the linear conformation, this being able to experience the core-ionization of Ni more directly. The situation for the $3\tilde{d}$ orbitals is relatively straightforward for NiNO. In the linear conformation, the $3\tilde{d}_{z^2}$ and $3\tilde{d}_{xz}$ orbitals which interact with the NO molecule lying along the z-axis do not contribute to the Ni_{2s} relaxation energy, whilst the $3\tilde{d}_{xy}$ and $3\tilde{d}_{x^2-y^2}$ orbitals, which do not interact at all with the NO molecule, contribute most significantly. On bending the NiNO molecule, the $3\tilde{d}_{xz}$ contribution decreases significantly, since now the oxygen atom of NO interacts even more with this orbital, whilst the remaining $3\tilde{d}$ orbitals stay essentially unchanged in contribution.

(c) Mulliken Population Analysis

For the linear $^2\Pi$ NiNO, the atomic populations on the nickel, carbon and oxygen atoms are 0.28, 0.05 and 0.33 respectively, as shown in Table 8.6. This contrasts somewhat with the situation for both $^3\Delta$ and $^1\Sigma$ linear NiCO, where the carbon atom had a significant population. The net effect of bending NiNO is very small compared with $^3\Delta$ NiCO, there being a small amount of electron transfer from Ni to C, with only slight changes in the bond overlap populations. This is in accord with the very small energy differences between the linear and bent NiNO conformations.

The creation of a core-hole on Ni gives rise to an almost unit decrease in population on the nickel, the populations on nitrogen and oxygen decreasing only slightly. The Ni-N bond overlap decreases slightly. For the bent conformations the changes in electron population are closely similar.

TABLE 8.6 Mulliken Population Analysis

$^2\Delta$ NiNO	Gross atomic population			Bond overlap	
	Ni	N	O	Ni-N	N-O
Linear					
Ground state	0.2834	0.0499	-0.3333	0.0293	0.0707
Ni 2s	1.0538	0.1065	-0.1604	-0.1414	0.0670
N 1s	1.3067	-0.1872	-0.1195	-0.0091	-0.1178
O 1s	1.1520	-0.0631	-0.0889	-0.0052	-0.1485
Bent, 17°					
Ground state	0.2816	0.0462	-0.3278	0.0292	0.0846
Ni 2s	1.0549	0.1016	-0.1564	-0.1418	0.0822
N 1s	1.3093	-0.1940	-0.1153	-0.0083	-0.1103
O 1s	1.1551	-0.0623	-0.0928	-0.0042	-0.1416
Bent, 34°					
Ground state	0.2751	0.0419	-0.3169	0.0289	0.1088
Ni 2s	1.0577	0.0926	-0.1503	-0.1423	0.1082
N 1s	1.0399	-0.0245	-0.0155	-0.1045	-0.0674
O 1s	1.0372	0.0394	-0.0766	-0.0899	-0.1362

Creation of a core-hole on nitrogen in the linear NiNO system leads to significant electron transfer from nickel and to a much lesser extent from oxygen; creation of a core-hole on oxygen leads to an analogous situation, most of the electron transfer again coming from nickel. This contrasts with the linear NiCO systems, where electron transfer from the metal was not so effective. For NiNO, there is little change in going to the 17^{o} bent conformation, with only slight change on bending to 34^{o}.

Whilst the main thrust of this Chapter has been concerned with a detailed analysis of the relaxation processes accompanying core-ionization in a NiCO model for CO adsorption on Ni, it is clear from this brief section on NO adsorption that the situation here is quite different. It is hoped that the use of single orbital relaxation contributions to relaxation energies accompanying core-ionization in such crude model systems for the adsorption of small molecules on metal surfaces may provide an alternative means of investigating the bonding at the metal surfaces, and the mechanism of relaxation upon core-ionization of such systems.

APPENDIX

APPENDIX

The Board of Studies in Chemistry requires that each postgraduate research thesis contain an appendix listing

(a) all research colloquia, research seminars and lectures (by external speakers) arranged by the Department of Chemistry since 1 October 1976; and (b) all research conferences attended and papers read out by the writer of the thesis, during the period when the research for the thesis was carried out.

1. Research Colloquia, Seminars and Lectures

1.1 1976-77

a) University of Durham Chemistry Colloquia

Wednesday, 20th October

Professor J.B. Hyne (University of Calgary), "New Research on an Old Element - Sulphur".

Wednesday, 10th November

Dr. J.S. Ogden (Southampton University), "The Characterization of High Temperature Species by Matrix Isolation".

Wednesday, 17th November

Dr. B.E.F. Fender (University of Oxford), "Familiar but Remarkable Inorganic Solids".

Wednesday, 24th November

Dr. M.I. Page (Huddersfield Polytechnic), "Large and Small Rate Enhancements of Intramolecular Catalysed Reactions".

Wednesday, 8th December

Professor A.J. Leadbetter (University of Exeter), "Liquid Crystals".

Wednesday, 26th January

Dr. A. Davis (ERDR), "The Weathering of Polymeric Materials".

Wednesday, 2nd February

Dr. M. Falk, (NRC Canada), "Structural Deductions from the Vibrational Spectrum of Water in Condensed Phases".

Wednesday, 9th February

Professor R.O.C. Norman (U. of York), "Radical Cations; Intermediates in Organic Reactions.

Wednesday, 23rd February

Dr. G. Harris (U. of St. Andrews), "Halogen Adducts of Phosphines and Arsines".

Friday, 25th February

Professor H.T. Dieck (Frankfurt U.), "Diazadienes - New Powerful Low-Valent Metal Ligands".

Wednesday, 2nd March

Dr. F. Hibbert (Birkbeck College, London), "Fast Reaction Studies of Slow Proton Transfers Involving Nitrogen and Oxygen Acids".

Friday, 4th March

Dr. G. Brink (Rhodes U., R.S.A.), "Dielectric Studies of Hydrogen Bonding in Alcohols".

Wednesday, 9th March

Dr. I.O. Sutherland (Sheffield U.), "The Stevans' Rearrangement: Orbital Symmetry and Radical Pairs".

Friday, 18th March

Professor Hans Bock (Frankfurt U.), "Photoelectron Spectra and Molecular Properties: A Vademecum for the Chemist".

Wednesday, 30th March

Dr. J.R. MacCallum (U. of St. Andrews), "Photooxidation of Polymers".

Wednesday 20th April

Dr. D.M.J. Lilley (G.D. Searle, Research Div.), "Tails of Chromatin Structure - Progress towards a Working Model".

Wednesday, 27th April

Dr. M.P. Stevens (Univ. of Hartford), "Photocycloaddition Polymerisation".

Wednesday, 4th May

Dr. G.C. Tabisz (Univ. of Manitoba), "Collision Induced Light Scattering by Compressed Molecular Gases".

Wednesday, 11th May

Dr. R.E. Banks (UMIST), "The Reaction of Hexafluoropropene with Heterocyclic N-Oxides".

Wednesday, 18th May

Dr. J. Atwood (Univ. of Alabama), "Novel Solution Behaviour of Anionic Organoaluminium Compounds: the Formation of Liquid Clathrates".

Wednesday, 25th May

Professor M.M. Kreevoy (Univ. of Minnesota), "The Dynamics of Proton Transfer in Solution".

Wednesday, 1st June

Dr. J. McCleverty (Univ. of Sheffield), "Consequences of Deprivation and Overcrowding on the Chemistry of Molybdenum and Tungsten".

Wednesday, 6th July

Professor J. Passmore (Univ. of Brunswick), "Adducts Between Group V Pentahalides and a Postscript on S_7I^+".

b) Durham University Chemical Society

Tuesday, 19th October

Dr. J.A. Salthouse (Univ. of Manchester), "Chemistry and Energy".

Tuesday, 26th October

Dr. R.E. Richards (Univ. of Oxford), "NMR Measurements on Intact Biological Tissue".

Tuesday, 2nd November

Dr. B. Sutcliffe (Univ. of York), "The Chemical Bond as a Figment of the Imagination".

Tuesday, 16th November

Mr. R. Ficken (Rohm & Haas), "The Graduate in Industry".

Tuesday, 30th November

Dr. R.J. Donovan (Univ. of Edinburgh), "The Chemistry of the Atmosphere".

Tuesday, 18th January

Professor I. Fells (Univ. of Newcastle), "Energy Storage: the Chemists' Contribution to the Problem".

Tuesday, 8th February

Dr. M.J. Cleare (Johnson Matthey Research Centre), "Platinum Group Metal Compounds as Anti-Cancer Agents".

Tuesday, 1st March

Professor J.A.S. Smith (Q.E. College, London), "Double Resonance".

Tuesday, 8th March

Professor C. Eaborn (Univ. of Sussex), "Structure and Reactivity".

1.2 1977-78

a) University of Durham Chemistry Colloquia

Tuesday, 27th September

Dr. T.J. Broxton (La Trobe Univ. Australia), "Interaction of Aryldiazonium Salts and Arylazoalkyl Ethers in Basic Alcoholic Solvents".

Wednesday, 19th October

Dr. B. Heyn (Univ. of Jena, D.D.R.), "σ-Organo-Molybdenum Complexes as Alkene Polymerisation Catalysts".

Thursday, 27th October

Professor R.A. Filler (Illinois Inst. of Technology, U.S.A.), "Reactions of Organic Compounds with Xenon Fluorides".

Wednesday, 2nd November

Dr. N. Boden (Univ. of Leeds), "NMR Spin-Echo Experiments for Studying Structure and Dynamical Properties of Materials Containing Interacting Spin-½ Pairs".

Wednesday, 9th November

Dr. A.R. Butler (Univ. of St. Andrews), "Why I lost Faith in Linear Free Energy Relationships".

Wednesday, 7th December

Dr. P.A. Madden (Univ. of Cambridge), "Raman Studies of Molecular Motions in Liquids".

Wednesday, 14th December

Dr. R.O. Gould (Univ. of Edinburgh), "Crystallography to the Rescue in Ruthenium Chemistry".

Wednesday, 25th January

Dr. G. Richards,(Univ. of Oxford), "Quantum Pharmacology".

Wednesday 1st February, 2.30 p.m.

Professor K.J. Ivin (Queens University, Belfast), "The olefin metathesis reaction: mechanism of ring-opening polymerisation of cycloalkenes".

Friday 3rd February

Dr A. Hartog (Free University, Amsterdam, Holland), "Surprising recent Studies in Organo-magnesium Chemistry".

Wednesday 22 February

Professor J.D. Birchall (Mond Division, I.C.I. Ltd.), "Silicon in the Biosphere".

Wednesday 1st March

Dr A. Williams (University of Kent), "Acyl Group Transfer Reactions".

Friday 3rd March

Dr G. van Koten (University of Amsterdam, Holland), "Structure and Reactivity of Arylkopper Cluster Compounds".

Wednesday 15 March

Professor G. Scott (University of Aston), "Fashioning Plastics to match the Environment".

Wednesday 22 March

Professor H. Vahrenkamp (University of Freiburg, Germany), "Metal-Metal Bonds in Organometallic Complexes".

Wednesday 19 April

Dr M. Barber (UMIST), "Secondary Ion Mass Spectra of Surfaces and Absorbed Species".

Tuesday 16th May

Dr P. Ferguson (C.N.R.S., Grenoble), "Surface Plasma Waves and Adsorbed Species on Metals".

Thursday 18th May

Professor M. Gordon (University of Essex), "Three Critical Points in Polymer Science".

Monday 22nd May

Professor D. Tuck (University of Windsor, Ontario), "Electrochemical Synthesis of Inorganic and Organometallic Compounds".

Wednesday - Thursday 24th, 25th May

Professor P. von R. Schleyer (University of Erlangen, Nürnberg),

I. "Planar Tetra-co-ordinate Methanes, Perpendicular Ethylenes, and Planar Allenes".

II. "Aromaticity in Three Dimensions".

III. "Non-classical Carbocations".

Wednesday 21st June

Dr S.K. Tyrlik (Academy of Science, Warsaw), "Dimethylglyoxime-cobalt Complexes - Catalytic Black Boxes".

Friday 23rd June

Professor W.B. Pearson (University of Florida), "Diode Laser Spectroscopy at 16 μm".

Friday 30th June

Professor G. Mateescu (Cape Western Reserve University), "A Concerted Spectroscopy Approach to the Characterization of Ions and Ion Pairs : Facts, Plans, and Dreams".

(b) Durham University Chemical Society

Thursday 13th October

Dr J. C. Young, Mr A.J.S. Williams (University of Aberystwyth), "Experiments and Considerations Touching Colour".

Thursday 20th October

Dr R.L. Williams (Metropolitan Police Forensic Science Dept.), "Science and Crime".

Thursday 3rd November

Dr G.W. Gray (University of Hull), "Liquid Crystals - Their Origins and Applications".

Thursday 24th November

Mr G. Russell (Alcan), "Designing for Social Acceptability".

Thursday 1st December

Dr B.F.G. Johnson (University of Cambridge), "Chemistry of Binary Metal Carbonyls".

Thursday 2nd February

Professor R.A. Raphael (University of Cambridge), "Bizarre Reactions of Acetylenic Compounds".

Thursday 16th February

Professor G.W.A. Fowles (University of Reading), "Home Winemaking".

Thursday 2nd March

Professor M.W. Roberts (University of Bradford), "The Discovery of Molecular Events at Solid Surfaces".

Thursday 9th March

Professor H. Suschitzky (University of Salford), "Fruitful Fissions of Benzofuroxans".

Thursday 4th May

Professor J. Chatt (University of Sussex), "Reactions of Co-ordinated Dinitrogen".

Tuesday 9th May

Professor G.A. Olah (Case Western Reserve University, Cleveland, Ohio), "Electrophilic Reactions of Hydrocarbons".

2. Research Conferences Attended

Institute of Petroleum 6th Conference of Molecular Spectroscopy (30th March - 2nd April 1976) Durham.

Summer School in Theoretical Organic Chemistry (13th - 27th June 1976) Teneriffe, Canary Islands.

1st Polymer Surfaces Symposium (21st - 24th March 1977) Durham

27th Annual Meeting of Nobel Prizewinners (9th in Chemistry) (27th June - 1st July 1977) Lindau, West Germany.

Meeting of the Chemical Society Theoretical Chemistry Group on "Molecules Adsorbed at Surfaces" (26th October 1977) London

NATO Advanced Study Institute on "Theoretical Aspects of the Electronic Structure and Properties of the Excited States of Atoms, Molecules and Solids" (4th - 18th June 1978) Kos, Greece.

REFERENCES

1. F.L. Pilar; "Elementary Quantum Chemistry", McGraw-Hill (1968).

2. H.F. Schaefer III; "The Electronic Structure of Atoms and Molecules", Addison-Wesley (1972).

3. W.G. Richards, J.A. Horsley; "Ab Initio Molecular Orbital Calculations for Chemists", Clarendon (1970).

4. D.B. Cook; "Ab Initio Valence Calculations in Chemistry", Butterworths (1974).

5. I.G. Csizmadia; "Theory and Practice of MO Calculations on Organic Molecules", Elsevier (1976).

6. E. Steiner, "The Determination and Interpretation of Molecular Wave Functions", CUP (1976).

7. a) R. McWeeny, B.T. Sutcliffe; "Methods of Molecular Quantum Mechanics", Academic Press (1969).

   b) R. McWeeny; "Quantum Mechanics: Principles and Formalism", Pergamon (1972).

8. A.C. Hurley; "Introduction to the Electron Theory of Small Molecules", Academic Press (1976).

9. M. Born, J. Oppenheimer; Ann. Physik., 84, 457 (1927).

10. Discussed in, e.g., Longuet-Higgins; Adv. in Spectroscopy, 2, 429 (1962).

11. C.E. Eckart; Phys. Rev., 36, 878 (1930).

12. a) D.R. Hartree; Proc. Camb. Phil. Soc., 24, 89 (1928).

    b) D.R. Hartree; Proc. Camb. Phil. Soc., 24, 111 (1928).

    c) D.R. Hartree; Proc. Camb. Phil. Soc., 24, 426 (1928).

13. V. Fock; Z. Physik., 61, 126 (1930).

14. J.C. Slater; Phys. Rev., 35, 210 (1930).

15. D.R. Hartree; "The Calculation of Atomic Structures", Wiley (1957).

16. C.C.J. Roothaan; Rev. Mod. Phys., 23, 69 (1951).

17. a) P.O. Löwdin; J. Chem. Phys., 18, 365 (1950).

    b) A recent review of interest is "On The Non-Orthogonality Problem", by P.O. Löwdin, in Adv. Quant. Chem., 5, 185 (1970).

18. C.C.J. Roothaan; Rev. Mod. Phys., 32, 179 (1960).

19. S. Huzinaga; Phys. Rev., 120, 866 (1960).

20. J.A. Pople, R.K. Nesbet; J. Chem. Phys., 22, 571 (1954).

21. P.S. Bagus, B. Liu, H.F. Schaefer III; Phys. Rev. A, 2, 555 (1970).

22. A useful method of projecting out the desired spin function starting from a single determinant is that of R.K. Nesbet; J. Math. Phys., 2, 701 (1961).

23. R.S. Mulliken; J. Chem. Phys., 23, 1833 (1955).

24. W.L. Jorgensen, L. Salem; "The Organic Chemist's Book of Orbitals", Academic Press (1973).

25. J.R. van Wazer, I. Absar; "Electron Densities in Molecules and Molecular Orbitals", Academic Press (1975).

26. R.F.W. Bader; Int. Rev. Sci., Phys. Chem. Ser. Two, 1, 43 (1975).

27. V.H. Smith, Jr.; Phys. Scripta, 15, 147 (1977).

28. Self-consistent perturbation theory is described, for example, by G. Diercksen, R. McWeeny, J. Chem. Phys., 44, 3554 (1966).

29. J.C. Slater; Phys. Rev., 36, 57 (1930).

30. E. Clementi, D.L. Raimondi; J. Chem. Phys., 38, 2686 (1963).

31. E. Clementi, D.L. Raimondi, W.P. Reinhardt; J. Chem. Phys., 47, 1300 (1967).

32. a) E. Clementi; J. Chem. Phys., 40, 1944 (1964).

b) E. Clementi, R. Matcha, A. Veillard; J. Chem. Phys., 47, 1865 (1967).

33. S. Huzinaga, C. Arnau; J. Chem. Phys., 53, 451 (1970).

34. R.K. Nesbet; Rev. Mod. Phys., 32, 272 (1960).

35. A.D. McLean, M. Yoshimine; "Tables of Linear Molecule Wavefunctions", supplement to IBM J. Res. Develop., 12, 206 (1968).

36. B. Roos, P. Siegbahn; Theoret. Chim. Acta, 17, 199 (1970).

37. S. Rothenberg, H.F. Schaefer III; J. Chem. Phys., 54, 2765 (1971).

38. T.H. Dunning; J. Chem. Phys., 55, 3958 (1971).

39. S.F. Boys; Proc. Roy. Soc. (London), A200, 542 (1950).

40. I. Shavitt; Methods Comp. Phys., 2, 1 (1963).

41. H. Preuss; Z. Naturforsch., 11, 823 (1956).

42. J.L. Whitten; J. Chem. Phys., 44, 395 (1966).

43. J.M. Foster, S.F. Boys; Rev. Mod. Phys., 32, 303 (1960).

44. W.J. Hehre, R.F. Stewart, J.A. Pople; J. Chem. Phys., 51, 2657 (1969).

45. W.J. Hehre, R. Ditchfield, R.F. Stewart, J.A. Pople; J. Chem. Phys., 52, 2769 (1970).

46. a) R. Ditchfield, W.J. Hehre, J.A. Pople; J. Chem. Phys., 54, 724 (1971).

b) W.J. Hehre, J.A. Pople; J. Chem. Phys., 56, 4233 (1972).

c) W.J. Hehre, W.A. Lathan; J. Chem. Phys., 56, 5255 (1972).

47. P.C. Hariharan, J.A. Pople; Chem. Phys. Lett., 16, 217 (1972).

48. E. Clementi, R. Davis; J. Comput. Phys., 2, 223 (1967).

49. T.H. Dunning; J. Chem. Phys., 53, 2823 (1970).

50. S. Huzinaga; J. Chem. Phys., 42, 1293 (1965).

51. J.P. Desclaux; At. Data Nucl. Data Tables, 12, 311 (1973).

52. K.-N. Huang, M. Aoyagi, M.H. Chen, B. Crasemann; At. Data Nucl. Data Tables, 18, 243 (1976).

53. P.O. Löwdin; Adv. Chem. Phys., 2, 207 (1959).

54. See, for example, D.T. Clark; Ann. Reports (B) Chem. Soc., 69, 40 (1972).

55. W.J. Hehre, R. Ditchfield, L. Radom, J.A. Pople; J. Am. Chem. Soc., 92, 4796 (1970).

56. An example of a quantative discussion of this topic is given by P.E. Cade, K.D. Sales, A.C. Wahl; J. Chem. Phys., 44, 1973 (1966).

57. A.C. Wahl; J. Chem. Phys., 41, 2600 (1964).

58. E.A. Hylleras; Z. Physik., 54, 347 (1929).

59. R.K. Nesbet; J. Chem. Phys., 43, 311 (1965).

60. I. Shavitt; J. Comput. Phys., 6, 124 (1970).

61. This topic is discussed in many standard texts, e.g., G. Hertzberg; "Spectra of Diatomic Molecules", Van Nostrand (1950).

62. a) P.O. Löwdin; Rev. Mod. Phys., 32, 328 (1960).

b) P.O. Löwdin; Rev. Mod. Phys., 36, 966 (1964).

63. J.C. Slater; Phys. Rev., 34, 1293 (1929).

64. A.C. Hurley; "Electron Correlation in Small Molecules", Academic Press (1976).

65. H.F. Schaefer III (Ed.); "Methods of Electronic Structure Theory", Plenum Press (1977).

66. All Enquiries and general correspondence should be directed to:

Quantum Chemistry Program Exchange,
Chemistry Department, Room 204,
Indiana University,
BLOOMINGTON, Indiana (47401).

67. E. Clementi, J. Mehl; "IBM System/360 IBMOL5 Program, Quantum Mechanical Concepts and Algorithms", IBM Research Laboratory, San José, California 95114 (1971).

68. D.B. Neumann, H. Basch, R.L. Kornegay, L.C. Snyder, J.W. Moskowitz, C. Hornback, S.P. Liebmann; QCPE 199.

69. U. Almöf; USIP Technical Report No. 7209, Stockholm.

70. A.D. McLean; Proc. Conf. Potential Energy Surfaces in Chemistry (1970), pg. 87 et seq., IBM Research Laboratory, San José, California 95114.

71. W.J. Hehre, W.A. Lathan, R. Ditchfield, M.D. Newton, J.A. Pople; QCPE 236.

72. M.F. Chiu, V.R. Saunders, M.F. Guest; Atlas Computor Laboratory, Science Research Council, Chilton, Didcot, Oxon OX11 0QX.

73. V.R. Saunders, M.F. Guest; Atlas Computing Division, Rutherford Laboratory, Chilton, Didcot, Oxon OX11 0QX.

74. V.R. Saunders; "An Introduction to Molecular Integral Evaluation" in "Computational Techniques in Quantum Chemistry and Molecular Physics", edited by G.H.F. Diercksen, B.T. Sutcliffe and A. Veillard, D. Reidel (1975).

75. I. Shavitt, M. Karplus; J. Chem. Phys., 43, 398 (1965).

76. A. Veillard; "The Logic of SCF Procedures" in "Computational Techniques in Quantum Chemistry and Molecular Physics", edited by G.H.F. Diercksen, B.T. Sutcliffe and A. Veillard, D. Reidel (1975).

77. C.C.J. Roothaan, P.S. Bagus in "Methods in Computational Physics, Vol. 2", edited by B. Alder, S. Fernbach and M. Rotenberg, Academic Press (1963).

78. S. Ehrenson; Theoret. Chim. Acta, 14, 136 (1969).

79. V.R. Saunders, I.H. Hillier; Int. J. Quantum Chem., 7, 699 (1973).

80. I.H. Hillier, V.R. Saunders; Proc. Roy. Soc. (London), A320, 161 (1970).

81. M.F. Guest, V.R. Sauders; Mol. Phys., 28, 819 (1974).

82. D.W. Turner, C. Baker, A.D. Baker, C.R. Brundle; "Molecular Photoelectron Spectroscopy", Wiley-Interscience (1970).

83. J.H.D. Eland; "Photoelectron Spectroscopy", Butterworths (1974).

84. D.A. Shirley; "Electron Spectroscopy: Proceeding of an International Conference at Asilomar", North-Holland (1972).

85. W. Dekeyser, et al.; "Electron Emission Spectroscopy", D. Reidel (1973).

86. R. Caudano, J. Verbist; "Electron Spectroscopy - Progress in Research and Applications", Elsevier (1974).

87. T.A. Carlsson; "Photoelectron and Auger Spectroscopy", Plenum (1975).

88. D. Briggs; "Handbook of Electron Spectroscopy", Heyden and Sons (1976).

89. C.R. Brundle, A.D. Baker; "Electron Spectroscopy, Volume 1: Theory, Techniques and Applications", Academic Press (1977).

90. K. Siegbahn, C. Nordling, A. Fahlman, R. Nordberg, K. Hamrin, J. Hedman, G. Johansson, T. Bergmark, S.E. Karlsson, I. Lindgren, B. Lindberg; "ESCA: Atomic, Molecular and Solid State Structure Studied by Means of Electron Spectroscopy", Almquist and Wiksells, Uppsala (1967).

91. K. Siegbahn, C. Nordling, G. Johansson, J. Hedman, P.F. Heden, K. Hamrin, U. Gelius, T. Bergmark, L.D. Werme, R. Manne, Y. Baer; "ESCA Applied to Free Molecules", North-Holland (1969).

92. C.S. Fadley; "Theoretical Aspects of X-ray Photoelectron Spectroscopy" in ref. 85 (1973).

93. D.A. Shirley; Adv. Chem. Phys., 23, 85 (1973).

94. H. Basch; J. Electron Spectrosc. Rel. Phenom., 5, 463 (1974).

95. M.E. Schwartz; Int. Rev. Sci., Theoret. Chem: Phys. Chem. Ser. 2, 1, 189 (1975).

96. M.E. Schwartz; "Electron Spectroscopy" in "Modern Theoretical Chemistry, Volume 4", edited by H.F. Schaefer, Plenum (1977).

97. a) H. Robinson, W.F. Rawlinson; Phil. Mag., 28, 277 (1914).

b) H. Robinson; Proc. Roy. Soc. (London), A104, 455 (1923).

c) H. Robinson; Phil. Mag., 50, 241 (1925).

98. M. de Broglie; Compt. Rend., 172, 274 (1921).

99. J.G. Jenkin, R.C.G. Leckey, J. Liesengang; J. Electron Spectrosc. Rel. Phenom., 12, 1 (1977).

100. W. Domcke, L.S. Cederbaum; J. Electron Spectrosc. Rel. Phenom., 12, 161 (1978).

101. C.R. Brundle, M.B. Robin, G.R. Jones; J. Chem. Phys., 52, 3383 (1970).

102. M.O. Krause, T.A. Carlson, R.D. Dismukes; Phys. Rev., 170, 37 (1968).

103. See, for example, R.L. Martin, D.A. Shirley; "Many-electron Theory of Photoemission", in ref. 89 (1977).

104. R. Manne, T. Åberg; Chem. Phys. Lett., 7, 282 (1970).

105. P. Auger; J. Phys. Radium, 6, 205 (1925).

106. P. Auger; Compt. Rend., 65, 180 (1925).

107. J.J. Lander; Phys. Rev., 91, 1382 (1953).

108. See, for example, the relevant section in ref. 87 (1975).

109. D. Coster, R. de L. Kronig; Physica, 2, 13 (1935).

110. E.H.S. Burhop; "The Auger Effect and Other Radiationless Transitions", CUP (1952).

111. A.E. Sandström in "Handbook of Physics", Vol. XXX. "X-rays", 164, ed. S.F. Flügge; Springer-Verlag (1957).

112. C.D. Wagner; Farad. Disc. Chem. Soc., 60, 306 (1975).

113. E.M. Purcell; Phys. Rev., 54, 818 (1938).

114. E. Sokolowski; Arkiv Fysik, 15, 1 (1959).

115. C. Nordling; Arkiv Fysik, 15, 397 (1959).

116. G. Johansson, J. Hedman, A. Berndtsson, M. Klasson, R. Nilsson; J. Electron Spectrosc. Rel. Phenom., 2, 295 (1973).

117. D.A. Shirley, R.L. Martin, S.P. Kowalczyk, F.R. McFeely, L. Ley; Phys. Rev. B, 15, 544 (1977).

118. S. Hagstrom, C. Nordling, K. Siegbahn; Z. Physik, 178, 439 (1964).

119. R.E. Watson, A.J. Freeman; in "Hyperfine Interactions", ed. A.J. Freeman, R.B. Frankel, Academic Press (1967).

120. J.H. van Vleck; Phys. Rev. Lett., 45, 405 (1934).

121. C.S. Fadley; pg. 781 et seq. in ref. 84 (1972).

122. D.W. Davis, D.A. Shirley; J. Chem. Phys., 56, 669 (1972).

123. J.C. Carver, C.A. Thomas, L.C. Cain, G.K. Schweitzer; pg. 803 et seq. in ref. 84.

124. T. Novakov, J.M. Hollander; Bull. Am. Phys. Soc., 14, 524 (1969).

125. T. Novakov, J.M. Hollander; Phys. Rev. Lett., 21, 1133 (1968).

126. See, for example, G.K. Wertheim; "Mössbauer Effect: Principles and Applications", Academic Press (1964).

127. G.M. Bancroft, I. Adams, H. Lampe, T.K. Sham; Chem. Phys. Lett., 32, 173 (1975).

128. R.L. Martin, D.A. Shirley; J. Chem. Phys., 64, 3685 (1976).

129. G.K. Wertheim, A. Rosencwaig; Phys. Rev. Lett., 26, 1179 (1971).

130. L.G. Parrat; Rev. Mod. Phys., 31, 616 (1959).

131. See, for example, R.G. Parr; "Quantum Theory of Molecular Electronic Structure", Benjamin (1964).

132. T. Koopmans; Physica, 1, 104 (1933).

133. W.G. Richards; J. Mass Spectrom. Ion Phys., 2, 419 (1969).

134. C.R. Brundle, M. Robin, H. Basch; J. Chem. Phys., 53, 2196 (1970).

135. D.B. Adams, D.T. Clark; Theoret. Chim. Acta, 31, 171 (1973).

136. P.S. Bagus; Phys. Rev., 139, A619 (1965).

137. M.E. Schwartz; Chem. Phys. Lett., 5, 50 (1970).

138. M.E. Schwartz, J.D. Switalski, R.E. Stronski; pg. 605 et seq. in ref. 84 (1972).

139. W. Meyer; J. Chem. Phys., 58, 1017 (1973).

140. W. Meyer; Int. J. Quant. Chem., S5, 341 (1971).

141. T.D. Thomas, R.W. Shaw; J. Electron Spectrosc. Rel. Phenom., 5, 1081, (1974).

142. P.S. Bagus, H.F. Schaefer III; J. Chem. Phys., 56, 224 (1972).

143. L.C. Snyder; J. Chem. Phys., 55, 95 (1971).

144. J.N. Murrel, B.J. Ralston; J. Chem. Soc. Faraday Trans. II, 68, 1393 (1972).

145. L.J. Aarons, M.F. Guest, I.H. Hillier; J. Chem. Soc. Faraday Trans. II, 68, 1866 (1972).

146. H. Siegbahn, UUIP-891 (1975).

147. U. Gelius, G. Johansson, H. Siegbahn, C.J. Allan, D.A. Allison, J. Allison, K. Siegbahn; J. Electron Spectrosc. Rel. Phenom., 1, 285 (1972-3).

148. M.F. Guest, I.H. Hillier, V.R. Saunders, M.H. Wood; Proc. Roy. Soc. (London), A333, 201 (1973).

149. D.T. Clark, I.W. Scanlan, J. Müller; Theoret. Chim. Acta, 35, 341 (1974).

150. U. Gelius, E. Basilier, S. Svensson, T. Bergmark, K. Siegbahn; J. Electron Spectrosc. Rel. Phenom., 2, 405 (1974).

151. K. Siegbahn, D. Hammond, H. Fellner-Feldegg, E.F. Barnett; Science, 176, 254 (1972).

152. E. McGuire; Phys. Rev., 185, 1 (1969).

153. G. Hertzberg; "Molecular Spectra and Molecular Structure, Volume III", Van Nostrand (1966).

154. J. Franck; Trans. Faraday Soc., 21, 536 (1926).

155. E.U. Condon; Phys. Rev., 28, 1182 (1926).

156. E.U. Condon; Phys. Rev., 32, 858 (1928).

157. F. Ansbacher; Z. Naturforsch., 14a, 889 (1959).

158. U. Gelius, S. Svensson, H. Siegbahn, E. Basilier, Å. Faxälv, K. Siegbahn; Chem. Phys. Lett., 28, 1 (1974).

159. S. Corvilain-Berger, G. Verhaegen; Chem. Phys. Lett., 50, 468 (1977).

160. A. Veillard, E. Clementi; J. Chem. Phys., 49, 2415 (1969).

161. E. Clementi; Chem. Rev., 68, 341 (1968).

162. C.W. Scherr, J.N. Siverman, F.A. Matsen; Phys. Rev., 127, 830 (1962).

163. C.S. Fadley, S.B.M. Hagstrom, M.P. Klein, D.A. Shirley; J. Chem. Phys., 48, 3779 (1968).

164. C.C.J. Roothaan, A.W. Weiss; Rev. Mod. Phys., 32, 194 (1960).

165. S. Corvilain, G. Verhaegen; Int. J. Quant. Chem., S7, 69 (1973).

166. C.M. Moser, R.K. Nesbet, G. Verhaegen; Chem. Phys. Lett., 12, 230 (1971).

167. W.L. Jolly, D.N. Hendrickson; J. Am. Chem. Soc., 92, 1863 (1970).

168. D.T. Clark, D.B. Adams; J. Chem. Soc. Faraday Trans. II, 68, 1819 (1972).

169. R. McWeeny, A.A. Velenik; Mol. Phys., 24, 1421 (1972).

170. D.T. Clark, J. Müller; Theoret. Chim. Acta, 41, 193 (1976).

171. M.M. Rohmer, A. Veillard; J. Chem. Soc. D, 250 (1973).

172. W. Meyer; "Configuration Expansion by Means of Pseudo-Natural Orbitals", pp. 413 in ref. 65 (1977).

173. a) O. Goscinski, B.T. Pickup, G. Purvis; Chem. Phys. Lett., 22, 167 (1973).

b) O. Goscinski, G. Howat, T. Åberg; J. Phys. B, 8, 11 (1975).

c) O. Goscinski, M. Hehenberger, B. Roos, P. Siegbahn; Chem Phys. Lett., 33, 427 (1975).

174. a) D.J. Rowe; Rev. Mod. Phys., 40, 153 (1968).

b) D.J. Rowe; Phys. Rev., 175, 1283 (1968).

175. a) J. Simons, W.D. Smith; J. Chem. Phys., 58, 4899 (1973).

b) J. Simons; Chem. Phys. Lett., 25, 122 (1974).

c) T.T. Chen, W.D. Smith, J. Simons; J. Chem. Phys., 61, 2670 (1974).

175. d) W.D. Smith, T.T. Chen, J. Simons; Chem. Phys. Lett., 26, 296 (1974).

e) K. Griffing, J. Simons; J. Chem. Phys., 62, 535 (1975).

176. a) D.P. Chong, F.G. Herring, D. McWilliams; J. Chem. Phys., 61, 78 (1974).

b) D.P. Chong, F.G. Herring, D. McWilliams; J. Chem. Phys., 61, 958 (1974).

c) D.P. Chong, F.G. Herring, D. McWilliams; Chem. Phys. Lett., 25, 568 (1974).

d) D.P. Chong, F.G. Herring, D. McWilliams; J. Chem. Phys., 61, 3567 (1974).

e) D.P. Chong, F.G. Herring, D. McWilliams; J. Electron Spectrosc. Rel. Phenom., 7, 445 (1975).

177. a) I. Hubač, V. Kvasnička, A. Holubec; Chem. Phys. Lett., 23, 381 (1973).

b) V. Kvasnička, I. Hubač; J. Chem. Phys., 60, 4483 (1974).

c) S. Biscupič, L. Valko, V. Kvasnička; Theoret. Chim. Acta, 38, 149 (1975).

178. Gy Csanak, H.S. Taylor, R. Yaris; Adv. At. Mol. Phys., 7, 287 (1971).

179. J. Linderberg, Y. Öhrn; "Propagators in Quantum Chemistry", Academic Press (1973).

180. For a recent review of both formalism and results, see L.S. Cederbaum, W. Domcke; Adv. Chem. Phys., 36, 205 (1977).

181. P.E. Cade, K.D. Sales, A.C. Wahl; J. Chem. Phys., 44, 1973 (1966).

182. L.S. Cederbaum, G. Hohlneicher, W. von Niessen; Chem. Phys. Lett., 18, 503 (1973).

183. See, for example, M.A. Robb; "Many Body Perturbation Theory Methods for Calculation of Excited States" and W. von Niessen; "On Green's Function Methods for the Study of Ionic States in Atoms and Molecules" in C.A. Nicolaides, D.R. Beck; "Theoretical Aspects of the Electronic Structure and Properties of the Excited States of Atoms, Molecules and Solids", Plenum (to be published, 1978).

184. J.J. Pireaux, S. Svensson, E. Basilier, P.-Å. Malmquist, U. Gelius, R. Caudano, K. Siegbahn; Phys. Rev., A14 2126 (1976).

185. T.D. Thomas; J. Chem. Phys., 52, 1373 (1970).

186. D.W. Davis, J.M. Hollander, D.A. Shirley, T.D. Thomas; J. Chem. Phys., 52, 3295 (1970).

187. D.B. Adams; J. Electron Spectrosc. Rel. Phenom., 9, 251 (1976).

188. D.T. Clark, I.W. Scanlan; J. Chem. Soc. Faraday Trans. II, 70, 1222 (1970).

189. For example, J.A. Pople; J. Am. Chem. Soc., 93, 5339 (1971).

190. J.A. Pople, M.S. Gordon; J. Am. Chem. Soc., 89, 4523 (1967).

191. U. Gelius, K. Siegbahn; J. Chem. Soc. Faraday Trans. II, 54, 257 (1972).

192. W.L. Jolly, T.F. Schaaf; J. Am. Chem. Soc., 98, 3178 (1976).

193. D.T. Clark, B.J. Cromarty, A. Dilks; J. Polym. Sci., Polym. Chem. Ed., in press (1978).

194. See, for example, the chapters in "Molecular Spectroscopy", edited by A.R. West, Heyden (1977) by D.T. Clark, E. Heilbronner and W.C. Price.

195. a) K. Thimm; J. Electron Spectrosc. Rel. Phenom., 5, 755 (1974).

b) H. Winick; SSRP Report No. 75/07 (1975).

196. See, for example, K. Siegbahn; UUIP-940 (1976).

197. W. Domcke, L.S. Cederbaum; Chem. Phys. Lett., 31, 582 (1975).

198. D.T. Clark, J. Müller; Chem. Phys., 23, 429 (1977).

199. D.T. Clark, L. Colling; J. Electron Spectrosc. Rel. Phenom., 13, 317 (1978).

200. D.T. Clark, L. Colling; Nouveau J. de Chemie, 2, 225 (1978).

201. R.L. Martin, D.A. Shirley; Phys. Rev. A, 13, 1475 (1976).

202. I.H. Hillier, J. Kendrick; J. Electron Spectrosc. Rel. Phenom., 8, 239 (1976).

203. W.R. Rodwell, M.F. Guest, T. Darko, I.H. Hillier, J. Kendrick; Chem. Phys., 22, 467 (1977).

204. M.F. Guest, W.R. Rodwell, T. Darko, I.H. Hillier, J. Kendrick; J. Chem. Phys., 66, 5447 (1977).

205. U. Wahlgren; Mol. Phys., 33, 1109 (1977).

206. P.S. Bagus, E.K. Viinikka; Phys. Rev. A, 15, 1486 (1977).

207. A.W. Potts, W.C. Price; Proc. Roy. Soc. (London), A326, 181 (1972).

208. A.W. Potts, T.A. Williams, W.C. Price; Faraday Disc. Chem. Soc., 54, 104 (1972).

209. J.J. Pireaux, R. Caudano; Phys. Rev. B, 15, 2242 (1977).

210. D.T. Clark, B.J. Cromarty; Chem. Phys. Lett., 49, 137 (1977).

211. L.S. Cederbaum, W. Domcke; J. Chem. Phys., 60, 2878 (1974).

212. A.D. Buckingham, N.C. Hardy, R.J. Whitehead; J. Chem. Soc. Faraday Trans. II, 1, 95 (1975).

213. E. Clementi, H. Popkie; J. Am. Chem. Soc., 94, 4057 (1972).

214. L.E. Sutton; "Tables of Interatomic Distances Supplement", Special Publications No. 18, London Chemical Society (1965).

215. C.E. Blom, P.J. Slingerland, C. Altona; Mol. Phys., 31, 1359 (1976).

216. J.J. Pireaux; private communication.

217. V. Buss, P. von R. Schleyer, L.C. Allen; "The Electronic Structure and Stereochemistry of Simple Carbonium Ions" in "Topics in Stereochemistry, Vol. 7", Ed. N.L. Allinger, E.L. Eliel, pp. 253 (1973).

218. W.A. Lathan, L.A. Curtiss, W.J. Hehre, J.B. Lisle, J.A. Pople; Prog. Phys. Org. Chem., 11, 175 (1974).

219. J.A. Pople; J. Mass Spectrom. Ion Phys., 19, 89 (1976).

220. W.J. Hehre; "Carbonium Ions: Structural and Energetic Investigations", in "Modern Theoretical Chemistry, Volume 4", ed. H.F. Schaefer III, Plenum (1977).

221. Ed. by G.A. Olah, P. von R. Schleyer; "Carbonium Ions, Volumes I- V", Wiley-Interscience (1976).

222. G.A. Olah, "Carbocations and Electrophilic Reactions", J. Wiley (1974).

223. G.M. Kramer; Adv. Phys. Org. Chem., 11, 177 (1975).

224. G.A. Olah; Acct. Chem. Res., 9, 41 (1976).

225. H.C. Brown; Tetrahedron, 32, 179 (1976).

226. H.C. Brown, with comments by P. von R. Schleyer; "The Non-classical Ion Problem", Plenum (1977).

227. G.A. Olah, Gh.D. Mateescu, L.A. Wilson, M.H. Gross; J. Am. Chem. Soc., 92, 7231 (1970).

228. D.T. Clark; 23rd IUPAC Congress (Boston), 1, 31 (1971).

229. G.A. Olah, Gh.D. Mateescu, J.L. Riemenschneider; J. Am. Chem. Soc., 94, 2529 (1972).

230. Gh.D. Mateescu, J.L. Riemenschneider, J.J. Svoboda, G.A. Olah; J. Am. Chem. Soc., 94, 7191 (1972).

231. Gh.D. Mateescu, J.L. Riemenschneider; in ref. 84, pp. 661 (1972).

232. G.A. Olah, G. Liang, Gh.D. Mateescu, J.L. Riemenschneider; J. Am. Chem. Soc., 95, 8698 (1973).

233. W.J. Hehre; Acct. Chem. Res., 8, 369 (1975).

234. L. Radom, J.A. Pople, P. von R. Schleyer; J. Am. Chem. Soc., 94, 5935 (1972).

235. R.M. Stevens; J. Chem. Phys., 52, 1397 (1970).

236. P.C. Hariharan, L. Radom, J.A. Pople, P. von R. Schleyer; J. Am. Chem. Soc., 96, 599 (1974).

237. O. Tapia, O. Goscinski; Mol. Phys., 29, 1653 (1975).

238. R.J. Abraham; in "Environmental Effects on Molecular Structure and Properties", edited by B. Pullman, pp. 41, D. Reidel (1976).

239. a) W.L. Jorgensen; J. Am. Chem. Soc., 99, 4272 (1977).

b) W.L. Jorgensen; J.E. Munroe; Tet. Lett., 6, 581 (1977).

240. D.T. Clark; D.M.J. Lilley; Tetrahedron, 29, 845 (1973).

241. D.W. Goetz, L.C. Allen; 23rd IUPAC Congress (Boston), 1, 51 (1972).

242. D.W. Goetz, H.B. Schlegel, L.C. Allen; J. Am. Chem. Soc., 99, 8118 (1977).

243. R.C. Bingham, M.J.S. Dewar, D.H. Lo; J. Am. Chem. Soc., 97, 1285 (1975).

244. M.J.S. Dewar, R.C. Haddon, A. Kormornicki, H. Rzepa; J. Am. Chem. Soc., 99, 377 (1977).

245. cf. D.T. Clark in ref. 85.

246. D.T. Clark, J. Peeling, L. Colling; Biochim. Biophys. Acta (P), 453, 533 (1976).

247. M.J.S. Dewar, D.H. Lo; Chem. Phys. Lett., 33, 298 (1975).

248. S. Bantle, R. Ahlrichs; Chem. Phys. Lett., 53, 148 (1978).

249. D.T. Clark, H.R. Thomas; J. Polym Sci., Polym. Chem. Ed., 15, 2843 (1977).

250. D.T. Clark, B.J. Cromarty; Theoret. Chim. Acta., 44, 181 (1977).

251. W.A. Lathan, W.J. Hehre, J.A. Pople; J. Am. Chem. Soc., 93, 6377 (1971).

252. P.C. Hariharan, W.A. Lathan, J.A. Pople; Chem. Phys. Lett., 14, 385 (1972).

253. B. Zurawski, R. Ahlrichs, W. Kutzelnigg; Chem. Phys. Lett., 21, 309 (1973).

254. L. Radom, J.A. Pople, V. Buss, P. von R. Schleyer; J. Am. Chem. Soc., 93, 1813 (1971).

255. "Hydrogen Bonding - Recent Developments in Theory and Experiment", edited by P. Schuster, G. Zundel, C. Sandorfy, North-Holland (1976).

256. P. Schuster; "Energy Surfaces for Hydrogen-Bonded Systems", pp. 26, in ref. 255 (1976).

257. P.A. Kollman; "Hydrogen Bonding and Donor-Acceptor Interactions" in "Modern Theoretical Chemistry, Volume 4", edited by H.F. Schaefer III, Plenum (1977).

258. W.C. Topp, L.C. Allen; J. Am. Chem. Soc., 96, 5291 (1974).

259. L.C. Allen; J. Am. Chem. Soc., 97, 6921 (1975).

260. J.D. Dill, L.C. Allen, W.C. Topp, J.A. Pople; J. Am. Chem. Soc., 97, 7220 (1975).

261. L.C. Allen; Proc. Nat. Acad. Sci. USA, 72, 4701 (1975).

262. K. Morokuma; J. Chem. Phys., 55, 1236 (1971).

263. K. Kitaura, K. Morokuma; Int. J. Quant. Chem., 10, 325 (1976).

264. H. Umeyama, K. Morokuma; J. Am. Chem. Soc., 99, 330 (1977).

265. H. Umeyama, K. Morokuma; J. Am. Chem. Soc., 99, 1316 (1977).

266. K. Morokuma; Accts. Chem. Res., 10, 294 (1977).

267. P.A. Kollman; Accts. Chem. Res., 10, 365 (1977).

268. P.A. Kollman; J. Am. Chem. Soc., 99, 4875 (1977).

269. J.O. Noell, K. Morokuma; J. Phys. Chem., 80, 2675 (1976).

270. M. Newton; J. Phys. Chem., 79, 2795 (1975).

271. M.D. Newton; J. Chem. Phys., 67, 5535 (1977).

272. H. Veillard; J. Am. Chem. Soc., 99, 7194 (1977).

273. O. Tapia; Theoret. Chim. Acta, 47, 157 (1978).

274. G. Diercksen, W. Kraemer, B. Roos; Theoret. Chim. Acta, 36, 249 (1975).

275. O. Matsuoka, E. Clementi, M. Yoshimine; J. Chem. Phys., 64, 1361 (1976).

276. P.A. Kollman, L.C. Allen; J. Am. Chem. Soc., 92, 6101 (1970).

277. A. Neckel, P. Kuzmany, G. Vinck; Z. Naturforsch., A26, 569 (1971).

278. C. Thomson, D.T. Clark, T.C. Waddington, H.D.B. Jenkins; J. Chem. Soc., Faraday Trans. II, 71, 1942 (1975).

279. J. Emsley, O.P.A. Hoyte, R.E. Overill; J. Chem. Soc. Chem. Comm., 225 (1977).

280. See, for example, C.R. Brundle, A.F. Carley; Disc. Farad. Soc., 60, 51 (1975).

281. K. Johnson, F. Herman, R. Kjellander; in "Electronic Structure of Polymers and Molecular Crystals", edited by J.M. André, J. Ladik; Plenum (1974).

282. P. Merlet, S.D. Peyerimhoff, R.J. Buenker; J. Am. Chem. Soc., 94 8301 (1972).

283. For example, see:

a) C.R. Brundle; Surf. Sci., 48, 99 (1975).

b) S.J. Atkinson, C.R. Brundle, M.W. Roberts; Disc. Faraday Soc., 58, 62 (1975).

284. H.A. Gebbie, W.J. Burroughs, J. Chamberlain, J.E. Harries, R.J. Jones; Nature, 221, 143 (1969).

285. a) J.A. Salthouse; Ph.D. Thesis (Univ. of Cambridge, 1965).

b) R.L. Benoit, M. Rinfret, R. Domain; Inorg. Chem., 11, 2603 (1972).

c) H.P. Dixon, H.D.B. Jenkins, T.C. Waddington; J. Chem. Phys., 57, 4388 (1972).

286. M.S. Banna, B.E. Mills, D.W. Davis, D.A. Shirley; J. Chem. Phys., 61, 4780 (1974).

287. U. Gelius; J. Electron Spectrosc. Rel. Phenom., 5, 985 (1974).

288. E. Clementi; J. Chem. Phys., 38, 1001 (1963).

289. O. Goscinski, A. Palma; Chem. Phys. Lett., 47, 322 (1977).

290. J. Cambray, J. Gasteigner, A. Streitwieser, Jr., P.S. Bagus; J. Am. Chem. Soc., 96, 5978 (1974).

291. G. Hertzberg; "Molecular Spectra and Molecular Structure, Volume I", Van Nostrand (1950).

292. G. Miksche, H. Miksche, H. Murauer, K. Persy; J. Electron Spectrosc. Rel. Phenom., 10, 423 (1977).

293. K. Burger, F. Tschismarov, H. Ebel; J. Electron Spectrosc. Rel. Phenom., 10, 461 (1977).

294. D.T. Clark, A. Dilks, H.R. Thomas, D. Shuttleworth; J. Polymer Sci., Polym. Chem. Ed., in press (1978).

295. K. Siegbahn; J. Electron Spectrosc. Rel. Phenom., 5, 3 (1974).

296. Yu. Ya. Kharitonov; Izv. Akad. Nauk SSSR, Otd. Khim. Nauk.,1953 (1962).

297. P.J. Bruna, S.D. Peyerimhoff, R.J. Buenker; Chem. Phys., 10, 323 (1975).

298. See, for example:

a) P.E. Cade, K.D. Sales, A.C. Wahl; J. Chem. Phys., 44, 1973 (1966).

b) H. Pritchard, A.G. Harrison; J. Chem. Phys., 50, 1043 (1969).

299. D.A. Shirley, R.L. Martin; J. Am. Chem. Soc., 96, 5299 (1974).

300. M. Barber, J.A. Connor, M.F. Guest, M.B. Hall, I.H. Hillier, W.N.E. Meredith; Farad. Disc. Chem. Soc., 54, 219 (1972).

301. P.K. Pearson, H.F. Schaefer III, U. Wahlgren; J. Chem. Phys., 62, 350 (1975).

302. J. Peslak, Jr., D.S. Klett, C.W. David; J. Am. Chem. Soc., 93, 5001 (1971).

303. P.K. Pearson, G.L. Blackman, H.F. Schaefer III, B. Roos, U. Wahlgren; Astrophys. J., 184, 49 (1973).

304. G.A. Gallup; Inorg. Chem., 14, 563 (1975).

305. A.A. Wu, S.D. Peyerimhoff, R.J. Buenker; Chem. Phys. Lett., 35, 316 (1975).

306. J.F. Ogilvie; J. Mol. Struct., 31, 407 (1976).

307. A.A. Wu; Chem. Phys., 21, 173 (1977).

308. C. Marian, P.J. Bruna, R.J. Buenker, S.D. Peyerimhoff; Mol. Phys., 33, 63 (1977).

309. U. Gelius; Phys. Script., 9, 133 (1974).

310. For a recent review, see, for example, C.R. Brundle; "Molecular Spectroscopy", Chapter 16, Ed. A.R. West, Heyden (1977).

311. D. Menzel; "Photoelectron Spectroscopy of Adsorption Layers", CRC Critical Review of Surface Science, Ed. R. Vaneslow, CRC Press (1977).

312. J. Pendry; "Low Energy Electron Diffraction", Academic Press (1974).

313. G. Blyholder; J. Vac. Sci. Technol., 11, 865 (1974).

314. G. Doyen, G. Ertl; Surf. Sci., 43, 197 (1974).

315. P.W. Anderson; Phys. Rev., 124, 41 (1971).

316. I.P. Batra, P.S. Bagus; Solid St. Comm., 16, 1097 (1975).

317. G. Apai, P.S. Wehner, R.S. Williams, J. Stöhr, D.A. Shirley; Phys. Rev. Lett., 37, 1497 (1976).

318. E.W. Plummer, T. Gustafsson; Science, 198, 165 (1977).

319. J.W. Davenport; Phys. Rev. Lett., 36, 945 (1976).

320. P.S. Bagus, K. Herman; Solid St. Comm., 20, 5 (1976).

321. K. Herman, P.S. Bagus; Phys. Rev. B, 16, 4195 (1977).

322. J.C. Tracy; J. Chem. Phys., 56, 2736 (1972).

323. S. Andersson; Solid St. Comm., 21, 5 (1977).

324. S. Andersson, J.B. Pendry; Surf. Sci., 71, 75 (1978).

325. R.W.G. Wyckoff; "Crystal Structures", 2nd Edition, Vol. II, 143, Interscience (1964).

326. T. Gustafsson, E.W. Plummer, D.E. Eastman, J.L. Freeouf; Solid St. Comm., 17, 391 (1975).

327. P.M. Williams, P. Butcher, J. Wood, K. Jacobi; Phys. Rev. B, 14, 3215 (1976).

328. H. Conrad, G. Ertl, J. Küppers, E.E. Latta; Surf. Sci., 50, 296 (1975).

329. I.P. Batra, C.R. Brundle; Surf. Sci., 57, 12 (1976).

330. D.W. Johnson, M.H. Matloob, M.W. Roberts; J. Chem. Soc., Chem. Comm., 40 (1978).

331. M.W. Roberts; Chem. Soc. Rev., 6, 373 (1976).